ISSN: 0218 – 1274

INTERNATIONAL JOURNAL OF

BIFURCATION AND CHAOS

IN APPLIED SCIENCES AND ENGINEERING

THEME ISSUE – Part I

Volume 8 • Number 8 • August 1998

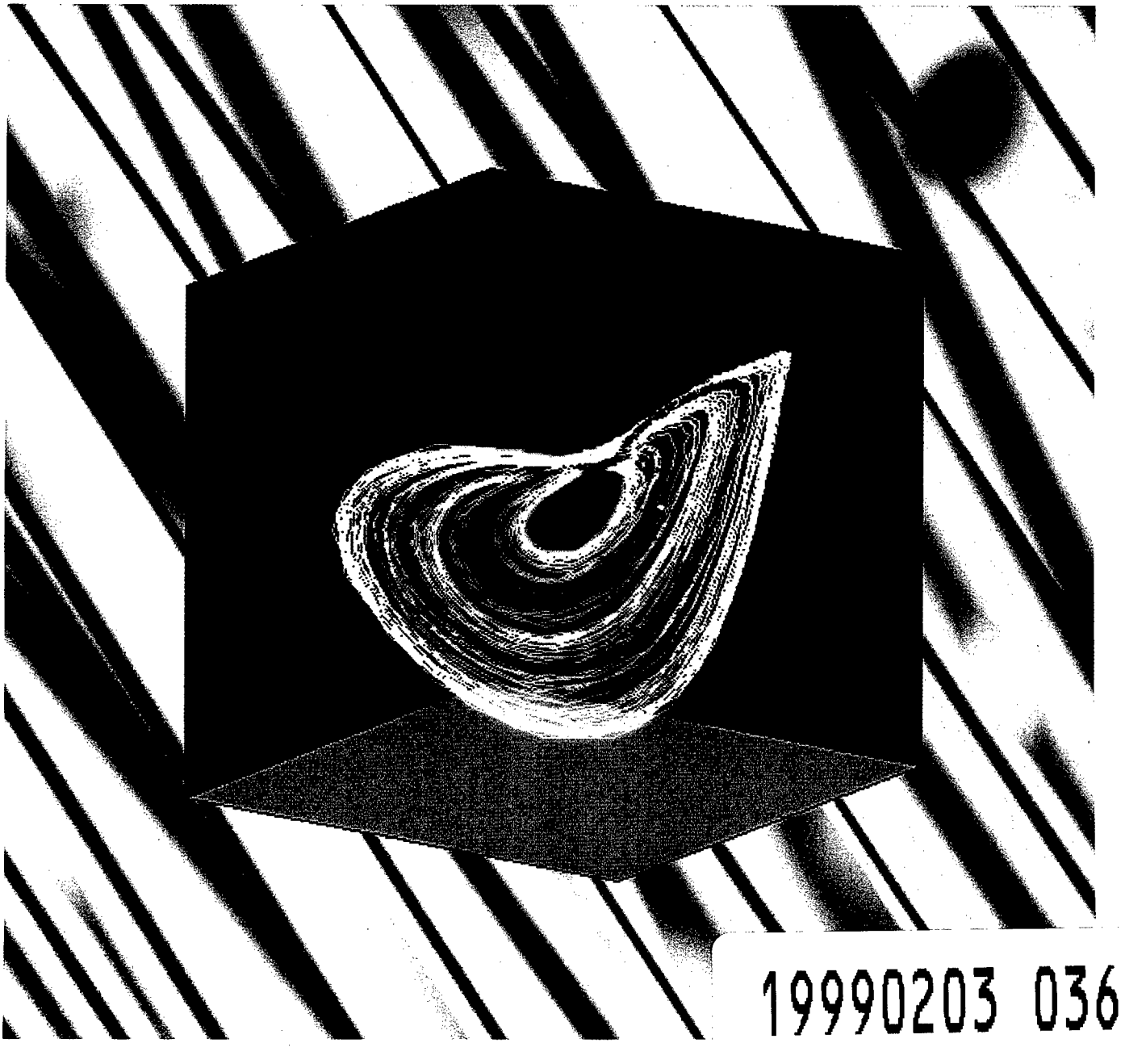

World Scientific
Singapore • New Jersey • London • Hong Kong

AIMS AND SCOPE

The discipline of *chaos* has created a universal paradigm, a scientific parlance, and a mathematical tool for grappling with *nonlinear* phenomena. In every field of the *applied sciences* (astronomy, atmospheric sciences, biology, chemistry, economics, geophysics, life and medical sciences, physics, social sciences, zoology, etc.) and *engineering* (aerospace, chemical, civil, computer, information, mechanical, software, telecommunication, etc.) the local and global manifestations of Chaos and Bifurcation have burst forth in an unprecedented universality, linking scientists heretofore unfamiliar with one another's fields, and offering an opportunity to reshape our grasp of reality.

The primary *objective* of this journal is to provide a single forum for this multidisciplinary discipline — a forum specifically designed for an interdisciplinary audience, a forum accessible and affordable to all. Real-world problems and applications will be emphasized. Our goal is to bring together, in one periodical, papers of the highest quality and greatest importance on every aspect of *nonlinear dynamics*, *phenomena*, *modeling*, and *complexity*, thereby providing a focus and catalyst for the timely dissemination and cross-fertilization of new ideas, principles, and techniques across a broad interdisciplinary front.

The *scope* of this journal encompasses *experimental*, *computational*, and *theoretical* aspects of **bifurcations**, **chaos** and **complexity** of biological, economic, engineering, fluid dynamic, neural, physical, social, and other dynamical systems. This broad but focused coverage includes, but is not restricted to, those areas of expertise provided by the members of the editorial board, whose composition will evolve continuously in order to respond to emerging new areas and directions in *nonlinear dynamics* and *complexity*. The philosophy and policy of this journal, as well as its commitment to readability and clarity, are articulated in an *Editorial* in the first issue (vol. 1, no. 1, 1991).

INFORMATION FOR AUTHORS

1. *International Journal of Bifurcation and Chaos* is a monthly journal consisting of
   - **papers**

     While the majority of papers will consist of original contributions, the Journal also welcomes well-written, incisive authoritative *tutorials* and *reviews* with long-lasting value to future researchers.
   - **letters to the Editor**

     These are mainly for the timely announcement of significant new results and discoveries (phenomena, algorithms, theorems, etc.). Though concise, letter manuscripts must include details and data so that referees can evaluate their validity and significance.
2. Once a paper or letter to the Editor is accepted for publication, the author is assumed to have transferred the copyright for it to the publisher.
3. Essential color pictures will be published at no cost to the authors.
4. There are no page charges for this journal.
5. 50 complimentary reprints will be given to the author(s) of each paper. For a multi-author paper, these will be sent to the author designated as the contact person. Orders for additional reprints may be made on forms which will be sent along with the proofs.

REPRODUCTION QUALITY NOTICE

This document is the best quality available. The copy furnished to DTIC contained pages that may have the following quality problems:

- Pages smaller or larger than normal.
- Pages with background color or light colored printing.
- Pages with small type or poor printing; and or
- Pages with continuous tone material or color photographs.

Due to various output media available these conditions may or may not cause poor legibility in the microfiche or hardcopy output you receive.

 If this block is checked, the copy furnished to DTIC contained pages with color printing, that when reproduced in Black and White, may change detail of the original copy.

REPORT DOCUMENTATION PAGE

Form Approved OMB No. 0704-0188

1. AGENCY USE ONLY (Leave blank)	2. REPORT DATE	3. REPORT TYPE AND DATES COVERED
	19 January 1999	Conference Proceedings

4. TITLE AND SUBTITLE

Control of Chaos: New Perspectives in Experimental and Theoretical Science

5. FUNDING NUMBERS

F6170897W0108

6. AUTHOR(S)

Conference Committee

7. PERFORMING ORGANIZATION NAME(S) AND ADDRESS(ES)

Instituto Nazionale di Ottica
Largo Enrico Fermi 6
Florence 50125
Italy

8. PERFORMING ORGANIZATION REPORT NUMBER

N/A

9. SPONSORING/MONITORING AGENCY NAME(S) AND ADDRESS(ES)

EOARD
PSC 802 BOX 14
FPO 09499-0200

10. SPONSORING/MONITORING AGENCY REPORT NUMBER

CSP 97-1053

11. SUPPLEMENTARY NOTES

2 Volumes

12a. DISTRIBUTION/AVAILABILITY STATEMENT

Approved for public release; distribution is unlimited.

12b. DISTRIBUTION CODE

A

13. ABSTRACT (Maximum 200 words)

The Final Proceedings for Control of Chaos: New Perspectives in Experimental and Theoretical Science, 16 May 1997 - 18 May 1997

nonlinear, adaptive and robust control; synchronization of chaotic processes; and applications of control of chaos in science and technology.

14. SUBJECT TERMS

EOARD, Control, Lasers, Non-linear Dynamics

15. NUMBER OF PAGES

16. PRICE CODE
N/A

17. SECURITY CLASSIFICATION OF REPORT	18. SECURITY CLASSIFICATION OF THIS PAGE	19. SECURITY CLASSIFICATION OF ABSTRACT	20. LIMITATION OF ABSTRACT
UNCLASSIFIED	UNCLASSIFIED	UNCLASSIFIED	UL

INTERNATIONAL JOURNAL OF
BIFURCATION AND CHAOS
IN APPLIED SCIENCES AND ENGINEERING
THEME ISSUE - Part I

Volume 8 • Number 8 • August 1998

CONTROL OF CHAOS: NEW PERSPECTIVES IN EXPERIMENTAL AND THEORETICAL NONLINEAR SCIENCE

Guest Editors

F. T. Arecchi
S. Boccaletti
M. Ciofini
G. Grebogi
R. Meucci

World Scientific
Singapore • New Jersey • London • Hong Kong

INTERNATIONAL JOURNAL OF
BIFURCATION AND CHAOS
IN APPLIED SCIENCES AND ENGINEERING
THEME ISSUE - Part I

Volume 8 • Numbers 8 & 9 • Aug & Sept 1998

CONTENTS (August 1998)

CONTENTS (September 1998)

Cover Illustration: From page 1762 [Fig. 6], Volume 8, Number 9.
Cover inset design represents a three-dimensional plot of an experimental chaotic attractor (yellow) with, superimposed, the stabilized period-1 limit cycle (blue).

Subscriptions, changes of address, single-copy orders should be addressed to Journal Department, World Scientific Publishing Co. Pte. Ltd., Farrer Road, P. O. Box 128, Singapore 912805, or Suite 1B, 1060 Main Street, River Edge, NJ 07661, USA, or 57 Shelton Street, Covent Garden, London WC2H 9HE, England.

The **International Journal of Bifurcation and Chaos** (ISSN 0218-1274) is published monthly by World Scientific Publishing Co. Pte. Ltd., Farrer Road, P. O. Box 128, Singapore 912805. Annual subscription rates are available upon request. Periodicals postage paid at Jamaica, N.Y. 11431.
US POST MASTER: Please send change of address to **International Journal of Bifurcation and Chaos**, c/o Publications Expediting Inc., 200 Meacham Avenue, Elmont, N.Y. 11003. Air freight & mailing in the US by Publications Expediting Inc., 200 Meacham Avenue, Elmont, N.Y. 11003 (Tel. 516-352-7300).

This journal is covered in *SciSearch*®, *Research Alert*®, *CompuMath Citation Index*® and *Science Citation Index*®.

International Journal of Bifurcation and Chaos, Vol. 8, No. 8 (1998) 1641–1642

EDITORIAL

The Third EuroConference on Nonlinear Dynamics in Physics and Related Sciences was held in Montecatini Terme, Tuscany, Italy, from 16–18 May, 1997, under the Auspices of a HCM granting programme (EEC Contract N. ERB4050PL934039). The title of the Conference was: *Control of Chaos: New Perspectives in Experimental and Theoretical Nonlinear Science.*

The aim of the workshop was to bring together researchers from different fields working on control and synchronization of chaos and spatiotemporal chaos, in order to assess the recent achievements in these areas, and to point out future directions.

The subjects covered in the conference include the control and tracking of unstable periodic orbits in experimental systems, the synchronization of chaos for secure communication systems, the control of chaotic laser dynamics, the stabilization of unstable periodic patterns in extended dynamical systems, the control of chemical reactions, and the targeting of chaotic trajectories to desired states.

The control of chaos refers to a process wherein a chaotic dynamics is slightly perturbed in order to stabilize some of the unstable periodic orbits which are embedded within the chaotic attractor. This process allows us to use a single chaotic system to produce an infinite variety of periodic behaviors, with great flexibility in switching from one to another. Chaos synchronization refers to a situation where two identical chaotic systems starting from different initial conditions are kept synchronized by means of the transmission of a signal. Finally, targeting of chaos is a process wherein tiny perturbations applied to the system are able to steer the trajectory emerging from a given initial condition to any desired point of the attractor in a finite (and usually very short) time.

In the last few years, these subjects have attracted more and more interest within the scientific community due to the extreme interdisciplinary nature of these research fields. For instance, applications of chaos synchronization range from building a secure communication system to the problem of bacterial replication. On the other hand, control of chaos has been experimentally tested in different dynamical situations, such as in laser dynamics, in electronic circuits, in the dynamics of the magnetoelastic ribbon, in the control of cardiac timing, in the control of chemical waves.

All the different achievements have faced different aspects of the same problem, and in many cases different methods have been used to control different dynamical situations.

More than 60 participants of the conference have profusely discussed these subjects from diverse points of view: from applied mathematics, to engineering, to laser physics, to chemistry, to electronics. We believe that the Montecatini Workshop has strongly contributed by bringing together different skills and expertises, and emphasizing the common achievements and the future directions of the field.

The present special issue summarizes the discussion that took place during the conference, by reporting most of the oral and poster presentations. This special issue also contains two tutorial papers, which are intended for the nonexpert readers as an introduction to the field.

We gratefully thank all colleagues who helped referee the papers in this issue. Their comments, suggestions and remarks have significantly improved the quality of the presentation of the reported papers. We would like to thank the EU representative, and all colleagues who chaired the different sections of the conference, who helped in putting up a successful and fruitful workshop. Special thanks also go to all the participants of the workshop and

to all the contributors to this special issue. We are particularly indebted to the following institutions for their contribution to the success of the conference:

— United States Air Force European Office of Aerospace Research and Development (E.O.A.R.D.)
— Istituto Nazionale di Ottica (Florence, Italy)
— Gruppo Nazionale di Elettronica Quantistica e Plasmi del Consiglio Nazionale delle Ricerche (G.N.E.Q.P.)

F. T. Arecchi
S. Boccaletti
M. Ciofini
G. Grebogi
R. Meucci

International Journal of Bifurcation and Chaos, Vol. 8, No. 8 (1998) 1643–1655

THE CONTROL OF CHAOS: THEORETICAL SCHEMES AND EXPERIMENTAL REALIZATIONS

F. T. ARECCHI*, S. BOCCALETTI†, M. CIOFINI and R. MEUCCI
Istituto Nazionale di Ottica, I-50125 Florence, Italy
**Department of Physics, University of Firenze, I-50125 Florence, Italy*
†*Department of Physics and Applied Mathematics, Universidad de Navarra, E-31080, Pamplona, Spain*
C. GREBOGI
University of Maryland, College Park, USA

Received July 31, 1997; Revised November 28, 1997

Controlling chaos is a process wherein an unstable periodic orbit embedded in a chaotic attractor is stabilized by means of tiny perturbations of the system. These perturbations imply goal oriented feedback techniques which act either on the state variables of the system or on the control parameters. We review some theoretical schemes and experimental implementations for the control of chaos.

1. Introduction

Controlling chaos consists in perturbing a chaotic system in order to stabilize a given unstable periodic orbit (UPO) embedded in the chaotic attractor (CA). The UPO's constitute the skeleton of chaotic dynamics, which, indeed, can be seen as a continuous irregular jumping process among neighborhoods of different periodic behaviors [Auerbach *et al.*, 1987]. Thus, control of chaos implies the extraction of desired periodic motions out of a chaotic one, through the application of judiciously chosen small perturbations. The process allows to exploit a single dynamical system for the production of a large number of different periodic behaviors, with an extreme flexibility in switching from one to another, so that the single system can carry out different performances with different yields.

The aim of this paper is to summarize some theoretical and experimental implementations of the above concepts. It is important to point out that the body of literature on this topic is very wide, and that the methodologies described here are by no means the only ones valid. Nevertheless, we hope that the reading of this paper may help researchers in entering this field, and in getting their bearings among the different methods.

In Sec. 2 we report the first control method, which was proposed by Ott *et al.* [1990] (OGY) and which consists in slight readjustments of a control parameter each time the trajectory crosses the Poincaré section (PS). Since a generic UPO is mapped on the PS by an ordered sequence of crossing points, OGY is able to stabilize such a sequence whenever the chaotic trajectory visits closely a neighborhood of one of the saddle PS points. The time lapse for a natural passage of the flow within the fixed neighborhood (hence for switching on the control process) can be very large. To minimize such a waiting time, a technique of targeting has been also introduced [Shinbrot *et al.*, 1993].

Another technique to constrain a nonlinear system $\mathbf{x}(t)$ to follow a prescribed goal dynamics $\mathbf{g}(t)$ [Plapp & Huebler, 1990] is based upon the addition to the equation of motion $d\mathbf{x}/dt = \mathbf{F}(\mathbf{x})$ of a term $\mathbf{U}(t)$ chosen in such a way that $|\mathbf{x}(t) - \mathbf{g}(t)| \to 0$ as $t \to \infty$. Plapp and Huebler choose $\mathbf{U}(t) = d\mathbf{g}/dt - \mathbf{F}(\mathbf{g}(t))$. The method provides robust

solutions, but in general the perturbation **U** would not be a small portion of the unperturbed dynamics **F**.

In other papers the effects of periodic [Lima & Pettini, 1990; Braiman & Goldhirsch, 1991; Azevedo & Rezende, 1991] and stochastic [Fahy & Hamann, 1992] perturbations is explored in producing dramatic changes in the dynamics, which eventually may lead to the selection of some UPO, even though they cannot be considered in general as goal oriented. This parametric perturbation avenue is explored in several companion papers of this issue.

Section 3 presents a method based upon the continuous application of a delayed feedback term in order to force the dynamical evolution of the system toward the desired periodic dynamics whenever the system visits such a periodic behavior closely [Pyragas, 1992].

Section 4 describes a frequency-domain control technique called "washout filter" [Tesi *et al.*, 1996; Basso *et al.*, 1997], based upon the insertion of a selective filter within a feedback loop.

Section 5 introduces the method of adaptive recognition [Arecchi *et al.*, 1994] and control [Boccaletti & Arecchi, 1995, 1996] of chaos. The method has later been successfully applied to chaos synchronization [Boccaletti *et al.*, 1997a], targeting of chaos [Boccaletti *et al.*, 1997b], filtering noise from chaotic data sets [Boccaletti *et al.*, 1997c], and eventually to the quenching of defects in an infinite dimensional dynamical system [Boccaletti *et al.*, 1997d]. The technique consists of a first step wherein the unperturbed features of the dynamics are extracted, and in a second step in which perturbations are done for the control of desired periodic orbits.

In Sec. 6 we review a few implementations of control of chaos in several experimental situations. The first experimental application of OGY was the stabilization of periodic orbits of a chaotic gravitationally buckled, amorphous magnetoelastic ribbon [Ditto *et al.*, 1990]. OGY inspired an easily realizable experimental technique called OPF (occasional proportional feedback), and demonstrated in a chaotic diode oscillator [Hunt, 1991].

Many other experimental systems have provided successful examples of chaos control. We recall among the others the thermal convection loop [Singer *et al.*, 1991], the yttrium iron garnet oscillator [Azevedo & Rezende, 1991], the optical multimode solid-state laser [Roy *et al.*, 1992], the Belouzov–Zabotinsky chemical reaction [Peng *et al.*, 1991; Petrov *et al.*, 1993], the optical fiber laser [Bielawski *et al.*, 1993], the CO_2 laser with modulation of losses [Meucci *et al.*, 1994], and the lead-salt diode laser [Chin *et al.*, 1996].

Finally, we discuss the experimental implementations of the "washout filter" technique of Sec. 4. The method has provided successful experimental applications both on autonomous [Meucci *et al.*, 1997] and nonautonomous [Ciofini *et al.*, 1997] chaotic CO_2 laser systems.

2. The OGY Control of Chaos

In this section we summarize the OGY method for the control of chaos [Ott *et al.*, 1990]. Even though such method holds regardless of the number of positive Liapunov exponents, for simplicity, we refer to a continuous-time chaotic dynamical system in a three-dimensional phase space, thus with a single positive Liapunov exponent. This is ruled by the differential equation

$$\frac{d\mathbf{x}}{dt} = \mathbf{F}(\mathbf{x}, p)\,, \tag{1}$$

where $\mathbf{x}$ is a D dimensional vector ($D = 3$), and p is a control parameter that we assume to be accessible for adjustments. The goal is to temporally program such adjustments so as to achieve stabilization of some UPO embedded within the chaotic attractor. Furthermore, we imagine that the functional form of $\mathbf{F}$ is not known, but that experimental time series of some scalar component $z(t)$ can be measured. By means of time-delay coordinates, and selecting an embedding time T, it is possible to reconstruct a $M + 1$ dimensional embedding space containing the vectors of the form

$$\mathbf{X}(t) \equiv [z(t),\, z(t-T),\, z(t-2T), \ldots,\, z(t-MT)]\,.$$

If one is interested in periodic orbits, one shall use $\mathbf{X}$ to obtain a surface of section, wherein any continuous-time-periodic orbit emerges as a discrete-time orbit cycling through a finite set of points. The requirement is that the embedding space has as many dimensions as there are coordinates of the point ($M = D - 1$), so that our surface of section is, in the present case, a two-dimensional surface. Let us now suppose that the control parameter p can be varied in a small interval about some nominal value p_0 (in the following, and without loss of generality, we take $p_0 = 0$), ranging within the interval $p_* > p > -p_*$. Again, let us

suppose that the experimental measurement contains many points in the surface of section for $p = 0$. By denoting such points as $\xi_1, \xi_2, \xi_3, \ldots, \xi_k$, then ξ_n are in general the coordinates at the nth intersection of the surface by the orbit $\mathbf{X}(t)$. A common choice of the surface is $z(t - MT) =$ constant, so that $\xi_n \equiv [z(t_n), \ldots, z(t_n - (M-1)T)]$, $t = t_n$ denoting the instant of the nth intersection.

Finally, let us denote by $\xi = \xi_F \equiv 0$ a given fixed point, by λ_s and λ_u respectively the stable and unstable eigenvalues of the surface at ξ_F, by $\mathbf{e}_s$ and $\mathbf{e}_u$ the unit vectors of the corresponding experimentally determined eigenvectors. When a change in p from $p = 0$ to some other value $p = \overline{p}$ is done, then the fixed point coordinate will shift correspondingly from 0 to some nearby point $\xi_F(\overline{p})$. For small $\overline{p}$ the following approximation holds

$$\mathbf{G} \equiv \frac{\partial \xi_F(p)}{\partial p} \simeq \frac{1}{\overline{p}} \xi_F(\overline{p})$$

which allows an experimental estimate of $\mathbf{G}$. On the surface and near $\xi = 0$, we can describe the dynamics with the linear map

$$\xi_{n+1} - \xi_F(p) \simeq \mathbf{M} \cdot [\xi_n - \xi_F(p)]$$

where $\mathbf{M}$ is a 2×2 matrix. Using $\xi_F(p) \simeq p\mathbf{G}$, the above equation reads

$$\xi_{n+1} \simeq p_n \mathbf{G} + [\lambda_u \mathbf{e}_u \mathbf{f}_u + \lambda_s \mathbf{e}_s \mathbf{f}_s] \cdot [\xi_n - p_n \mathbf{G}] \quad (2)$$

where $\mathbf{f}_s$ and $\mathbf{f}_u$ are controvariant basis vectors defined by $\mathbf{f}_s \cdot \mathbf{e}_s = \mathbf{f}_u \cdot \mathbf{e}_u \equiv 1$, $\mathbf{f}_s \cdot \mathbf{e}_u = \mathbf{f}_u \cdot \mathbf{e}_s \equiv 0$. Let us assume ξ_n be located within a neighborhood of the desired fixed point. The control method consists in selecting p_n so as ξ_{n+1} be put onto the stable manifold of $\xi = 0$, which implies to select p_n so that $\mathbf{f}_u \cdot \xi_{n+1} = 0$. When ξ_{n+1} falls on the stable manifold of the desired fixed point, the parameter can be set again to $p = 0$, because, by subsequent natural evolution, the dynamics will approach the desired fixed point at a geometrical rate λ_s.

Dotting (2) with $\mathbf{f}_u$, we obtain

$$p_n = \frac{\lambda_u}{\lambda_u - 1} \frac{\mathbf{f}_u \cdot \xi_n}{\mathbf{f}_u \cdot \mathbf{G}}$$

which can be used provided the magnitude of the right-hand side be smaller than p_*. In the opposite case, p_n is set to 0. As a consequence, the perturbation is activated only when ξ_n is located within a narrow strip $|\xi_n^u| < \xi_*$, $\xi_n^u = \mathbf{f}_u \cdot \xi_n$ and $\xi_* = p_* |(1 - \lambda_u^{-1}) \mathbf{G} \cdot \mathbf{f}_u|$.

This way, a stable periodic orbit is obtained out of the chaotic evolution of the dynamics. As we mentioned, the control of chaos gives flexibility. By turning the small controlling perturbations off, one can switch the time asymptotic behavior from one periodic orbit to another. In some situations, where flexibility offered by the ability to do such switching is desirable, it may be advantageous to design the system so that it is chaotic. In other situations, where one is presented with a chaotic system, the method may allow one to eliminate chaos and achieve great improved behavior at relatively low cost. The OGY ideas can also be applied to stabilize a desired chaotic trajectory, which has potential applications to problems such as synchronization of chaotic systems [Lai & Grebogi, 1993], conversion of transient chaos into sustained chaos [Lai & Grebogi, 1994], communication with chaos [Hayes *et al.*, 1993, 1994; Rosa *et al.*, 1997; Bollt *et al.*, 1997], and selection of a desired phase [Nagai & Lai, 1995].

3. The Pyragas' Method

An alternative time-continuous method [Pyragas, 1992] considers a dynamical system ruled by a set of unknown ordinary differential equations, and having some scalar variable accessible for measurements. Furthermore, the system possesses at least one input accessible for external forcing. The above assumptions are met by the following model

$$\frac{dy}{dt} = P(y, \mathbf{x}) + F(t); \quad \frac{d\mathbf{x}}{dt} = \mathbf{Q}(y, \mathbf{x}) \quad (3)$$

where y represents the output scalar variable, $\mathbf{x}$ the remaining hidden variables of the dynamical system, $F(t)$ is an input signal which disturbs the dynamical evolution of the variable y, and P and $\mathbf{Q}$ are two nonlinear functions.

Let us imagine that system (3) produces chaotic dynamics for $F = 0$. In general, a large number of the UPO's within a chaotic attractor can be obtained from a single scalar variable through the standard method of delay coordinates. Therefore, one can extract from the measured variable y various periodic signals of the form $y = y_i(t)$, $y_i(t + T_i) = y_i(t)$, where T_i represents the period of the ith unstable periodic orbit.

To achieve stabilization of the selected UPO, let us design an external feedback line which reinjects into the system the difference $D(t)$ between

the signals $y(t)$ and $y(t-\tau)$ as a control signal:

$$F(t) = K[y(t-\tau) - y(t)] \tag{4}$$

where the weight K has to provide a negative feedback ($K < 0$) and τ represents a time delay. Stabilization of the ith UPO is achieved when τ equals the period T_i.

The method can be extended by adding information on previous periods, that is, replacing (4) with [Bleich & Socolar, 1996]

$$F(t) = K\left(y(t) - (1-R)\sum_{k=1}^{\infty} R^{k-1} y(t-k\tau)\right), \tag{5}$$

with $0 < R < 1$ a suitable real parameter, and k integer.

Notice that use of the perturbations (4) or (5) transforms the Ordinary Differential Equation (3) to a Delay Differential Equation. This requires some warning. As a delayed dynamical system is richer than an instantaneous one, care should be put in stabilizing a true UPO of the original unperturbed system, rather than a spurious UPO introduced artificially by the delay.

4. The Washout Filter

Control of chaos can be achieved by negative feedback of suitable spectral components of a system variable [Meucci *et al.*, 1996; Tesi *et al.*, 1996; Basso *et al.*, 1997; Ciofini *et al.*, 1997]. The set up consists in a feedback loop wherein all unwanted frequencies present in the chaotic spectrum are transmitted as correction signals by means of a selective filter ("washout filter"). In this way, the system is allowed to oscillate at the only frequency which is not fed back, namely, that of the unstable orbit to be stabilized. This control scheme is very easy to be implemented, besides having the relevant advantage of being robust and fast.

Consider a dynamical system modeled by ordinary differential equations in the form

$$\begin{aligned} \dot{x}_1 &= F(x_1, x_2) \\ \dot{x}_2 &= G(x_1, x_2), \end{aligned} \tag{6}$$

F and G being a linear and a nonlinear function, respectively. The forthcoming considerations still hold in case the system is nonautonomous. Considering a stationary periodic regime where each variable can be approximated by $x_k \sim e^{st}$ ($s = i\omega$), let us introduce in the first equation a suitable negative feedback loop for x_1 through a "washout filter", characterized by a certain transfer function $C(s)$:

$$sx_1 = F(x_1, x_2) - x_1 C(s).$$

The above equation can be also rewritten as

$$x_1 = \frac{F(x_1, x_2)}{s + C(s)}.$$

In order to stabilize a given orbit with pulsation Ω introducing a minimal perturbation, $C(s)$ should vanish for $\omega = 0$ and $\omega = \Omega$ (which implies that the feedback does not alter the fixed point and the limit cycle solutions of the unperturbed system). Moreover, depending on the route to chaos, it is useful to choose $C(s)$ so that it presents a maximum in correspondence to the frequency characteristic of the transition to chaos. Whenever the above conditions are fulfilled, the only frequency component which is not affected by the feedback is that of the cycle to be stabilized, while all the other components are sent back as a correction signal.

For example, in the case of the subharmonic route to chaos, the filter structure for stabilizing the period-1 (fundamental frequency $\tilde{f} = \Omega/2\pi$) orbit can be modeled as

$$C(s) = \beta \frac{s(s^2 + \Omega^2)}{\left(s^2 + \xi\Omega s + \dfrac{\Omega^2}{4}\right)(s + \mu\Omega)}$$

where $\xi = 0.4$, $\mu = 1.5$ and β is the gain factor. The amplitude and phase responses of the above transfer function are shown in Fig. 1 for $\tilde{f} = 110$ kHz; the maximum of $C(s)$ is set approximately at $\Omega/2$.

We add some remarks on the applications to real experimental conditions.

(i) This control scheme can be in principle very fast; indeed, the feedback loop can be entirely realized by analog electronics.

(ii) The control is also very robust since it is independent of parameter fluctuations.

(iii) Regarding the possibility of stabilizing more complex orbits (i.e. a period-2 orbit or a torus), one has just to design a different filter $C(s)$, with several zeroes corresponding to all the frequency components of the cycle to be stabilized.

(iv) The basic structure of Eqs. (6) (called Lur'e form) is peculiar of dynamical systems widely studied in the literature, such as the Chua circuit, the Rössler model and the Duffing oscillator [Genesio *et al.*, 1993].

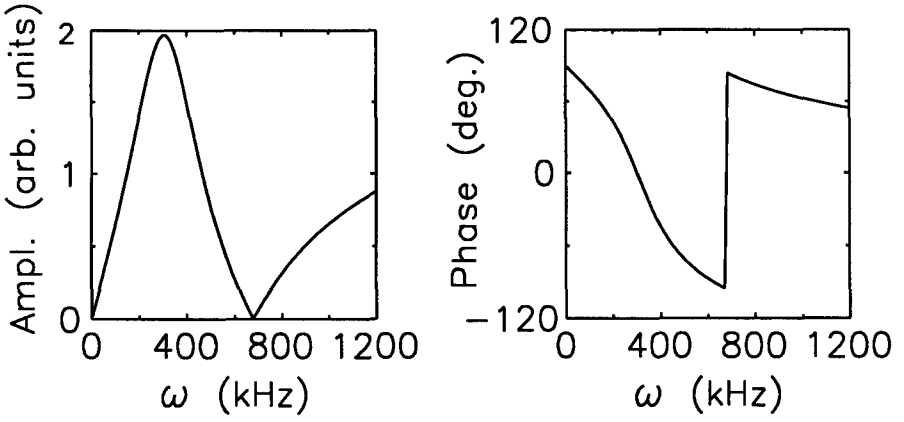

Fig. 1. Amplitude and phase response curves of the washout filter as a function of ω.

As a final consideration, we observe that this method presents several similarities with the time-delayed autosynchronization method [Pyragas, 1992; Basso *et al.*, 1997], despite the conceptual difference between these two techniques. In the frequency domain, the Pyragas' method can be seen as a negative feedback loop with a high-pass filter whose amplitude response goes to zero at the fundamental frequency Ω and for all its multiples $n\Omega$. In this way, the stabilized limit cycle is exactly the same as that of the unperturbed system since it contains all the harmonics, while the perturbation vanishes.

5. The Adaptive Algorithm

Let us consider a dissipative dynamics ruled by Eq. (1). The adaptive control technique consists in two successive steps, the first one, in which the unperturbed features of the dynamics are extracted [Arecchi *et al.*, 1994] and the periods of the UPO's are measured, and the second one whereby adaptive perturbations are applied in order to stabilize the selected UPO [Boccaletti & Arecchi, 1995, 1996].

We consider an observer "blind" to the main coordinate position x_i $(i = 1, \ldots, D)$ and interested only in its variation

$$\delta x_i(t_{n+1}) = x_i(t_{n+1}) - x_i(t_n)\,, \tag{7}$$

where $t_{n+1} - t_n = \tau_n$ is the nth adjustable interval, to be specified. In order to assign τ_{n+1} we consider the local variation rate

$$\lambda_i(t_{n+1}) = \frac{1}{\tau_n} \ln \left| \frac{\delta x_i(t_{n+1})}{\delta x_i(t_n)} \right| . \tag{8}$$

Here τ_{n+1} is the minimum of all $\tau_{n+1}^{(i)}$ corresponding to the different i, and defined by the rule

$$\tau_{n+1}^{(i)} = \tau_n^{(i)}(1 - \tanh(\sigma\lambda_i(t_{n+1})))\,. \tag{9}$$

Equation (9) arises from the following considerations. To obtain a sequence of geometrically regular δx_i, we shrink (stretch) the time intervals whenever the actual value of δx_i is larger (smaller) than the previously observed one. The hyperbolic tangent function maps the whole range of $\sigma\lambda_i$ into the interval $(-1, +1)$. The constant σ, strictly positive, is chosen in such a way as to forbid $\tau_n^{(i)}$ from going to zero. It may be taken as an *a priori* sensitivity, however, a more sensible assignment would consist in fixing σ by a moving average procedure, looking at the unbiased dynamical evolution for a while and then taking a σ value smaller than the reciprocal of the maximal λ recorded in that time span. Notice that a moving sensitivity is mandatory whenever the adaptive recognition is specialized to the measurement of a periodic orbit [Arecchi *et al.*, 1994].

We thus obtain a sequence of observation times starting from t_0

$$t_0, t_1 = t_0 + \tilde{\tau}\,,\ t_2 = t_1 + \tau_1, \ldots,\ t_{n+1} = t_n + \tau_n, \ldots \tag{10}$$

corresponding to which the variations of $\delta x_i(t_n)$ can be reduced below a preassigned value.

The observations performed at these times provide a "regularized" window, and the time sequence (10) now includes the chaotic information which was in the original geometric sequence $\mathbf{x}(t)$. The sequence (10) contains the relevant information on the dynamics, and we can characterize chaos as

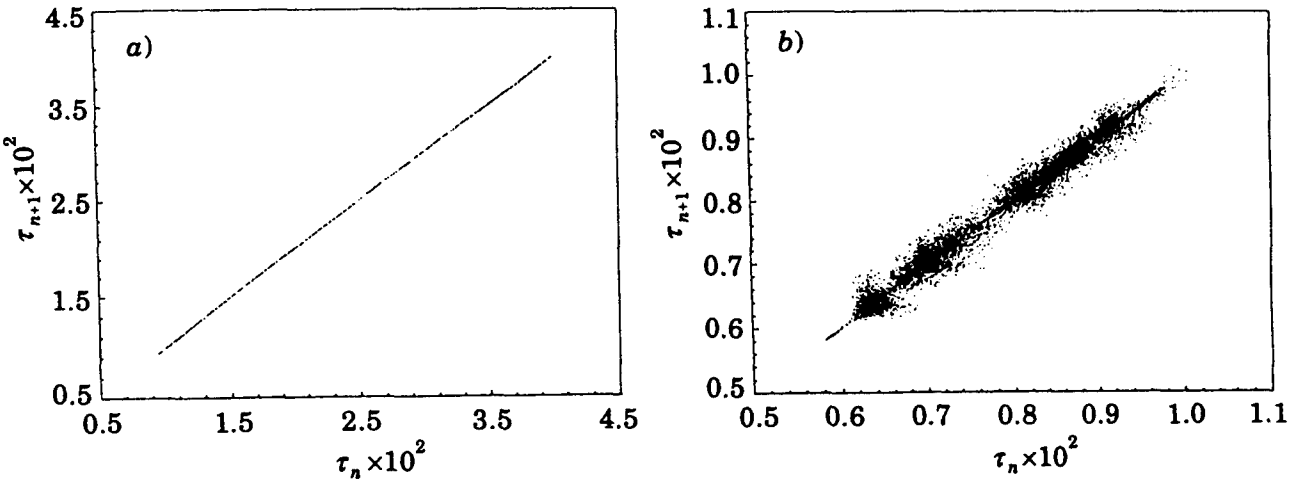

Fig. 2. Return maps τ_{n+1} versus τ_n for (a) Ro4 and (b) Ro4 with an additional 1% white noise. Initial conditions: $x(0) = -20$, $y(0) = z(0) = 0$, $w(0) = 15$. $g = 0.000048$.

follows. Since in Eq. (9) $|\sigma\lambda_i| \ll 1$, then two successive τ_n must be strongly correlated. As a result, even though the set of τ_n may be spread over a rather wide support, the return map τ_{n+1} versus τ_n must cluster along the diagonal. The residual deviations, averaged over many successive n's, provide the decorrelation trend, and hence yield an accurate assignment of the maximum Liapunov exponent. However, presence of large deviations from the diagonal denotes an uncorrelated perturbation. This may be some additive noise, which eventually can be filtered out, thus extracting the deterministic dynamics [Boccaletti *et al.*, 1997c].

In the following we will summarize the application of such a method to the Roessler four-dimensional (Ro4) model [Roessler, 1979] for a vector state $\mathbf{x} \equiv (x_1, x_2, x_3, x_4)$. For particular initial conditions ($x_1(0) = -20$, $x_2(0) = x_3(0) = 0$, $x_4(0) = 15$) and control parameters, Ro4 undergoes a hyperchaotic dynamics with two positive Liapunov exponents.

Figure 2 reports the return map of the τ_n for Ro4 and for Ro4 with 1% noise.

Since we are interested in stabilizing periodic dynamics, we need to extract the periods of UPO's embedded within the CA. For this purpose, instead of considering the single step map, we construct the maps τ_{n+k} versus τ_n, $k = 1, 2, \ldots$ and we plot the r.m.s. $\eta(k)$ of the point distribution around the diagonal of such maps as functions of the step interval k. For chaotic dynamics, temporal selfcorrelation lasts only for a finite time, hence one should expect to obtain a monotonically increasing function $\eta(k)$. In fact, the chaotic dynamics steers the phase-space trajectory toward neighborhoods of different UPO's. As the trajectory gets close to an UPO of period T_j, temporal selfcorrelation is rebuilt after T_j and the distribution of τ includes windows of correlated values appearing as minima of η versus k around $k_j = T_j/\langle\tau\rangle$, $\langle\tau\rangle$ being the average of the τ distribution.

To give an exemple, we report in Fig. 3 the η-k plot for Ro4, from which one can extract the different UPO's periods looking to the minima of the η curve. In fact, during the observation, the

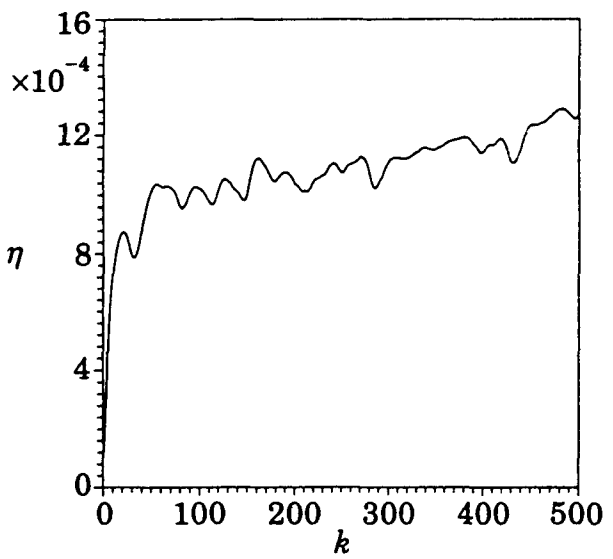

Fig. 3. η-k plot for Ro4 attractor. Initial conditions and control parameters as in the text. The recognition task has been performed with $g = 0.01$. Vertical axis has to be multiplied for 10^{-4}.

time intervals are changing, and a more rigorous determination of the period is provided by minimizing a suitable cost function in the vicinity of each minimum of the η curve [Boccaletti & Arecchi, 1995].

Once the periods T_j ($j = 1, 2, \ldots$) of the UPO's have been measured, stabilization of each one can be achieved when the system naturally visits closely phase space neighborhoods of that UPO. For a nonauthonomous system, a period T may correspond to many degenerate UPO's. In this case, selection of the desired one can be achieved by the study of the topology of all UPO's corresponding to the same period and by switching-on the control task when the system is shadowing the selected UPO. Several topological approaches to the UPO's detection have been developed [Cvitanovic *et al.*, 1988; Gunaratne *et al.*, 1989; Mindlin *et al.*, 1990; Tufillaro *et al.*, 1990].

The control procedure is done by use of the following modified algorithm. At each new observation time $t_{n+1} = t_n + \tau_n$ and for each component i of the dynamics, instead of Eq. (7), we evaluate the differences between actual and desired values

$$\delta x_i(t_{n+1}) = x_i(t_{n+1}) - x_i(t_{n+1} - T_j)\,, \qquad (11)$$

and the local variation rates λ's now read

$$\lambda_i(t_{n+1}) = \frac{1}{\tau_n} \log \left| \frac{x_i(t_{n+1}) - x_i(t_{n+1} - T_j)}{x_i(t_n) - x_i(t_n - T_j)} \right| . \qquad (12)$$

We keep Eq. (9) and the choice of the minimum for the updating process of τ's. Defining $\mathbf{U}(t)$ as the vector with ith component (constant over each observation time interval) given by

$$U_i(t_{n+1}) = \frac{1}{\tau_{n+1}} (x_i(t_{n+1} - T_j) - x_i(t_{n+1}))\,, \qquad (13)$$

we add such a vector to the evolution equation, which then becomes

$$\frac{d\mathbf{x}}{dt} = \mathbf{F}(x, p) + \mathbf{U}(t)\,. \qquad (14)$$

Notice that the λ's given by Eq. (12) track the rate of separation of the actual trajectory from the desired one. Indeed, λ negative means that locally the true orbit is collapsing into the desired one and hence the actual dynamics is shadowing the desired UPO, while λ positive implies that the actual trajectory is locally diverging away from the desired one and control has to be performed in order to constrain the orbit to shadow the desired UPO.

As a consequence, contraction or expansion of τ's now reflects the need to perturb the dynamics more or less robustly in order to stabilize the desired UPO. This appears as a weight to the correction of Eq. (13), which, once a given T_j has been chosen by the operator, is selected by the same adaptive dynamics.

Once again, the introduced adaptive weighting procedure in Eq. (13) assures the effectiveness of the

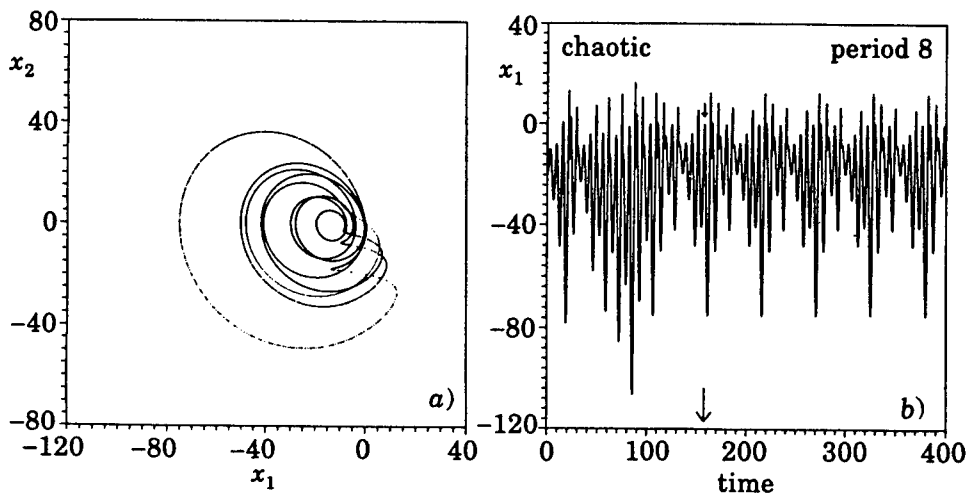

Fig. 4. (a) (x_1, x_2) projection of the phase space portrait for the controlled period-8 of Ro4 attractor. Control task has been performed with period-8 extracted from Fig. 3 and $g = 10^{-5}$. (b) Time evolution of the first component x_1 of Ro4 before and after control. Arrows indicate the instant at which control task begins.

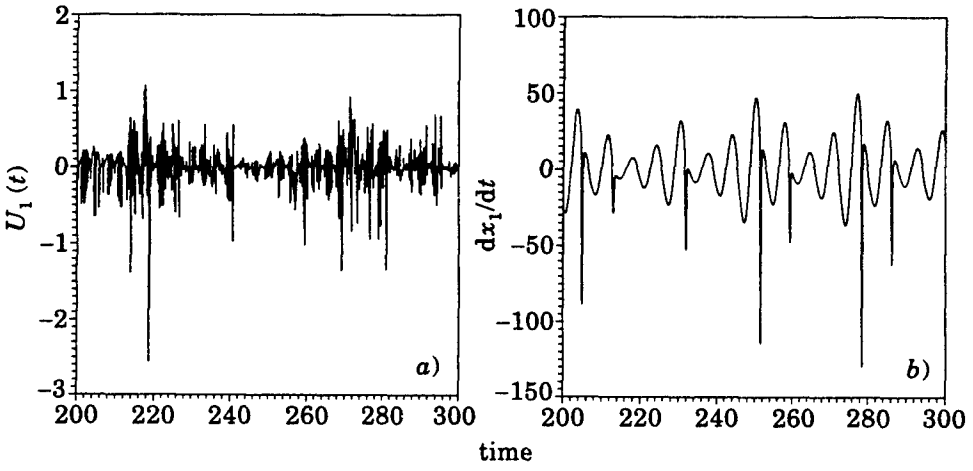

Fig. 5. (a) Temporal evolution of the first component of the additive controlling term U_1 during the control of period-8 of Ro4 and (b) temporal evolution of the uncontrolled dx_1/dt. The adaptive correction term is between two and three orders of magnitude smaller than the natural evolution of the dynamics. Same stipulation for controlling task as mentioned in the caption of Fig. 4.

method (perturbation is larger or smaller whenever it has to be) as well as the fact that the additive term **U** is much smaller than the unperturbed dynamics **F**.

In Fig. 4 we show the control of period-8 of Ro4.

Figure 5 reports the perturbation $U_1(t)$ and the unperturbed dynamics G_1 for the Ro4 model during the control task of period-8, in order to show that the former is between two and three orders of magnitude smaller than the latter as expected by the above discussion.

Notice that the limit $\sigma = 0$ of the above algorithm recovers [Pyragas, 1992]. Choosing $\sigma \neq 0$ implies an adaptive nature of the forcing term [Eq. (13)] which is inversely proportional to the time intervals and hence is weighted by the information extracted from the dynamics itself.

Applications of this method have been already reported in the introductory section.

6. Review of Some Control Experiments

The OGY method described in Sec. 2 has found applications in several experimental situations. As an example, we herewith report the first experimental realization of chaos control which was done in 1990 by Ditto *et al.* [1990].

In this case, the theoretical background of Sec. 2 has been applied to an experimental system consisting of a gravitationally buckled, amorphous magnetoelastic ribbon. The ribbon exhibits large reversible changes of its Young's modulus when small magnetic fields are applied. It is clamped at the base, yielding a free vertical length greater than the Euler buckling length, thus providing an initial buckling configuration. The ribbon is placed within three mutually orthogonal pairs of Helmoltz coils, allowing to compensate for the Earth's magnetic field. Finally, a uniform vertical magnetic field is applied along the ribbon. In this configuration, the Young's modulus of the ribbon is varied due to the applied vertical magnetic field which has the form $H = H_{\rm dc} + H_{\rm ac}\cos(2\pi f t)$. Both amplitudes have been set typically in the range 0.1–2.5 Oe. A measurement of the curvature of the ribbon near the base is provided by a sensor.

The experimental data consist in time series voltages $V(t)$ acquired from the output of the sensor and sampled at the drive period of the ac magnetic field (i.e. at times $t_n = n/f$). The sampled voltages are considered as iterates of the map $X_n = V(t_n)$ and the control theory in Sec. 2 is applied, taking as control parameter the amplitude of the continuous component of the magnetic field $H_{\rm dc}$. Selecting $H_{\rm ac}$, $H_{\rm dc}$ and f so as to produce chaotic dynamics, control of period-1 UPO is achieved for over 200 000 iterates (approximately 64 hours) with maximum perturbation of about 1% of the unperturbed control parameter. With the same setup, control of one of the period-2 UPO is also achieved.

A modification of the OGY method, called occasional proportional feedback (OPF) has been used to stabilize unstable orbits in a chemical system

[Peng *et al.*, 1991, Petrov *et al.*, 1993] and in a diode resonator [Hunt, 1991]. This technique consists in feeding back deviations of the chaotic variable within a specified window from a reference point to perturb a control parameter. The chemical experiment deals with the Belousov–Zhabotinsky reaction carried out in a continuous-flow stirred-tank reactor. The flow rate μ of the reactants into the tank ultimately determines whether the system shows steady state, periodic and chaotic behaviors. The control algorithm takes advantage of the predictable evolution of the chaotic system in the vicinity of a fixed point in the next-amplitude return map of a suitable variable A (dimensionless concentration). The position of the period-1 fixed point is given by the intersection of the map with the bisectrix, where $A_{n+1} = A_n = A_s$. The map can be shifted to target the fixed point by applying a perturbation to the bifurcation parameter μ according to the difference between the system state and the fixed point

$$\Delta\mu = \frac{A_n - A_s}{g}$$

where g is a suitable constant. In an analogous manner (changing A_s and g) period-2 and period-4 unstable orbits have been stabilized.

The electronic experiment consists of a p-n junction rectifier in series with an inductor. The system exhibits the period-doubling route to chaos when driven with an increasing sinusoidal voltage. The current through the diode provides a convenient chaotic variable; if the peak current I_n falls within a given window, the driving voltage is amplitude modulated with a signal proportional to the difference between I_n and the center of the window. By changing the level and the width of the window, or the gain of the feedback signal, several unstable orbits are stabilized, up to the period-23.

The OPF has been also applied by Roy *et al.* [1992] to an autonomously chaotic multimode laser, that is, a high dimensional system for which the chaotic attractor is not characterized by a low-dimensional map. The experimental setup consists of a diode-laser-pumped solid state Nd-doped yttrium aluminum garnet (Nd:YAG) laser containing a KTP doubling crystal. The source of chaotic behavior in this laser is the coupling of the longitudinal modes through the nonlinear process of sum-frequency generation. This process destabilizes the relaxation oscillations which are normally damped in a system without the intracavity KTP crystal. The total laser output intensity is sampled within a window of selected offset and width, and a signal proportional to the deviation from the center of the window is applied to perturb the injection current of the pumping laser diodes. With this configuration period-1, -4 and -9 limit cycles have been successfully stabilized with relative perturbation amplitude less than 10%.

The control scheme proposed by Pyragas (discussed in Sec. 3) has been first experimentally demonstrated in an electronic circuit [Gauthier *et al.*, 1994] and in a modulated laser [Bielawski *et al.*, 1994]. In the first experiment, the setup is similar to that reported by Hunt, the only difference being that the resonator has been modified to operate at higher frequency (10 MHz). The control is derived by directing half of the voltage signal (proportional to the resonator current) directly into one input of a summing amplifier, while the other half, delayed and inverted, is sent to the second input. The delay line consists of a cable with length precisely adjusted so that it provides a delay τ corresponding to the period of the desired UPO. The control signal is reinjected into the resonator as an additive perturbation of the driving voltage. In this way, a close reproduction of the control Eq. (4) is achieved, allowing stabilization and tracking of period-1, -2 and -4 unstable limit cycles.

The second experiment deals with a CO_2 laser with cavity loss modulation, obtained by driving an intracavity electro-optic crystal with an external sinusoidal voltage. In this case, the chaotic variable is the infrared (10 μm) laser light, monitored by a fast photovoltaic detector. The detector voltage is used to modulate a laser diode emitting at 845 nm so that a time delayed voltage can be obtained by propagating the laser diode light in a long fiber and detecting it at the end. Finally, the difference between the CO_2 laser intensity and its delayed version is added to the modulation signal after suitable amplification. With such a configuration the unstable period-1 orbit is stabilized and tracked along a wide range in the bifurcation diagram.

The experimental implementation of the control scheme based on the washout filter has been tested in the chaotic regimes of both a nonautonomous system [Meucci *et al.*, 1996; Ciofini *et al.*, 1997] (a CO_2 laser with externally modulated losses) and of an autonomous system [Meucci *et al.*, 1997] (a CO_2 laser with intensity feedback), obtaining stabilization and tracking of different unstable periodic orbits, with perturbation amplitudes of the order of few percent.

The experimental setup consists of a single mode CO_2 laser with an intracavity electro-optic crystal which can be driven by an external voltage $V(t)$ to modulate the cavity losses k. In the nonautonomous case, the driving voltage $V(t)$ is a sinusoidal signal, so that the cavity loss parameter k becomes: $k = k_0[1+m\sin(2\pi ft)]$, where $f = 110$ kHz is the modulation frequency and the modulation depth m, proportional to the amplitude of $V(t)$, is the control parameter. By increasing m the system undergoes the transition to chaos through a sequence of subharmonic bifurcations. The period-1 orbit is stable up to $m = 0.1$, and a further increase of m drives the system to period-2 and period-4 orbits, followed by the first chaotic region and, finally, by a period-3 stable solution. The control was implemented with a negative feedback loop where the laser intensity, revealed by a fast detector, is first filtered and then subtracted from $V(t)$. The characteristic curves in Fig. 1 have been closely reproduced by a two-stage passive filter (a band-pass stage combined with a Notch stage) entirely realized by analog circuitry (Fig. 6).

Figure 7 reports the experiment. Figure 7(a) is the chaotic laser oscillations ($m = 0.18$) observed

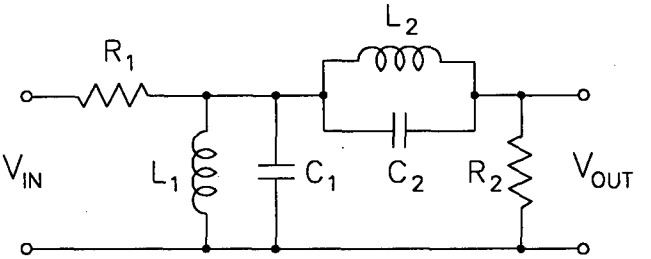

Fig. 6. Electronic scheme of the washout filter: $R_1 = 1$ kΩ, $L_1 = 6.5$ mH, $C_1 = 0.1$ nF, $R_2 = 6.7$ kΩ, $L_2 = 12.4$ mH and $C_2 = 0.2$ nF.

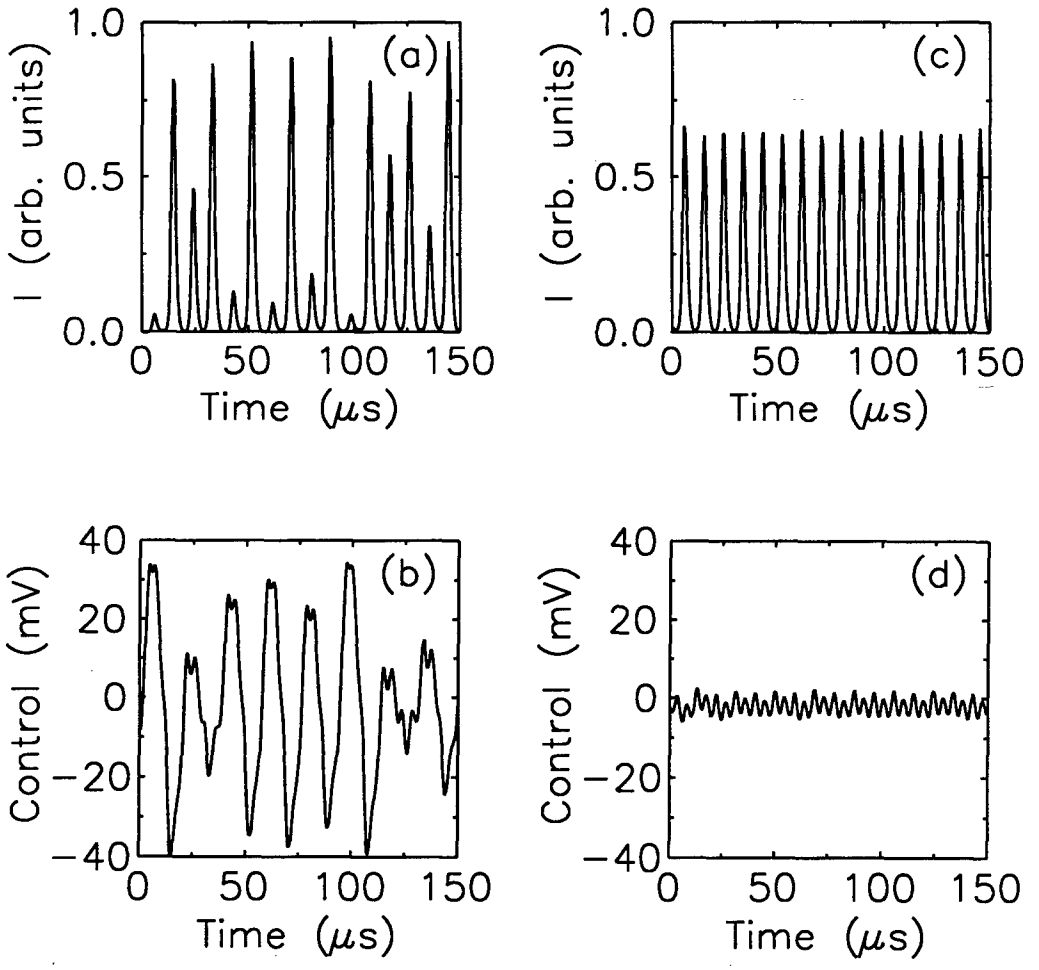

Fig. 7. Experimental results: (a) chaotic laser intensity without control and (b) corresponding control signal; (c) and (d) represent the same signals as (a) and (b), respectively, but in the case of activated control.

with open control loop, while Fig. 7(b) is the corresponding control signal. The same signals are reported in Figs. 7(c) and 7(d), respectively, but in the case of a closed control loop. The control signal amplitude of Fig. 7(b) provides a 1.25% perturbation of the driving signal. This result confirms that the method allows stabilization of unstable orbits slightly different from those embedded in the unperturbed system.

Following the above criteria, a second filter has been prepared allowing stabilization of the period-2 limit cycle, and both filters have been used to track the corresponding trajectory along the whole bifurcation diagram. The unperturbed bifurcation diagram has been measured by increasing the control parameter m at fixed steps, and processing the laser intensity in order to extract the maxima (Fig. 8). The same measurements have been repeated after the insertion of the feedback loops with the two filters. Figures 8(a) and 8(b) show the superposition of the unperturbed bifurcation diagram (dots) with the tracked period-1 and period-2 orbits (circles), respectively. In both cases the tracking has been achieved without any readjustment of the gain of the feedback loop over the whole explored range, and with relative perturbation amplitudes less than 3%.

In a different experiment, the control has been tested on a CO_2 laser made chaotic by an intensity feedback. In this case the system is autonomous, since the modulator voltage $V(t)$ carries information on the output intensity. Indeed it is obtained by detecting the laser output and then amplifying such a signal. The equation for $V(t)$ is

$$\dot{V} = -\beta\left(V - B + \frac{RI}{1+\alpha I}\right)$$

where β is the damping rate of the feedback loop, I is the laser intensity, B a bias voltage acting as the control parameter and R the total gain of the loop (the term αI represents the saturation of the detection apparatus).

Starting from constant laser output and increasing B, the system passes to a limit cycle through a Hopf bifurcation, and then it reaches the chaotic region after a subharmonic cascade. The spectral analysis of the chaotic signal for $B = 360$ V shows the presence of a peak at $\tilde{f} = 22$ kHz, remnant of the Hopf bifurcation. This property suggests to prepare a suitable washout filter with zero amplitude in correspondence of $\tilde{f}$. Figure 9 shows

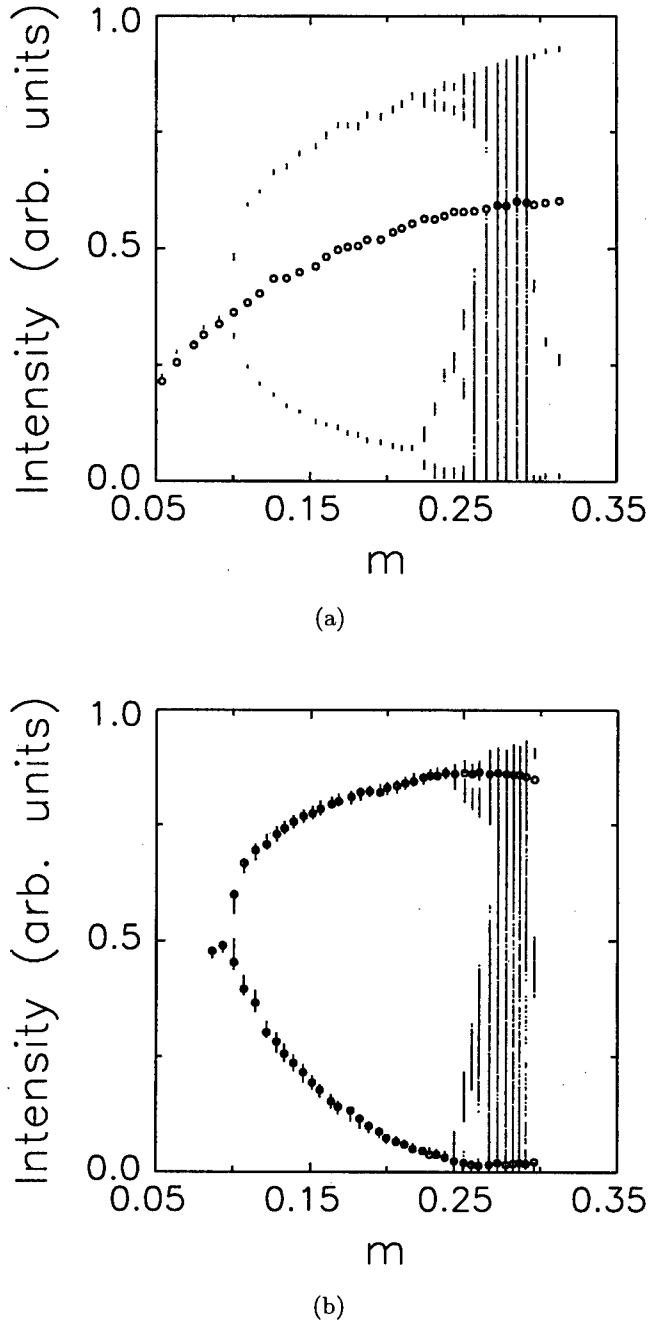

Fig. 8. Experimental results of the tracking of (a) period-1 unstable orbit and (b) period-2 unstable orbit. Circles and points: maxima in the laser output signal with and without the control loop, respectively.

the three-dimensional reconstruction of the chaotic attractor and the stabilized period-1 orbit obtained with a relative perturbation of about 7%.

All the experimental results can be adequately reproduced by numerical integration of a CO_2 laser model based on rate equations for the intensity and for the populations of the resonant levels coupled by collisions with the rotational manifolds.

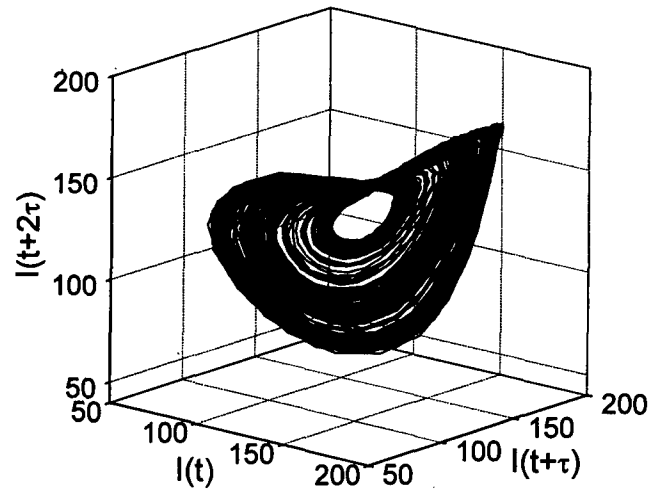

(a)

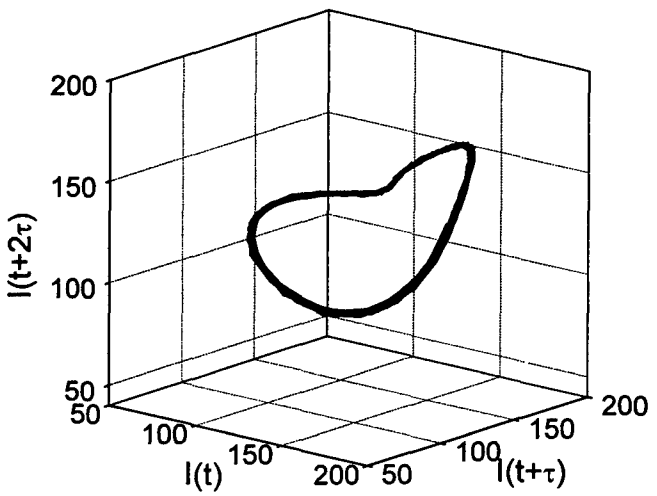

(b)

Fig. 9. (a) Three-dimensional reconstruction of the chaotic attractor and (b) stabilized period-1 orbit.

References

Arecchi, F. T., Basti, G., Boccaletti, S. & Perrone, A. L. [1994] "Adaptive recognition of a chaotic dynamics," *Europhys. Lett.* **26**, 327–332.

Auerbach, D., Cvitanovic, P., Eckmann, J.-P., Gunaratne, G. & Procaccia, I. [1987] "Exploring chaotic motion through periodic orbits," *Phys. Rev. Lett.* **58**, 2387–2390.

Azevedo, A. & Rezende, S. M. [1991] "Controlling chaos in spin-wave instabilities," *Phys. Rev. Lett.* **66**, 1342–1345.

Basso, M., Genesio, R. & Tesi, A. [1997] "Controlling chaos in a CO_2 laser," *Proc. 4th European Control Conference, Bruxelles.*

Bielawski, S., Derozier, D. & Glorieux, P. [1993] "Experimental characterization of unstable periodic orbits by controlling chaos," *Phys. Rev.* **A47**, R2492–2495.

Bielawski, S., Derozier, D. & Glorieux, P. [1994] "Controlling unstable periodic orbits by a delayed continuous feedback," *Phys. Rev.* **E49**, R971–974.

Bleich, M. E. & Socolar, J. E. S. [1996] "Stability of periodic orbits controlled by time-delay feedback," *Phys. Lett.* **A210**, 87–94.

Boccaletti, S. & Arecchi, F. T. [1995] "Adaptive control of chaos," *Europhys. Lett.* **31**, 127–132.

Boccaletti, S. & Arecchi, F. T. [1996] "Adaptive recognition and control of chaos," *Physica* **D96**, 9–16.

Boccaletti, S., Farini, A. & Arecchi, F. T. [1997a] "Adaptive synchronization of chaos for secure communication," *Phys. Rev.* **E55**, 4979–4982.

Boccaletti, S., Farini, A., Kostelich, E. J. & Arecchi, F. T. [1997b] "Adaptive targeting of chaos," *Phys. Rev.* **E55**, R4845–4848.

Boccaletti, S., Giaquinta, A. & Arecchi, F. T. [1997c] "Adaptive recognition and filtering of noise using wavelets," *Phys. Rev.* **E55**, 5393–5400.

Boccaletti, S., Maza, D., Mancini, H., Genesio, R. & Arecchi, F. T. [1997d] "Control of defects and spacelike structures in delayed dynamical systems," *Phys. Rev. Lett.* **79**, 5246–5249.

Bollt, E., Lai, Y. C. & Grebogi, C. [1997] "Coding, channel capacity and noise resistance in communication with chaos," *Phys. Rev. Lett.* **79**, 3787–3790.

Braiman, Y. & Goldhirsch, I. [1991] "Taming chaotic dynamics with weak periodic perturbations," *Phys. Rev. Lett.* **66**, 2545–2548.

Chin, G., Senesac, L. R., Blass, W. E. & Hillman, J. J. [1996] "Stabilizing lead-salt diode lasers: Understanding and controlling chaotic frequency emission," *Science* **274**, 1498–1501.

Ciofini, M., Labate, A. & Meucci, R. [1997] "Tracking unstable periodic orbits in a modulated laser," *Phys. Lett.* **A227**, 31–36.

Cvitanovic, P., Gunaratne, G. H. & Procaccia, I. [1988] "Topological and metric properties of Hénon-type strange attractors," *Phys. Rev.* **A38**, 1503–1520.

Ditto, W. L., Rauseo, S. N. & Spano, M. L. [1990] "Experimental control of chaos," *Phys. Rev. Lett.* **65**, 3211–3214.

Fahy, S. & Hamann, R. D. [1992] "Transition from chaotic to nonchaotic behavior in randomly driven systems," *Phys. Rev. Lett.* **69**, 761–764.

Gauthier, D. J., Sukow, D. W., Concannon, H. M. & Socolar, J. E. S. [1994] "Stabilizing unstable periodic orbits in a fast diode resonator using continuous time-delay autosynchronization," *Phys. Rev.* **E50**, 2343–2346.

Genesio, R., Tesi, A. & Villoresi, F. [1993] "A frequency approach for analyzing and controlling chaos in nonlinear circuits," *IEEE Trans. Circuits Syst. I: Fundamental Theor. Appl.* **40**, 819–828.

Gunaratne, G. H., Linsay, P. S. & Vinson, M. J. [1989] "Chaos beyond onset: A comparison of theory and experiment," *Phys. Rev. Lett.* **63**, 1–4.

Hayes, S., Grebogi, C. & Ott, E. [1993] "Communication with chaos," *Phys. Rev. Lett.* **70**, 3031–3034.

Hayes, S., Grebogi, C., Ott, E. & Mark, A. [1994] "Experimental control of chaos for communication," *Phys. Rev. Lett.* **73**, 1781–1784.

Hunt, E. R. [1991] "Stabilizing high-period orbits in a chaotic system: The diode resonator," *Phys. Rev. Lett.* **67**, 1953–1956.

Lai, Y. C. & Grebogi, C. [1993] "Synchronization of chaotic trajectories using control," *Phys. Rev.* **E47**, 2357–2360.

Lai, Y. C. & Grebogi, C. [1994] "Converting transient chaos into sustained chaos by feedback control," *Phys. Rev.* **E49**, 1094–1099.

Lima, R. & Pettini, M. [1990] "Suppression of chaos by resonant parametric perturbations," *Phys. Rev.* **A41**, 726–733.

Meucci, R., Gadomski, W., Ciofini, M. & Arecchi, F. T. [1994] "Experimental control of chaos by means of weak parametric perturbations," *Phys. Rev.* **E49**, R2528–2531.

Meucci, R., Ciofini, M. & Abbate, R. [1996] "Suppressing chaos in lasers by negative feedback," *Phys. Rev.* **E53**, R5537–5540.

Meucci, R., Labate, A. & Ciofini, M. [1997] "Controlling chaos by negative feedback of subharmonic components," *Phys. Rev.* **E56**, 2829–2834.

Mindlin, G. B., Hou, X.-J., Solari, H. G., Gilmore, R. & Tufillaro, N. B. [1990] "Classification of strange attractors by integers," *Phys. Rev. Lett.* **64**, 2350–2353.

Nagai, Y. & Lai, Y. C. [1995] "Selection of desirable chaotic phase using small feedback control," *Phys. Rev.* **E51**, 3842–3848.

Ott, E., Grebogi, C. & Yorke, J. A. [1990] "Controlling chaos," *Phys. Rev. Lett.* **64**, 1196–1199.

Peng, B., Petrov, V. & Showalter, K. [1991] "Controlling chemical chaos," *J. Phys. Chem.* **95**, 4957–4959.

Petrov, V., Gaspar, V., Masere, J. & Showalter, K. [1993] "Controlling chaos in the Belousov–Zhabotinsky reaction," *Nature* **361**, 240–242.

Plapp, B. B. & Huebler, A. W. [1990] "Nonlinear resonances and suppression of chaos in the rf-biased Josephson junction," *Phys. Rev. Lett.* **65**, 2302–2305.

Pyragas, K. [1992] "Continuous control of chaos by self-controlling feedback," *Phys. Lett.* **A170**, 421–428.

Roessler, O. E. [1979] "An equation for hyperchaos," *Phys. Lett.* **71A**, 155–157.

Rosa, E., Hayes, S. & Grebogi, C. [1997] "Noise filtering in communication with chaos," *Phys. Rev. Lett.* **78**, 1247–1250.

Roy, R., Murphy Jr., T. W., Maier, T. D., Gills, Z. & Hunt, E. R. [1992] "Dynamical control of a chaotic laser: Experimental stabilization of a globally coupled system," *Phys. Rev. Lett.* **68**, 1259–1262.

Shinbrot, T., Grebogi, C., Ott, E. & Yorke, J. A. [1993] "Using small perturbations to control chaos," *Nature* **363**, 411–417.

Singer, J., Wang, Y.-Z. & Bau, H. H. [1991] "Controlling a chaotic system," *Phys. Rev. Lett.* **66**, 1123–1126.

Tesi, A., Abed, E. H., Genesio, R. & Wang, O. H. [1996] "Harmonic balance analysis of period-doubling bifurcations with implications for control of nonlinear dynamics," *Automatica* **32**, 1255–1271.

Tufillaro, N. B., Solari, H. G. & Gilmore, R. [1990] "Relative rotation rates: Fingerprints for strange attractors," *Phys. Rev.* **A41**, R5717–R5720.

International Journal of Bifurcation and Chaos, Vol. 8, No. 8 (1998) 1657–1669

APPLICATIONS OF CHAOTIC DIGITAL CODE-DIVISION MULTIPLE ACCESS (CDMA) TO CABLE COMMUNICATION SYSTEMS

TAO YANG and LEON O. CHUA
Electronics Research Laboratory and
Department of Electrical Engineering and Computer Sciences,
University of California at Berkeley,
Berkeley, CA 94720, USA

Received December 15, 1997; Revised February 24, 1998

In this paper the technical details of chaotic digital code-division multiple access ($(CD)^2MA$) communication systems used in cable communication systems are presented. The cable communication system may be a pure coaxial RF cable network, a hybrid fiber-coax network, or a pure optical fiber network for high-capacity data link. As an example of its many potential applications in cable communication systems, $(CD)^2MA$ is used to support the upstream digital data communications in cable TV systems occupying the very noisy 5–40 MHz portion of spectrum. Although the $(CD)^2MA$ proposed in this paper is only used to support current Internet services via cable TV networks, it can also be used to support the high-speed data-link provided in the 550–750 MHz band in hybrid fiber-coax networks.

$(CD)^2MA$ is a new communication framework which uses band-limited chaotic carriers instead of linear ones. For the purpose of generality, in this paper the band-limited chaotic carriers are approximated by groups of linear sub-carriers, which distribute within the same bandwidth with a fixed amplitude, random phases and uniformly distributed frequencies. The theoretical result of the performance of $(CD)^2MA$ is given. We also provide the simulation results of the bit-error-rate (BER) performances of a synchronous $(CD)^2MA$ used in cable communication systems. The results show that the $(CD)^2MA$ system has a better performance than the synchronous CDMA system proposed for the same cable communication system. Technical details of $(CD)^2MA$ are also presented for the future design of prototype systems. We present the framework of the whole $(CD)^2MA$ system including carrier synchronization, timing recovery and the details of nonlinear carrier generators.

1. Introduction

Currently, the main networks connecting American homes to the Internet are telephone lines. However, the twisted pair copper telephone wire cannot provide much more bandwidth than 56 to 64 kbps. For this reason, many American families have to install separate telephone lines for their PCs.

Cable television system is a kind of communication system which was originally designed to broadcast television signals via coaxial RF cables rather than through the air [Baer, 1974]. More than 50 years older, the cable television system has covered almost every corner of North America and Europe. Today, cable TV companies have direct access to more than 63 million U.S. homes. Recently, due to the rapid growth of the Internet market, the functions of cable television systems have been changed from sending only analog television signals to sending both analog television signals *and* digital Internet information. In view of this conceptual change of usage of the cable television system, a brand new television set called *WebTV* (shown in Fig. 1) will

Fig. 1. The outline of a WebTV system.

usher in a new era of television [Tomari *et al.*, 1997], where entertainment and information services are combined into single devices. The main advantage of a cable TV network is its ability to transmit high-bandwidth video, voice and data. Furthermore, a cable TV network integrated with digital information sources can also create new Internet services such as interactive TV programs, high-speed on-line services and videophone services.

Being a mature technical and widespread commercial service, it has become very expensive to upgrade the existing cable TV system. For example, by using optical fibers, the bandwidth of a cable TV system can be enlarged by 50%, from 40–550 MHz to 40–750 MHz. In addition, the optical fiber is more reliable than a coaxial cable. However, even for a small city, it would cost $20 million to upgrade its cable system to fiber-optic lines.

A less costly approach is to keep the hardware framework of the cable TV systems unchanged but exploit optimally the channel capacity of existing networks. One of these methods is *synchronous*

code division multiple access (S-CDMA) proposed by Terayon Communication Systems.[1] Terayon's S-CDMA can provide a very robust transmission with a full 10 Mbps per 6 MHz channel upstream and downstream over a fiber-coax cable system. So far, since only a very small portion of the bandwidth, namely 5–40 MHz, can be used to provide two-way, high-speed data links between a subscriber and the Internet, the channel capacity of this portion of spectrum becomes very critical to the service quality for cable subscribers to access the Internet via cable TV networks.

Besides upgrading the cable TV network, a cable modem for converting the data stream to radio frequency should be plugged into a PC. The current price of a cable modem is about \$250 to \$600 [Huffaker, 1995]. Since today's PCs usually include pre-installed modems for accessing the Internet via telephone lines, a user may object to the extra cost of installing the cable modem. To overcome this objection, a cable modem should be cheap enough for the cable TV company to provide each user with a free cable modem at the outset. In designing the application of (CD)²MA to cable TV Internet services, we must always bear this consideration in mind such that all costly and sophisticated devices are concentrated at the fiber node, or at the head-end, to reduce the expense of the overall network.

We have shown in [Yang & Chua, 1997] that an asynchronous (CD)²MA technology can double the channel capacity of an asynchronous CDMA system in a wireless communication environment. In this paper, we propose a synchronous (CD)²MA technology and show that better performance than the S-CDMA can be achieved. Instead of employing a linear carrier, a (CD)²MA system uses a chaotic carrier. Whenever a chaotic carrier is used the nonlinearity of the channel can be exploited to make the carriers more distinguishable from each other by reducing the correlation of the different chaotic carriers generated by the same chaotic generator structure in different transmitters. For linear communication systems, however, any nonlinearity will change the waveforms of the linear carriers such that it is more difficult to recover the modulated information because the current design principle is to maintain the waveform unchanged all along the channel. Although beautiful theoretical analysis can be formulated in view of the simplicity of linearity, the price a linear communication system must pay is to ensure that *all* devices along the channel are operating only in linear regions. This makes the whole communication system expensive because nonlinearity is wasted as useless excess baggage.

The organization of this paper is as follows. In Sec. 2, the layout of today's cable TV system with Internet service is presented. In Sec. 3, The layout of the (CD)²MA system used in upstream and downstream cable TV systems is presented. In Sec. 4, the theoretical model of our proposed (CD)²MA scheme for cable TV systems is given. In Sec. 5, theoretical results on the performance of our (CD)²MA system are presented. In Sec. 6, a comparison between the performance of the S-CDMA system and the (CD)²MA system for the 5–40 MHz band in the same cable TV system is presented. Finally, some concluding remarks are given in Sec. 7.

2. Cable TV Systems

Figure 2(a) shows the outline of a typical current cable communication system, which is not only a two-way analogue TV broadcast system but a two-way information network. However, unlike telephone networks, a cable TV network is very asymmetric, with over 90% capacity used for downstream and the rest for the upstream. The functional change of cable communication systems from one-way to two-way is driven by the rapid growth of the demand for bandwidth on the Internet. The central node of a cable TV system is the *headend.* Signals from different sources, such as satellite and terrestrial broadcast, Internet, as well as local originating programming, are modulated onto radio frequency carriers and combined together for distribution over the cable system. Supertrunks (high-quality microwave, fiber optic, or cable links) connect the head-end to local distribution centers, known as *hubs.* Several trunks may originate from a hub to provide coverage over a large contiguous area. Figure 2(b) shows a single trunk of a typical cable TV system. Trunk amplifiers are installed along the trunk to maintain the signal level and compensate for cable transmission characteristics. The bridge amplifier serves as a high-quality tap, providing connection between the main trunk and multiple high-level branches. The line extender is a type of amplifier that maintains the signal level along the branch.

[1]At the URL: http://www.terayon.com

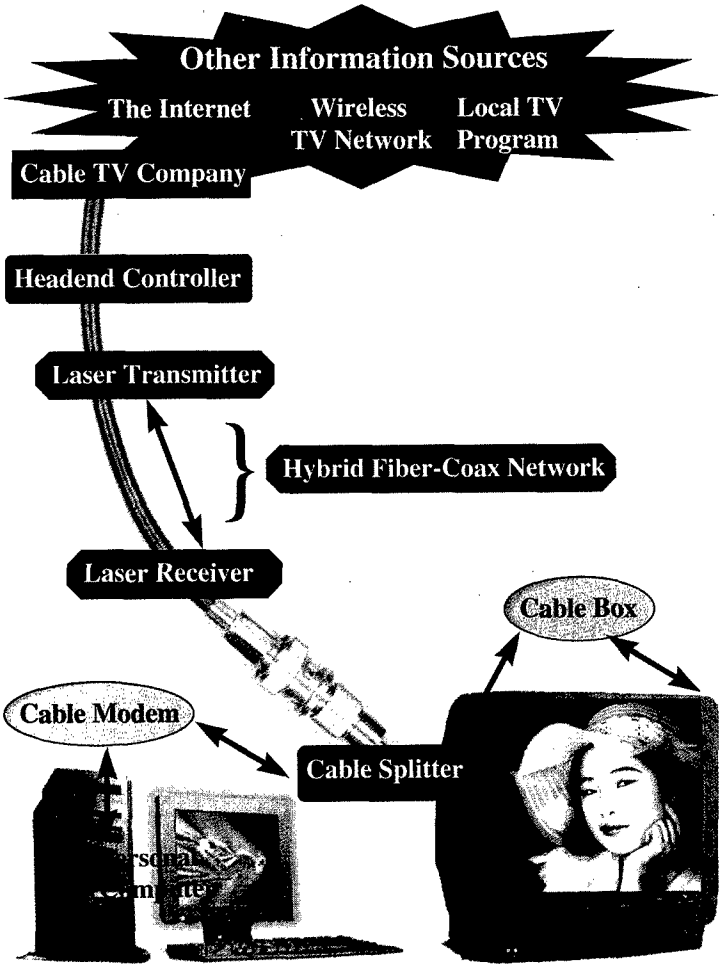

(a)

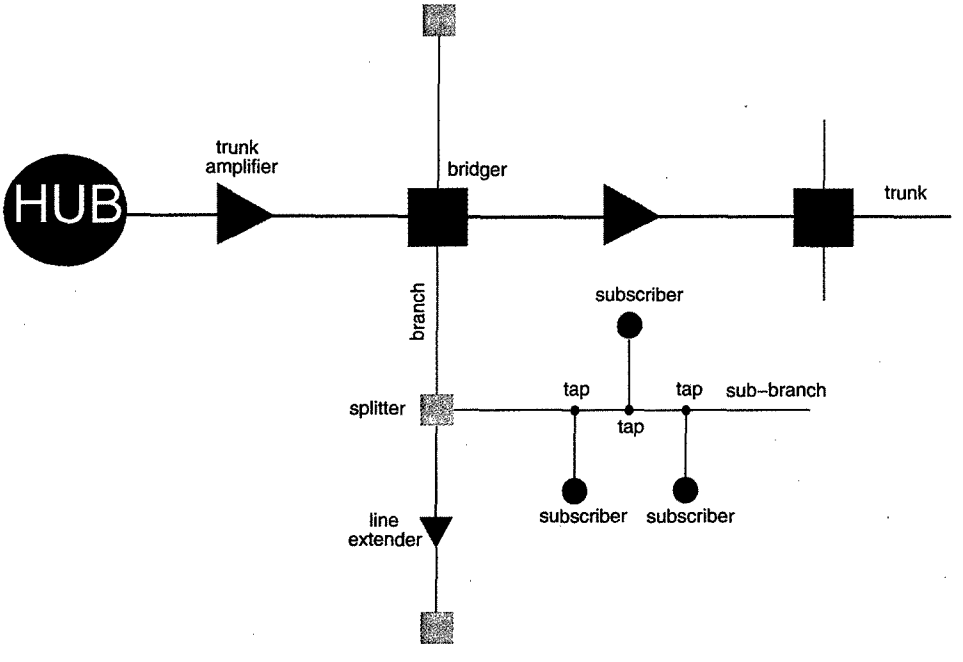

(b)

Fig. 2. The outline of typical current cable communication systems. (a) Block diagram of a typical cable communication system. (b) The block diagram of a single trunk.

The splitter connects a subbranch to a branch. Subscriber drops are connected to passive taps along the subbranch. Many cable TV companies support 500 subscribers per fiber node in hybrid fiber-coax networks [Huffaker, 1995]. If each subscriber has a 64 kbps modem for its PC, then a 32 Mbps per fiber node should be designed for peak hours. However, the available bandwidth is always swamped by more advanced Internet services such as teleconference where real time audio and video data streams are sent.

Technical limitations on channel capacity are set principally by cable amplifiers. The coaxial cable service occupies the 40–550 MHz portion of the spectrum, while the hybrid fiber-coax cable service occupies the 40–750 MHz portion of the spectrum. Since each commercial analog TV channel occupies a 6 MHz bandwidth, a cable TV system may provide up to 100 TV channels. In the future, a fully upgraded hybrid optical-coax cable network may use the 550–750 MHz band to provide digital video, high-speed data and telephone services. In this spectrum band, $(CD)^2MA$ can also find applications. For a two-way cable TV system, the spectrum slot located at 5–40 MHz provides subscribers with an upstream data-link to the outside world through the fiber-coax cable system. Formally, this upstream link can only provide a low speed data-link due to two main noise sources in this spectral slot (shown in Fig. 3). The first is impulsive noise from the electrical devices in PCs, TV sets, hair dryers, vacuum cleaner and etc., as well as vehicle emission systems. The second is narrowband interference picked up by the cable network itself such as Ham radio and Voice of America broadcasts.

In the Terayon S-CDMA system, it was reported that a total capacity of 10 Mbps per 6 MHz channel can be achieved in the 5–40 MHz band. While this represents a big advance in technology, this channel capacity may be too small to match the rapid future growth of demand of the Internet service, accompanied by the occupation of PCs and WebTVs in subscriber homes. Although the soft-degradation of the service quality of current CDMA systems can provide a barely satisfactory

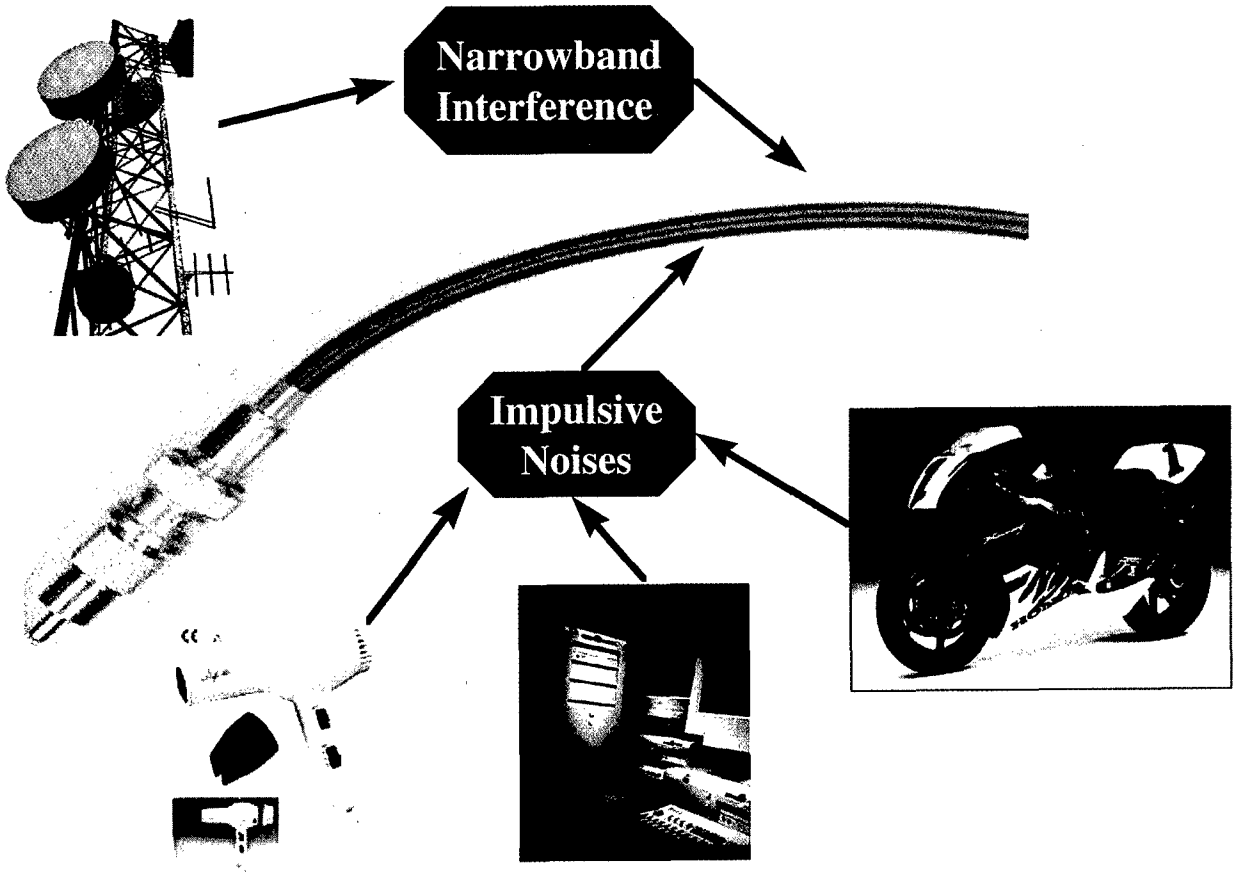

Fig. 3. Two main noise sources in the 5–40 MHz band of a cable TV system.

service to each subscriber during peak periods, such degradation of service can still be felt by subscribers if they are in the process of downloading image files, or some other data-intensive services, such as teleconferencing.

3. (CD)²MA for Cable Communication System

The main problems in using the 5–40 MHz band in cable TV systems are impulsive and narrowband noises. The multipath fading problem in wireless environments [Viterbi, 1995] does not occur in cable systems and the delay from each link can be measured *a priori*. Since the price that a subscriber is willing to pay for updating his cable service is relatively low, the transmitter and the receiver of the (CD)²MA system at the subscriber's end should be as simple as possible. The layout of the (CD)²MA transmitter for upstream communication is shown in Fig. 4. Since the hardware structure of a cable communication system is fixed during its operation, each head-end controller can broadcast a local clock signal to synchronize the local clocks of all subscribers under the same headend. The timing recovery in a cable communication system is thus solved.

The chaotic carrier used in the (CD)²MA system can be generated by an array of chaotic digital circuits, such as a "chaotic" (pseudo-chaotic) cellular automata [Toffoli, 1987], or a reversible cellular neural network [Crounse *et al.*, 1996; Yang *et al.*, 1996]. For manufacturing convenience, the hardware for each chaotic digital circuit is chosen to be the same in every transmitter. To ensure that at every moment the chaotic carriers in the same channel are orthogonal to each other, the headend controller must dynamically assign each transmitter a user ID number as the initial states of the digital chaotic generator whenever a subscriber begins sending information. Then, the output of the digital chaotic generator (which may be 8 or 12 bits) is fed into a D/A converter, whose output is sent to a frequency step-up for transferring the chaotic carrier to a different spectral band. Since the D/A converter may work at a clock speed of 1 MHz, we may have to shift this output to some prescribed 6 MHz channel within the 5–40 MHz band.

A frequency step-up is used to transfer the nonlinear carrier to an appropriate spectral band. This is accomplished by a *frequency multiplier*, which consists of a nonlinear circuit followed by a bandpass filter, as shown in Fig. 5(a). While there are many choices for the nonlinear device, the simplest one is a transistor biased in the nonlinear region. The frequency multiplier based on a transistor is shown in Fig. 5(b). If a bandpass signal $v_{\text{in}}(t)$ is fed into a frequency multiplier, the output $v_{\text{out}}(t)$ will appear in a frequency band at the nth harmonic of the input frequency(range). However, the multiplication factor n that can be provided by this circuit is usually small with a typical value of 3 or 5 because the nonlinearity of a transistor is too "smooth". To get a large gain, we need to find some device which has much more irregular nonlinearities such as breakpoints.

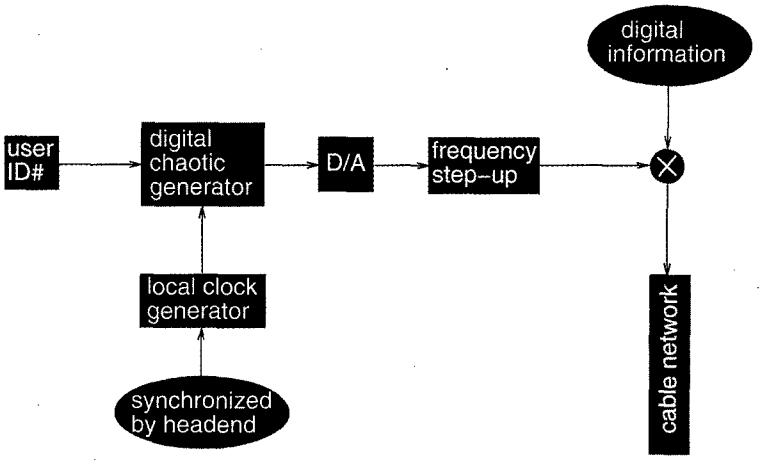

Fig. 4. The block diagram of the upstream transmitter at subscriber's end.

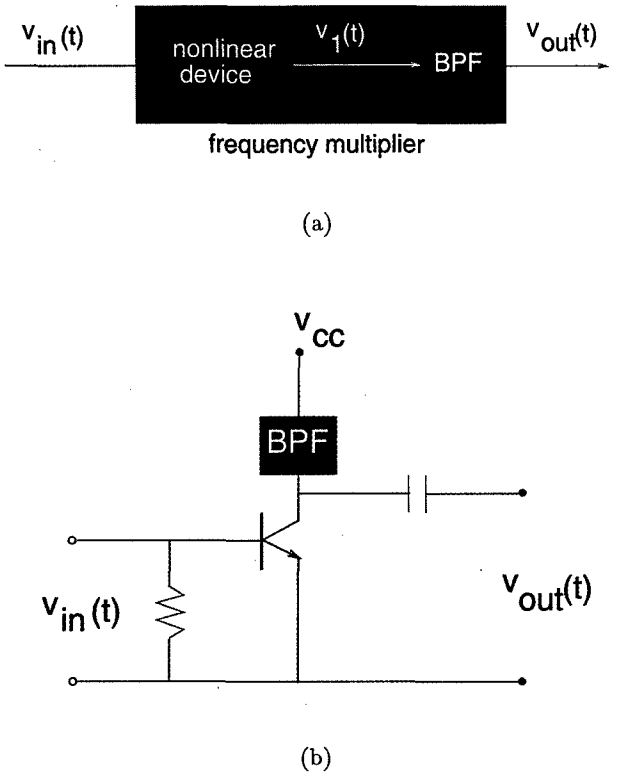

Fig. 5. A frequency multiplier used for the frequency step-up. (a) The block diagram of a frequency multiplier. (b) The circuit implementation of a frequency multiplier.

The block diagram of the receiver at the head-end controller for retrieving the digital signal from the ith user is shown in Fig. 6. Since the delay of the ith subscriber has been previously measured, the receiver in the headend controller can find the pre-measured time delay from a lookup table and generate the corresponding chaotic carrier with the corresponding delay. The signal received by the cable network is a mixture of noises and interferences from the other subscribers. The received signal is then multiplied by the regenerated carrier at the receiver. The result is low-pass filtered by a $[0, T]$ integrator and then thresholded and sampled to give the recovered digital signal. The timing signal used in sampling is provided by the local clock signal at the head-end controller. This recovered signal is then sent out to the Internet from the headend controller.

The downstream communication is almost the same as that of the upstream except that before the headend sends a chaotic carrier to user i, a time delay is compensated at the transmitter end. By doing this, the receiver at the subscriber's end is almost the same as its transmitter except for an additional $[0, T]$ integrator, a thresholding and a sampling circuit. The block digram of the receiver at the

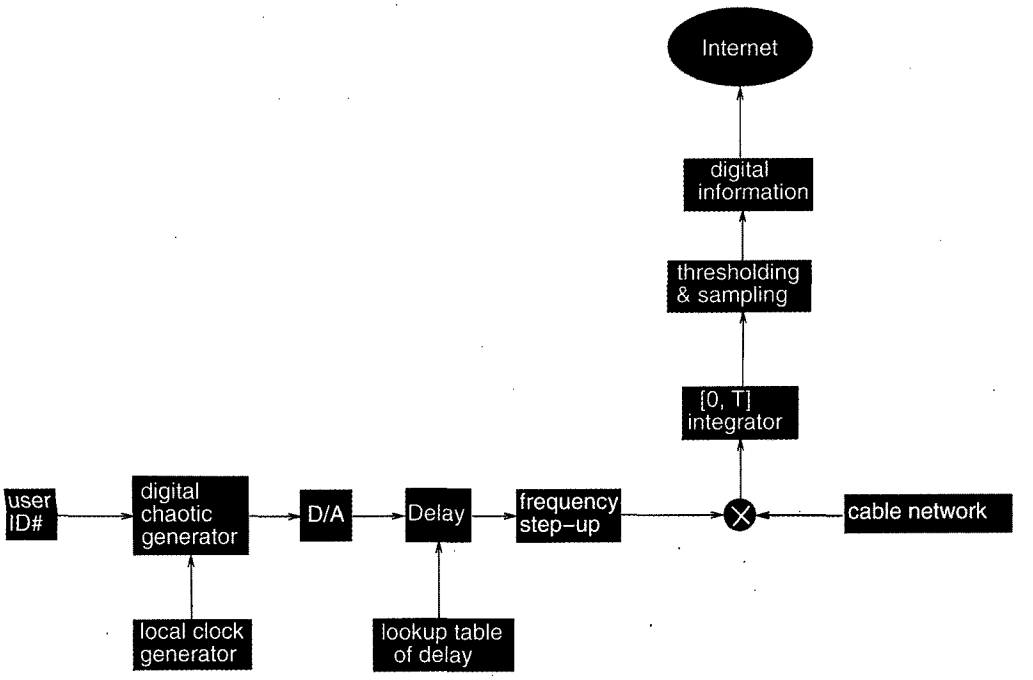

Fig. 6. The block diagram of the receiver at the headend controller for upstream communication.

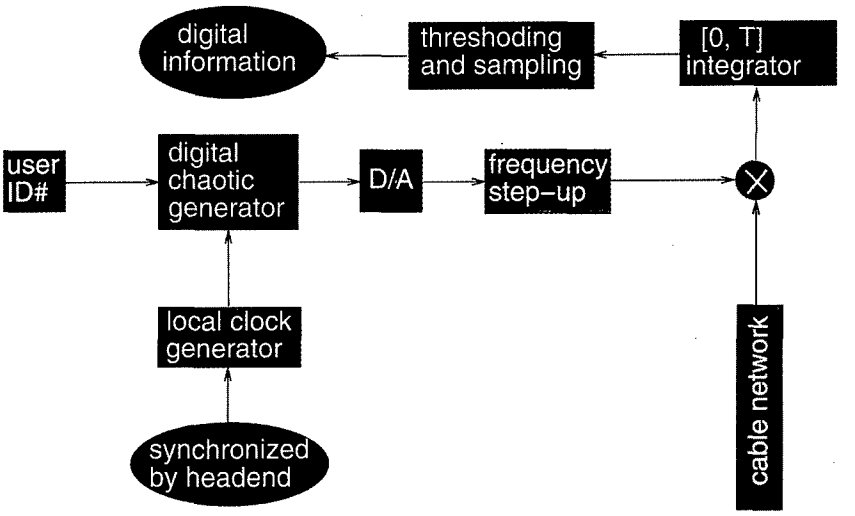

Fig. 7. The block diagram of the receiver at the subscriber's end for downstream communication.

subscriber's end is shown in Fig. 7. Observe that the main part of the transmitter is shared by the receiver. Since the synchronization signal is broadcast through the whole network, the expensive synchronization circuit is not installed in the subscriber's transmitter/receiver. Hence, the additional equipment in the subscriber's home is relatively inexpensive.

Under ideal conditions, the power levels of the chaotic carriers from different users at the fiber node (or the headend) should be the same. This is the power control problem, which had been extensively studied in wireless CDMA systems [Lee, 1989]. However, in view of the fixed hardware structures of cable TV networks, amplifiers can be designed to satisfy this condition. In this paper, perfect power control is assumed.

4. Model of Chaotic Digital CDMA Communication Systems

The difference between classical CDMA and $(CD)^2MA$ is that the former uses a pseudo-random digital NRZ signal as a nonlinear sub-carrier and this carrier is then used to modulate a linear carrier for central frequency shift. The latter uses chaotic carriers directly in the desired spectral band. To clarify the difference between them, in this section we present examples to show the different principles used in these two schemes.

Since in $(CD)^2MA$ systems many candidates of chaotic RF waveforms can be used as chaotic carriers, we give a theoretical model for a chaotic carrier which has a flat enough spectrum in the bandwidth we are interested in. The chaotic carrier for the ith user is given by

$$c_i(t) = \sum_{n=1}^{N} a_{i,n}(t)\cos(\omega_n t + \theta_{i,n}) = \mathrm{Re}\left\{\sum_{n=1}^{N} a_{i,n}(t)\exp(j\omega_n t + j\theta_{i,n})\right\},\ N \to \infty \tag{1}$$

where $j \triangleq \sqrt{-1}$, and $a_{i,n}(t) \in \Re$, $\omega_n \in$ [prescribed spectral band] and $\theta_{i,n} \in (-\pi, \pi]$ are respectively the amplitude, frequency and phase of the nth component of the chaotic carrier. Since $c_i(t)$ is a nonlinear wave, at least one of $a_{i,n}$, $n = 1, \ldots, N$, must be time-varying. Observe that the single tune carrier is a special case of $c_i(t)$ with $a_{il} \neq 0$ and $a_{ij} = 0$ if $j \neq l$ for a given l.

Similarly, the carrier for the jth user is modeled by

$$c_j(t) = \sum_{n=1}^{N} a_{j,n}(t)\cos(\omega_n t + \theta_{j,n}) = \mathrm{Re}\left\{\sum_{n=1}^{N} a_{j,n}(t)\exp(j\omega_n t + j\theta_{j,n})\right\},\ N \to \infty \tag{2}$$

Since in $(CD)^2MA$ systems, we usually use a $[0, T]$ integrator as the low-pass filter (LPF), the moving

average of the cross-correlation between $c_i(t)$ and $c_j(t)$, $i \neq j$ with time window T is given by

$$
\begin{aligned}
r_{ij}(t) &= \frac{1}{T}\int_{t-T}^{t} c_i(t)c_j(t)dt \\
&= \frac{1}{T}\int_{t-T}^{t} \sum_{n=1}^{N} a_{i,n}(t)\cos(\omega_n t+\theta_{i,n}) \sum_{n=1}^{N} a_{j,n}(t)\cos(\omega_n t+\theta_{j,n})dt \\
&= \frac{1}{T}\int_{t-T}^{t} \sum_{n=1}^{N} a_{i,n}(t)\cos(\omega_n t+\theta_{i,n})a_{j,n}(t)\cos(\omega_n t+\theta_{j,n})dt \\
&\quad + \frac{1}{T}\int_{t-T}^{t} \sum_{n=1}^{N} a_{i,n}(t)\cos(\omega_n t+\theta_{i,n}) \sum_{m=1,\, m\neq n}^{N} a_{j,m}(t)\cos(\omega_m t+\theta_{j,m})dt \\
&= \frac{1}{2T}\int_{t-T}^{t} \sum_{n=1}^{N} a_{i,n}(t)a_{j,n}(t)\cos(\theta_{i,n}-\theta_{j,n})dt + \frac{1}{2T}\int_{t-T}^{t} \sum_{n=1}^{N} a_{i,n}(t)a_{j,n}(t)\cos(2\omega_n t+\theta_{i,n}+\theta_{j,n})dt \\
&\quad + \frac{1}{T}\int_{t-T}^{t} \sum_{n=1}^{N} a_{i,n}(t)\cos(\omega_n t+\theta_{i,n}) \sum_{m=1,\, m\neq n}^{N} a_{j,m}(t)\cos(\omega_m t+\theta_{j,m})dt\,, N\to\infty
\end{aligned} \tag{3}
$$

Assuming that the phase of each subcomponent of a chaotic carrier is a random variable distributed uniformly over the interval $(-\pi, \pi]$, then $\theta_{i,n}-\theta_{j,n}$ distributes over $(-2\pi, 2\pi)$. Hence, we can choose T large enough so that $r_{ij}(t)$ will be small enough.

In CDMA systems, binary pseudo-random sequences (chip sequences) are used to spread the bandwidth of the modulated signals over the larger transmission bandwidth, *and* to distinguish the different user signals by using the same transmission bandwidth. Then the chip sequence is modulated by a linear sinusoidal waveform using different modulation methods. The most commonly used method is QPSK modulation [Viterbi, 1995]. However, for simplicity and without loss of generality, let us choose the simplest "phase shift" method ("bit 1" shifts the 0 phase of the linear carrier while "bit 0" shifts the π phase) for demonstration purposes. The ith carrier in a CDMA system is given by

$$
c_i(t) = a_i \cos\left(\omega t+\theta_i+\sum_{k=0}^{[t/T_c]}\psi_i(k)\right) \tag{4}
$$

where the two constants a_i and ω are respectively the amplitude and frequency of the ith carrier; T_c is the chip bit duration defined as the time span of a bit in the chip sequence; $[x]$ denotes the biggest integer less than x; and $\psi_i(k)$ is the phase shift caused by the kth chip value p_k; namely,

$$
\psi_i(k) = \begin{cases} 0, & p_k = 1 \\ \pi, & p_k = 0 \end{cases} \tag{5}
$$

Similarly, the carrier for the jth user is given by

$$
c_j(t) = a_j \cos\left(\omega t+\theta_j+\sum_{k=0}^{[t/T_c]}\psi_j(k)\right) \tag{6}
$$

The moving average of the cross-correlation between $c_i(t)$ and $c_j(t)$ with time window T is given by

$$
\begin{aligned}
&r_{ij}(t) \\
&= \frac{1}{T}\int_{t-T}^{t} c_i(t)c_j(t)dt \\
&= \frac{1}{T}\int_{t-T}^{t} a_i \cos\left(\omega t+\theta_i+\sum_{k=0}^{[t/T_c]}\psi_i(k)\right) a_j \\
&\quad \times \cos\left(\omega t+\theta_j+\sum_{k=0}^{[t/T_c]}\psi_j(k)\right) dt \\
&= \frac{1}{2T}\int_{t-T}^{t} a_i a_j \cos\left(\theta_i-\theta_j+\sum_{k=0}^{[t/T_c]}\psi_i(k)-\psi_j(k)\right) dt \\
&\quad + \frac{1}{2T}\int_{t-T}^{t} a_i a_j \cos\left(2\omega t+\theta_i+\theta_j+\sum_{k=0}^{[t/T_c]}\psi_i(k)+\psi_j(k)\right) dt
\end{aligned} \tag{7}
$$

For both chaotic CDMA and linear CDMA systems, the main goal is to make $r_{ij}(t) \to 0$ whenever $i \neq j$. Comparing Eqs. (3) and (7) we can see that the chaotic CDMA and the linear CDMA achieve this goal by using different strategies. In chaotic CDMA, the goal is to make the term

$$\frac{1}{2T}\int_{t-T}^{t}\sum_{n=1}^{N} a_{i,n}(t)a_{j,n}(t)\cos\left(\theta_{i,n}-\theta_{j,n}\right)dt \qquad (8)$$

as small as possible, but in linear CDMA the goal is to make the term

$$\frac{1}{2T}\int_{t-T}^{t} a_i a_j \cos\left(\theta_i-\theta_j+\sum_{k=0}^{[t/T_c]}\psi_i(k)-\psi_j(k)\right)dt \qquad (9)$$

as small as possible. To reduce the value of Eq. (9) we can reduce the transmitting energy of each carrier (restricted by the noise level), increase T (restricted by the bit-rate of the message signal), increase the bit-rate of the chip sequence (restricted by bandwidth) and make $\psi_i(k) - \psi_j(k)$ as random as possible (restricted by the pseudo-random algorithm for generating the chip sequence).

To reduce the value of Eq. (8) we can also reduce the transmitting energy of each carrier and increase T. However, instead of increasing the bit-rate of the chip sequence, we need to use as many sub-carrier components as possible; instead of making $\psi_i(k) - \psi_j(k)$ random, we need to make $\theta_{i,n} - \theta_{j,n}$ random enough. We can then conclude that the main difference between a linear CDMA and a chaotic CDMA is that the former explores the spectrum resource from the time-domain, while the latter does it in the frequency-domain.

5. The BER Performance of (CD)²MA

In this section we study the bit-error-rate (BER) performance of (CD)²MA. This is a very important benchmark for measuring service performance. Throughout this section we assume that all signals are at constant power throughout the transmission period.

Suppose $y_i(t)$ is the output of the demodulator of the ith user and $x_{i,n}(t)$ is the nth bit of the message signal of the ith user. As with any digital communication system, spread spectrum or not, there are four components in the demodulator output:

- the desired output, which depends only on $x_{i,n}(t)$;
- the inter-symbol interference components, which depend only on $x_{i,n+m}(t)$, $m \neq 0$;
- the component due to background noise, which we assume to be white with a one-side density equal to N_0 watts/Hz;
- the other-user interference components, which depend on $x_{j,n+m}(t)$ for all $i \neq j$ and all m.

Let T_b be the bit duration of the message signal, and choose a $[0, T_b]$ integrator as the LPF. Thus,

$$\Gamma = \int_0^{T_b} y_i(t)dt \qquad (10)$$

The sign of this measurement is used to decide whether the message bit is $+1$ or -1. The mean of Γ is given by

$$\begin{aligned} E[\Gamma] &= \int_0^{T_b} E[y_i(t)|x_{i,n}(t)]dt \\ &= \sqrt{P_i}\int_0^{T_b} x_{i,n}(t)dt \\ &= \pm T_b\sqrt{P_i} \end{aligned} \qquad (11)$$

where P_i is the power of ith chaotic carrier. The second equality is satisfied because we have assumed that every signal has constant power throughout the transmission period. Here, the sign depends on the sign of $x_{i,n}(t)$, which is constant over $[0, T_b]$.

Since the noise components are essentially uncorrelated,

$$\begin{aligned} \mathrm{Var}[\Gamma] &= \int_0^{T_b} \mathrm{Var}[y_i(t)|x_{i,n}(t)]dt \\ &= T_b(V_I + V_N + V_O) \end{aligned} \qquad (12)$$

where V_I, V_N and V_O are the variances of the inter-symbol interference, background noise and interference from all the other users, respectively.

Then the bit-error-rate (BER) is given by

$$\begin{aligned} \mathrm{BER} &= \Psi\left(\sqrt{\frac{(E[\Gamma])^2}{\mathrm{Var}[\Gamma]}}\right) \\ &= \Psi\left(\sqrt{\frac{T_b P_i}{V_I + V_N + V_O}}\right) \end{aligned} \qquad (13)$$

where

$$\Psi(x) \triangleq \frac{1}{\sqrt{2\pi}}\int_x^{\infty} e^{-s^2/2}ds\,. \qquad (14)$$

Assuming the inter-symbol interference to be negligible or zero, and since the other two components (background white noise and other-user interference) are independent of $x_{i,n}(t)$ for all i, it follows that the variance due to background noise is just the effect of a white noise with one-sided density N_0 on the receiver filter whose transfer function is $H^*(f)$, and must therefore contribute

$$V_N = (N_0/2)\int_{-\infty}^{\infty} |H(f)|^2 df = N_0/2\,. \quad (15)$$

This is because the filter gain is normalized, so that

$$\int_{-\infty}^{\infty} |H(f)|^2 df = 1\,. \quad (16)$$

To the user i any other user j has a constant carrier power P_j modulated as $c_j(t)x_{j,n}(t)$ which is independent of and generally unsynchronized with that of user i. In addition, the carrier phase of the jth user's modulator will differ from that of the ith user. Hence, the effect of the jth user's signal on the kth user's demodulator will be that of a white noise with a two-sided density P_j passing through the tandem combination of two filters in the transmitter and the receiver with a combined transfer function $|H(f)|^2$. Hence,

$$V_O = \sum_{j\neq i} \frac{P_j}{2}\int_{-\infty}^{\infty} |H(f)|^4 df\,. \quad (17)$$

It follows from Eqs. (13), (15) and (17) that

$$\mathrm{BER} = \Psi\left(\sqrt{\frac{2T_bP_i}{N_0 + \sum_{j\neq i} P_j\int_{-\infty}^{\infty}|H(f)|^4 df}}\right) \quad (18)$$

The numerator is just twice the bit energy, E_b, and the denominator is the effective interference density. Thus,

$$\mathrm{BER} = \Psi\left(\sqrt{\frac{2E_b}{I_0}}\right) \quad (19)$$

where

$$\frac{E_b}{I_0} = \frac{T_bP_i}{N_0 + \sum_{j\neq i} P_j\int_{-\infty}^{\infty}|H(f)|^4 df} \quad (20)$$

Since $(CD)^2$MA systems are interference limited rather than noise limited, let us ignore the background noise (i.e. $N_0 = 0$) and assume that because of perfect power control, all users are received by the base station (headend or fiber node) receiver at the same power $P_i = P_j = P_c$ for any i and j. Then for a given E_b/I_0 level, determined from Eq. (19) for the required BER, the maximum number of users, $K_{\max}$, obtained from Eq. (20), is given by

$$K_{\max} - 1 = \frac{1}{E_b/I_0}\frac{T_b}{\int_{-\infty}^{\infty}|H(f)|^4 df} = \frac{1}{E_b/I_0}\frac{W/R}{W\int_{-\infty}^{\infty}|H(f)|^4 df} \quad (21)$$

where W is the bandwidth, R is the bit rate and the integral in the denominator is lower-bounded by unity. Consequently,

$$K_{\max} - 1 \leq \frac{W/R}{E_b/I_0} \quad (22)$$

and the maximum bit-rate, $R_{\max}$, that this channel can support is given by

$$R_{\max} \leq \frac{W}{E_b/I_0} + R \quad (23)$$

For a given BER, the actual E_b/I_0 depends on the system design and error-correction code. It may approach but is never equal to the theoretical calculations. In the next section, we use simulation results to find the performance of $(CD)^2$MA systems.

6. Comparison of BER Between S-CDMA and $(CD)^2$MA Systems

In the upstream, the headend receives all the chaotic carriers from active subscribers, additive impulsive noises and narrowband noises from the cable network. The channel model of the upstream data-link located at the 5–40 MHz band in cable TV systems is only a noisy channel with narrowband interference and random impulsive noise with duration up to 100 μs. Since multipath fadings usually encountered in wireless mobile communication systems [Lee, 1989] do not occur here, a

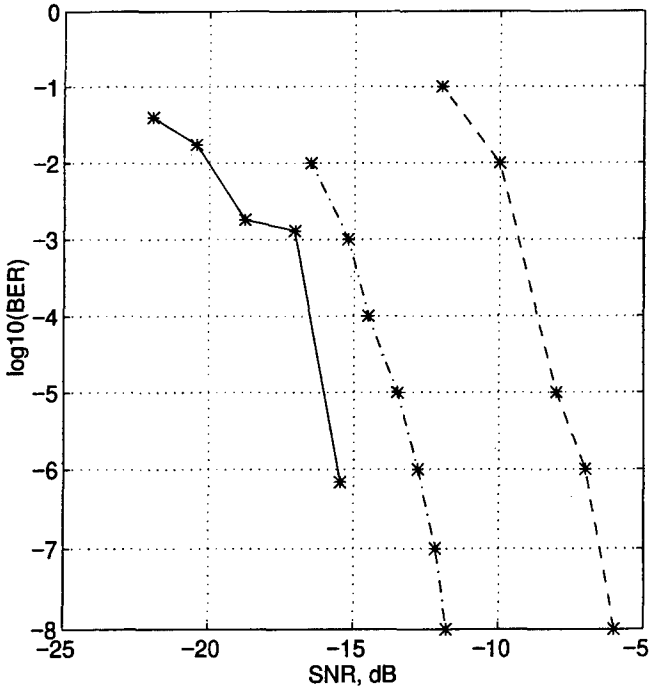

Fig. 8. The BER performance of the $(CD)^2MA$ system used in a cable communication system. The dashed line and the dash-dotted line are the corresponding results of the S-CDMA system under "normal mode" (dashed line) and "fall back mode" (dashdotted line), respectively.

spread spectrum communication system can be used much more easily in this channel than in a wireless communication channel. Furthermore, since the delay in a cable system is a fixed characteristic which can be measured, it is possible to use synchronous spread spectrum communication schemes, such as S-CDMA and synchronous $(CD)^2MA$.

Our simulation results of the $(CD)^2MA$ system are shown in Fig. 8. The solid line shows the BER performance when $N = 200$ sub-carriers are used to model the chaotic carrier of each subscriber. The parameters for the $[0, T]$ integrator at the receivers are chosen as $T = T_b = 1/64$ ms. One should note that the interference from the other users in the same 6 MHz channel is also considered as noise here. For comparison, the results of the Terayon's S-CDMA system in both normal mode and fall back mode are also shown in the same figure. We can see that the performance of $(CD)^2MA$ systems is much better than the S-CDMA scheme in its "fall back mode", which is the best operating mode that the Terayon's S-CDMA scheme can provide.

The quantitative comparison of the channel capacities of the S-CDMA in its fall back mode and the $(CD)^2MA$ is shown in Table 1. From Table 1 we

Table 1. The relationship between the channel capacities of the $(CD)^2MA$ system and the S-CDMA system in its fall back mode.

BER	10^{-6}	10^{-5}	10^{-4}	10^{-3}	10^{-2}
Capacity rate: $\frac{(CD)^2MA}{CDMA}$	1.50	1.50	1.40	1.35	1.41

can see that $(CD)^2MA$ can support a much higher bit-rate than S-CDMA when the BER is smaller than 10^{-5}. A 1.5 times higher bit-rate in this case means that a $(CD)^2MA$ system can support a capacity of 15 Mbps per 6 MHz upstream.

7. Conclusions

In this paper, we apply $(CD)^2MA$ to cable communication systems by using the 5–40 MHz band which is very noisy for other narrow band communication schemes, such as the QPSK method. Time division multiple access (TDMA) and frequency division multiple access (FDMA) also cannot be used efficiently in this noisy portion of the spectrum because narrowband interference and long duration impulsive noises can introduce many errors in TDMA and FDMA systems. We also compare our $(CD)^2MA$ system to Terayon's S-CDMA system and found that the $(CD)^2MA$ system can perform much better than the S-CDMA system by increasing the channel capacity 1.5 times more than the best performance by an S-CDMA system.

In this paper, we emphasize the application of our $(CD)^2MA$ on the almost "useless" spectrum band in today's cable TV networks because its potential commercial benefit can easily be realized even without upgrading existing cable TV networks. However, readers should not form the wrong impression that $(CD)^2MA$ can only be used in coaxial networks. In fact, the $(CD)^2MA$ principle can also be used in future high-capacity digital data links based on pure optical fibers to enable a high bandwidth efficiency. On the other hand, since $(CD)^2MA$ systems are interference limited but not dimension-limited, it can provide more flexible performance choices for different services.

Acknowledgment

This work is supported by the Office of Naval Research under grant No. N00014-97-1-0463.

References

Baer, W. S. [1974] *Cable Television: Franchising Considerations* (Crane, Russak, NY).

Crounse, K. R., Yang, T. & Chua, L. O. [1996] "Pseudorandom sequence generation using the CNN universal machine with applications to cryptography," in *Proc. Fourth IEEE Int. Workshop on Cellular Neural Networks and Their Applications*, June 24–26, IEEE Catalog Number 96TH8180 and ISBN 0-7803-3261, pp. 433-438.

Huffaker, M. [1995] "Take the coax route [internet access through cable modems]," *Telephony* **229**(22), 44, 46, 48, 50–1, 27.

Lee, W. C. Y. [1989] *Mobile Cellular Telecommunications Systems* (McGraw-Hill, NY).

Toffoli, T. [1987] *Cellular Automata Machines: A New Environment for Modeling* (MIT Press, Cambridge).

Tomari, Y., Saito, M., Okada, N. & Yoshida, R. [1997] "Design and implementation of Internet-TV," *IEEE Trans. Consumer Electron.* **43**(3), 953–960.

Viterbi, A. J. [1995] *CDMA: Principles of Spread Spectrum Communication*, Wireless Communications Series (Addison-Wesley, Reading, MA).

Yang, T. & Chua, L. O. [1997] "Chaotic digital code-division multiple access (CDMA) systems," *Int. J. Bifurcation and Chaos* **7**(12), 2789–2805.

Yang, T., Chua, L. O. & Crounse, K. R. [1996] "Application of discrete-time cellular neural networks to image copyright labeling," in *Proc. Fourth IEEE Int. Workshop on Cellular Neural Networks and Their Applications*, June 24–26, IEEE Catalog Number 96 TH8180 and ISBN 0-7803-3261, pp. 19–24.

International Journal of Bifurcation and Chaos, Vol. 8, No. 8 (1998) 1671–1674

ADAPTIVE MODE SELECTION USING ON–OFF SWITCHING OF CHAOS

PETER DAVIS*
ATR Adaptive Communications Research Labs.,
2-2 Hikaridai, Seika-cho, Soraku-gun, Kyoto 619-0288 Japan

Received July 31, 1997

Onset of chaotic mode transitions can be used in a simple and robust mechanism for adaptation in multimode systems. We present an idealized model of adaptive mode selection using on–off switching of chaotic basin transitions in a multistable system. A stochastic description obtained in the limit of large switching intervals gives search times in terms of projections of the chaotic state onto basins of multistability.

1. Introduction

This paper relates to work on harnessing the onset of chaotic dynamics for adaptive mode selection in multimode systems. This work is based on a general view of self-reorganization in which chaos can play an important role in finding "fit" modes. It is often the case that whether a particular mode of a multimode system, such as a laser, or a neural network, for example, is satisfactory or "fit", is known by the external response seen when the system is in that mode. When working on the problem of mode selection in a particular high-dimensional nonlinear optical system, we proposed that bifurcation to intermittent mode transitions (also called chaotic itinerance) could be harnessed to automatically search for fit modes among a set of candidate modes by simply feeding back external fitness responses to a bifurcation parameter [Davis, 1990]. The general idea of adaptive mode selection using chaos is to couple the fitness response signal to the multimode in such a way that bad responses result in mode transitions, and good responses result in suppression of mode transitions. Specifically, the fitness response signal can be used to drive the system between a multistable regime and a chaotic mode transition regime.

The effectiveness and practicality of this scheme has been demonstrated in numerical [Davis, 1990] and physical experiments [Aida & Davis, 1994] using an opto-electronic oscillator, and in numerical experiments on a neural network [Nara & Davis, 1992]. A variation of this idea has also been used in experiments on a signal generator spontaneously adapting its output signal mode to avoid signal collisions [Liu & Davis, 1997].

The purpose of this paper is to present a simple model of this method, involving adaptive switching between two idealized dynamical regimes. It allows an easy derivation of a state transition diagram describing the mode search process, including the effects of "false-alarms".

2. Model System

The basic model for adaptive mode selection is as follows. The multimode system is described by a parameter p and a dynamical variable $\mathbf{X}$. The control parameter has two particular parameter

*E-mail: davis@acr.atr.co.jp

values p_- and p_+, corresponding to the two dyamical regimes — multistability regime and mode transition regime, respectively. In the multistability regime, there is a set of modes which are all stable for the same parameter; that is, there are multiple basins of attraction, and which mode is excited depends on the location of the initial state. In the mode transition regime, the modes are unstable, and there is a single chaotic attractor which extends to the neighborhoods of the previously stable modes. The system receives a response E which is some arbitrary function of $\mathbf{X}$ and its history over some time interval. The response E takes two values, say 0 and 1 respectively, corresponding to "good" and "bad" fitness. The response signal causes the multimode to switch between the two dynamical regimes at p_- and $p+$, as shown in Fig. 1.

The mode search algorithm is represented by 3 steps. The fitness of the mode is evaluated, returning a value of signal $E = 0$ or 1. Then the parameter is adjusted, to p_- in the case of a good response, $E = 0$, or p_+ in the case of a bad response, $E = 1$. Then the system is allowed to freely evolve for a time T.

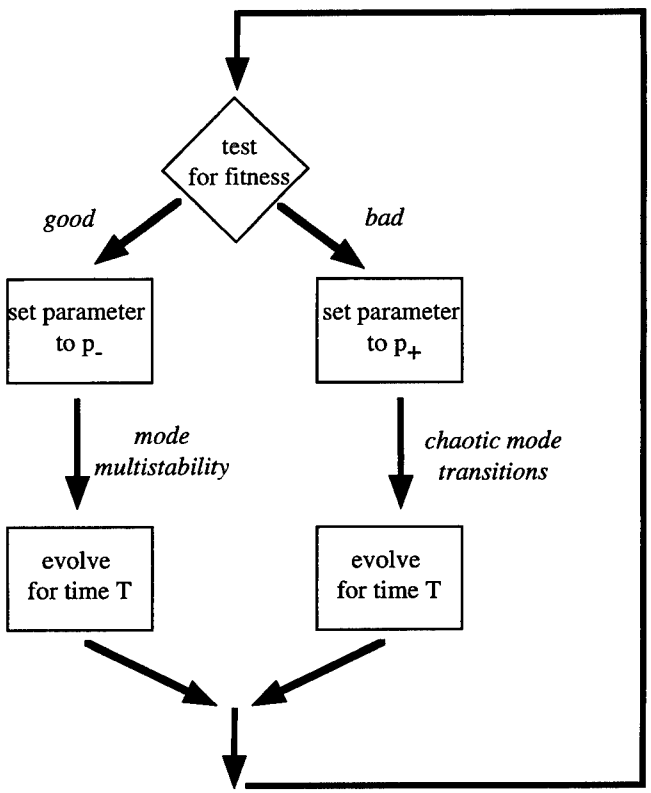

Fig. 1. Control algorithm for adaptive mode search using on–off switching of chaos. It is assumed that at "test" there is a response signal from the environment which indicates whether the current state is "good" or "bad".

Note that we do not exclude the possibility that more than one mode gets a good response. And it is functionally reasonable for the system to make a spontaneous selection of any one of multiple good modes.

3. State Transition Representation

The dynamics of the search process defined in Fig. 1 can be described by the state transition diagram shown in Fig. 2(a). The combined state of the multistable system plus environment is completely described by the parameter p, dynamical state $\mathbf{X}$, and response E. We sample the state of the system immediately after the parameter has been adjusted. Then there is one-to-one correspondence between the state of the combined system and states of $\mathbf{X}$. First we define two states, the set S_B of $\mathbf{X}$ states which get a bad response, and the set S_G of $\mathbf{X}$ states which get a good response. One iteration of the search algorithm gives one of four transitions in the transition diagram: $S_B \to S_B$, $S_B \to S_G$, $S_G \to S_G$, or $S_G \to S_B$.

Now, it is useful to further decompose S_G, as shown in Fig. 2(b), into "trap" states S_T which do not lead to transitions back to bad states S_B, and "nontrap" states S_{NT} which do lead to transitions back to bad states S_B. If there is a transition from a good state in S_G, *or any of its iterates*, to a bad state S_B, then it belongs to the nontrap set S_{NT}. The S_{NT} states will be called "false-alarm" states. False-alarm states exist when there is a mismatch between the external fitness criterion and the basin structure. States $\mathbf{X}$ which get a good response but which are located in the basin of a bad mode are straightforward examples of false-alarm states. However, there may also be false-alarm states in the basins of "good" modes. Note that under certain conditions, the scheme defined in Fig. 1 can eventually reach a good mode even if there is such a mismatch causing false alarms. This is a key point for the usefulness of this adaptation mechanism.

4. Accessibility of Fit Modes

Now we consider if and when the system will be able to find and lock onto a good mode. That is, do trap states exist and can they be reached from arbitrary initial states? If one or more of the

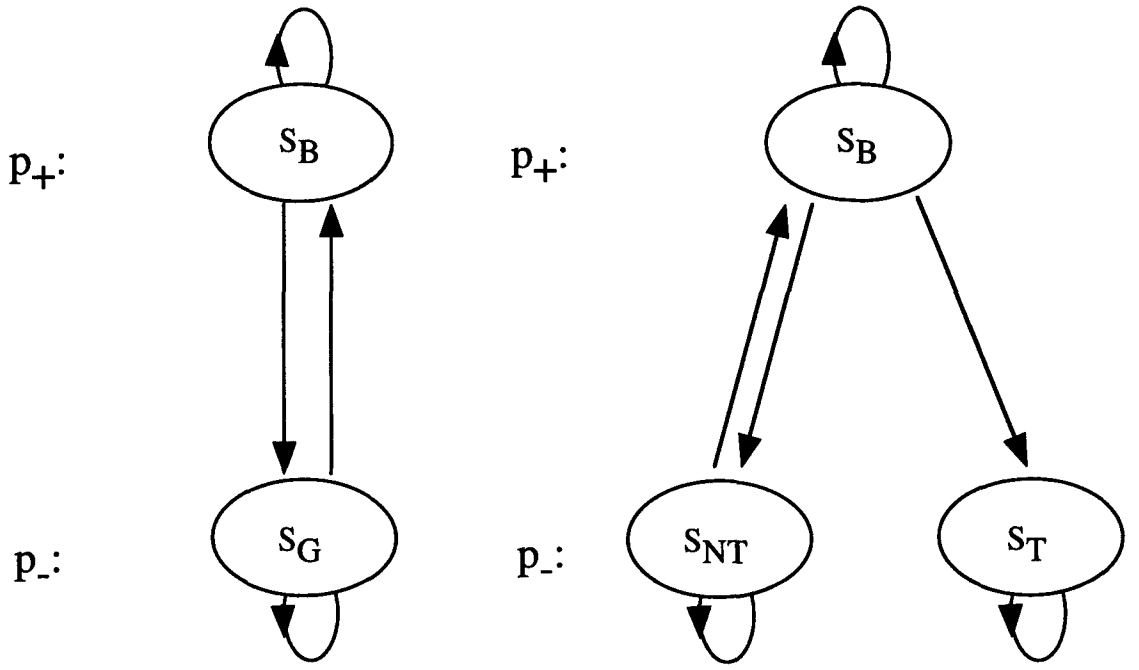

Fig. 2. (a) State transition representation of the search process. S_G and S_B are sets of states $\mathbf{X}$ of the multimode system which get "good" and "bad" responses, respectively. For this transition diagram, states are defined just after the switch of parameter and before the free evolution stage. (b) As for (a) but with the S_G states split into trapping states S_T and nontrapping (or false-alarm) states S_{NT}.

multistable modes at parameter p_- satisfy the fitness criterion, then the set of trap states in Fig. 2(a) is not empty, i.e. $S_T \neq \emptyset$. If the orbit of the chaos at parameter p_+ passes through states which are in the trap set, then the trap set is accessible from at least some initial conditions. For a given system, such states may be easy to identify. However, in general, it is difficult to say whether trap sets can be reached from arbitrary initial states. Regardless of the ergodicity on the chaotic attractor at parameter p_+, the on–off switching may alter the distribution of the search dynamics to the extent that local accesibility is not enough to guarantee global accessibility.

In order to establish a condition where we can guarantee global accessibility for the trap set, let us take the limit of large switching intervals. Let us assume that the interval T is much longer than characteristic times for relaxation to the invariant measures at both p_- and p_+. Also, we will assume that each of the attractors at p_- contains only either good or bad states and not both. (A counterexample is a mode which is a limit-cycle through good and bad states.) Then the transition diagram can be written as in Fig. 3, as a markov stochastic transition diagram. A transition between states can now be described as a stochastic transition characterized by a probability which depends only on the current state. The probabilities for transitions from the S_B state are obtained by projecting the invariant measure of the chaotic attractor. The probability $P_{B,T}$ for transition $S_B \rightarrow S_T$ is the relative measure of states visited by chaos which are also in the trapping set S_T. The probability $P_{B,NT}$ for transition $S_B \rightarrow S_{NT}$ is the relative measure of states visited by chaos which are in the false-alarm set. Now, the probability $P_{T,T}$ of the $S_T \rightarrow S_T$ transition is just unity by definition. The probability $P_{NT,B}$ of the $S_{NT} \rightarrow S_B$ transition is also unity from the assumption about the uniqueness of the fitness type of the states in each multistable mode.

It can be seen immediately from Fig. 3 that in this limit of large switching intervals, there is convergence to the trap set S_T so long as $P_{B,T}$ is nonzero. It is also straightforward to calculate the average time τ to reach the trap set,

$$\tau = T\frac{P_{B,T}(1 - P_{B,NT} + 2P_{B,NT}^2 + 2P_{B,T}P_{B,NT})}{(1 - P_{B,NT})^2(P_{B,T} + P_{B,NT})^2}. \quad (1)$$

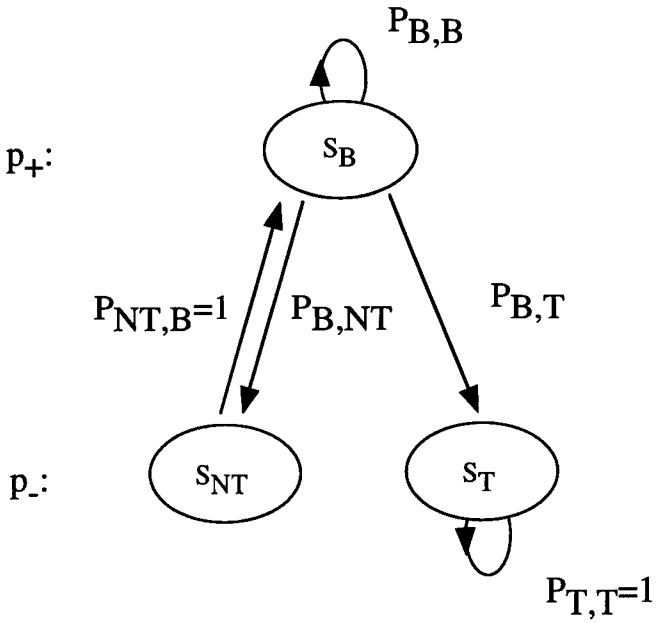

Fig. 3. Stochastic transition diagram obtained with assumption of free evolution time T longer than characteristic times for relaxation to invariant measures. Transitions are marked with corresponding transition probabilities.

In the particular case where there are no false alarms, $P_{B,NT} = 0$, then the average search time is just

$$\tau = \frac{T}{P_{B,T}} = \frac{T}{P_{B,G}}, \tag{2}$$

where $P_{B,G}$ is the probability of a chaotic transition from a bad state to a good state, $P_{B,G} \equiv P_{B,T} + P_{B,NT}$. Clearly, the adaptive mode selection process will be faster if the measure of the chaotic dynamics is localized on the neighborhoods of the candidate modes, and the environment responses match the mode basins, so that the probability of false alarms is reduced. Also, in practice, one would not want to have switch interval T any longer than was necessary. In this regard, for example, it would be desirable to avoid situations where there are good responses to states, such as those near fractal boundaries, which correspond to long transients at p_-.

By way of comparison, we could consider a method in which the multimode system is allowed to evolve in chaos at p_+ for time T, then unconditionally switched to p_- where it is allowed to evolve for another interval T before being tested. (Note that in this case the response signal alone is not enough to switch the parameter, and supplementary parameter dynamics are needed.) A similar analysis for the case of long switch intervals gives an average search time τ of

$$\tau = \frac{2T}{P_{B,G}}. \tag{3}$$

In this method, the average search time may be twice as long as that for the method of Fig. 1 in the case when $P_{B,NT} = 0$. However, this method has the advantage that there are cases in which it may allow convergence to a good mode even when the method in Fig. 1 does not do so.

5. Conclusions

We have presented a simple model of the method proposed in [Davis, 1990] for adaptive mode selection using adaptive bifurcation between multistability and chaotic mode transition regimes in a multimode system. In actual implementations of this method, in particular to high-dimensional multimode systems, such as in the experiment by Aida and Davis [1994], it can be difficult to analyze the search dynamics, for example to estimate search times. The simple model presented here involves adaptive switching between two ideal dynamical regimes of multistability and chaos. It allows easy derivation of a state transition diagram describing the mode search process, including the effects of "false-alarms". This provides a useful framework for further analysis of particular systems. In particular, in the limit of large switching intervals, it can be seen that the mode search depends on just the projection of the chaotic attractor on the states which get good responses, and on their distributions in the basins of stable modes.

References

Aida, T. & Davis, P. [1994] "Oscillation mode selection using bifurcation of chaotic mode transitions in a nonlinear ring resonator," *IEEE J. Quantum Electron.* **30**, 2986–2997.

Davis, P. [1990] "Application of optical chaos to temporal pattern search in a nonlinear optical resonator," *Jpn. J. Appl. Phys.* **29**, L1238–L1240.

Davis, P. [1994] "Functional optical chaos," in *Towards Harnessing Chaos*, ed. Yamaguchi, Y. (Elsevier Science B. V., NY), pp. 169–185.

Liu, Y. & Davis, P. [1997] "Adaptive optical sequence generation for collision avoidance using chaos," *Electron. Lett.* **33**, 68–69.

Nara, S. & Davis, P. [1992] "Chaotic wandering and search in a cycle memory neural network," *Prog. Theor. Phys.* **88**, 845–855.

International Journal of Bifurcation and Chaos, Vol. 8, No. 8 (1998) 1675–1684

PARAMETRIC RESONANT CONTROL OF CHAOS

RICARDO LIMA*
Centre de Physique Théorique du C.N.R.S.,
Luminy Case 907, F-13288 Marseille, France

MARCO PETTINI†
Osservatorio Astrofisico di Arcetri,
Largo E. Fermi 5, I-50125 Firenze, Italy

Received July 31, 1997

A concise account is given of the early motivations for introducing parametric methods to achieve control of chaos. The heuristic argument that made us think that this kind of method could have been successful is also given. A key study is then reviewed. This concerns a parametric perturbation of a damped and forced Duffing–Holmes oscillator in a chaotic regime. The theoretical analysis, based on the Melnikov treatment of homoclinic tangles, provides a clear understanding of the intimate mechanism that controls chaos. Numerical results confirm and extend the theoretical predictions. A brief discussion of an experimental test on a magneto-elastic device is finally presented.

1. Introduction

It is well known that chaos is rather ubiquitous in both physical and nonphysical nonlinear systems. Sometimes chaos can be useful; this is for instance the case of the ergodic divertor in tokamaks, where a stochastic layer of magnetic field is produced at the plasma edge to improve the confinement. In other cases chaos can have harmful consequences: Plenty of engineering devices could be mentioned [Moon, 1987].

Among physical systems where chaos is harmful, we want to mention an example that motivated our contribution to the field of control of chaos: Magnetic confinement devices for controlled thermonuclear fusion. Here the intrinsic chaoticity of particle dynamics is responsible for an enhanced diffusion across the confining magnetic field; this chaotic (anomalous) transport is much larger than the loss rate predicted by collisional transport theory (see e.g. [Pettini *et al.*, 1988]). The destruction of regular magnetic surfaces, due to chaotic instability, is another unpleasant effect in these systems [Rosenbluth *et al.*, 1966].

Also particle accelerators of betatron type are afflicted by chaotic instabilities, these can be caused by beam–beam interactions in storage-ring colliders [Scandale & Turchetti, 1991].

In some cases one can *a priori* suggest how a machine should be designed in order to avoid the onset of chaos: An example has been given for stellarators [Hanson & Cary, 1984] for which the dangerous parameter ranges have been investigated.

More generally, if a given physical or nonphysical system is satisfactorily described by some nonlinear dynamical model, then by studying — analytically or numerically — its parameter space, it is possible to know how chaos could be avoided.

But, let us consider those situations where one cannot make a system operate in a safe domain of parameter space. In other words, assume that chaos

*E-mail: lima@cptsg2.univ-mrs.fr
†Also at INFN, Sezione di Firenze, and INFM, unità di Firenze, Largo E. Fermi 2, 50125 Firenze, Italy.
E-mail: pettini@arcetri.astro.it

is unavoidable for the operating conditions of your system. For example, this is the case of anomalous transport of energy and particles in tokamaks. Then the only thing you can dream of is to *perturb* your system in a skilful way to reduce or even suppress chaos. This idea, obviously, is not new and dates back to an old preprint (in Russian) [Izrailev & Chirikov, 1974]. These authors studied how a perturbation of an area preserving map can change dramatically the phase space structure, hence the diffusion properties of the model; the drawback is in the choice of the perturbation, which is critical, and on its amplitude, which is not small.

Later on, in a more recent paper [Matsumoto & Tsuda, 1983], a white noise, added to a map modeling the Belusov–Zhabotinsky reaction, was proved useful to reduce or suppress chaos. The explanation is related to the peculiar structure of the invariant density $\rho(x)$ of the map, which is strongly peaked in the region of $|\partial f/\partial x|$ that gives the largest contribution to the Lyapunov characteristic exponent. The introduction of additive noise smears out this peak of $\rho(x)$ thus reducing chaos.

In two subsequent papers (in Russian) [Loskutov, 1987; Alexeev & Loskutov, 1987], a parametric control of chaos has been proved effective in the case of the Rössler attractor and for a system of ODE that models a simple ecosystem. These works are based only upon numerical simulations.

A first account of a theoretical understanding of how chaos can be controlled was given in [Pettini, 1988], where it was presented the possibility of reducing or suppressing chaos by means of parametric excitations on the basis of both analytical and numerical results. Moreover, the suggested method relies upon a "resonant" effect, therefore a *small* relative variation of a parameter is effective, provided that some "resonance" condition is satisfied. Thinking of the practical application of this method, its advantage is that the hardware of a given chaotic system should be only slightly modified, whereas the addition — for example — of new couplings in the system often requires nontrivial modifications.

Then, at the beginning of the '90s, an impressive flourishing of papers occurred on the subject of control of chaos [Chen & Dong, 1993]. At present four main strategies can be roughly identified, they group into two different classes: (1) adaptive — *closed loop* or *feed-back* — methods, requiring an online data acquisition and treatment of the chaotic signal; (2) nonadaptive — *open loop* or *non feedback* — methods, requiring good model equations of the chaotic system. Both of these classes then split into two subclasses: (1) additive methods, where the orbits are directly acted upon; (2) parametric methods, where one or more parameters are varied in time in order to achieve the control of the dynamics.

Claiming that one method is superior to another would be senseless, much depends on the specific problem one has to tackle. Sometimes a feedback method can be implemented, sometimes it is *a priori* unconceivable because following the individual trajectories of a system is impossible; this is the case, for example, of chaotic trajectories of charged particles in a plasma, where an open-loop parametric method is the only hope to control chaos.

Let us now give a heuristic argument which led us to guess that parametric excitations could work. The idea arises from the following observations:

(a) parametric perturbations can modify the stability properties of fixed points of linear (or linearized) systems [Arnold, 1976];
(b) Jacobi equation for the spread of a geodesic flow is a linear equation whose stable and unstable solutions correspond to regular and chaotic flows respectively.

The first item means that the elliptic fixed point $(\dot{x}(0), x(0)) = (0, 0)$ of the linearized pendulum equation

$$\ddot{x} + \omega_0^2 x = 0 \tag{1}$$

can be made unstable substituting $\omega_0^2 \to \omega_0^2(1 + \varepsilon f(t))$, where $f(t) = f(t + T)$. This is a parametrically excited oscillation.

Near the hyperbolic fixed point $(\dot{x}(0), x(0)) = (0, -\pi)$ the same equation reads

$$\ddot{x} - \omega_0^2 x = 0 \tag{2}$$

and the same substitution can make stable the unstable position $(0, -\pi)$ provided that the pivot of the reversed pendulum is in sufficiently rapid oscillation (thus ε has to be large) [Arnold, 1976].

The second item is used *only heuristically* as follows. At least for Newtonian systems, Lagrange equations of motion describe the geodesics of the configuration space manifold equipped with the Riemannian metric [Pettini, 1993] $g_{ij}(\mathbf{x}) = 2[E - U(\mathbf{x})]\delta_{ij}$, where E is the total energy of the system and $U(\mathbf{x})$ is the potential energy; then the

Jacobi equation for the second variation of the action functional describes the local stability of geodesics with respect to a reference geodesic γ : $\{x^i = x^i(s)\}$; when expressed in local coordinates it reads [Pettini, 1993]

$$\nabla^2_{\dot{x}}\xi^i + R^i_{jkl}\dot{x}^j\xi^k\dot{x}^l = 0 \tag{3}$$

where $\nabla_{\dot{x}}$ is the covariant derivative, R^i_{jkl} is the curvature tensor associated to g_{ij}, s is the natural parameter along the geodesic and ξ^i is the Jacobi field of geodesic variation.

For two-dimensional manifolds of constant curvature Eq. (3) simplifies to

$$\frac{d^2\xi_\perp}{ds^2} + K\xi_\perp = 0 \tag{4}$$

where $\xi_\perp$ is the perpendicular component of the Jacobi field ξ and K is the Gaussian curvature of the manifold.

From Eq. (4) it is clear that on a sphere $\mathbb{S}^2$ the geodesics are stable because $K > 0$. At variance, on a compact hyperbolic manifold the geodesics are unstable because $K < 0$ everywhere, and thus the geodesic flow is chaotic. Loosely speaking, to describe regular and chaotic dynamics we have recovered — at another level — Eqs. (1) and (2). Letting $K \to K(1 + \varepsilon f(t))$, as with Eq. (1), one can make exponentially unstable nearby geodesics on a positively curved manifold as a consequence of curvature fluctuations "felt" by the geodesics; this is actually a major mechanism responsible of chaos in Hamiltonian flows of physical relevance [Cerruti-Sola & Pettini, 1996; Pettini & Valdettaro, 1995; Casetti *et al.*, 1996]. Therefore it is also conceivable that a suitable parametric perturbation of Eq. (4) might act to stabilize the exponentially unstable (chaotic) trajectories, when $K < 0$, in analogy with the reversed pendulum Eq. (2). Within this analogy the sign of K should periodically change in time.

This argument is only heuristic because, in general chaotic flows are not topologically equivalent to geodesic flows on manifolds of *constant* negative curvature, if this were the case one should have structural stability (after the Lobatchevsky–Hadamard theorem [Arnold & Avez, 1968]), thus ergodicity, mixing, etc., but this is not the generic situation. In principle this heuristic argument — of differential geometric kind — could be also repeated for dissipative systems using the geometry of Finsler spaces, but this goes far beyond the aim of the present contribution.

The conjecture given above is tested using a dynamical system where, to some extent, chaos can be tackled also analytically.

2. A Paradigmatic System

In [Lima & Pettini, 1990] we chose the so-called Duffing–Holmes oscillator. This model, defined by the equation

$$\ddot{x} - \alpha x + \beta x^3 = -\delta\dot{x} + \gamma\cos\omega t \tag{5}$$

is one of the simplest nonlinear dissipative ODE undergoing a chaotic transition. With some approximations of Galerkin type [Guckenheimer & Holmes, 1983], it can be derived from a PDE describing the dynamics of a buckled beam; in a different context, it can also be used to describe plasma oscillations [Laval & Gresillon, 1979]. Equation (5) can be trivially rewritten as (we set $\alpha = 1$ without loss of generality)

$$\begin{pmatrix}\dot{x}\\ \dot{y}\end{pmatrix} = \begin{pmatrix} y \\ x - \beta x^3\end{pmatrix} + \varepsilon\begin{pmatrix} 0 \\ -\dfrac{\delta}{\varepsilon}y + \dfrac{\gamma}{\varepsilon}\cos\omega t\end{pmatrix} \tag{6}$$

which is in the form

$$\dot{\mathbf{x}} = \mathbf{f}_0(\mathbf{x}) + \varepsilon\mathbf{f}_1(\mathbf{x}, t)\,. \tag{7}$$

The unperturbed part $\dot{\mathbf{x}} = \mathbf{f}_0(\mathbf{x})$ can be derived from the Hamiltonian

$$H = \frac{1}{2}y^2 - \frac{1}{2}x^2 + \frac{1}{4}\beta x^4 \tag{8}$$

and is integrable. Its phase space has only one hyperbolic fixed point from which an "eight-shaped" separatrix originates. The motion on this separatrix is given by

$$\begin{aligned} x^{(0)}(t) &= \sqrt{\frac{2}{\beta}}\operatorname{sech} t\,, \\ \dot{x}^{(0)}(t) &= -\sqrt{\frac{2}{\beta}}\operatorname{sech} t\ \tanh t\,. \end{aligned} \tag{9}$$

The separatrix, parametrically defined by Eq. (9), is also called homoclinic loop and results from the superposition of the so-called stable and unstable manifolds, W^s and W^u, respectively tangent at the origin to the stable and unstable eigenspaces E^s and E^u of the hyperbolic point. W^s and W^u are defined as those trajectories which converge asymptotically

to the hyperbolic fixed point: W^s for $t \to +\infty$ and W^u for $t \to -\infty$ respectively. When the system $\dot{\mathbf{x}} = \mathbf{f}_0(\mathbf{x})$ is perturbed only by a dissipative term, the two manifolds $W^{s,u}$ never meet and the solutions are still regular. If a forcing term is also added (i.e. an energy supply is added to balance friction losses) then $W^{s,u}$ may have an homoclinic intersection and hence an infinity of subsequent intersections [Guckenheimer & Holmes, 1983]. We briefly recall how Melnikov's method works to determine the condition of homoclinic intersection of W^s and W^u and so of the onset of chaos. Let $\Gamma^{(0)}(t) = (\dot{x}^{(0)}(t), x^{(0)}(t))^T$ be the unperturbed motion on the homoclinic loop, write

$$W^{s,u}(t, t_0) \simeq \Gamma^{(0)}(t - t_0) + \varepsilon W^{s,u}{}_1(t, t_0) \qquad (10)$$

to describe how $W^{s,u}$ are perturbed up to first order in ε [due to $\mathbf{f}_1$ in Eq. (7)] starting from $\Gamma^{(0)}$; t_0 is an arbitrary reference time and $W^{s,u} \equiv (\dot{x}^{s,u}, x^{s,u})^T$ are column vectors. One gets

$$\frac{d}{dt} W^{s,u}{}_1 = \mathbf{J}(\Gamma^{(0)}(t - t_0)) W^{s,u}{}_1 + \varepsilon \mathbf{f}_1(\Gamma^{(0)}(t - t_0), t) \qquad (11)$$

where $\mathbf{J}$ is the Jacobian matrix of $\mathbf{f}_0$ computed at $\Gamma^{(0)}(t - t_0)$.

Then the Melnikov distance is defined as

$$\Delta(t, t_0) = \mathbf{n} \cdot (W_1^s(t, t_0) - W_1^u(t, t_0)) \qquad (12)$$

where $\mathbf{n}$ is the normal to $\Gamma^{(0)}(t - t_0)$.

After some algebra one finally finds the Melnikov function

$$\Delta(t_0) = -\int_{-\infty}^{\infty} dt (\mathbf{f}_0 \wedge \mathbf{f}_1)_{\Gamma^{(0)}(t - t_0)} \qquad (13)$$

which in principle can be explicitly computed; if $\Delta(t_0)$ changes sign for some t_0, then an infinity of homoclinic intersections between W^u and W^s will take place and chaos will set in. This is the only *general* predictive method to study the condition for the onset of chaos in dissipative ODE.

Notice that for Hamiltonian systems there are always homoclinic intersections when a nonintegrable perturbation $\varepsilon \mathbf{f}_1(\mathbf{x}, t)$ is added to an integrable system; in this case the Melnikov function [Chirikov, 1979] is

$$M(t_0) = -\int_{-\infty}^{\infty} dt \{H_0, H_1\}_{\Gamma^{(0)}(t - t_0)}, \qquad (14)$$

where curly brackets are Poisson brackets, of the unperturbed Hamiltonian H_0 with the perturbation Hamiltonian H_1, computed along the unperturbed separatrix $\Gamma^{(0)}$; $M(t_0)$ is useful to evaluate the thickness of the stochastic layer. The analytical computation of $\Delta(t_0)$ for Eq. (6) is standard and yields

$$\Delta(t_0) = 2\pi \sqrt{\frac{2}{\beta}} \gamma \omega \operatorname{sech}\left(\frac{\pi\omega}{2}\right) \sin \omega t_0 + \frac{4\delta}{3\beta}. \qquad (15)$$

Unfortunately there are not so many models for which explicit computation of $\Delta(t_0)$ can be performed. Therefore we chose Duffing–Holmes model because it is not difficult to compute $\Delta(t_0)$ when a parametric perturbation is introduced.

Let us modify Eq. (6) to

$$\begin{pmatrix} \dot{x} \\ \dot{y} \end{pmatrix} = \begin{pmatrix} y \\ x - \beta(1 + \eta \cos \Omega t) x^3 \end{pmatrix} + \varepsilon \begin{pmatrix} 0 \\ -\dfrac{\delta}{\varepsilon} y + \dfrac{\gamma}{\varepsilon} \cos \omega t \end{pmatrix}, \qquad (16)$$

if $\eta \ll 1$ we are allowing a periodic modulation of small amplitude of the parameter β.

Accounting for the modulating term $\beta\eta \cos \Omega t\, x^3$ in the perturbation function $\mathbf{f}_1$, the new Melnikov function $\Delta_p(t_0)$ is given by

$$\Delta_p(t_0) = \Delta(t_0) - \frac{\eta}{\beta} \int_{-\infty}^{\infty} dt\, \dot{x}^{(0)}(t - t_0) \times [x^{(0)}(t - t_0)]^3 \cos \Omega t \qquad (17)$$

using (10), after simple but tedious computations, one finds [Lima & Pettini, 1990, 1993]

$$\Delta_p(t_0) = 2\pi \sqrt{\frac{2}{\beta}} \gamma \omega \operatorname{sech}\left(\frac{\pi\omega}{2}\right) \sin \omega t_0 + \frac{4\delta}{3\beta} - \frac{\pi\eta}{6\beta} (\Omega^4 + 4\Omega^2) \operatorname{cosech}\left(\frac{\pi\Omega}{2}\right) \sin \Omega t_0 . \qquad (18)$$

Let us now consider a set of parameters for which $\Delta(t_0)$ changes sign, thus predicting the existence of chaos; then we add the parametric perturbation as in Eq. (16) and we compute, from the numerical tabulation of Eq. (18), the time needed between two successive homoclinic intersections of W^u and W^s, let us denote it by τ_M.

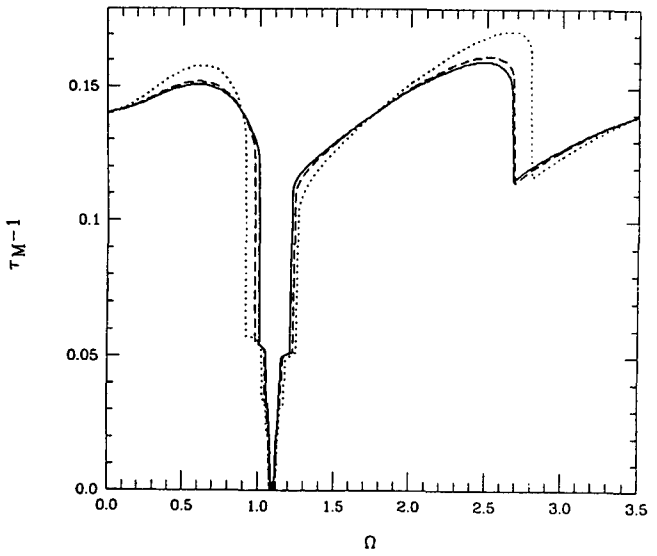

Fig. 1. The inverse of the time τ_M elapsed between two successive homoclinic intersections, computed using Eq. (18), is plotted versus the parametric perturbation frequency Ω. Again $\beta = 4$, $\delta = 0.154$, $\gamma = 0.088$, $\omega = 1.1$. Continuous line corresponds to $\eta = 0.09$, dashed line to $\eta = 0.1$ and dotted line to $\eta = 0.15$.

In Fig. 1, τ_M^{-1} is reported versus the parametric perturbation frequency Ω for the following set of parameters: $\gamma = 0.088$, $\delta = 0.154$, $\omega = 1.1$, $\beta = 4$, $\eta = 0.1$.

A "resonance line" is found which is centered at $\Omega \equiv \omega$; for this value of Ω, τ_M becomes infinite; this means that W^u and W^s never intersect, hence chaos should disappear.

If η is smaller than some critical value η_c, then τ_M remains finite and homoclinic intersections are not suppressed. By increasing η above η_c, a *line broadening* is observed (see Fig. 1). Finally, outside the interval of Ω where the quartic polynomial in Eq. (18) is negative, there is no way to avoid intersections of W^u and W^s.

Similar results are obtained for different sets of parameters.

Accurate numerical experiments can be performed to make a comparison with these predictions. Equation (16) is integrated using a Hammings modified predictor-corrector of fourth order, time integration steps $\Delta t = 0.001 - 0.003$ and integration times of $t = 10\,000 - 20\,000$ after a transient of $t = 500$. By means of a standard technique [Benettin *et al.*, 1979], the largest Lyapunov characteristic exponent λ is computed to detect chaos and measure its strength.

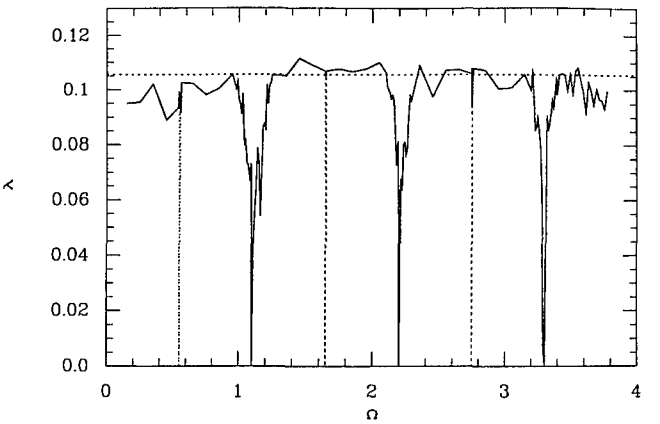

Fig. 2. The largest Lyapunov characteristic exponent λ is reported versus Ω. This result corresponds to $\beta = 4$, $\delta = 0.154$, $\gamma = 0.088$, $\omega = 1.1$, $\eta = 0.03$. The dotted line refers to $\eta = 0$ (unperturbed case) for which $\lambda = 0.1056$. Dotted lines are also used for subharmonic resonances whose existence depends on the starting point in phase space.

For the same set of parameters in Fig. 1, except for η which is 0.03, λ is computed for different values of the parametric perturbation frequency Ω. The results are shown in Fig. 2 and are rather striking. The resonance line displayed in Fig. 1 by $\tau_M^{-1}(\Omega)$, $\Omega \sim \Omega_R^0 = 1.1$ corresponds to the first order resonance of $\lambda(\Omega)$ in Fig. 2. Moreover, other resonances show up: at $\Omega = 2.2$ and $\Omega = 3.3$, second and third harmonics of Ω_R^0 respectively, at $\Omega = 0.55$ and $\Omega = 2.75$, i.e. at the first subharmonic of Ω_R^0 and at the third harmonic of the subharmonic. These last resonances are very narrow and correspond to suppression of chaos ($\lambda = 0$) only if the initial conditions belong to a suitable domain.

In Fig. 3 it is shown that a *resonance broadening* is produced at increasing perturbation amplitude, which is at least in qualitative agreement with the analytical result reported in Fig. 1.

Another way to get a hold of what happens to the dynamics when the parametric perturbation frequency approaches a resonant value, is to look at the autocorrelation function $\langle x(t + \Delta t)x(t)\rangle$ of the solution of Eq. (5). In [Lima & Pettini, 1990] some of them are reported and show an increasing correlation time — thus a decreasing chaoticity -- when Ω approaches a resonant value (in this case $\Omega_R^{(1)}$).

We thus have a paradigmatic example showing that chaos can be reduced or eliminated in a dissipative system by means of parametric perturbations. A 3% modulation of a parameter, when the modulation frequency is resonant with the forcing frequency, is able to make regular the chaotic

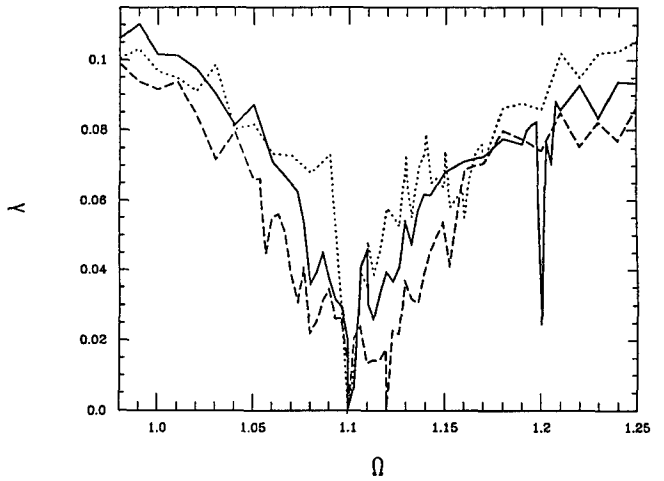

Fig. 3. λ versus Ω for $\beta = 4$, $\delta = 0.154$, $\gamma = 0.088$, $\omega = 1.1$ at different parametric perturbation amplitude. Dotted line corresponds to $\eta = 0.03$, continuous line to $\eta = 0.05$ and dashed line to $\eta = 0.07$.

dynamics. Let us just spend few words about Hamiltonian systems. We have already mentioned that in this case chaos is always present, therefore one can "only" hope either to stabilize some broken KAM tori, or to modify the diffusion properties of the model. Some attempts made with the Hamiltonian version of the Duffing–Holmes oscillator and with the systems of [Pettini *et al.*, 1988], show that sometimes several small and sticky islands can be produced by parametric perturbations; the major consequence is a slowing down of diffusion in phase space due to intermittent trapping near islands. An increase of intermittency is revealed by a worse convergence of maximal Lyapunov exponent caused by enhanced fluctuations of local divergence rate of nearby trajectories. In general, stronger perturbations are necessary to produce measurable effects.

3. An Experimental Confirmation

The model equation above studied is well suited also for an experimental test of the practical applicability of the method [Fronzoni *et al.*, 1991].

The experimental apparatus consists of a magnetoelastic device schematically represented in Fig. 4: A steel-made elastic beam is clamped at one end and is left free at the other end; near the free end of the beam two magnets create a two-well potential with two stable equilibria. The whole system is put in vibration by means of an electromagnetic shaker. If the forcing is not too strong,

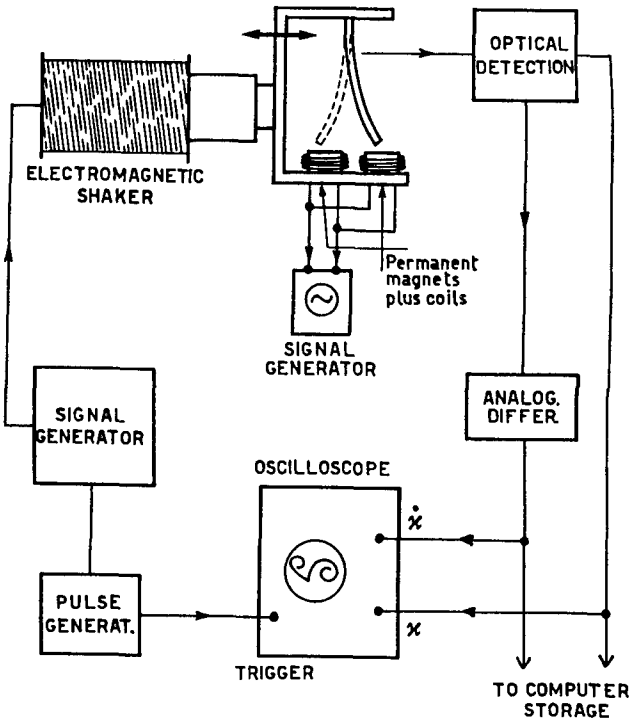

Fig. 4. Sketch of the experimental apparatus.

a one mode approximation of Galerkin type can be done on the partial differential equation that describes this flexible pendulum [Marsden & Holmes, 1980], so that the single mode amplitude obeys the Duffing–Holmes ordinary differential Eq. (5). In order for a parametric perturbation to act upon the system, the permanent magnets of the experimental apparatus are surrounded by coils of copper wires. An oscillating electric current in the coils gives a modulation of the magnetic field at the end of the beam so that α and β in Eq. (5) become

$$\alpha \to \alpha[1 + \varepsilon \cos(2\pi\nu_M t)], \quad \varepsilon \ll 1 \qquad (19)$$

$$\beta \to \beta[1 + \eta \cos(2\pi\nu_M t)], \quad \eta \ll 1. \qquad (20)$$

The bending of the beam can be measured by an optical device: A thin screen fixed on the elastic beam makes an occultation of a light source, then the resulting light intensity, measured by a photoresistence, reveals the fundamental mode amplitude of the deflection which is described in Eq. (5).

The dynamics of the system can be examined with the aid of an oscilloscope where the portraits $(x, \dot{x})$ of the Poincaré sections of the phase space are obtained by modulating the z-axis of the oscilloscope with a signal synchronized to the driving signal of the vibrator. A typical Poincaré section, obtained when chaotic vibrations are present, is

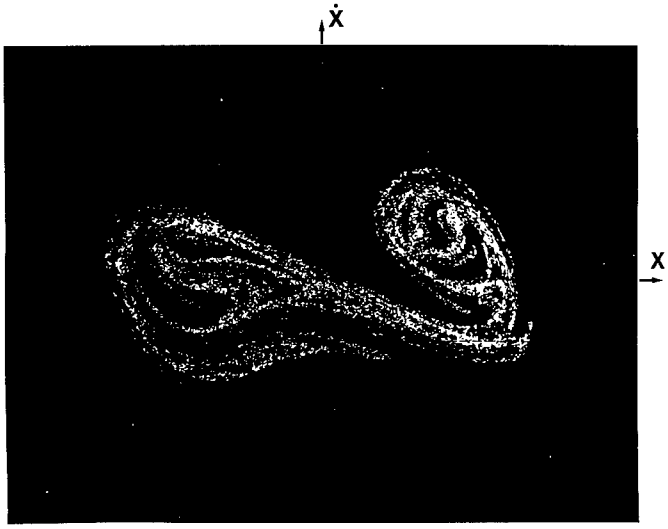

Fig. 5. Poincaré section obtained with 300 seconds of acquisition time. About 1000 points are displayed. $\nu_F = 13.03$ Hz, $A/A_c = 1.33$, $\varepsilon = \eta = 0$.

reproduced in Fig. 5. Long runs (several hours) of the experimental apparatus ensure that chaos is stable in the system.

A current flowing through the coils around the permanent magnets changes the magnetic field intensity at the end of the elastic beam, this means that the parameters α and β are modified according to Eq. (20).

When a modulation voltage is applied to the coils, the response is like in Fig. 6, where the voltage output (proportional to $x(t)$) is displayed versus time. At modulation frequencies ν_M close to the forcing frequencies ν_F chaotic vibration is alternated by ordered vibrations. Ordered phases are almost periodic oscillations around one of the two minima of the potential with $x(t)$ locked to the forcing signal.

The average duration of the regular vibrations increases when $|\nu_F - \nu_M|$ is reduced. Roughly speaking, the parametric perturbation makes the system intermittent and by approaching a resonance between ν_F and ν_M the laminar phase has an increasing weight with respect to the chaotic phase. Complete regularization of the dynamics shows up only at exact resonance. A modulation of the 10% of the unperturbed value of α (i.e. $\varepsilon = 0.1$) is needed to produce the result reported in Fig. 6.

A less qualitative description of phenomenon is given in Fig. 7, where the amplitude output of a Lock-in measurement device is reported versus the perturbation frequency ν_M when the forcing signal

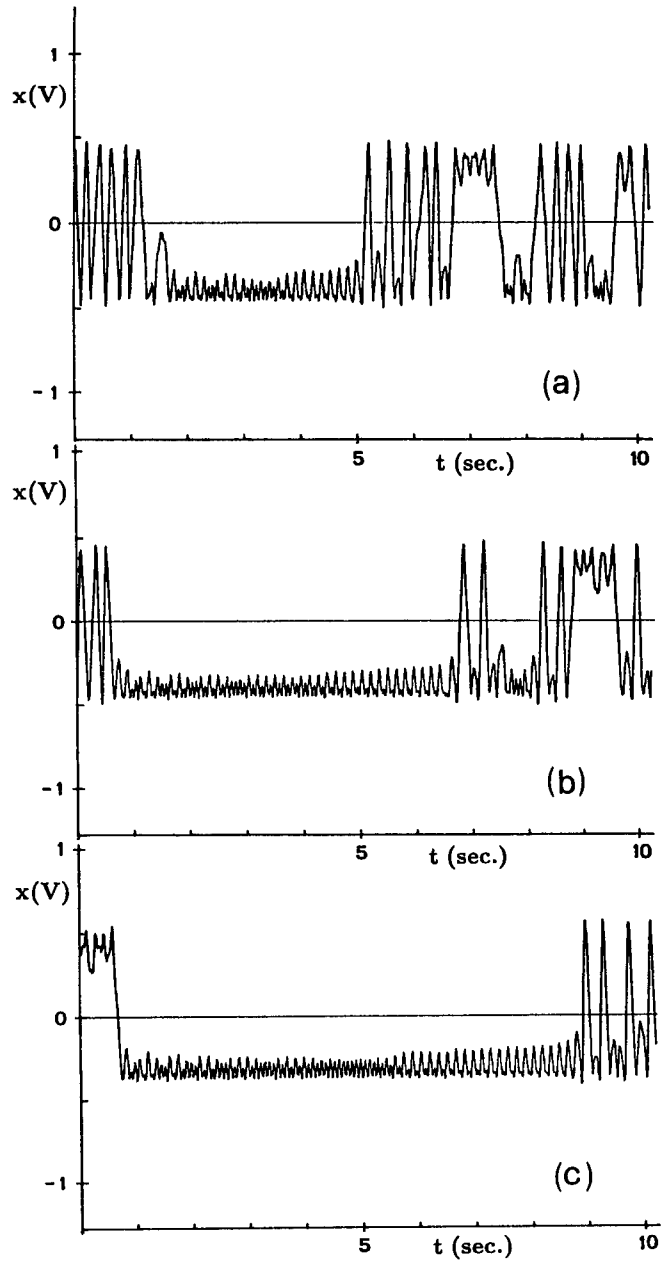

Fig. 6. Oscillation amplitude $x(t)$, measured in Volts, at $\nu_F = 13.03$ Hz, $\varepsilon = 0.1$, $\eta = 0.08$, $A/A_c = 1.33$. (a) $\nu_M = 13.06$ Hz; (b) $\nu_M = 13.07$ Hz; (c) $\nu_M = 13.08$ Hz.

is sent also to the reference of the Lock-in. The tracings display typical resonance patterns. These show how the relative weight of laminar phases with respect to chaotic phases changes as a function of parametric modulation frequency. The two upper curves correspond to different amplitudes of the modulation ($\varepsilon = 0.16$ and $\varepsilon = 0.1$ from top to bottom) and show a resonance broadening at increasing ε. The maxima of the peaks correspond to $\nu_M \simeq \nu_F$. The same effect of parametric

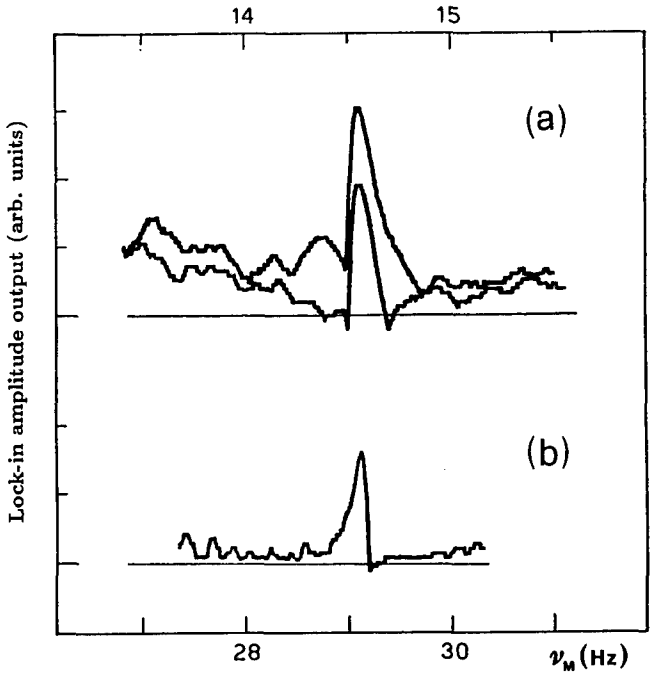

Fig. 7. Lock-in amplitude output (arbitrary units) versus ν_M. Sweep time: 1175 sec/Hz. Lock-in integration time: 300 sec. $\nu_F = 14.59$ Hz and $A/A_c = 1.33$. (a) upper curve refers to $\varepsilon = 0.16$; lower curve refers to $\varepsilon = 0.1$. (b) second harmonic resonance, $\varepsilon = 0.12$.

modulation is found at $\nu_M \simeq 2\nu_F$ and this too is reported in Fig. 7 (lower curve).

In the experimental device it is not possible to avoid the contemporary modulation of α and β, therefore one has to adapt the above theoretical analysis to this case. The Melnikov function must be computed for Eq. (5) with the modulations given by Eq. (20). The new result — (setting $\Omega = 2\pi\nu_M$ and $\omega = 2\pi\nu_F$) — reads

$$\Delta(t_0) = 2\pi\omega A\sqrt{\frac{2}{\beta}}\,\mathrm{sech}\left(\frac{\pi\omega}{2\sqrt{\alpha}}\right)\sin(\omega t_0) + \left[\frac{\pi\epsilon\alpha^2}{\beta}\left(\frac{\Omega^2}{\alpha}-1\right) - \frac{\pi\eta}{6\beta}(\Omega^4+4\Omega^2)\right] \times \mathrm{cosech}\left(\frac{\pi\Omega}{2\sqrt{\alpha}}\right)\sin(\Omega t_0) + \frac{4\gamma\alpha^{3/2}}{3\beta}. \quad (21)$$

At $\eta = \varepsilon = 0$, if the parameters are such that the function $\Delta(t_0)$ changes sign then homoclinic intersections are present and hence the existence of chaotic solutions is inferred. At $\varepsilon, \eta \neq 0$, as the sign of the polynomial function of Ω is indefinite, the second term of Eq. (21) can act as a counterterm of the first one. As a consequence, also choosing the unperturbed system in a chaotic phase, it is again possible to prevent $\Delta(t_0)$ from changing sign (i.e. to eliminate chaos), provided that Ω is resonant and that the other parameters are in suitable domains.

4. Concluding Remarks

We have briefly shown that open-loop parametric control of chaos is successful. The model here discussed is somehow paradigmatic because, beside the general heuristic argument, we have at disposal an analytical prediction — based on the only predictive method existing at present (Melnikov's theory) — and numerical simulations confirming the theoretical analysis, and finally an experimental confirmation on a physical system.

Numerical simulations confirmed the analytical predictions revealing at the same time a richer phenomenology, which is not surprising because Melnikov's theory is based on an approximate method.

The experimental confirmation is crucial at least for two reasons: The obvious one is to show that the method can be successfully implemented in real systems, the other is that the possibility of controlling chaos by parametric perturbations turns out to be *robust*, in fact our experimental system is only *roughly* modeled by a Duffing–Holmes equation, nevertheless the method works, this suggests that the choice of good model equations is certainly important but not critical.

Many problems are open and need a deeper understanding. Among the open questions we mention that:

(i) The development of a more general theoretical framework requires to go beyond Melnikov's theory which is undoubtely general but it applies to weakly perturbed systems and it is of practical utility only in a few simple cases. An interesting direction for further research work on this topic could be provided by optimal control theory, *à la* Pontrjaguin, i.e. to minimize the functional

$$J = \int_{t_0}^{t_1} dt\, A(\mathbf{x}(t), u(t)) + \mu\int_{t_0}^{t_1} dt \sum_{i=1}^{N}[\dot{x}_i - f_i(\mathbf{x}(t), u(t))]^2 \quad (22)$$

where the dynamic constraints $\dot{x}_i = f_i(\mathbf{x}(t), u(t))$ have been introduced with a Lagrange

multiplier μ and where the (vector) function $u(t)$ represents the control(s) with respect to which the functional J has to be minimized. Here the problem is to find a good function $A(\mathbf{x}(t), u(t))$ that attains its minimum in correspondence of ordered motions.

(ii) The above results raise an intriguing problem in connection with the so-called "stability dogma" [Guckenheimer & Holmes, 1983]: If you observe chaos in real systems it must be structurally stable (in the strong sense) and the same should hold for the theoretical models used. In fact theoretical models will never take into account all the interactions, perturbations, noise, etc. which are present in real systems. Attempts to soften the definition of structural stability have been proposed some years ago [Zeeman, 1988].

(iii) In this context it is not out of place to mention that, after the Birkhoff–Smale homoclinic theorem [Guckenheimer & Holmes, 1983], the existence of homoclinic intersections for the Duffing–Holmes oscillator ensures the existence of a hyperbolic invariant set Λ. Other considerations [Guckenheimer & Holmes, 1983] rule out, for the same model, the possibility for Λ to be an attractor. There are several reasons to believe that noise, which is always present both in real systems and in numerical models, plays an important role together with Λ to stabilize chaotic transients or, at least, to make them very long with respect to practical observational times.

References

Alexeev, V. V. & Loskutov, A. Yu. [1987] "Destochastization of a system with a strange attractor by parametric interaction," *Dokl. Akad. Nauk SSSR* **293**, 1346–1349.

Arnold, V. I. [1976] *Les Méthodes Mathématiques de la Méchanique Classique* (Editions MIR, Moscow).

Arnold, V. I. & Avez, A. [1968] *Ergodic Problem of Classical Mechanics* (W. A. Benjamin Inc., NY).

Benettin, G., Galgani, L. & Strelcyn, J. M. [1976] "Kolmogorov entropy and numerical experiments," *Phys. Rev.* **A14**, 2338–2345.

Casetti, L., Clementi, C. & Pettini, M. [1996] "Riemannian theory of Hamiltonian chaos and Lyapunov exponents," *Phys. Rev.* **E54**, 5969–5984.

Cerruti-Sola, M. & Pettini, M. [1996] "Geometric description of chaos in two-degrees of freedom Hamiltonian systems," *Phys. Rev.* **E53**, 179–188.

Chirikov, B. V. [1979] "A universal instability of many-dimensional oscillator systems," *Phys. Rep.* **52**, 263–379.

Chen, G. & Dong, X. [1993] "From chaos to order — Perspectives and methodologies in controlling chaotic nonlinear dynamical systems," *Int. J. Bifurcation and Chaos* **3**, 1363–1409.

Fronzoni, L., Giocondo, M. & Pettini, M. [1991] "Experimental evidence of suppression of chaos by resonant parametric perturbations," *Phys. Rev.* **A43**, 6483–6487.

Guckenheimer, J. & Holmes, P. [1983] *Nonlinear Oscillations, Dynamical Systems, and Bifurcations of Vector Fields* (Springer-Verlag, NY).

Hanson, J. D. & Cary, J. R. [1984] "Elimination of stochasticity in stellarators," *Phys. Fluids* **27**, 767–769.

Izrailev, F. M. & Chirikov, B. V. [1974] *Numerical Experiments on Stabilization of Stochastic Instability with the Use of Computer in Interactive Regime* (in Russian), I.Ya.F. preprint 74-13, Novosibirsk.

Lima, R. & Pettini, M. [1990] "Suppression of chaos by resonant parametric perturbations," *Phys. Rev.* **A41**, 726–733.

Lima, R. and Pettini, M. [1993] "Reply to comment on suppression of chaos by resonant parametric perturbations," *Phys. Rev.* **E47**, 4630–4631.

Loskutov, A. Yu. [1987] *Parametric Destochastization of a System with a Strange Attractor of a Spiral Type* (in Russian), preprint n. 4802-B87, Phys. Dept. Univ. Moscow.

Laval, G. & Gresillon, D. (eds.) [1979] "Intrinsic stochasticity in plasmas," (Les Edition de Physique Courtaboeuf, Orsay).

Marsden, J. E. & Holmes, P. J. [1980] "A horseshoe in the dynamics of a forced beam," in *Nonlinear Dynamics*, ed. Helleman, R. H. G. (The New York Academy of Science, NY).

Matsumoto, K. & Tsuda, I. [1983] "Noise induced order," *J. Stat. Phys.* **31**, 87–106.

Moon, F. C. [1987] *Chaotic Vibrations. An Introduction for Applied Scientists and Engineers* (John Wiley, NY).

Pettini, M. *et al.* [1988] "Chaotic diffusion across a magnetic field in a model of electrostatic turbulent plasma," *Phys. Rev.* **A38**, 344–363, and references quoted therein.

Pettini, M. [1988] "Controlling chaos through parametric excitations," in *Dynamics and Stochastic processes*, eds. Lima, R., Streit, L. & Vilela-Mendes, R. V. (Springer-Verlag, NY), pp. 242–250.

Pettini, M. [1993] "Geometrical hints for a nonperturbative approach to Hamiltonian dynamics," *Phys. Rev.* **E47**, 828–850, and general references quoted therein.

Pettini, M. & Valdettaro, R. [1995] "On the

Riemannian description of chaotic instability in Hamiltonian dynamics," *Chaos* **5**, 646–652.

Rosenbluth, M. N., Sagdeev, R. Z., Taylor, J. B. & Zaslavsky, G. M. [1966] "Destruction of magnetic surfaces by magnetic field irregularities," *Nucl. Fusion* **6**, 297–300.

Scandale, W. & Turchetti, G. (eds.) [1991] *Nonlinear Problems in Future Particle Accelerators* (World Scientific, Singapore).

Zeeman, E. C. [1988] "Stability of dynamical systems," *Nonlinearity* **1**, 115–155.

International Journal of Bifurcation and Chaos, Vol. 8, No. 8 (1998) 1685–1691

ADAPTIVE MODE SELECTION BASED ON CHAOTIC SEARCH IN A FABRY–PEROT LASER DIODE

YUN LIU* and PETER DAVIS
ATR Adaptive Communications Research Laboratories,
2-2 Hikaridai, Seika-cho, Soraku-gun, Kyoto 619-0288, Japan

Received July 31, 1997; Revised December 9, 1997

This paper describes mode-transition dynamics of a compound-cavity, multimode, Fabry–Perot (FP) semiconductor laser and the basic idea of adaptive wavelength selection using chaotic search. In the presence of external feedback, the laser is shown to exhibit different mode-competition dynamics including single-mode, multistability, and chaotic mode-transition states. A chaotic search technique is proposed to adaptively select a dominant lasing mode which fits the environment by switching a control parameter (feedback level or bias injection) between multistability and chaotic mode-transition states. The effectiveness of the adaptive mode selection is verified through a computer simulation and the robustness as well as the experimental implementation of the technique are discussed.

1. Introduction

Applications of chaotic dynamics have received much attention in recent studies of nonlinear dynamics. One promising topic is adaptive mode selection using chaotic search [Davis, 1990] which utilizes the global properties of a chaotic system and the bifurcation from multistable regime to chaotic regime. This method was successfully applied to adaptive oscillation mode selection in an electro-optical system [Aida & Davis, 1994; Liu & Davis, 1997].

This paper describes the application of the chaotic search to a multimode FP semiconductor laser with external optical feedback. Experiments have revealed that the external reflectivity as well as the external cavity length exert essential influences on dynamical and spectral behaviors of a laser diode in an external cavity (e.g. [Mørk *et al.*, 1992; Uenishi *et al.*, 1996]). The purpose of this paper is to investigate the mode-competition dynamics in the external cavity laser and to verify whether it has a bifurcation structure which is suitable for performing adaptive mode (wavelength) selection using chaotic search, that is, multistability of modes and an onset of chaotic transitions among the different modes.

The paper is organized as follows. In the next section, we first introduce a numerical model of a multimode laser with external feedback and compare numerical results for the spectral distribution with experimental observations. The mode-competition dynamics are characterized by mode power and dominant mode distributions, and based on these measures, the laser output is classified into three different regimes: single dominant mode regime (only one mode dominates the lasing), multistability regime (different modes become dominant depending on initial condition), and chaotic mode-transition regime. In particular, we show that it is possible to switch between the multistability and chaotic mode transition regimes by switching a control parameter: external feedback strength or injection current. In Sec. 3, we show that adaptive mode selection using chaotic search can be performed by

*E-mail: y-liu@acr.atr.co.jp

coupling the control parameter to an external evaluation signal. The effectiveness of the adaptive mode selection technique is verified by computer simulations. The robustness and possible experimental implementation of the technique are also discussed. The last section summarizes the paper with a comment on potential applications of the proposed chaotic search scheme to other lasers.

2. Mode-Competition Dynamics and Bifurcation Diagrams

As a reference for the numerical modeling, we first show an experimental optical spectrum of a typical laser diode with moderate optical feedback ($1 \sim 10\%$). The laser employed in the observation of Fig. 1 is a AlGaAs laser diode with a center mode wavelength of about 782 nm at the threshold bias current of 45 mA. It is well known that a FP semiconductor laser subject to moderate to strong feedback often exhibits multimode behavior. In this experiment, it is found that about 10 modes have power levels within 10% of that of the peak mode power.

The dynamics of the above laser can be described by a set of multimode rate equations including the external feedback and Langevin noise [Byrne, 1992; Ryan *et al.*, 1994].

$$\frac{dE_m(t)}{dt} = i(\omega_m - \omega_{\text{th}})E_m(t) + \frac{1}{2}(1 - i\alpha)(G_m - \gamma)E_m(t) + \kappa E_m(t - \tau)\exp(i\omega_m\tau) - \frac{1}{2}\sum_k \theta_{mk}|E_k(t)|^2 E_m(t) + F_m(t)\,, \quad (1)$$

$$\frac{dN(t)}{dt} = J - \frac{N(t)}{\tau_s} - \sum_{j=1}^{M} G_j|E_j(t)|^2 + F_N(t)\,. \quad (2)$$

Here, E_m is the complex optical field of the mth ($m = 1, 2, \ldots, M$) longitudinal mode and is scaled so that $|E_m|^2$ corresponds to the photon number within the laser cavity, $N(t)$ is the carrier number within the laser cavity, ω_m, λ_m, G_m are respectively the angular frequency, wavelength, and gain of the mth mode. γ is the loss coefficient of the laser, τ_s is the life time of carriers, τ is the time delay in the external feedback, ω_{th} is the angular frequency of the solitary laser without external feedback, α is the linewidth enhancement factor, θ_{mk} is the coefficient for cross-saturation between modes m and k, J is the bias injection, and F_m, F_N are Langevin noise terms. We did not include noises in the current simulations in order to distinguish effects of deterministic chaos from stochastic noise. The expression for the mode gain G_m is given by

$$G_m = g[N(t) - N_0][1 - (\lambda_m - \lambda_p)^2/\Delta\lambda_g^2]\,, \quad (3)$$

where g is the gain coefficient, N_0 is the carrier number at transparency, λ_p is the wavelength of the peak gain, and $\Delta\lambda_g$ is the full width half maximum (FWHM) value of the parabolic gain curve. The feedback level κ is given by

$$\kappa = (1 - r_0^2)r_1/\tau_{\text{in}}r_0\,, \quad (4)$$

where τ_{in} is the round-trip time of the laser cavity and r_0 and r_1 are internal cavity reflection

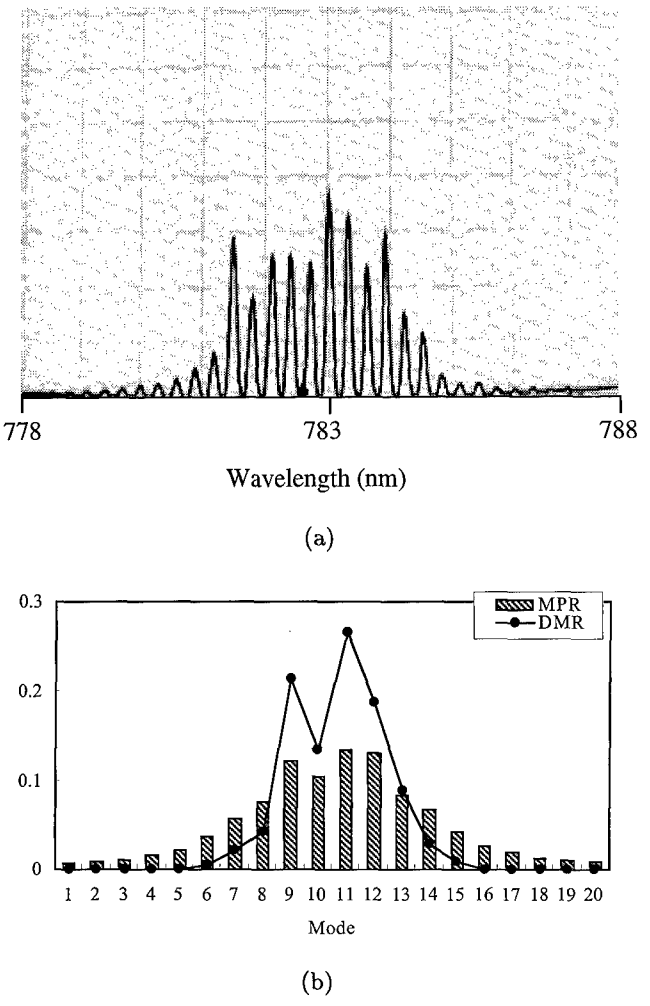

Fig. 1. Optical spectra of a FP laser diode with external feedback. (a) Experimental and (b) simulation results. The vertical scale of (a) is 50 nW/div.

Table 1. Some parameter values for the laser diode used in the numerical calculations.

Symbol	Parameter	Value
λ	Center wavelength	780 nm
$\delta\lambda_m$	Wavelength separation	0.28 nm
$\delta\lambda_g$	FWHM of laser gain	100 nm
l	Laser cavity length	250 mm
r_0	Facet reflectivity	0.5556
g	Gain coefficient	1639 s^{-1}
γ	Loss coefficient	5.3×10^{11} s^{-1}
α	Linewidth enhancement factor	3
N_0	Carrier number at transparency	1.75×10^8
$N_{\rm th}$	Carrier number at threshold	4.99×10^8
τ_s	Life time of carrier	2.0 ns
$\tau_{\rm in}$	Round-trip time of laser cavity	5.9 ps
θ_{mm}	Saturation coefficient	2.8×10^4 s^{-1}
θ_{mk}	Cross-saturation coefficient	2.5×10^4 s^{-x1}

and external reflection coefficients (both in amplitude), respectively. Modes couple with each other through the depletion of the commonly shared carriers [Eq. (2)] and the gain cross-saturation effect. We neglect the small contribution from spontaneous emission to the lasing mode. This factor is evaluated to be much smaller (less than one percent) than the feedback term (at $r_1 = 1\%$) and negligible compared with both the gain and loss factors. Based on the observed optical spectrum, we assume the bandwidth of the laser gain to be 100 nm with the center wavelength at 780 nm and the total mode number M to be 20 which is large enough to cover the experimental spectrum. Other parameters and parameter values employed in the calculation are listed in Table 1 [Lang & Kobayashi, 1980; Mørk *et al.*, 1992; Ryan *et al.*, 1994].

We have numerically simulated Eqs. (1) and (2) by employing a fourth order Runge–Kutta algorithm and investigated dynamical states for different parameter conditions. Figure 1(b) shows a numerical result for the optical spectrum of the laser with external feedback. The spectrum is quite similar to the experimental result in Fig. 1(a) and this justifies the numerical model and the parameter values used.

To characterize mode states of the multimode LD, we introduced two measures, namely, mode–power–ratio (MPR) and dominant–mode–ratio (DMR). MPR stands for a long-term average of the light power of each mode. The distribution of MPR shows the optical spectrum of the laser during a specified time interval. Meanwhile, DMR shows how frequently a specific mode dominates the laser output. The two factors are respectively defined as

$$(\mathrm{MPR})_i = \int |E_i(t)|^2 dt \Big/ \sum_j \int |E_j(t)|^2 dt\,, \quad (5)$$

and

$$(\mathrm{DMR})_i = \int \left\{ \prod_{j \neq i} \theta[E_i(t) - E_j(t)] \right\} dt \Big/ \int dt\,, \quad (6)$$

where $\theta(x)$ is a step function and takes 1 for $x > 0$ and 0 otherwise.

We mention that nonlinear dynamics and mode interactions of multimode lasers have been studied in various experimental systems and numerical models. For example, Byrne [1992] calculated the averaged response and the stochastic response of a multimode laser under Gb/s modulation. Bracikowski and Roy [1991] investigated periodic pulsing of a multimode solid-state laser and found antiphase cycling among different modes. Ryan *et al.* [1994] investigated intensity noise features of a multimode laser diode with external feedback and observed mode transitions in the time evolution of the laser output. Recently, Szwaj *et al.* [1996] observed wave propagation in the

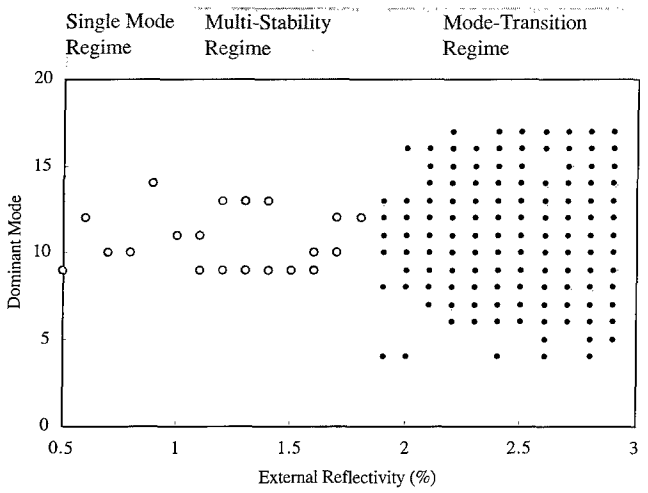

Fig. 2. Bifurcation diagram of mode-competition states versus external reflectivity. White circles and solid dots denote respectively stable and temporary dominant modes. Parameters are $I_b = 1.5\ I_{\rm th}$ and $L_{\rm ext} = 15$ cm.

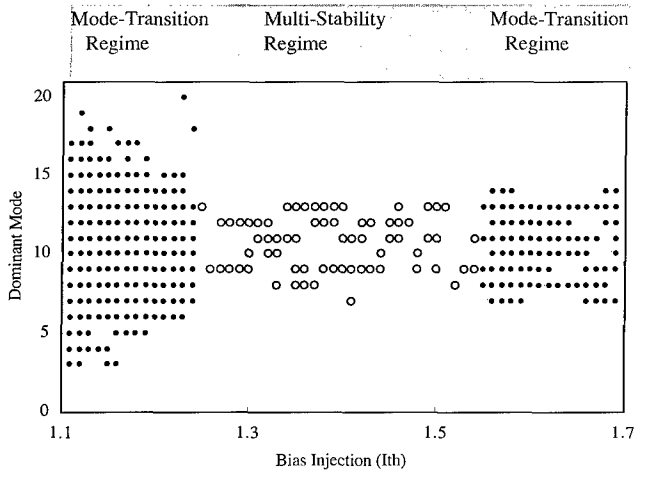

Fig. 3. Bifurcation diagram of mode-competition states versus bias injection. White circles and solid dots denote respectively stable and temporary dominant modes. Parameters are $L_{\rm ext} = 36$ cm and $R_{\rm ext} = 1.0\%$.

spectrum as a result of coupling between modes in a strongly multimode fiber laser. In this paper, we focus on the bifurcation of mode-competition dynamics when the external feedback level or the bias injection are varied. In particular, we use the measures of DMR and MPR to classify different laser states and investigate how the bifurcation of mode-competition dynamics results in changes in laser states.

Figures 2 and 3 show the bifurcation diagrams of laser states versus the external reflectivity and the bias injection, respectively. In these diagrams, white circles denote stable dominant modes whose DMR is unity for some initial condition. Multiple circles at a fixed parameter value indicate multistability of the dominant mode. On the other hand, solid dots denote temporary dominant modes, i.e. the dominant mode changes from one to another in time and each marked mode is only dominant for a short time interval. It is stressed that the blank area in the bifurcation diagram does not necessarily mean the output power of the mode there is truly zero, it only means the mode never becomes dominant during the observation time.

In the above bifurcation diagrams, the parameter domain can be divided into three different regimes corresponding to different mode-competition states: (i) single mode regime where only one specific mode becomes dominant (which means DMR = 1) and the mode takes most of the output power all the time; (ii) the multistability regime where different dominant modes exist depending on initial conditions; and (iii) the chaotic

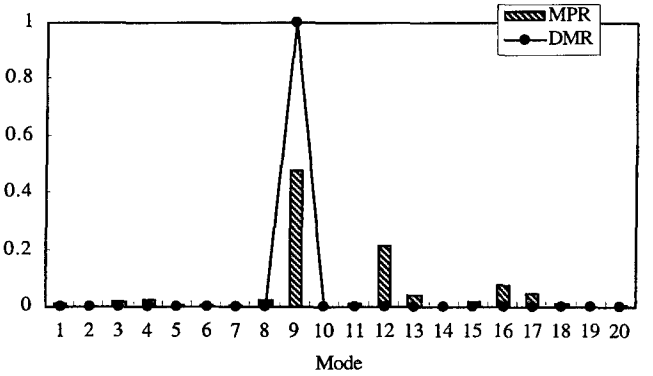

(a)

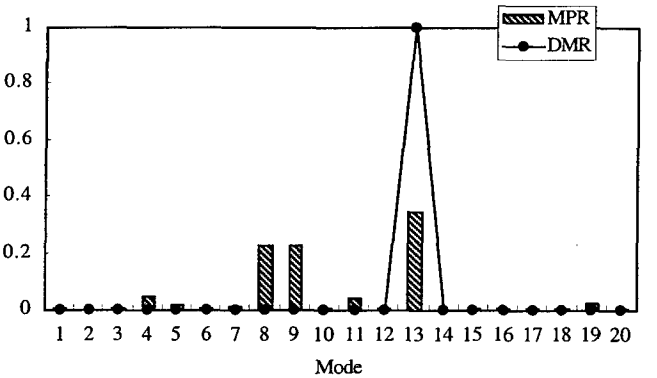

(b)

Fig. 4. Mode distributions in multistability regime for $I_b = 1.5\ I_{\rm th}$, $L_{\rm ext} = 15$ cm, and $R_{\rm ext} = 1.4\%$. Dominant mode is (a) No. 9 and (b) No. 13.

mode-transition regime where no particular mode becomes dominant during the observation time.

Examples of mode distributions for multistable states are shown in Figs. 4(a) and 4(b). The histograms show DMR distributions while the lines indicate MPR values. In both figures, there exists one mode whose DMR becomes unity, although the MPR shows that the mode does not take all of the laser output power.

3. Adaptive Mode Selection Using Chaotic Search

A method for adaptive mode selection using chaotic search was proposed by Davis [1990]. Here the word "mode" could mean an oscillation pattern, a bit sequence, or the dominant lasing wavelength as in the current case. The method is applicable to systems which exhibit multistability of modes and an onset of chaotic transitions among the different modes. It is further assumed that the "fitness" of a particular mode is shown by an external response signal obtained when the system is in that mode, with different response signal levels corresponding to good fitness and bad fitness. The general idea of adaptive mode selection using chaotic search is to couple the fitness response signal to the control parameter of the system in such a way that bad responses result in mode transitions and good responses result in mode stability.

As shown in the last section, a multimode FP laser diode with external feedback has multistability and chaotic mode-transition states as well as bifurcation between these two regimes upon the continuous variation of laser parameters. Thus, we are able to apply the chaotic search idea to the multimode FP semiconductor laser for the purpose of adaptive mode selection. The chaotic search consists of two steps: mode evaluation and parameter adjustment. In the first step the system output is evaluated and external response is generated and in the second step the control parameter is adjusted using the external response signal. In the first step, we detect the output of each mode and calculate the DMR during the fixed mode-evaluation time interval. The mode-evaluation time is chosen as several times the relaxation time of the laser. For the second step, the control parameter is chosen as a two-level variable for simplicity, with parameter value μ^c corresponding to chaotic mode-transition regime and parameter value μ^0 to multistability regime. Thus the search is performed as follows. When a mode gets a good external response, the control parameter is set to μ_0. If the laser output falls into a different mode which gets a bad response, the control parameter is reset to μ^c and the search loop is repeated.

Two typical examples of chaotic search are shown in Figs. 5 and 6. In the case of Fig. 5, the

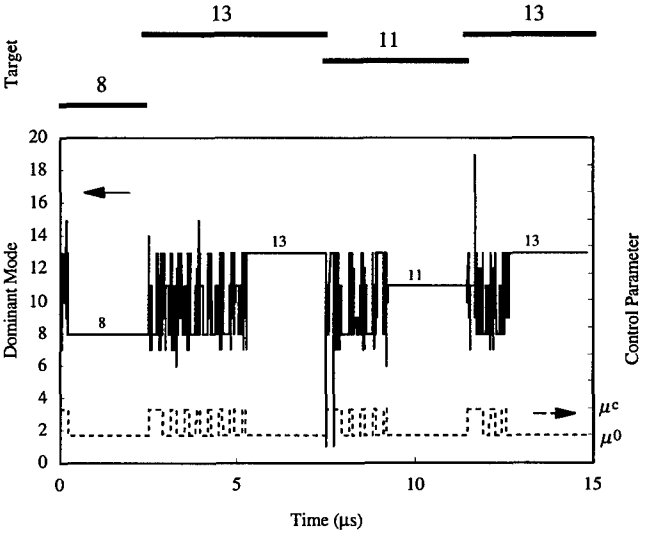

Fig. 5. Mode search process. Target modes are mode 8, 13, 11, and 13. The control parameter (bias injection I_b) is switched between $\mu^c = 1.15\ I_{\text{th}}$ and $\mu^0 = 1.35\ I_{\text{th}}$. Other parameters are $L_{\text{ext}} = 36$ cm and $R_{\text{ext}} = 1.0\%$. Upper trace: Dominant mode DMR. Lower trace: The control signal.

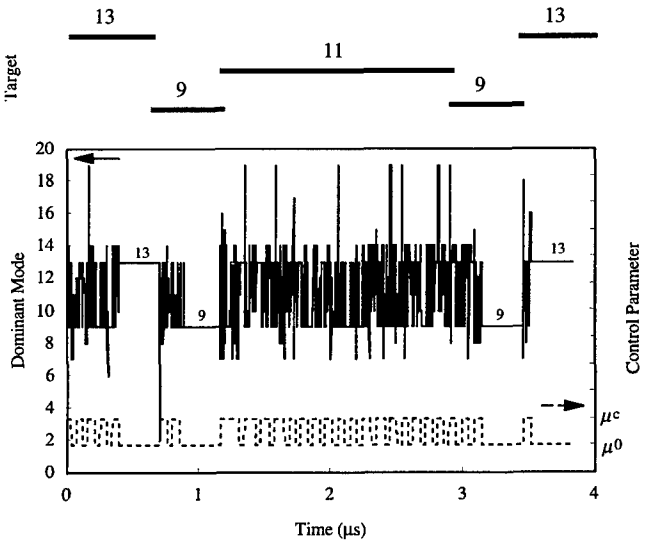

Fig. 6. Mode search process. Target modes are mode 13, 9, 11, 9, and 13. The control parameter (external reflectivity R_{ext}) is switched between $\mu^c = 2.8\%$ and $\mu^0 = 1.4\%$. Other parameters are $I_b = 1.5\ I_{\text{th}}$ and $L_{\text{ext}} = 15$ cm. Upper trace: Dominant mode DMR. Lower trace: The control signal.

bias injection is taken as the control parameter and is switched between chaotic mode-transition regime at $\mu^c = 1.15\ I_{\rm th}$ and multistability regime at $\mu^0 = 1.35\ I_{\rm th}$. Three modes (mode 8, 11, and 13) were alternatively set as targets. During each search loop, there are several switch-on and -off processes. Such behavior is typical in this adaptive mode selection method due to mismatch between the external classification of output states and the basins of attraction. When the target mode appears, the laser is set in multistability regime ($\mu = \mu^0$) and the output mode converges to one of the multiple stable modes. If the output converges to the target mode, the good response will keep the control parameter at μ^0; if the output falls into some other mode, the change of the external response will automatically reset the control parameter to be μ^c. Chaotic search can also be performed using the external reflectivity as the control parameter as shown in Fig. 6. Here, again three states (modes 9, 11, and 13) were set as targets. We purposely chose mode 11 as one of the targets to show a case when the search fails to converge. Since mode 11 is not among the multistable states at μ^0 (see Fig. 2), the laser output cannot converge to this mode. This search method can only converge to modes which are stable at μ^0.

The influence of the parameter value for the onset of chaos on the search process has been investigated. Figure 7 shows the effects of μ^c on the average search time which was calculated from 50 search events. It can be seen from Fig. 7 that the mode search time varies in a complicated way on the control parameter, the reflectivity. The mode search time depends on the details of the chaotic mode transition dynamics [Davis, 1998], which can have complicated structure depending on the control parameter. More detailed analysis of this is a subject for future work. However, it is important to note that Fig. 7 shows that there is a parameter interval over which the variation of the search time is small enough for the search method to be considered robust. On the other hand, for $\mu^c \leq 2.1\%$, the average search time shows significant increase and the search fails when $\mu^c < 2\%$. The increase of the search time near the boundary of the chaotic mode-transition regime, where the mode-transition rate decreases, shows that chaotic mode-transition is essential in the adaptive mode selection.

We briefly discuss the feasibility of experimentally implementing the above mode selection method. For experimental convenience, we could substitute the mode-evaluation method used in the current simulation with a more simple method: To detect the light power for a particular wavelength and compare it with a preset threshold, i.e. to evaluate MPR instead of DMR. We numerically tested this simplified version of the search technique and obtained successful mode selection provided the threshold is appropriately chosen. The experimental implementation could be realized by using a diffraction grating and a photodiode whose bandwidth corresponds to the mode-evaluation time, and an amplifier with a preset threshold voltage. The target mode can be set by varying the angle of the grating and hence the wavelength of the light incident upon the detector. The detected signal for a specific wavelength could be compared with the preset threshold and the deviation signal employed to adjust the injection current of the laser or the electric port of an acousto-optical modulator which controls the external reflectivity.

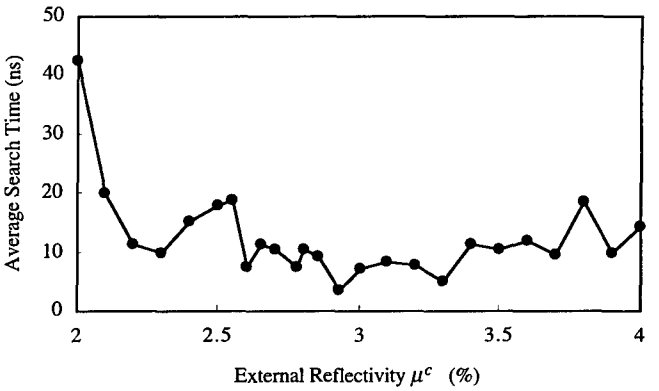

Fig. 7. The dependence of average mode search time on control parameter μ^c. The control parameter is external reflectivity $R_{\rm ext}$. Other parameters are $I_b = 1.5\ I_{\rm th}$ and $L_{\rm ext} = 15$ cm. Dependence on bias injection is similar.

4. Conclusion

In summary, we have investigated mode-competition dynamics of a multimode FP semiconductor laser and demonstrated that different mode-competition states exist when external feedback or bias injections are varied and these states and their bifurcation structure are suitable for performing adaptive mode (wavelength) selection using chaotic search. For a solitary multimode laser, all modes are excited and no particular mode dominates the light output. When external feedback or injection modulation are introduced, the laser exhibits complex mode-competition dynamics. Three different parameter regimes have been verified namely a

single-mode regime, a multistability regime, and a chaotic mode-transition regime.

Switching between the multistability regime and the chaotic mode-transition regime makes it possible to adaptively select a dominant lasing mode by using a chaotic search method. In this method, the laser is initially set in the chaotic mode-transition regime. When a particular wavelength gets a good external response, the external response stabilizes that mode as the dominant mode of the laser by driving the control parameter (reflectivity or injection) into the multistability regime. We have performed computer simulations of the search technique and demonstrated that the proposed method is quite effective over a wide parameter range in spite of its simplicity. It is noted that the proposed method may also be applicable to the strongly multimode class-B lasers [Szwaj *et al.*, 1996] where hundreds of lasing modes oscillate simultaneously. Adaptive mode selection may provide a promising way for applying such lasers in adaptive communication or adaptive data transmission networks.

References

Aida, T. & Davis, P. [1994] "Oscillation mode selection using bifurcation of chaotic mode transitions in a nonlinear ring resonator," *IEEE J. Quantum Electron.* **30**(12), 2986–2997.

Bracikowski, C. & Roy, R. [1991] "Chaos in a multimode solid-state laser system," *Chaos* **1**(1), 49–64.

Byrne, D. M. [1992] "Accurate simulation of multifrequency semiconductor laser dynamics under gigabits-per-second modulation," *J. Lightwave Technol.* **10**(8), 1086–1096.

Davis, P. [1990] "Application of optical chaos to temporal pattern search in a nonlinear optical resonator," *Jap. J. Appl. Phys.* **29**(7), L1238–L1240.

Davis, P. [1998] "Adaptive mode selection using on–off switching of chaos," *Int. J. Bifurcation and Chaos* **8**(8), 1671–1674.

Lang, R. & Kobayashi, K. [1980] "External optical feedback effects on semiconductor injection laser properties," *IEEE J. Quantum Electron.* **16**(2), 347–355.

Liu, Y. & Davis, P. [1997] "Adaptive optical sequence generation for collision avoidance using chaos," *Electron. Lett.* **33**(1), 68–69.

Mørk, J., Tromborg, B. & Mark, J. [1992] "Chaos in semiconductor lasers with optical feedback: Theory and experiment," *IEEE J. Quantum Electron.* **28**(1), 93–108.

Ryan, A. T., Agrawal, G. P., Gray, G. R. & Gage, E. C. [1994] "Optical-feedback-induced chaos and its control in multimodal semiconductor lasers," *IEEE J. Quantum Electron.* **30**(3), 668–679.

Szwaj, C., Bielawski, S. & Derozier, D. [1996] "Propagation of waves in the spectrum of a multimode laser," *Phys. Rev. Lett.* **77**(22), 4540–4543.

Uenishi, Y., Honma, K. & Nagaoka, S. [1996] "Tunable laser diode using a nickel micromachined external mirror," *Electron. Lett.* **32**(13), 1207–1208.

International Journal of Bifurcation and Chaos, Vol. 8, No. 8 (1998) 1693–1698

CONTROLLING CHAOS WITH PARAMETRIC PERTURBATIONS

LEONE FRONZONI
Department of Physics, University of Pisa, Italy
MICHELE GIOCONDO
Department of Physics, University of Calabria, Italy

Received July 31, 1997

We consider the effects of parametric perturbation on the onset of chaos in different dynamical systems. Favoring or suppression of chaos was observed depending on the phase or the frequency of the periodic perturbation. A lowering of the threshold of chaos was observed in an electronic device simulating a Josephson-Junction model and the suppression of chaos was obtained in a bistable mechanical device. We showed that in case of spatial instability in a sample of liquid crystal, the action of the parametric perturbation is to modify the velocity and the onset of the defects.

Considering that the emergence of defects precedes the threshold of spatio-temporal chaos, we infer that parametric perturbation can modify the threshold of chaos in this spatial dynamical system.

1. Introduction

In 1965, an interesting paper appeared where Wehrmann [1965] was able to suppress turbulence behind a cylinder in a moving fluid. The basic idea was to put in vibration the cylinder with a suitable feed-back using the same fluctuations present in the turbulent fluid. A complete laminarization was obtained. Turbulence is a phenomena related to a system with infinite degrees of freedom and it is natural to wonder if parametric perturbations can modify the onset of chaos in low dimensional system as well. In 1990, Lima and Pettini [1990] showed with rigorous theoretical consideration that resonant parametric perturbation can remove chaos in low dimensional systems. They confirmed this prediction with numerical simulation. Furthermore, Cicogna [1990] showed, using a Melnikov Integral [Melnikov, 1963], how to modify the threshold of chaos by resonant parametric modulation. Considering that these works were essentially of theoretical nature, it was particularly interesting to try to verify these predictions in real systems with an experimental point of view. In spite of the development of other methodologies for the control of chaos, e.g. [Ott *et al.*, 1990; Pyragas, 1992] and more recently [Boccaletti & Arecchi, 1995], the techniques for controlling chaos with parametric perturbations remain a good method when it becomes impossible to apply feedback on the systems. In the next sections we will reassume the experimental results that have allowed us to verify these predictions [Cicogna & Fronzoni, 1990; Fronzoni *et al.*, 1991]. The validity of this kind of methodology has been verified in other experiments performed in several laboratories [Azevedo & Rezende, 1991; Braiman & Goldhirsch, 1991; Meucci *et al.*, 1994; Ding *et al.*, 1994; Chizhevsky & Glorieux, 1995; Chizhevsky & Corbalan, 1996].

2. The Influence of Parameter Perturbations in a Josephson-Junction Model

We considered a model that describes a wide class of phenomena that can be reduced to a pendulum in the presence of forcing and viscosity. This equation can be resumed in the following equation:

$$\frac{d^2\phi}{dt^2} + \delta\frac{d\phi}{dt} + D\,\sin\,\phi + \gamma\,\cos(\omega t) = 0 \qquad (1)$$

where δ means the viscosity coefficient, γ the amplitude of forcing and ω the frequency.

This system behaves chaotic in a range of parameters γ and D as widely described in an experiment [D'Humieres *et al.*, 1982], where an electronic device was used to simulate Eq. (1).

We repeated this experiment but with an important improvement, which is to consider the coefficient D as a modulated control parameter:

$$D = D_0[1 + \xi\,\cos(\Omega t + \theta)] \qquad (2)$$

where Ω means the frequency modulation, ξ is the amplitude and θ is the difference of phase between the modulation and the forcing.

In Fig. 1 we show the scheme of the circuit which simulated Eq. (1) using minimum components technique [Fronzoni, 1989].

The main element of this device is the Voltage Control Oscillator (VCO) that provides an output with frequency depending on the input V_1 according to the relation

$$\omega_{\rm vco} = KV_1\,. \qquad (3)$$

$M1$ and $M2$ are multipliers, and without going into great detail, it is important to know that the phase ϕ of the voltage at the VCO-output is described by the following relation:

$$V_0(1 + \xi\,\cos\,\Omega t)\frac{\sin\,\phi}{R_5} + \frac{\dot\phi}{KR_1} + \frac{V_\gamma}{R_\gamma} + \frac{C}{K}\ddot\phi = 0\,. \qquad (4)$$

With suitable time-scaling this relation is equivalent to Eq. (1) which includes the modulation term. To study the influence of the modulation we fixed the amplitude and the frequency of the modulation, then the forcing was increased until it reached the threshold of chaos. In this experiment we used forcing and modulation locked with $\theta = 0$.

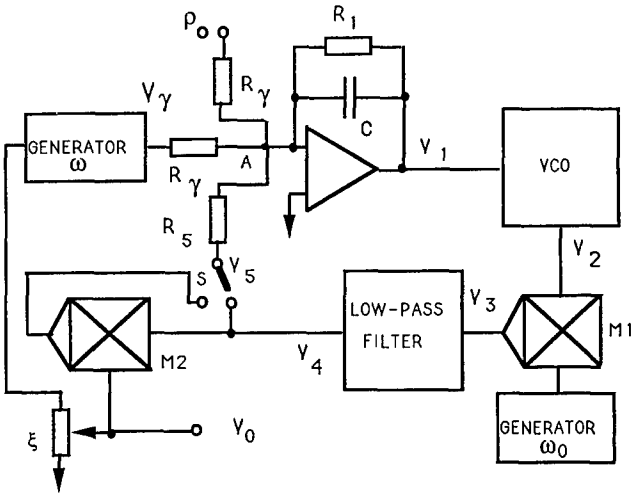

Fig. 1. Scheme of circuit for simulating Eq. (1).

The prediction of the chaos threshold can be obtained by means of the Melnikov Integral. After some approximation [Cicogna & Fronzoni, 1990] one deduces a simple relation for this quantity

$$M(t_0) = -A\,\cos(\Omega t_0) + B\,\mathrm{sen}(\Omega t_0 + \theta)\,, \qquad (5)$$

with

$$A = 8\delta \pm 2\pi\gamma\,\mathrm{sech}(\omega\pi/2) \qquad (6)$$

and

$$B = 2\pi\xi\Omega^2\,\mathrm{csch}(\Omega\pi/2)\,. \qquad (7)$$

Assuming $\xi > 0$, chaos does not appear if

$$\gamma\,\mathrm{sech}(\omega\pi/2) + \xi\Omega^2\,\mathrm{csch}(\Omega\pi/2) < 4\delta/\pi\,. \qquad (8)$$

It is important to observe that the sign of $M(t_0)$ depends on the sign of ξ and θ. In other words the threshold of chaos is defined by the relation of sign between the amplitude modulation ξ and the phase θ. For instance, $\xi > 0$ and $\theta > 0$ provide a lowering of the threshold of chaos.

Figure 2 shows the results, which are justified by this theory where one has to expect a lowering of the threshold of chaos versus the amplitude of the modulation. The quantitative differences between the experimental data and the theoretical predictions are due to the approximations used in the computation of the Melnikov Integral.

When we performed this experiment we were not interested in observing the suppression of chaos, nevertheless the Cicogna' s theory predicts this possibility. Only favoring chaos was experimentally

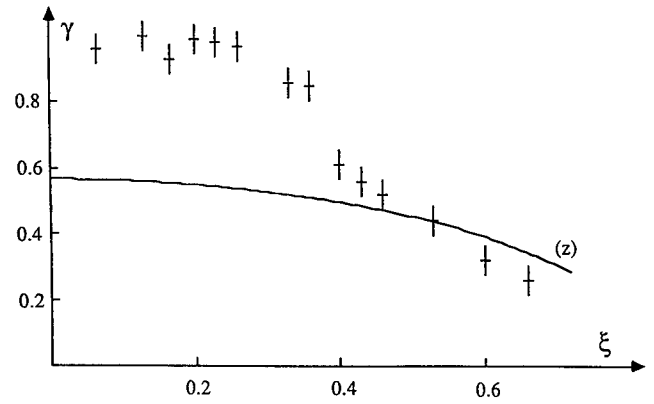

Fig. 2. Experimental results and theoretical predictions (z-line) for threshold chaos as function of the amplitude modulation with $\theta = 0$, $\delta = 0.25$, $\omega = 0.75$ and $\Omega = 0.75$.

verified with this kind of apparatus. Prodded by the theory of Lima and Pettini we performed another experiment with the specific intention to verify the suppression of chaos in a real mechanical system.

3. Suppression of Chaos in a Bistable Mechanical Device

The motivation behind this choice arises from the fact that the theoretical predictions could be invalidated by the incomplete correspondence of the model with the reality. This could cause doubts on the true possibility to remove chaos in a real system. For this purpose we restricted our choice to a bistable system as illustrated in Fig. 3 and modeled by a Duffing–Holmes forced oscillator [Moon, 1997].

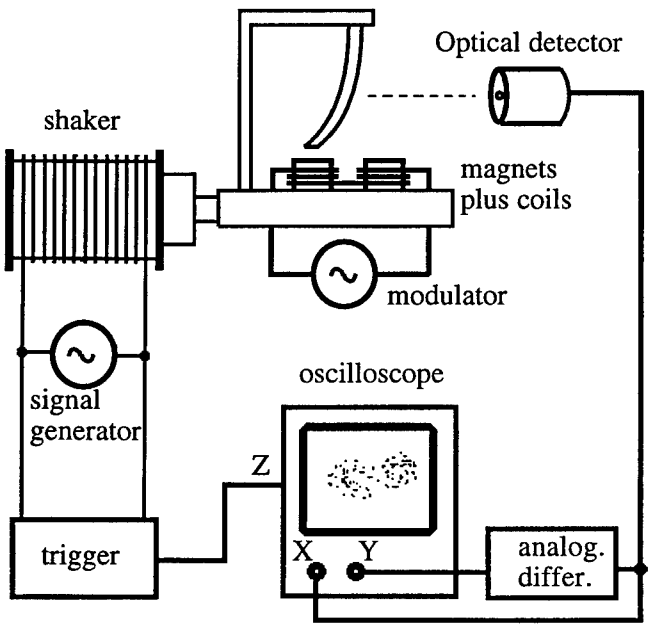

Fig. 3. Scheme of mechanical device and the experimental configuration.

A metal beam was fixed over an oscillating plate. Two electromagnets are located near the free-end of the beam. This system is approximately described by this equation:

$$\ddot{\phi} = \alpha\phi - \beta\phi^3 - \gamma\dot{\phi} + A\cos(2\pi\nu_f t)\,. \tag{9}$$

The parameters α and β are obtained by a direct measurement of the equilibrium position $\pm x_0$ and resonant frequencies ν_0 for small perturbations, according to the following relations:

$$\alpha = \frac{1}{2}(2\pi\nu_0)^2\,, \tag{10}$$

$$\beta = \frac{1}{2x_0^2}(2\pi\nu_0)^2\,. \tag{11}$$

We get the modulation by sending a periodic current into the electromagnets and this modifies the parameters α and β:

$$\alpha \to \alpha[1 + \varepsilon\cos(2\pi\nu_m t)]\,, \tag{12}$$

$$\beta \to \beta[1 + \eta\cos(2\pi\nu_m t)]\,. \tag{13}$$

ε and η are the modulation amplitudes and ν_m the frequency modulation. Figure 3 shows the experimental configuration used to control chaos.

The shaker drove the plate with a frequency forcing ν_f. An optical detector read the oscillation amplitude of the beam. This signal and its derivative were sent to the x–y input of an oscilloscope. If the z-axis of the oscilloscope was triggered by the forcing, a Poincaré section appeared on the screen. With this technique we were able to know in real time the state of the system without computations. Fixed dots on the screen indicated order and spread points on the screen indicated chaotic dynamics. According to the Lima–Pettini theory it is possible to suppress chaos if the frequency of the perturbation approaches the values of the characteristic frequencies of the system, including harmonics.

To observe the suppression of chaos we used the following procedure: We fixed the driving amplitude and its frequency to observe a strange attractor on the screen and then we sent a periodic current into the coils. The frequency of this perturbation was swept around the values of the driving frequency or around the harmonics.

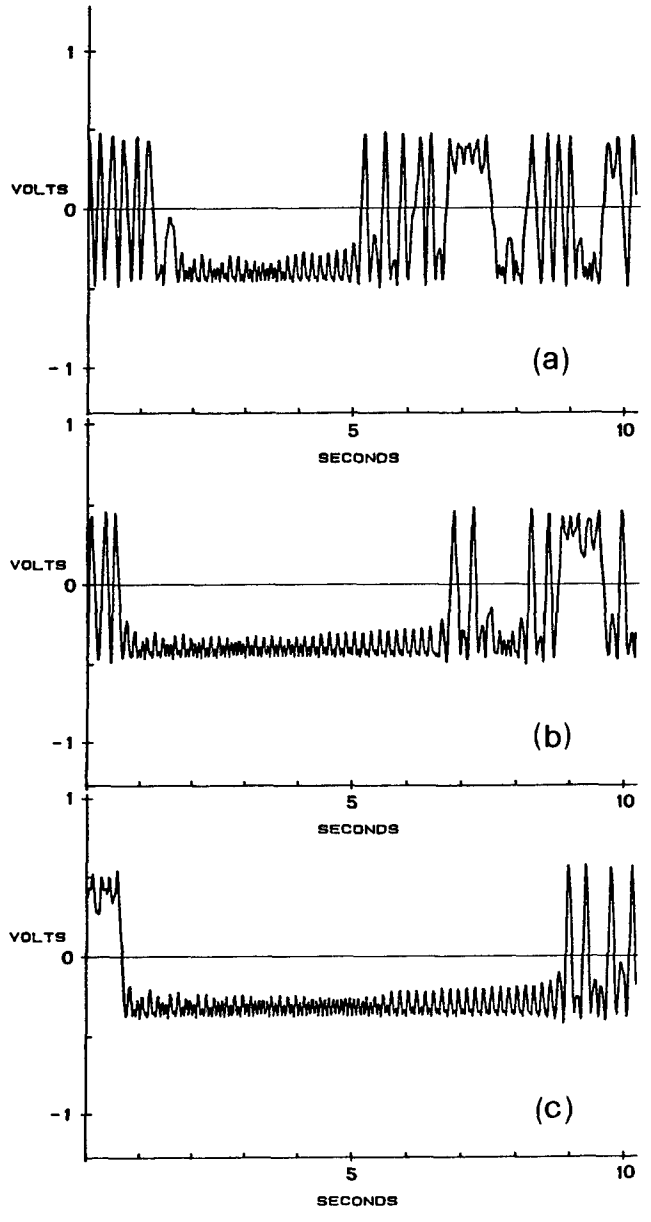

Fig. 4. Time evolution of voltage at the output of Optical Detector in presence of modulation. $\nu_f = 13.03$ Hz, $\varepsilon = 0.1$, $\eta = 0.08$, and $A/A_{\text{chaos}} = 1.13$. (a) $\nu_m = 13.08$ Hz, (b) $\nu_m = 13.07$ Hz, (c) $\nu_m = 13.06$ Hz.

Figure 4 shows the voltage of the optical detector versus the time for different modulation frequencies. The beam angle amplitude ϕ is proportional to this quantity. It results in:

(a) Chaotic vibrations of the beam were alternated with ordered oscillations.
(b) The ordered states were characterized by periodic oscillation around one of the two equilibrium positions. The beam amplitude was synchronized with the forcing.

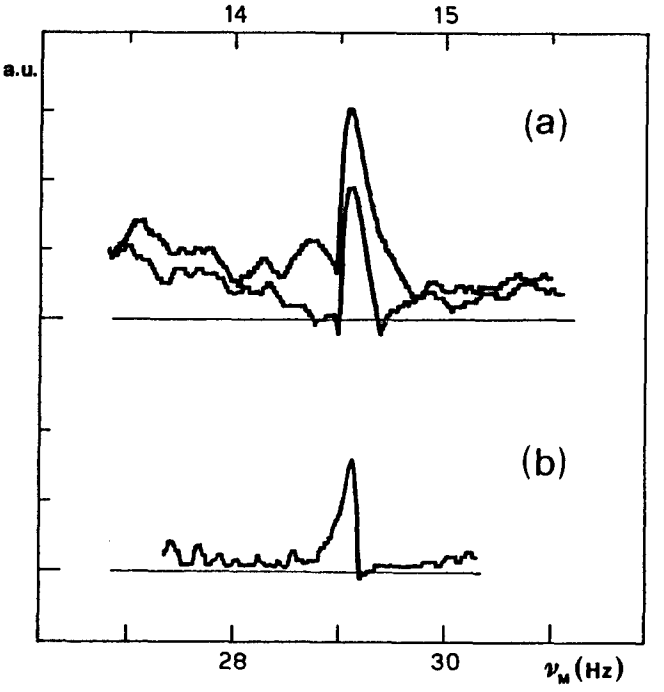

Fig. 5. Amplitude Lock-in output versus frequency modulation ν_m (a) first-harmonic resonance, upper curve $\varepsilon = 0.16$, lower curve $\varepsilon = 0.1$. (b) second-harmonic resonance $\varepsilon = 0.12$. Sweep time 1175 sec/Hz, integration time 300 sec and $A/A_{\text{chaos}} = 1.33$.

(c) The average duration of the ordered phases was proportional to the reciprocal of the difference $\Delta\nu = \nu_f - \nu_m$.

A way to get numerical evaluation of the resonance phenomena, was to send the derivative of ϕ-voltage to the input of a Lock-in instrument using the amplitude modulation as reference signal. Peaks in the response of the Lock-in indicate ordered state synchronized with the modulation signal. Figure 5 shows the Lock-in output versus the frequencies modulation. Resonance at the forcing frequency and at the second harmonics are evident. These results are well explained by the theory [Lima & Pettini, 1990].

4. Parametric Perturbation on Spatio-Temporal Instability

The onset of chaos in spatio-temporal dynamics is characterized by the appearance of defects or topological defects. The behavior of these defects become more complex when a control parameter approaches the chaos threshold. For instance, the number and the velocity of these objects are increasing with the control parameter.

Due to the absence of regularity in the behavior of these defects its results are too ambiguous to define the threshold of the spatio-temporal chaos. In fact, in spite of the presence of a few defects in the structure, they assume chaotic motion just for a small increase of the control parameter.

To study the influence of parametric perturbations on this kind of system, we considered an electrohydrodynamic instability [Williams, 1963] that appears in samples of nematic liquid crystals in the presence of electric field. Nematics are organic elements characterized by molecules with rod like shape. These properties induce an ordered configuration where the molecules prefer to stay in a well defined orientation around a mean value. A vector n called "director" defines this orientation. In our experiment the nematic was closed between two conducting glass plates. The internal plate surface was rubbed in a well defined direction. In this configuration the molecules assume an orientation parallel to the rubbing direction. When an electric field is applied on the sample, fluctuations of the molecular orientation induce spatial charges inside the nematic. The charges are generated by a current perpendicular to the field because of the anisotropy of the nematic conductibility. The interaction of the spatial charges with an electric field cause movement in the fluid. This motion arises over a critical threshold of the field and a regular pattern appears on the sample, as shown in Fig. 6. The image is obtained observing the cell with a polarized microscope. Dark and white lines correspond to opposite velocities of the fluid in the sample with rotation axes parallel to the plates. As the electric field is increased topological defects broke the regularity of the structure. Two examples of these defects are shown in Fig. 6. These defects are well described by the Landau–Ginsburg theory [Ginsburg & Pitaevs, 1958].

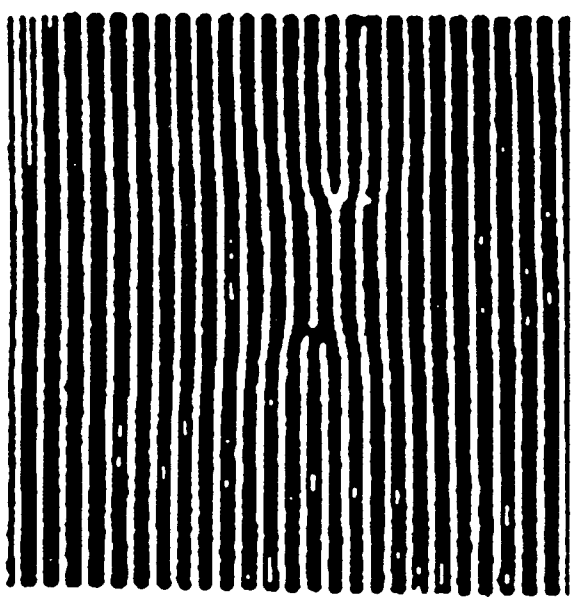

Fig. 6. Microscopic image of liquid crystals cell in presence of Williams' domains. Two defects are present in the structure.

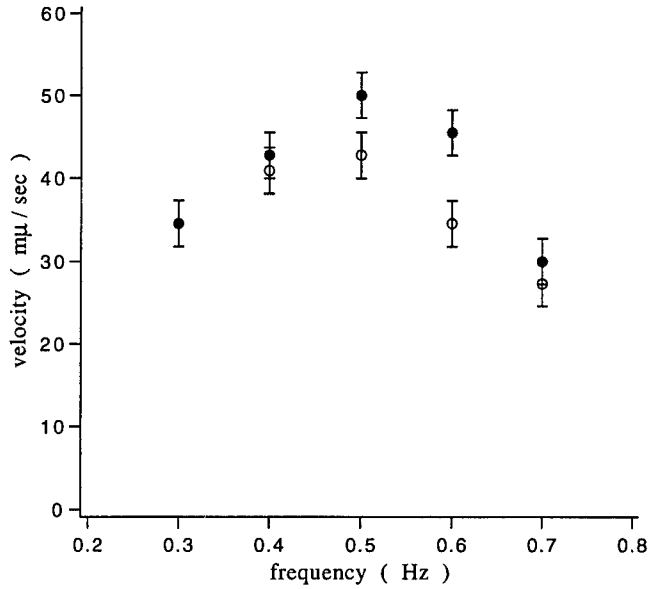

Fig. 7. Velocity of defects versus frequency modulation. Open circles correspond to the data of repeated experiment 30 days later.

In our experiment we used MBBA (Methoxybenzilidenebutylaniline) inside square glass plates of 2 cm size and separated by 20 μm. We applied on the sample an alternating voltage at the frequency of 10 Hz. We perturbed the system by means of voltage amplitude modulation of the order of 10%. Figure 7 shows the velocity of the defects against the frequency of periodic amplitude modulation and a resonance behavior is evident. This experiment was repeated with the same sample 30 days later obtaining a good reproducibility of the phenomena.

It is important to note that a modulation of 10% of the forcing at $\nu_m = 0.5$ Hz induced an increase of the order of 50% of the defects velocity. Considering that the increase of defects velocity precedes the onset of chaos means that parametric perturbation induces a lowering of the threshold of chaos in this kind of instability.

5. Conclusions

In these experiments we obtained suppression or favoring of chaos depending on the frequency and phase of periodic perturbation applied on different systems. Moreover an interesting result was obtained in a sample of liquid crystal where the influence of perturbation modifies the velocity of defects in spatial structures. This behavior suggests that parametric modulation can modify the onset of chaos as a consequence of modifications of the dynamic properties of the defects in proximity to the turbulence threshold. In order to explain these last results we have developed a phenomenological model and are in the progress of further laboratory experimentation.

References

Azevedo, A. & Rezende, S. M. [1991] "Controlling chaos in spin-wave instabilities," *Phys. Rev. Lett.* **66**, 1342–1345.

Braiman, Y. & Goldhirsch, I. [1991] "Taming chaotic dynamics with weak periodic perturbations," *Phys. Rev. Lett.* **66**, 2545–2548.

Boccaletti, S. & Arecchi, F. T. [1995] "Adaptive control of chaos," *Europhys. Lett.* **31**(3), 127–132.

Chizhevsky, V. N. & Corbalan, R. [1996] "Experimental observation of perturbation-induced intermittency in the dynamics of CO_2 laser," *Phys. Rev.* **E54**, 4576–4579.

Chizhevsky, V. N. & Glorieux, P. [1995] "Targeting unstable orbits," *Phys. Rev.* **E51**, R2701–R2704.

Cicogna, G. [1990] "Changing the threshold of chaos by resonant parametric modulation," *Nuovo Cim.* **B105**, 813–815.

Cicogna, G. & Fronzoni, L. [1990] "Effects of parametric perturbation on the onset of chaos in the Josephon-junction model: Theory and analog experiments," *Phys. Rev.* **A42**, 1901–1906.

Cicogna, G. & Fronzoni, L. [1993] "Modifying the onset of homoclinic chaos. Application to bistable potential," *Phys. Rev.* **E47**(6), 4585–4588.

D'Humieres, D., Beasley, M. R., Huberman, B. A. & Libchaber, A. [1982] "Chaotic states and routes to chaos in the forced pendulum," *Phys. Rev.* **A26**, 3483–3496.

Ding, W. X., She, H. Q., Huang, W. & Yu, C. X. [1994] "Controlling chaos in a discharge plasma," *Phys. Rev. Lett.* **72**, 96–99.

Fronzoni, L. [1989] "Analogue simulations of stochastic processes by means of minimum component electronic devices," *Noise in Nonlinear Dynamical Systems*, eds. Moss, F. & McClintock, P. V. E., Vol. 3 (Cambridge University Press, Cambridge), pp. 222–241.

Fronzoni, L., Giocondo, M. & Pettini, M. [1991] "Experimental evidence of suppression of chaos by resonant parametric perturbations," *Phys. Rev.* **A43**, 6483–6487.

Ginzburg, V. L. & Pitaevs, L. [1958] *JETP* **34**, 1240.

Helfrich, W. [1969] "Conduction-imduced alignment of nematic liquid crystals: Basic model and stability considerations," *J. Chem. Phys.* **51**, 4092–4105.

Lam, L. & Prost, J. [1991] *Solitons in Liquid Crystals* (Springer-Verlag).

Lima, R. & Pettini, M. [1990] "Suppression of chaos by resonant parametric perturbation," *Phys. Rev.* **A41**, 726–733.

Melnikov, V. K. [1963] *Trans. Moskow Math. Soc.* **12**, 1.

Meucci, R., Gadomski, W., Ciofini, M. & Arecchi, F. T. [1994] "Experimental control of chaos by means of weak parametric perturbations," *Phys. Rev.* **E49**, R2528–R2531.

Moon, F. C. [1987] *Chaotic Vibration* (Wiley, NY).

Ott, E., Grebogi, C. & York, J. A. [1990] "Controlling chaos," *Phys. Rev. Lett.* **64**, 1196–1999.

Pettini, M. [1990] *Dynamics and Stocastic Processes*, eds. Lima, R., Streit, L. & Vilela Mendes, R., *Lecture Notes in Physics*, Vol. 355 (Springer-Verlag, Berlin).

Pyragas, K. [1992] "Continuous control of chaos by self-controlling feedback," *Phys. Lett.* **A170**, 421–428.

Wehrmann, O. [1965] "Reduction of velocity fluctuation in a Kármán vortex street by a vibrating cylinder," *Phys. Fluids* **8**, 760–761.

Williams, R. J. [1963] "Domains in liquid crystals," *J. Chem. Phys.* **39**, 384–388.

International Journal of Bifurcation and Chaos, Vol. 8, No. 8 (1998) 1699–1706

ON OPTIMAL STABILIZATION OF PERIODIC ORBITS VIA TIME DELAYED FEEDBACK CONTROL

M. BASSO, R. GENESIO*, L. GIOVANARDI, A. TESI and G. TORRINI
Dipartimento di Sistemi e Informatica, University of Florence,
Via S. Marta 3-50139, Firenze, Italy

Received July 31, 1997

The paper considers the problem of designing time delayed feedback controllers to stabilize unstable periodic orbits of a class of sinusoidally forced nonlinear systems. This problem is formulated as an absolute stability problem of a linear periodic feedback system, in order to employ the well-known circle criterion. In particular, once a single test is verified by an unstable periodic orbit of the chaotic system, our approach directly provides a procedure for designing the optimal stabilizing controller, i.e. the one ensuring the largest obtainable stability bounds. Even if the circle criterion provides a sufficient condition for stability and therefore the obtained stability bounds are conservative in nature, several examples, as the one presented in this paper, show that the performance of the designed controller is quite satisfactory in comparison with different approaches.

1. Introduction

The problem of controlling chaos has recently received a lot of attention and many theoretical as well as experimental contributions coming from several areas have considered different aspects of this problem (see e.g. [Shinbrot *et al.*, 1993; Ogorzalek, 1993; Chen & Dong, 1993; Abed & Wang, 1995; Hu *et al.*, 1995] and references therein). One of the most frequent objectives consists in the stabilization of chaotic behaviors to periodic regimes and, in particular, many methods are directed towards the stabilization of one of the infinite unstable periodic orbits that coexist in the chaotic attractor. This problem was first considered by Ott, Grebogi and Yorke in a paper [Ott *et al.*, 1990] that has originated, with related extensions and modifications (see e.g. [Romeiras *et al.*, 1992; Hunt, 1991; Dressler & Nitsche, 1992]), the so-called OGY methods. A distinct technique was proposed by Pyragas [1992], again forming the basis for other related works [Socolar *et al.*, 1994; Kittel *et al.*, 1995; Just *et al.*, 1997], which are referred to as time-delayed auto-synchronization or time-delayed or simply Pyragas methods. These two classical approaches, based on quite different properties and design procedures and successfully applied to various physical experiments, lead to feedback controllers utilizing small perturbation signals and they really exploit the peculiar characteristics of chaos. Also for this reason, the above methods and in general most literature on control of chaos appear to be distinct from what is called control theory, although some evident links are present.

The purpose of the present paper is to contribute (see also [Basso *et al.*, 1997a]) to the results of feedback control theory in order to optimize, in a certain sense, the solution obtainable via the Pyragas approach, and also to indicate a means of designing the related controller. In particular, we consider periodically forced chaotic systems, for which the Pyragas methods are quite appealing,

*E-mail: genesio@dsi.unifi.it

and we formulate the periodic orbit stabilization as an absolute stability problem [Vidyasagar, 1992] of a linear periodic feedback system. Therefore, a well-known frequency criterion, the circle criterion [Vidyasagar, 1992], is employed to compute the largest obtainable stability bounds. Once a single test is verified by the unstable periodic orbit of the chaotic system, our approach directly provides a procedure for designing the "optimal" stabilizing controller, i.e. the one maximizing the stability bounds. Even if the method is based on a sufficient condition and therefore the bounds are conservative in nature, several examples show that the performance of the optimal controller is quite satisfactory.

The remainder of the paper is organized as follows. Section 2 formulates the problem and develops the main results, while Sec. 3 presents in some detail one example showing the application of these results, also in comparison with different approaches. Some brief comments end the paper in Sec. 4.

2. Main Results

The notation adopted hereafter is pretty standard. For instance, $X(s)$ denotes the Laplace transform of the time-domain signal $x(t)$, f' stands for the derivative of a function f. A transfer function is said to be stable if its impulse response belongs to L_1, the space of time-domain signal $x(t)$ such that $\int_0^\infty |x(t)|dt$ is finite. If the transfer function is rational, this reduces to the usual notion of stability, i.e. all the poles must have a negative real part.

To motivate our problem of stabilizing unstable periodic solutions, we consider one of the most studied problems in controlling chaos, i.e. the elimination of a period doubling bifurcation sequence [Abed & Wang, 1995].

Consider the periodically forced (Lur'e) system depicted in Fig. 1, where $G(s)$ is the transfer function of a stable finite dimensional linear time-invariant system and $n(\cdot)$ is a sufficiently smooth nonlinear function such that $n(0) = 0$ and $n'(0) = 0$. These latter hypotheses on the function $n(\cdot)$ are quite general (see also the example of Sec. 3) and are posed to ensure that the origin is a locally stable equilibrium point of the uncontrolled system (i.e. $u(t) = 0$), when the amplitude A of the forcing term is zero. For increasing values of the amplitude A the uncontrolled system exhibits a stable

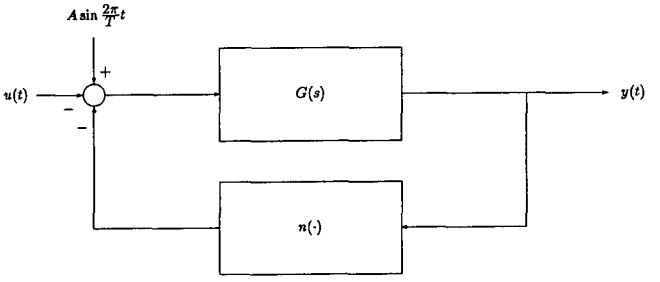

Fig. 1. Feedback system.

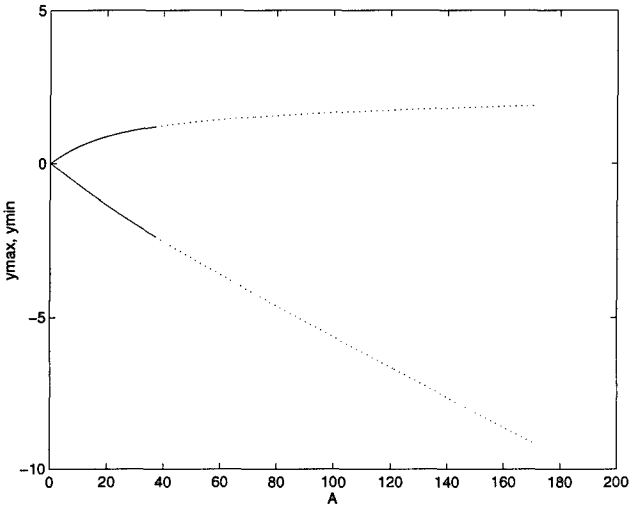

Fig. 2. The solid (dotted) curves correspond to stable (unstable) T-periodic solutions. ($y_{\max} := \max_{t\in[0,T]} y_A(t)$, $y_{\min} := \min_{t\in[0,T]} y_A(t)$).

T-periodic solution up to a certain value, where a first period doubling bifurcation appears. After this value the system possesses an unstable T-periodic solution and a stable $2T$-periodic solution, until this latter solution undergoes a new period doubling bifurcation, and so on according to the well-known sequence which usually leads to chaos. This scenario is illustrated in Fig. 2 where only the T-periodic solutions are indicated explicitly. The basic idea for eliminating the bifurcation sequence is to stabilize the unstable T-periodic solution (the dashed one in Fig. 2), thus inhibiting the first period doubling bifurcation. Obviously, this calls for the design of a controller that stabilizes the family of T-periodic solutions corresponding to the largest possible interval of amplitudes A of the forcing term.

To proceed, consider the problem of stabilizing an unstable T-periodic solution $y_A(t)$ of the uncontrolled system (i.e. $u(t) = 0$) of Fig. 1 corresponding to a given amplitude A of the forcing term. Such a problem requires the design of a linear

time-invariant feedback controller of transfer function $C(s)$, i.e.

$$U(s) = C(s)Y(s), \tag{1}$$

such that $y_A(t)$ becomes a stable T-periodic solution of the controlled system.

It is easily recognized that the controller transfer function must satisfy the condition

$$C\left(jn\frac{2\pi}{T}\right) = 0 \quad for \quad n = 0, 1, 2, \ldots \tag{2}$$

to ensure that the T-periodic solution $y_A(t)$ is still a solution of the controlled system. This fact implies that the transfer function of such a controller has the form

$$C(s) = F(s)(1 - e^{-sT}) \tag{3}$$

where $F(s)$ is in general not restricted to be rational. For instance, $F(s)$ is a constant gain K in [Pyragas, 1992], while it has the form $K(1 - Re^{-sT})^{-1}$ in [Socolar *et al.*, 1994], where R is a suitable constant. A generalization of this latter structure has been used in [Basso *et al.*, 1997a].

To investigate the stability of $y_A(t)$, the linearization of the Lur'e system around the periodic solution is performed. This leads to the linear periodic system of Fig. 3, where the transfer function $L(s)$ of the linear subsystem is given by the feedback interconnection of $G(s)$ and $C(s)$, i.e.

$$L(s) = \frac{G(s)}{1 + C(s)G(s)} \tag{4}$$

and the periodic gain in the feedback path has the form

$$k_A(t) = \left.\frac{dn}{dy}\right|_{y=y_A(t)}. \tag{5}$$

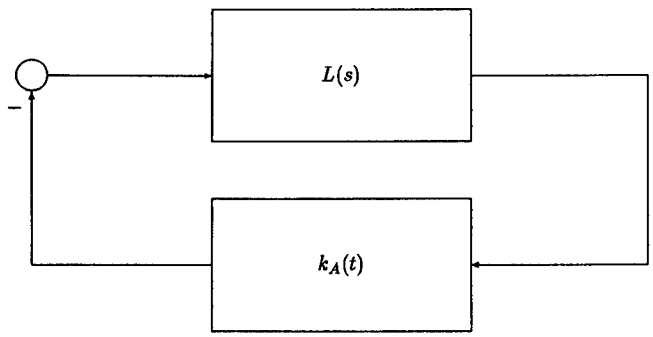

Fig. 3. Linear periodic feedback system.

It is well known that the stability of $y_A(t)$ is guaranteed by the stability of the origin of the linearized system of Fig. 3 [Vidyasagar, 1992]. Here, we refer essentially to input-output stability, even if quite mild assumptions on the feedback interconnection of $G(s)$ and $C(s)$ allow one to consider asymptotic stability [Basso *et al.*, 1997a].

To assess the stability of the system of Fig. 3 and consequently the stability of $y_A(t)$, we can employ the well-known circle criterion [Vidyasagar, 1992]. The two quantities

$$\alpha := -\frac{1}{\max_{t\in[0,T]} k_A(t)} \qquad \beta := -\frac{1}{\min_{t\in[0,T]} k_A(t)} \tag{6}$$

are introduced to state the following stability result.

Theorem 1. *Let $\alpha < 0$ and $\beta > 0$. Then, the controller $C(s)$ stabilizes $y_A(t)$ if*

1. *$L(s)$ is stable;*
2. *the following inequality holds:*

$$\left|L(j\omega) - \frac{\alpha+\beta}{2}\right| < \frac{\beta-\alpha}{2} \qquad \forall\omega \geq 0. \tag{7}$$

Remark 1. Condition (7) has a simple graphical interpretation in terms of the Nyquist plot of $L(s)$. Indeed, the Nyquist plot must lie inside the circle of center $((\beta+\alpha)/2, 0)$ and radius $(\beta-\alpha)/2$.

Remark 2. Similar results can also be given for general values of α and β. However, for the purposes of this paper, it is enough to consider the case $\alpha < 0$ and $\beta > 0$.

From condition (2) and Eq. (4), it follows that $L(jn2\pi/T) = G(jn2\pi/T)$ for $n = 0, 1, 2, \ldots$. Therefore, it is evident that Theorem 1 can ensure stability of $y_A(t)$ only if $L(s)$ is stable and the following inequalities

$$\left|G\left(jn2\frac{\pi}{T}\right) - \frac{\alpha+\beta}{2}\right| < \frac{\beta-\alpha}{2} \text{ for } n = 0, 1, 2, \ldots. \tag{8}$$

hold. Note that the inequalities above rely on the uncontrolled system, thus resulting in an *a priori* test for the guaranteed stabilizability of $y_A(t)$.

Now, the major question is the following: If the *a priori* test (8) is satisfied for $y_A(t)$, is it possible to design a controller $C(s)$ such that Theorem 1

ensures stability of $y_A(t)$? Fortunately, the answer is affirmative as shown by the next result.

Theorem 2. *Let $y_A(t)$ satisfy condition (8) and define $\Phi(s) = 1 - e^{-sT}$. Then, it is always possible to find a stable rational (with stable inverse) approximation $\Phi_{\rm ap}(s)$ of $\Phi(s)$ and a stable rational transfer function $W(s)$ such that the controller*

$$C(s) = \frac{1}{G(s)} \cdot \frac{\left(1 - \frac{\alpha+\beta}{2G(s)}\right)\frac{\Phi(s)}{\Phi_{\rm ap}(s)}W(s)}{1 - \left(1 - \frac{\alpha+\beta}{2G(s)}\right)\frac{\Phi(s)}{\Phi_{\rm ap}(s)}W(s)} \quad (9)$$

stabilizes $y_A(t)$.

Sketch of the proof (see [Basso et al., 1997b] for details):

The stability of $L(s)$ follows directly from the stability of $G(s)$, $\Phi_{\rm ap}^{-1}(s)$, $W(s)$ and $\Phi(s)$. Indeed, from Eqs. (4) and (9) it turns out that

$$L(s) = G(s) - \left(G(s) - \frac{\alpha+\beta}{2}\right)\frac{\Phi(s)}{\Phi_{\rm ap}(s)}W(s)\,.$$

Consider the inequality (7). After some manipulations, it can be rewritten in the form

$$\left|\left(G(j\omega) - \frac{\alpha+\beta}{2}\right)\left(1 - \frac{\Phi(j\omega)}{\Phi_{\rm ap}(j\omega)}W(j\omega)\right)\right| < \frac{\beta-\alpha}{2} \qquad \forall\omega \geq 0$$

and, equivalently,

$$\left|\left(1 - \frac{\Phi(j\omega)}{\Phi_{\rm ap}(j\omega)}W(j\omega)\right)\right| < \frac{\frac{\beta-\alpha}{2}}{\left|\left(G(j\omega) - \frac{\alpha+\beta}{2}\right)\right|} \qquad \forall\omega \geq 0\,. \quad (10)$$

Now, the ratio at the right hand side of inequality (10) is greater than one for the set of ω such that $G(j\omega)$ is inside the circle of center $((\beta+\alpha)/2,\ 0)$ and radius $(\beta-\alpha)/2$ (see Remark 1). For this set, which contains $\omega = n2\pi/T$ for $n = 0,\ 1,\ 2, \ldots$, as ensured by condition (8), it is enough to put $W(j\omega)$ close to zero in order that condition (10) holds. For the remaining values of ω, i.e. those such that the ratio at the right hand side of inequality (10) is equal or less than one, we select $\Phi_{\rm ap}$ such that the ratio $\Phi(j\omega)/\Phi_{\rm ap}(j\omega)$ is arbitrarily close to one. This can always be done since at such frequencies $\Phi(j\omega)$ is always different from zero. At this point it is enough to choose $W(j\omega)$ close to one to fulfill condition (10) also for these frequencies. The fact that rational transfer functions are dense in the L_1 space concludes the proof.

Remark 3. A possible way to select $\Phi_{\rm ap}$ is to use the standard odd Padé approximation of e^{-sT}. However, the resulting $\Phi_{\rm ap}$ has its zeros on the imaginary axis. This drawback is simply eliminated by slightly shifting the zeros into the left half plane, thus arriving at a new $\Phi_{\rm ap}$ that has a stable inverse. Increasing the order of the Padé approximation, it is easily verified that the ratio $\Phi(j\omega)/\Phi_{\rm ap}(j\omega)$ is quite close to one at all frequencies, except for $\omega = n2\pi/T$ for $n = 0,\ 1,\ 2, \ldots$. The choice for W is based on the idea of not using the controller ($W(j\omega) = 0$) at the frequencies ω where $G(j\omega)$ is already inside the circle of center $((\beta+\alpha)/2,\ 0)$ and radius $(\beta-\alpha)/2$, and to use the controller at the remaining frequencies to force $L(j\omega)$ towards the center of such a circle. Finally, we note that it is often possible to simplify the controller (9) via a suitable order reduction.

Despite the complicated aspect of Eq. (9), the implementation of the controller is rather simple. Indeed, the controller is obtained via the positive feedback scheme reported in Fig. 4 that makes clear the presence of a unique delay element and two rational filters, $G(s)$ and

$$H(s) = \left(1 - \frac{\alpha+\beta}{2G(s)}\right)\frac{W(s)}{G(s)\Phi_{\rm ap}(s)}\,. \quad (11)$$

Let us now consider the problem of stabilizing the family of T-periodic solutions corresponding to the largest interval of amplitudes A of the forcing term. To this purpose, let A_0 denote the largest possible value of A such that condition (8) holds where $\alpha = \alpha_0$ and $\beta = \beta_0$, being α_0 and β_0 defined as

$$\alpha_0 = \max_{A\in[0,A_0]} \alpha \qquad \beta_0 = \min_{A\in[0,A_0]} \beta\,. \quad (12)$$

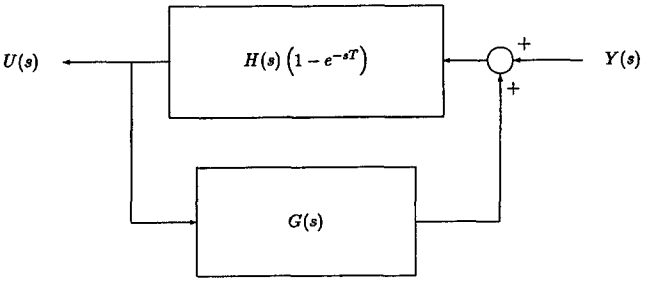

Fig. 4. Controller structure.

Clearly, the application of Theorem 2 guarantees that all the T-periodic solutions corresponding to amplitudes $A \leq A_0$ are stabilized by the controller $C(s)$.

Finally, we recall that Theorem 2 provides a sufficient condition for the stability of $y_A(t)$, i.e. $y_A(t)$ may be stable even if condition (8) is far from being satisfied (see the example in the next section). However, several application examples have shown that the controller designed via our approach performs much better than other controllers that do not satisfy condition (7). This is illustrated via the example developed in the next section.

3. Example

Consider the equation of the driven Toda oscillator

$$\ddot{y} + 0.8\dot{y} + 25(e^y - 1) = A \sin 2\pi t - u(t)\,. \quad (13)$$

This system has been extensively studied in [Just *et al.*, 1997], where the analysis of the Floquet exponents showed the presence of a set of stable orbits of period $T = 1$ in the range $A \in (0, 37)$ of the forcing input. For larger values of the amplitude the system undergoes a sequence of period doubling bifurcations leading to chaos. The stable (solid curve) and unstable (dotted curve) T-periodic solutions of the uncontrolled system are reported in Fig. 2. The upper and the lower curves represent the maximum and minimum, respectively, of the periodic solution $y_A(t)$, as a function of the system parameter A.

The control technique proposed in this paper can be fruitfully exploited to derive a unique time-delayed feedback controller such that the controlled system has stable periodic solutions for a much larger range of the parameter A. It is easily recognized that system (13) can be recast in the classical Lur'e structure of Fig. 1, where

$$G(s) = \frac{1}{s^2 + 0.8s + 25} \quad (14)$$

and

$$n(y) = 25(e^y - y - 1)\,. \quad (15)$$

Note that $G(s)$ is stable and $n(0) = n'(0) = 0$.

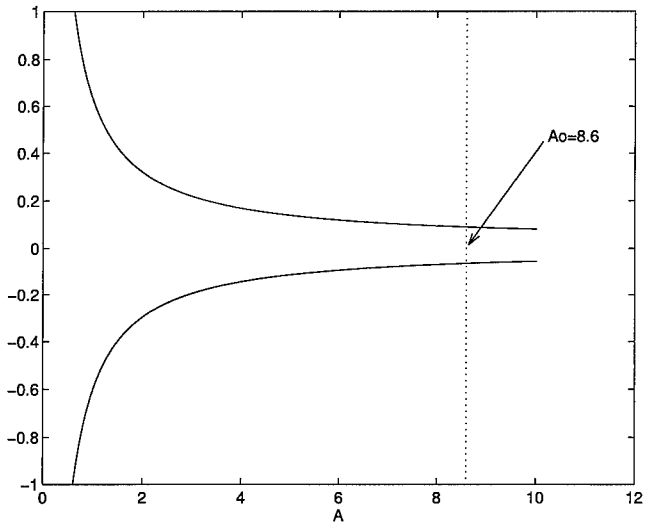

Fig. 5. $\alpha(A)$ (lower curve), $\beta(A)$ (upper curve).

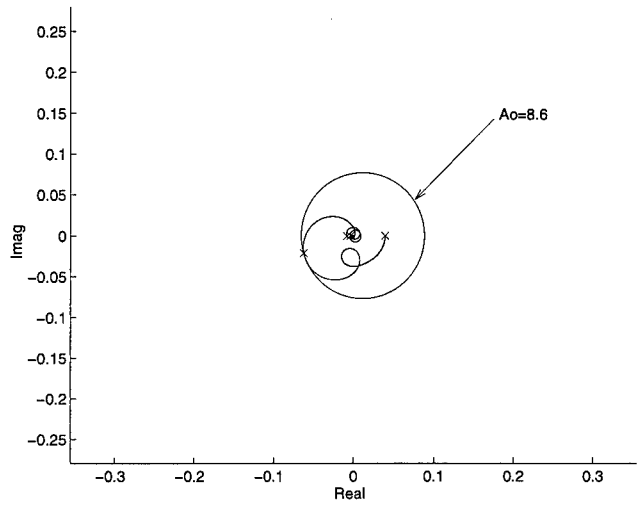

Fig. 6. Nyquist plot of $L(s)$ using controller (16).

From the bifurcation diagram of Fig. 2 and using expressions (5), (6) and (15) we can derive the two functions α and β of the amplitude A, shown in Fig. 5.

From these functions, we compute A_0, i.e. the largest possible value of A satisfying condition (8), that is the smallest circle that includes the fixed complex points at the frequencies $2n\pi$, $n = 0, 1, \ldots$ ('x' marks in Figs. 6–8). It turns out that $\alpha_0 = -0.064$, $\beta_0 = 0.088$ and $A_0 = 8.6$.

Based on Theorem 2 and the structure in Fig. 4, the following controller is obtained

$$C(s) = \frac{H(s)(1 - e^{-s})}{1 - G(s)H(s)(1 - e^{-s})}\,, \quad (16)$$

where

$$H(s) = \frac{1.3s^2 + s + 32.5}{5 \cdot 10^{-7}s^3 + 1.3 \cdot 10^{-4}s^2 + 1.6 \cdot 10^{-2}s + 1} \cdot \Phi_{\text{ap}}^{-1}(s)\,. \tag{17}$$

Here, the stable filter

$$\Phi_{\text{ap}}(s) = \frac{2s^5 + 20s^4 + 899s^3 + 4598s^2 + 35720s + 108900}{s^5 + 30s^4 + 420s^3 + 3360s^2 + 15120s + 30240} \tag{18}$$

follows directly from the fifth order Padé approximation of e^{-s}.

The Nyquist plot of the corresponding closed loop transfer function $L(s)$ is indicated in Fig. 6 together with the circle intersecting the real axis in α_0 and β_0.

Simulations show that the designed controller (16) stabilizes the periodic orbits of system (13) over the range $A \in (0, 1500)$, where the upper bound is only due to numerical problems in integrating the system at large values of A.

We can compare the results obtained by our controller with those presented in [Just *et al.*, 1997], where a Pyragas controller was designed exploiting Floquet theory. The derived control law was

$$u(t) = 2.4[\dot{y}(t) - \dot{y}(t-1)]\,, \tag{19}$$

or, equivalently,

$$C(s) = F(s)(1 - e^{-s}) = 2.4s(1 - e^{-s})\,. \tag{20}$$

Such a controller is optimal among the controllers with the same structure but different gains (i.e. $F(s) = Ks$), in the sense of minimizing the Floquet exponents at the given input amplitude $A = 105$.

Figure 7 shows the application of Theorem 1 to the system (13) and the controller (20). From the Nyquist diagram we can derive $A = 4$, $\alpha = -0.149$ and $\beta = 0.173$ (circle with solid curve). For comparison, Fig. 7 also reports the optimal circle at $A_0 = 8.6$ (dotted curve).

Finally, we note that the controller (20) is also optimal with respect to Theorem 1 in the sense that maximizes the amplitude A among the controllers with the same structure but different gains.

Simulations on the controlled system show that the controller (20) can stabilize all the orbits of period 1 in the much restricted range $A \in (0, 131)$.

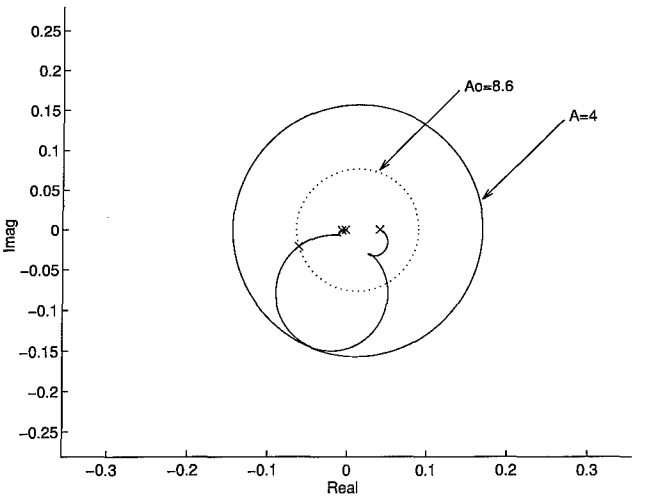

Fig. 7. Nyquist plot of $L(s)$ using controller (20).

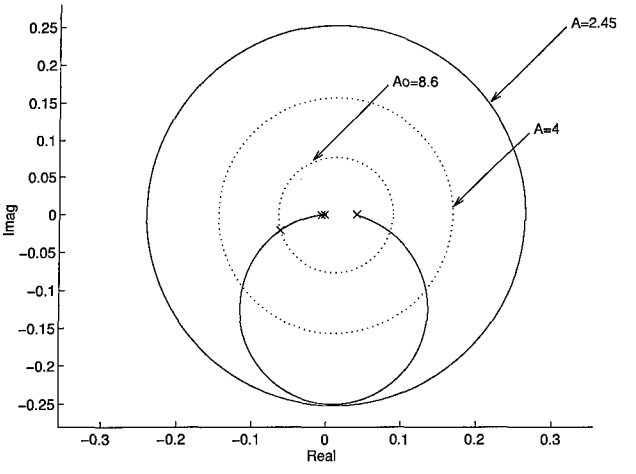

Fig. 8. Nyquist plot of $G(s)$.

Table 1. Results of the example.

$C(s)$	Guaranteed Stability Range	Simulated Stability Range
0	$A \in (0, 2.45)$	$A \in (0, 37)$
$2.4s(1 - e^{-s})$	$A \in (0, 4)$	$A \in (0, 131)$
Eq. (16)	$A \in (0, 8.6)$	$A \in (0, 1500)$

To conclude, Theorem 1 is applied to the uncontrolled system [see the Nyquist plot of the linear subsystem (14) in Fig. 8] determining the values of $\alpha = -0.241$, $\beta = 0.266$ and $A = 2.45$ (solid circle in Fig. 8).

We summarize the results obtained in Table 1, which definitely supports our claim that

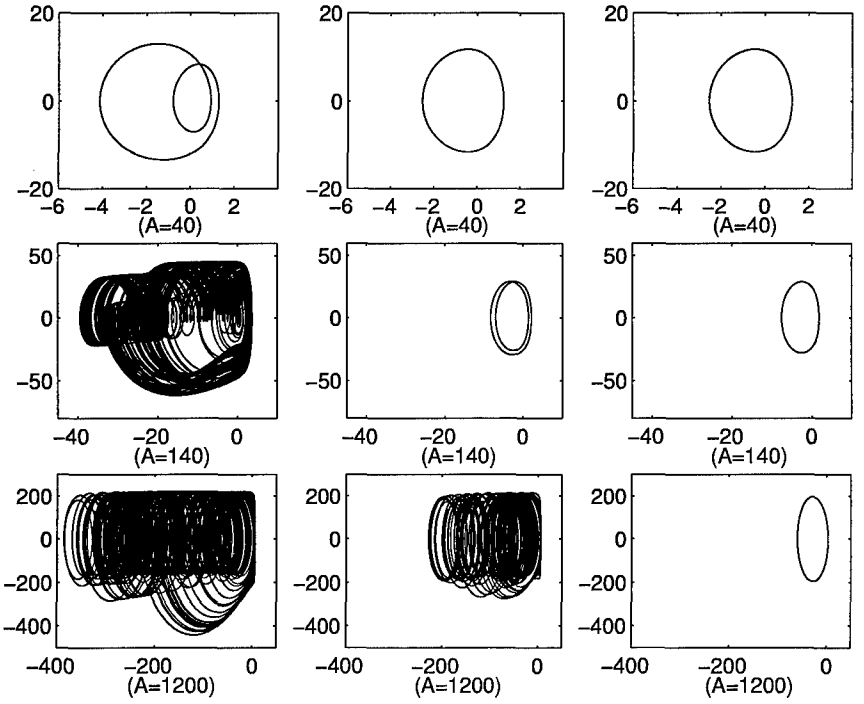

Fig. 9. Simulations in the $(y, \dot{y})$ plane: Each row denotes a different value of the parameter A $(40, 140, 1200)$, while each column indicates a different controller, i.e. column 1 $C(s) = 0$, column 2 controller (20), column 3 controller (16).

the larger the amplitude of the system input fulfilling Theorem 1, the larger the range that is stabilized in practice. For completeness, we have also reported some of the simulation results in Fig. 9 for different values of the parameter A and for the controllers presented in the example.

4. Conclusion

The paper has dealt with the problem of designing time delayed feedback controllers to stabilize unstable periodic orbits, a problem of great interest in the control of chaos. For an important class of sinusoidally forced nonlinear systems, we have formulated such a problem as an absolute stability problem of a linear periodic feedback system, in order to employ classical stability tools.

Our main contribution is a simple procedure for designing the optimal stabilizing linear time-invariant feedback controller, i.e. the one that guarantees the largest stability bounds obtainable via the well-known circle criterion. Several examples have shown that the performance of the designed optimal controller is quite satisfactory also in comparison with different approaches. This has been illustrated in the application example, where also the possible use of the proposed approach for eliminating the period doubling bifurcation sequence has been shown.

References

Abed, E. H. & Wang, H. O. [1995] "Feedback control of bifurcations and chaos in dynamical systems," in *Recent Developments in Stochastic and Nonlinear Dynamics: Applications to Mechanical Systems*, eds. Namachchivaya, N. S. & Kliemann, W. (CRC Press), pp. 153–173.

Basso, M., Genesio, R. & Tesi, A. [1997a] "Stabilizing periodic orbits of forced systems via generalized Pyragas controllers," *IEEE Trans. Circuits Syst. I* **44**, 1023–1027.

Basso, M., Genesio, R. & Tesi, A. [1997b] "Stabilization of periodic orbits of forced systems: State of the art and new proposals," Research Report 29/97, Dipartimento di Sistemi e Informatica, Firenze.

Chen, G. & Dong, X. [1993] "From chaos to order. Perspective and methodologies in controlling chaotic nonlinear dynamical systems," *Int. J. Bifurcation and Chaos* **3**, 1363–1409.

Dressler, U. & Nitsche, G. [1992] "Controlling chaos using time delayed coordinates," *Phys. Rev. Lett.* **68**, 1–4.

Hu, G., Qu, Z. & He, K. [1995] "Feedback control of chaos in spatiotemporal systems," *Int. J. Bifurcation and Chaos* **5**, 901–936.

Hunt, E. R. [1991] "Stabilizing high-period orbits in chaotic system: The diode resonator," *Phys. Rev. Lett.* **67**, 1953–1955.

Just, W., Bernard, T., Ostheirer, M., Reibold, E. & Benner, H. [1997] "Mechanism of the time-delayed feedback control," *Phys. Rev. Lett.* **78**, 203–206.

Kittel, A., Parisi, J. & Pyragas, K. [1995] "Delayed feedback control of chaos by self-adapted delay time," *Phys. Lett.* **A198**, 433–436.

Ogorzalek, M. J. [1993] "Taming chaos — Part II: Control," *IEEE Trans. Circuits Syst.* **40**, 700–706.

Ott, E., Grebogi, C. & Yorke, J. A. [1990] "Controlling chaos," *Phys. Rev. Lett.* **64**, 1196–1199.

Pyragas, K. [1992] "Continuous control of chaos by self-controlling feedback," *Phys. Lett.* **A170**, 421–428.

Romeiras, F. J., Grebogi, C., Ott, E. & Dayawansa, W. P. [1992] "Controlling chaotic dynamical systems," *Physica* **D58**, 165–192.

Shinbrot, T., Grebogi, C., Ott, E. & Yorke, J. A. [1993] "Using small perturbations to control chaos," *Nature* **363**, 411–417.

Socolar, J. E. S., Sukow, D. W. & Gauthier, D. J. [1994] "Stabilizing unstable periodic orbits in fast dynamical systems," *Phys. Rev.* **E50**, 3245–3248.

Vidyasagar, M. [1992] *Nonlinear System Analysis*, 2nd edition (Prentice Hall, Englewood Cliffs, NJ).

International Journal of Bifurcation and Chaos, Vol. 8, No. 8 (1998) 1707–1711

CONTROL OF CHAOTIC MAPS BY OPTIMIZED PERIODIC INPUTS

R. METTIN
Drittes Physikalisches Institut, Universität Göttingen,
Bürgerstraße 42-44, D-37073 Göttingen, Germany

Received July 31, 1997; Revised December 16, 1997

It has been established that chaotic iterated maps can be transferred to a periodic motion by application of periodic signals. As a next step, we investigate the optimization of such signals with respect to a small norm. This method employs a cost function on the space of periodic inputs. By means of a direct optimization search in this space, the approach stabilizes periodicity with small forces. The results for increasing driving periods are compared.

1. Introduction

In recent years, many authors considered the problem of controlling chaotic systems (see [Chen & Dong, 1993; Shinbrot, 1995] for reviews). A common goal is to force the chaotic system into a periodic state. Other intentions might be a migration of the system to certain phase space regions, synchronization with an arbitrary signal, or the enhancement of chaos in the system. In this paper we will focus on the conversion of chaos to periodicity. There are two aspects of this approach: (i) some advantage of a periodic behavior over a chaotic one (e.g. reduced drag, higher mean output, limited peak values, or simple predictability), and (ii) the proximity of the chaotic motion to (infinitely many) unstable periodic solutions. The second point is the reason why it may take very little effort to control the system. This paper investigates a method to systematically reduce periodic control inputs that remove chaos in iterated maps.

Removal of chaos with very little effort by use of its own specific complex phase space structure is the main aspect pursued in the chaos control field. In this regard, many proposed methods aim to exactly stabilize a pre-existing unstable periodic orbit (UPO) embedded in the chaotic attractor. Such techniques usually require some type of feedback since the control forces correct deviations from the desired orbit. In principle (i.e. in absence of noise, modeling errors, etc.) control forces vanish if the goal is reached ("noninvasive" controls). By contrast there are "invasive" methods that always influence the system. The particular invasive technique we consider is called "open-loop" since it foregoes any additional feedback. The control forces are applied permanently and irrespective of the actual system state. If one wants to achieve a periodic goal motion by an open-loop control, the forces have to be periodic, too. The only possible goal trajectories are asymptotically stable solutions of the periodically driven system — which are typically not pre-existing unstable system solutions like UPOs. It might be possible, however, to control a goal close to a UPO. For instance, a pendulum can be stabilized in a vibrating state near to its unstable inverted position by periodic up and down motion of the suspension (vibrational control, see e.g. [Bellman *et al.*, 1986]).

The history of periodic control of chaotic systems dates back to Alekseev [1987] who sinusoidally modulated a parameter of a chaotic population system modeled by an ordinary differential equation. More recent work has focused on driven

oscillators, often employing an analytical treatment by Melnikov's method [Lima & Pettini, 1990; Braiman & Goldhirsch, 1991; Chacón, 1995]. Interesting effects of periodic and stochastic parameter modulation of iterated maps have been investigated by Rössler *et al.* [1989]. Subsequent experimental work has employed periodic modulation for removal of chaos [Azevedo & Rezende, 1990; Fronzoni *et al.*, 1991; Ciofini *et al.*, 1995].

A somewhat different approach of open-loop control was proposed by Hübler & Lüscher [1989]. They constructed control forces starting from an explicit goal trajectory of the system (whereas simple periodic modulation methods do not provide *a priori* knowledge of the eventual controlled orbit). Their entrainment control method is not limited to chaotic systems, and the goal trajectory need not be periodic. Nevertheless, authors often deal with the chaos to periodicity conversion problem [Jackson & Hübler, 1990; Jackson, 1991; Jackson & Kodogeorgiou, 1992; Mettin *et al.*, 1995].

Modulation can be simple and fast, which is the main advantage of the open-loop approaches over the feedback approach as long as one accepts larger permanent control signals. An attempt to reduce the control power by a suitable shaping of the modulation was proposed for chaotic continuous flows [Mettin & Kurz, 1995]. It was demonstrated that multimode signals can scale down the control and switch between different goal states. Now we consider the control of chaotic iterated maps in the same manner. Therefore, the control problem is restated in terms of an optimization problem. We seek to find convenient periodic control inputs that (i) introduce asymptotically stable periodic solutions in the chaotic system, and (ii) are small in a given sense. With respect to smallness, there are several considerations. In principle, the power needed by noninvasive methods to keep an originally chaotic system in periodic motion is negligible. Intuitively, one expects that the finite power an open-loop control needs is less the closer the goal is to the uncontrolled, natural dynamics. This might depend on the exact definitions of "power" and "close". However, if this expectation holds, orbits resulting from small signal periodic modulation may emerge near to UPOs. On the other hand, the underlying UPO structure may facilitate a periodic modulation approach.

The optimization problem and the control signal search are stated in detail in Sec. 2. In Sec. 3 the method is applied to a map that models driven dissipative oscillators, and the results for increasing control signal period are compared. A discussion is given in Sec. 4.

2. Optimization Problem and Direct Search Approach

We consider an iterated map dynamics subject to a periodic control signal input,

$$\mathbf{x}^{(n)} = \mathbf{f}(\mathbf{x}^{(n)}, \mathbf{u}^{(n)}), \quad \mathbf{u}^{(n+N)} = \mathbf{u}^{(n)}, \qquad (1)$$

where $n \in Z$ is the discrete time, N is the period of the control, and $\mathbf{x} \in \mathbb{R}^d$, $\mathbf{u} \in \mathbb{R}^k$, $\mathbf{f} : \mathbb{R}^d \times \mathbb{R}^k \mapsto \mathbb{R}^d$. Without control, i.e. if all $\mathbf{u}^{(n)} = \mathbf{0}$, we assume chaotic motion of the system. The task is to find a convenient set $\mathbf{U}_N = \{\mathbf{u}^{(n)}\}_{n=0,\ldots,N-1}$ such that (i) there exists an asymptotically stable periodic solution of Eq. (1), and (ii) some norm of the input set is small.

To determine the quality of a test set $\mathbf{U}_N$, information must first be gained about existence of an asymptotically stable periodic solution under its action. This is used in connection with the control signal's norm for evaluation of a cost function like

$$\text{cost} = \begin{cases} \|\mathbf{U}_N\| : & \text{stable period} \\ c_p : & \text{otherwise} \end{cases} \qquad (2)$$

where c_p is some large (penalty) number. An optimization algorithm performs the task of finding a test set that minimizes the cost function. It turns out that the cost landscape defined by Eq. (2) can be very complicated and rough or fractal-like. Therefore we expect to find sufficient but not optimal control forces.

The optimization works directly on the (kN)-dimensional space of control signal sequences $\mathbf{U}_N$. The detection of the existence of an asymptotically stable periodic solution is done by a recurrence check for different initial conditions. For simplicity in this initial study, we do not include statements about the basin of attraction so as to avoid excessive numerics needed to check for coexisting attractors. Thus we are content with periodicity for a few selected initial states $\mathbf{x}^{(0,j)}$ and an *a posteriori* test of the basin after the complete optimization. If all tested initial $\mathbf{x}^{(0,j)}$ lead (after M transient iterations) to a periodic recurrence of the same response period $\tilde{N}$, it is concluded that a stable periodic solution exists under the influence of the control signal, and that the basin of attraction has some larger extent. Then the tested control signal is assigned a cost value according to its norm.

To decrease the cost, the optimization algorithm directly manipulates the control sequence $\mathbf{U}_N$ what we call a direct search. It is also possible to implement an indirect search that manipulates goal trajectories instead of the control forces. The latter corresponds to a transfer of the optimized entrainment control approach [Mettin, 1997] to iterated maps, and it will be investigated in future work.

3. Example

As an example we consider a two-dimensional map introduced by Parlitz *et al.* [1991]. It models a class of driven dissipative oscillators and reads

$$\begin{aligned} x_1^{(n+1)} &= \gamma(x_1^{(n)} \cos\beta - x_2^{(n)} \sin\beta) \\ x_2^{(n+1)} &= \gamma(x_1^{(n)} \sin\beta + x_2^{(n)} \cos\beta) + a + u^{(n)} \end{aligned} \tag{3}$$

where $u^{(n)}$ is the (scalar) control, and

$$\gamma = e^{-dT/2}, \quad \beta = T + |x_1^{(n)}|^2 + |x_2^{(n)}|^2 . \tag{4}$$

The parameters correspond to a damping d, a driving period T, and a driving amplitude a (where the control acts upon). They were set to $T = 1.0$, $d = 0.9162$, $a = 1.5$ which results in a chaotic dynamics. As a cost function we chose Eq. (2) with $c_p = 10$ and the L_2 norm of the control inputs $\mathbf{U}_N$ written as an N-dimensional vector, divided by the control period N:

$$\|\mathbf{U}_N\| = \frac{1}{N} \left(\sum_{n=0}^{N-1} |u^{(n)}|^2 \right)^{\frac{1}{2}} . \tag{5}$$

The recurrence was checked up to period 32 with five different initial conditions $\mathbf{x}^{(0,j)} = (2j-1)(0.1, 0.1)$, $j = 1, \ldots, 5$. The check was done after $M = 100$ transients and for a recurrence of 10^{-3}. For the search of small cost values in the N-dimensional control signal space the numerical optimization algorithm **amebsa**, a variant of simulated annealing, from [Press *et al.*, 1992] was employed.

Figure 1 shows a bifurcation diagram of the parameter a near the chosen value for the uncontrolled oscillator map. It can be seen that the chaotic region reaches from about $a = 1.32$ upwards, and a few, narrow periodic windows are visible. Periodic control is equivalent to a periodic shift of the driving amplitude a. Note, however, that a is never reduced below 1.32 by application of all in the following reported optimized signals.

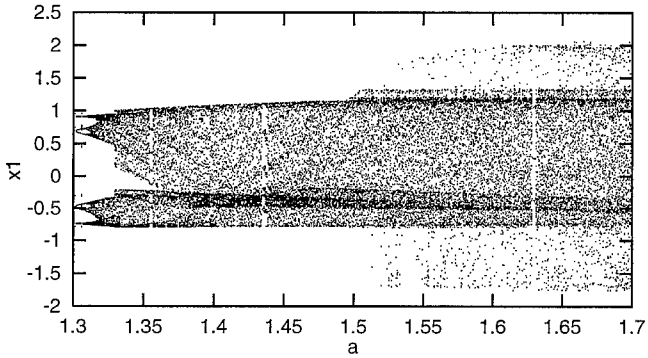

Fig. 1. Bifurcation diagram of the uncontrolled oscillator map Eq. (3): first coordinate x_1 versus parameter a.

A period 1 control signal corresponds to a constant parameter shift of a, and the nearest low-periodic window to $a = 1.5$ can be found at $a_1 = 1.4356$ (response period $\tilde{N} = 28$). This is in some sense the only obvious nonoptimized control signal as it can easily be extracted from a codimension one bifurcation diagram. Such an initial guess is not straightforward in the higher dimensional control signal spaces (besides the trivial set of identical $u^{(n)} = a - a_1 = 0.0644$). Therefore the purpose of the optimzation procedure is twofold: first to find a nontrivial stabilizing sequence $\mathbf{U}_N$ at all, and second to reduce the norm of such a sequence.

Control inputs of periods N from 2 to 12 were used for optimization. For all control periods N the algorithm easily found nontrivial stabilizing sets. Further optimization reduced the norm on average by a factor of 2. The computations were terminated when no further improvement of the cost criterion (2) could be found within a given time. The runs were repeated a few times, and arbitrary sequences as well as results from lower periods (extended to an integer multiple control period) were used as initial guesses. The overall best results from all runs have been taken. The expenditure for obtaining the individual optimized results was moderate but similar for the various N. Therefore a comparison of these is justified, though the results are supposed to provide only some local cost minima. Figure 2 presents the magnitude of the best signals found in different norms versus the driving period N. The L_2-type norm used for optimization [Eq. (5)] is indicated by the squares connected by the solid curve. The dashed line connects for the same control inputs the arithmetic mean of the absolute values

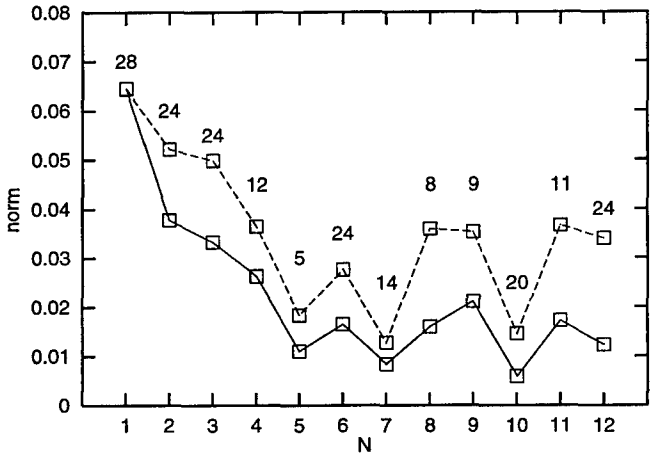

Fig. 2. Magnitude of the optimized control signals versus their period: the solid line connects the values of norm Eq. (5), the dashed line of norm Eq. (6).

(L_1-type norm):

$$\|\mathbf{U}_N\|_1 = \frac{1}{N}\sum_{n=0}^{N-1}|u^{(n)}|\,. \qquad (6)$$

Note that Eq. (6) is a better criterion for comparison with the trivial control ($N = 1$) than Eq. (5) since the latter gives smaller values for the same signal written in a multiple period. The numbers above the squares indicate the actual system response period $\tilde{N}$ that is achieved by control (always an integer multiple of the driving period N). All control signals have rather small norm values, and the resulting stable periodic orbits turn out to lie close to the chaotic attractor. It can be seen that there is the tendency of the norm to decrease for higher periods, which is plausible because of more degrees of freedom in the search space. However, the control cost does not decline monotonously, but seems to saturate except for some selected minima (at control periods $N = 5$, 7, and 10). Therefore the gain of an optimized periodic driving with respect to constant parameter shift (trivial periodic control) depends to some extent on the specific period of the applied control signal. In Fig. 3, the optimized period-7 control is shown (lower plot). The resulting orbit was detected as a period 14, and its first coordinate is shown in the upper plot (diamonds connected by the solid line). It runs close to a UPO of period 7 (dotted line). In fact, all emerging stable periodic states are adjacent to pre-existing unstable periodic orbits, but a detailed analysis of this is beyond the scope of the paper. In particular, a certain hierarchy of the different UPOs might

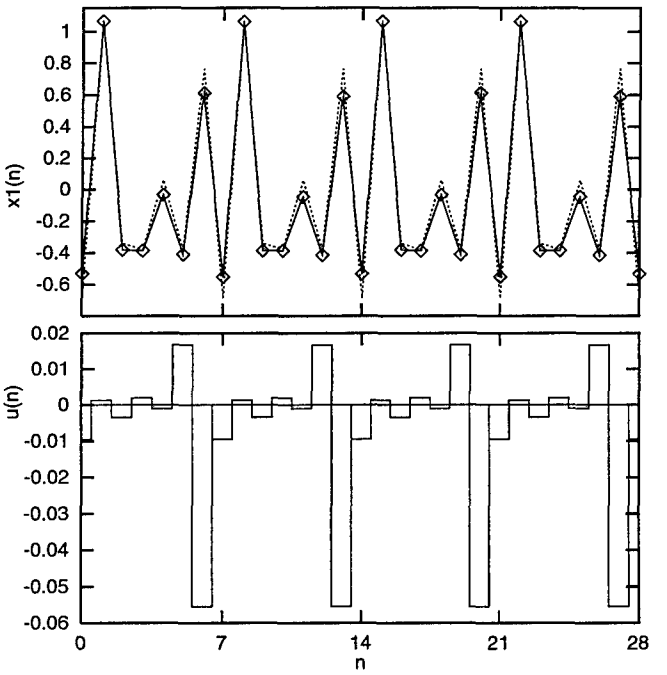

Fig. 3. Optimized control signal u of period 7 versus discrete time n (lower plot), and resulting periodic orbit (diamonds in the upper plot). An adjacent UPO is indicated by the dotted line.

underly the effort necessary to stabilize the system in their vicinity.

Finally, the result of the optimization depends on the chosen cost function. Here a quadratic mean of the applied signal was minimized, which does not avoid relatively large single inputs (compare the relative peak of $u^{(6)}$ shown in Fig. 3). To minimize the largest control amplitude, one might choose the maximum norm for the cost evaluation.

4. Discussion

It was demonstrated that a chaotic iterated map can be controlled to return eventual periodic motions by means of small optimized inputs of various periodicity. The optimization of the cost function corresponds to a search for periodic windows in the control signal parameter space near to the origin. The possibility of finding such a window should in principle increase with the dimension (the control signal period). Accordingly, the example shows a trend of decreasing control forces for higher driving periods, with some periods being preferred. This might be related to the underlying structure of UPOs, as controlled trajectories appeared near them. Besides the pure reduction of open-loop control forces, this connection of stabilized periodic states and pre-existing

UPOs provides an interesting result. Further investigations about the stabilizing mechanisms would be relevant not only for control applications but also for synchronization studies. Besides the role of unstable orbits, the investigation of chaotic transients of the periodically controlled maps might be of some further interest since they can strongly vary for neighbored initial conditions.

Acknowledgments

The author thanks John Allen for carefully reading the manuscript.

References

Alekseev, V. V. & Loskutov, A. Yu. [1987] "Control of a system with a strange attractor through periodic parametric action," *Dokl. Akad. Nauk. SSSR* **293**, 1346–1348.

Azevedo, A. & Rezende, S. M. [1991] "Controlling chaos in spin-wave instabilities," *Phys. Rev. Lett.* **66**, 1342–1345.

Bellman, R. E., Bentsman, J. & Meerkov, S. M. [1986] "Vibrational control of nonlinear systems: Vibrational stabilizability," *IEEE Trans. Automat. Contr.* **AC-31**, 710–716.

Braiman, Y. & Goldhirsch, I. [1991] "Taming chaotic dynamics with weak periodic perturbations," *Phys. Rev. Lett.* **66**, 2545–2548.

Chacón, R. [1995] "Geometrical resonance as a chaos eliminating mechanism," *Phys. Rev. Lett.* **77**, 482–485.

Chen, G. & Dong, X. [1993] "From chaos to order — Perspectives and methodologies in controlling chaotic nonlinear dynamical systems," *Int. J. Bifurcation and Chaos* **3**(6), 1363–1409.

Ciofini, M., Meucci, R. & Arecchi, F. T. [1995] "Experimental control of chaos in a laser," *Phys. Rev.* **E52**, 94–97.

Fronzoni, L., Giocondo, M. & Pettini, M. [1991] "Experimental evidence of suppression of chaos by resonant parametric perturbations," *Phys. Rev.* **A43**, 6483–6487.

Hübler, A. & Lüscher, E. [1990] "Resonant stimulation and control of nonlinear oscillators," *Naturwissenschaften* **76**, 67–69.

Jackson, E. A. & Hübler, A. [1990] "Periodic entrainment of chaotic logistic map dynamics," *Physica* **D44**, 407–420.

Jackson, E. A. [1991] "On the control of complex dynamic systems," *Physica* **D50**, 341–366.

Jackson, E. A. & Kodogeorgiou, A. [1992] "Entrainment and migration controls of two-dimensional maps," *Physica* **D54**, 253–265.

Lima, R. & Pettini, M. [1989] "Suppression of chaos by resonant parametric perturbations," *Phys. Rev.* **A41**, 726–733.

Mettin, R., Hübler, A., Scheeline, A. & Lauterborn, W. [1995] "Parametric entrainment control of chaotic systems," *Phys. Rev.* **E51**, 4065–4075.

Mettin, R. & Kurz, T. [1995] "Optimized periodic control of chaotic systems," *Phys. Lett.* **A206**, 331–339.

Mettin, R. [1997] "Entrainment control of chaos near unstable periodic orbits," *IUTAM Symp. Interactions between Dynamics and Control in Advanced Mechanical Systems*, ed. van Campen, D. H. (Kluwer), pp. 231–238.

Parlitz, U., Scheffczyk, C., Kurz, T. & Lauterborn, W. [1991] "On modeling driven oscillators by maps," *Int. J. Bifurcation and Chaos* **1**(1), 261–264.

Press, W. H., Teukolsky, S. A., Vetterling, W. T. & Flannery, B. R. [1992] *Numerical Recipes in C*, 2nd edition (Cambridge University Press).

Rössler, J., Kiwi, M., Hess, B. & Markus, M. [1989] "Modulated nonlinear processes and a novel mechanism to induce chaos," *Phys. Rev.* **A39**, 5954–5960.

Shinbrot, T. [1995] "Progress in the control of chaos," *Adv. Phys.* **44**(2), 73–111.

International Journal of Bifurcation and Chaos, Vol. 8, No. 8 (1998) 1713–1718

CLUSTERING BIFURCATION AND SPATIOTEMPORAL INTERMITTENCY IN RF-DRIVEN JOSEPHSON JUNCTION SERIES ARRAYS

FAGEN XIE
Institute of Theoretical Physics, Academia Sinica, Beijing 100080, China
HILDA A. CERDEIRA
The Abdus Salam International Center for Theoretical Physics, P.O. Box 586, 34100 Trieste, Italy

Received July 13, 1997; Revised December 16, 1997

We study the spatiotemporal dynamics of the underdamped Josephson junction series arrays (JJSA) which are globally coupled through a resistive shunting load and driven by an rf bias current. Clustering bifurcations are shown to appear. In particular, cluster-doubling induced period-doubling bifurcations and clustering induced spatiotemporal chaos are found. Furthermore, an interesting spatiotemporal intermittency is also found. These phenomena are closely related to the dynamics of the single cell.

The dynamics of globally chaotic systems has been of great interest in recent years. They arise naturally in studies of Josephson junctions arrays, multimode laser, charge-density wave, oscillatory neuronal system, and so on. Some rather surprising and novel features, such as clustering, splay state, collective behavior, and violation of the law of large numbers are revealed in these continuous and discrete globally coupled models [Benz *et al.*, 1990; Bhattacharya *et al.*, 1987; Chernikov & Schmidt, 1995; Domínguez *et al.*, 1991; Domínguez & Cerdeira, 1995; Eikmans & van Himbergen, 1991; Fisher, 1983; Free *et al.*, 1990; Hadley & Beasley, 1987; Hadley *et al.*, 1988; Hebboul & Garland, 1991; Kaneko, 1989; Kvale & Hebboul, 1991; Lee *et al.*, 1992; Middleton *et al.*, 1992; Strogatz & Mirollo, 1993; Tchiastiakov, 1996; Tsang *et al.*, 1991; Tsang & Schwartz, 1992; Watanabe & Strogatz, 1993; Wiesenfeld *et al.*, 1996].

Being a paradigm for the study of nonlinear dynamical systems with many degrees of freedom, Josephson junction series arrays (JJSA) have been a subject of active research. After scaling the parameters [Domínguez *et al.*, 1991], the dynamical equations of an underdamped JJSA shunted by a resistive load, and subject to an rf-bias current $I(t) = I_{\rm dc} + I_{\rm rf}\sin(\omega_{\rm rf}t)$, [Hadley & Beasley, 1987; Hadley *et al.*, 1988; Tsang *et al.*, 1991; Tsang & Schwartz, 1992] are

$$\begin{aligned} &\ddot{\phi}_i + g\dot{\phi}_i + \sin\phi_i + i_L = i_{\rm dc} + i_{\rm rf}\sin(\Omega_{\rm rf}\tau)\,, \\ &i_L = \sigma v(\tau) = \frac{\sigma}{N}\sum_{j=1}^{N} g\dot{\phi}_j\,, \quad i = 1,\ldots,N\,, \end{aligned} \tag{1}$$

where ϕ_i is the superconducting phase difference across the junction i. N is the total number of Josephson junctions or system size. Here, we use reduced units, with currents normalized by the critical current, $i = I/I_c$; time normalized by the plasma frequency $\omega_p t = \tau$, with $\omega_p = (2eI_c/\hbar C)^{1/2}$ and C the capacitance of the junctions; and voltages by rI_c, with r the shunt resistance of the junctions. i_L is the current flowing through the resistive load; $g = (\hbar/2eCr^2I_c)^{1/2} = \beta_c^{-1/2}$, with β_c the

McCumber parameter [McCumber, 1968; Stewart, 1968]; $v = V_{\text{total}}/N$ is the total voltage across the array per junction; $\sigma = rN/R$, with R the resistance of the shunting load, represents the strength of the global coupling in the array; and the normalized rf frequency is $\Omega_{\text{rf}} = \omega_{\text{rf}}/\omega_p$. Equation (1) exhibits rich spatiotemporal behavior, including phase locking, bifurcations, chaos, solitonic excitation, and pattern formation, breaking the law of large numbers and novel pseudo-Shapiro steps emerge in turbulence [Benz *et al.*, 1990; Domínguez *et al.*, 1991; Domínguez & Cerdeira, 1995; Eikmans & van Himbergen, 1991; Free *et al.*, 1990; Hebboul & Garland, 1991; Kvale & Hebboul, 1991; Lee *et al.*, 1992]. However, to the best of our knowledge, the mechanism of the transitions among these dynamical phases, specially the transition from coherence to turbulence, has never been discussed. In this paper we study the interesting spatiotemporal intermittency, clustering bifurcation and clustering induced spatiotemporal chaos in the system (1).

For a single cell (i.e. $N = 1$), the dynamical equation reduces to

$$\ddot{\phi} + \overline{g}\dot{\phi} + \sin\phi = i_{\text{dc}} + i_{\text{rf}}\sin(\Omega_{\text{rf}}\tau)\,, \qquad (2)$$

with $\overline{g} = (1+\sigma)g$. It is well known that Eq. (2) can exhibit chaotic behavior in the underdamped regime, i.e. $\overline{g} < 1$ and $\Omega_{\text{rf}} < 1$ [Ben-Jacob *et al.*, 1982; Bhagavatula *et al.*, 1992; Huberman *et al.*, 1980; Iansiti *et al.*, 1984; Jensen *et al.*, 1984; Kautz & Monaco, 1985; Octavio & Raedi Nasser, 1984]. In Figs. 1(a) and 1(b) we show the bifurcation diagrams, for $\overline{g} = 0.2$, $\Omega_{\text{rf}} = 0.8$, as a function of i_{rf} and i_{dc} respectively. In Fig. 1(a) with $i_{\text{dc}} = 0.03$, the following points are to be remarked: First, the motion of the system (2) is period-1, then as i_{rf} increases to a critical value 0.662, in the system takes place a period-doubling bifurcation to period-2. Second, as i_{rf} continuously increases, the system undergoes a series of period-doubling bifurcation leading to a small scale region of chaos. At $i_{\text{rf}} \approx 0.832$, this chaotic attractor suddenly expands, and is replaced by a large scale chaotic motion. After the expanding transition the system acquires a rotating motion, and the time-averaged voltage becomes nonzero. The bifurcation diagram as a function of i_{dc}, with $i_{\text{rf}} = 0.61$, is shown in Fig. 1(b). The bifurcation behavior is essentially different from that of Fig. 1(a). As i_{dc} increases, the period-1 orbit first loses its stability, then a new period-2 solution arises via period-doubling bifurcation. The most

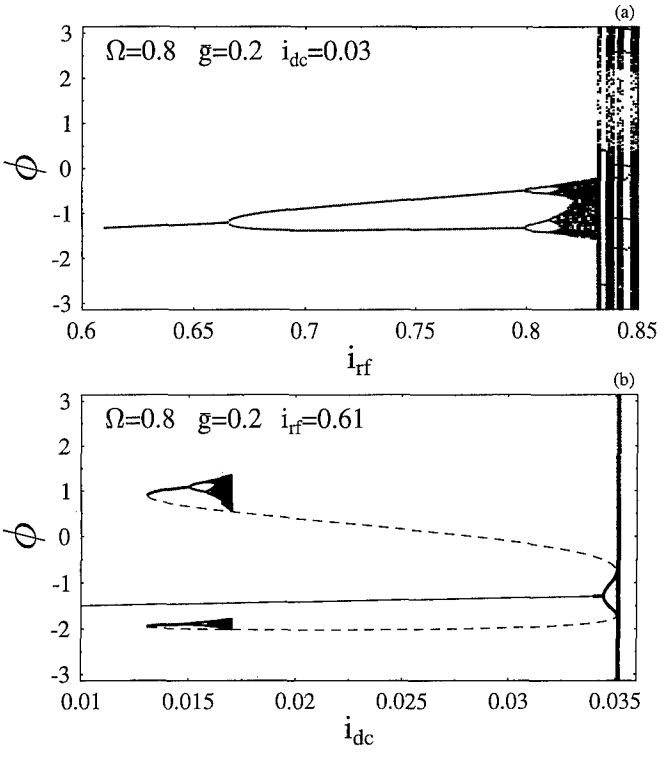

Fig. 1. Plots of ϕ at $t = nT(T = 2\pi/\Omega_{\text{rf}})$, with n being large enough to exclude the transient process.

interesting and surprising point is that this period-doubling solution meets with an unstable period-2 orbit (the dashed lines), and they suddenly disappear via inverse tangent (saddle-node) bifurcation as i_{dc} reaches a critical value $i_{\text{dc}} \approx 0.035076$. Beyond this *threshold*, the behavior of the system is rotating and the motion is chaotic in a large scale region, and has the characteristic of type-I intermittency [Pomeau & Manneville, 1980]. In Fig. 1(b), it is clear that another period-2 orbit appears via tangent bifurcation for i_{dc} near zero. Increasing i_{dc}, this period-2 solution first bifurcates into a small region of chaos through a series of continuous period-doubling bifurcations, then this chaotic motion coincides with the unstable period-2 orbit, and suddenly disappears due to a boundary crisis [Grebogi *et al.*, 1983]. The two attractors form an interesting hysteresis phenomenon. In the following we investigate the complicated spatiotemporal dynamics in JJSA and how it originates from that of a single Josephson junction.

An important concept in a model for globally coupled systems is "clustering". This means that even when the interaction between all elements is identical, the dynamics can break into different clusters, each of which consists of fully synchronized

elements. After the system falls in an attractor, we say that the elements i and j belong to the same cluster if $\phi_i \equiv \phi_j$ for all time. Therefore, the behavior of the whole system can be characterized by the number of clusters $n_{\rm cl}$, and the number of elements of each cluster $(M_1, M_2, \ldots, M_{n_{\rm cl}})$ [Domínguez & Cerdeira, 1995; Kaneko, 1989].

The simplest attractor of the system (1) is the spatially homogeneous configuration, so called *coherent* state, i.e. $\phi_i(\tau) \equiv \phi(\tau)$, $n_{\rm cl} = 1$, $M_1 = N$. Linearizing Eq. (1) around the $\phi(\tau)$ state

$$\delta\ddot{\phi}_i + g\delta\dot{\phi}_i + \cos\,\phi\delta\phi_i + \frac{\sigma}{N}\sum_{j=1}^{N} g\delta\dot{\phi}_j = 0\,, \qquad i = 1, \ldots, N\,. \tag{3}$$

Introducing the following coordinates defined by

$$X = \sum_{j=1}^{N} \delta\phi_j\,, \qquad Y_k = \delta\phi_k - \delta\phi_{k+1}\,, \quad k = 1, \ldots, N-1 \tag{4}$$

After simple algebra, the critical stability boundaries of this coherent state are determined by the following set of linearizing equations:

$$\ddot{X} + \overline{g}\dot{X} + \cos\,\phi X = 0\,, \qquad \ddot{Y}_k + g\dot{Y}_k + \cos\,\phi Y_k = 0\,, \quad k = 1, \ldots, N-1\,. \tag{5}$$

The first equation in (5) is nothing but the equation obtained from linearizing the single cell case [Eq. (2)]. The second one characterizes the evolution of the difference of two cell perturbations. The interesting point here is that the second one has the same structure as the other except that it has g instead of the renormalized $\overline{g}$. Since the difference between the two is proportional to σ, the system recovers the single cell scenario when $\sigma = 0$. The critical boundaries of the coherent state in the σ versus $i_{\rm rf}$ parameter plane are shown in Fig. 2(a) with $\overline{g} = 0.2$, $i_{\rm dc} = 0.03$ and $N = 128$. In the white region, the coherent state (motion in time may be regular and irregular) is *locally* stable, while in the shaded region, the coherent state loses its stability, and bifurcates to a multicluster state. As the coupling strength σ decreases to zero, the instability regions collapse to the discrete bifurcation points for a single cell ($\sigma = 0$). After the coherent state loses the stability, lots of multiclusters are created in the JJSA. A class of interesting states are multiclusters with a uniform distribution of junctions per cluster (i.e. $M_1 = \cdots = M_{n_{\rm cl}}$, with M_i, being the number of elements in the ith cluster), and each cluster may have the same motion except for uniformly distributed phase shifts. We focus on this kind of states, a period-m state with k clusters will be called TmCk state, and $N = k \times n$, $n = 1, 2, 3, \ldots$. It often happens that $m = k$, then the dynamics of the TkCk state is reduced to

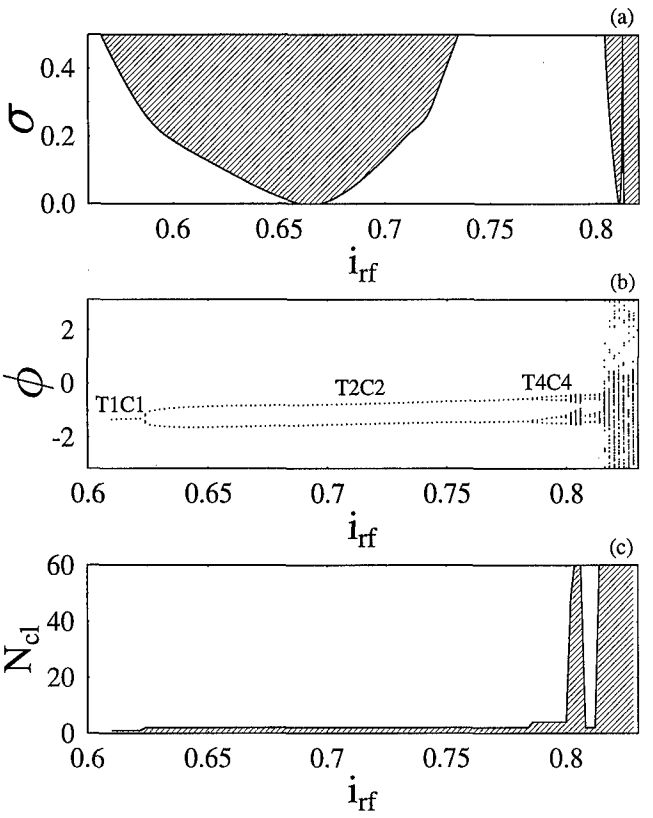

Fig. 2. (a) Bifurcation diagram for the homogeneous or coherent state in σ versus $i_{\rm rf}$ plane with $N = 128$. In the shaded region the coherent state is unstable due to the clustering bifurcation. (b) Bifurcation sequences plotted versus $i_{\rm rf}$ for $\overline{g} = 0.2$, $\Omega_{\rm rf} = 0.8$, $i_{\rm dc} = 0.03$, $\sigma = 0.1$ and $N = 128$. (c) The number of cluster, $n_{\rm cl}$ versus $i_{\rm rf}$ for the state of Fig. 2(b).

$$\ddot{\phi}(\tau) + g\dot{\phi}(\tau) + \sin\,\phi(\tau) + \frac{\sigma}{k}\sum_{j=1}^{k} g\dot{\phi}\left(\tau + \frac{2\pi}{\Omega_{\rm rf}}j\right) = i_{\rm dc} + i_{\rm rf}\sin(\Omega_{\rm rf}\tau)\,. \tag{6}$$

To investigate the clustering bifurcations in JJSA with nonzero coupling, we show the asymptotic state of the system (1) in Fig. 2(b) as a function of $i_{\rm rf}$ with $\sigma = 0.1$, $N = 128$ and the other parameters equal to those of Fig. 1(a). However, the bifurcation diagram is essentially different from that of Fig. 1(a). The T1C1 (coherent) state first

undergoes a cluster-period-doubling bifurcation at $i_{rf} \approx 0.624$ to create a stable T2C2 state. By increasing i_{rf}, the state undergoes further cluster-period-doubling bifurcations leading to spatiotemporal chaos. Figure 2(b) is interesting due to the following novel features. First, we find a cluster-doubling induced period-doubling. The bifurcation point value is below the period-doubling condition for a single Josephson junction. Global coupling leads to cluster doubling at this parameter, which induces period doubling in time. Second, we find a cluster-doubling sequence 1-2-4 (and the induced period-doubling sequence). We expect that this clustering doubling cascade will proceed to a very large number of clusters and long periods. In our case this cascade is interrupted at $k = 4$ by a Hopf bifurcation, i.e. the modulus of another couple of complex eigenvalues is greater than *one*. Nevertheless, the tendency of cluster doubling bifurcations leading to spatiotemporal chaos can still be seen in Fig. 2(c), where we plot number of clusters versus i_{rf} for the state described in Fig. 2(b). Therefore, we conclude that spatiotemporal chaos is made possible by clusterization, and call it "clustering induced spatiotemporal chaos". Moreover, these cluster-doubling sequences grow from the period-doubling sequences of the single cell due to the nonzero global coupling. As σ decreases to zero, the clustering-doubling sequences is identified as the period-doubling sequence of the single cell. If the period-doubling sequence of the single cell is broken off, then the character of the clustering bifurcation in JJSA also changes suddenly. This can be clearly seen in Fig. 3(a) which shows the asymptotic state of the system (1) along the i_{dc} axis, with $\sigma = 0.6$ and the other parameters are the same as those of Fig. 1(b). The T1C1 state first undergoes a cluster-period-doubling bifurcation at $i_{dc} \approx 0.02087$ to create a stable T2C2 state. However, since the period-doubling period-2 solution in the single cell [see Fig. 1(b)] is destroyed by the inverse saddle-node bifurcation by increasing i_{dc}, the T2C2 state in the JJSA is suddenly destroyed by the spatiotemporal intermittency transition near $i_{dc} = 0.02143$. In Figs. 2(b) and 3(a), first we run Eqs. (1) to get the coherent (period-1) state from random initial conditions, then we compute Eqs. (1) by gradually increasing the parameter value (i_{dc} or i_{rf}) and by

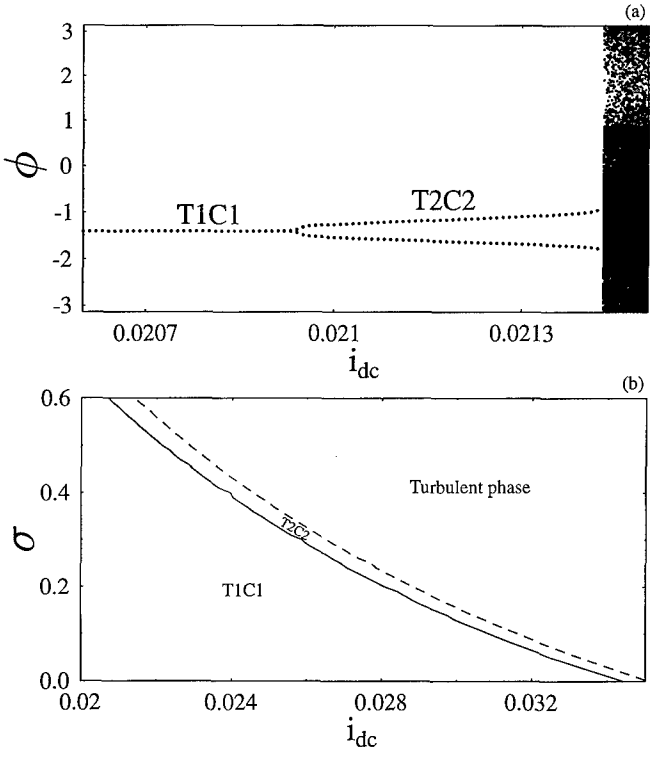

Fig. 3. (a) Bifurcation sequences plotted versus i_{dc} for $\overline{g} = 0.2$, $\Omega_{rf} = 0.8$, $i_{rf} = 0.61$, $\sigma = 0.6$ and $N = 128$. (b) The critical boundaries among the T1C1 state, the T2C2 state and the turbulent phase in i_{dc}–σ plane with the parameters of (a).

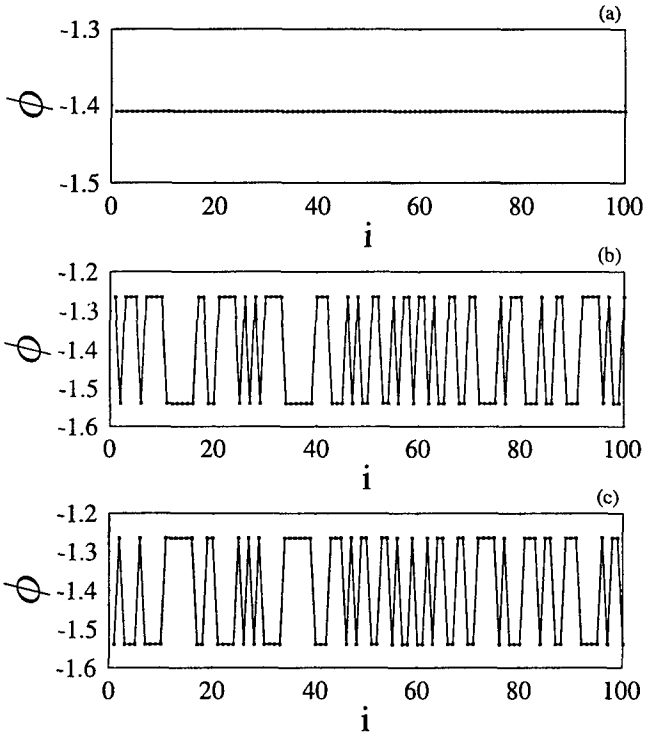

Fig. 4. Snapshot of the asymptotic solution of the system (1) after the transient process for $\overline{g} = 0.2$, $i_{rf} = 0.61$, $\Omega_{rf} = 0.8$, $\sigma = 0.6$, and $N = 100$. (a) $i_{dc} = 0.0206$, (b) and (c) are two successive snapshots for $i_{dc} = 0.0210$.

using the final state for the previous parameter value as the initial state for the new parameter value, in this way we can surely get clusters with a uniform distribution of cells for all cluster-doubling cascades. Figure 3(b) shows the phase diagram among T1C1 state, T2C2 state and the turbulent phase in the σ versus i_{dc} plane. The two critical transition curves in Fig. 3(b) are obtained by the numerical simulation of the system (1). It is clear that the regime of the T2C2 state is very narrow. Figures 4 shows the snapshots of ϕ for the T1C1 state and T2C2 state after a long transient process. The features of coherence and two-cluster are clearly observed in Figs. 4(a), and 4(b)–4(c), respectively. The most interesting phenomenon is that the system suddenly evolves to a very complicated rotating motion as i_{dc} is increased beyond a critical value ($i_{dc} \approx 0.02143$ for $\sigma = 0.6$), i.e. after the T2C2 state loses its stability. The system falls in a large $n_{cl} \sim N$ clusters motion with all M_j small. Figure 5 shows the space-time evolution after a very long and complicated transient process for $i_{dc} = 0.0215$ and $\sigma = 0.6$. The turbulent character of the motion is very clear. The evolution of ϕ_1 (the first junction) is displayed in Figs. 6(a) at the same parameters values as those of Fig. 5. The motion displays periodic behavior (2P) for a long time, it is suddenly interrupted by large

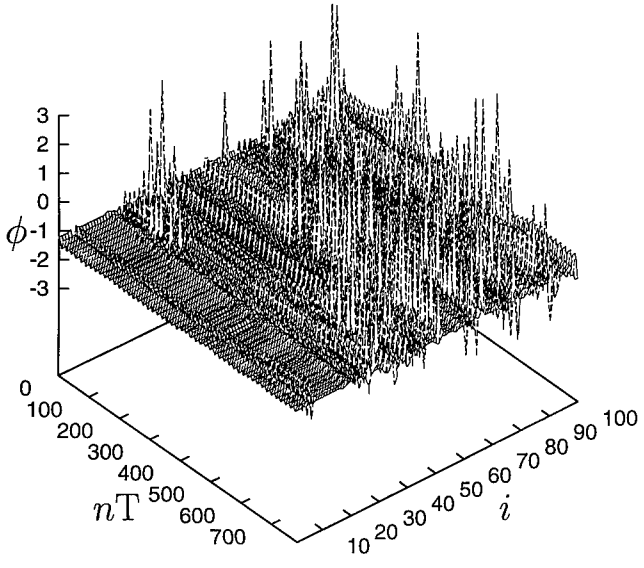

Fig. 5. The time-space evolution of the system (1) for $i_{dc} = 0.0215$ and the other parameters the same as those of Fig. 4. The plots are at $t = nT$ after some transient process, where T is the same as in Fig. 1. The features of turbulence are clearly observed.

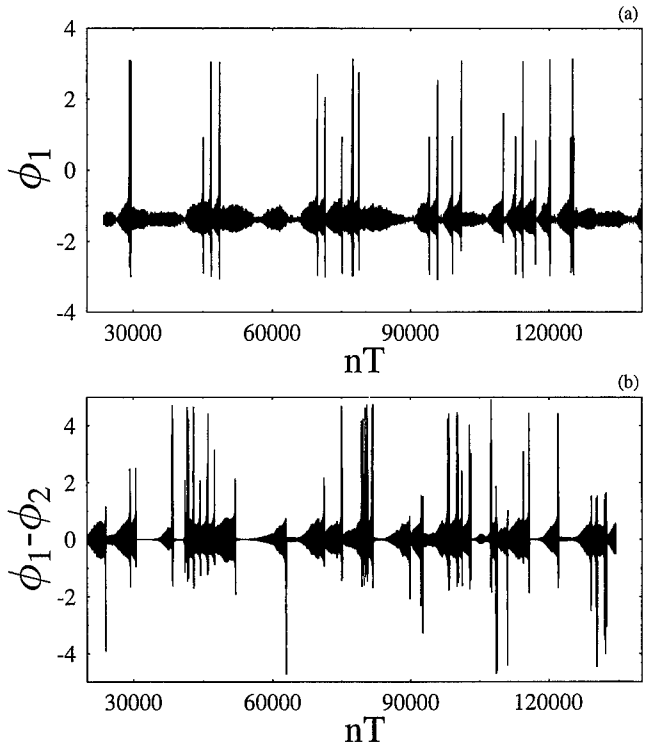

Fig. 6. The evolution of ϕ_1 and $\phi_1 - \phi_2$ with the same parameters as those of Fig. 5. The features of spatiotemporal intermittency are clear.

bursts and quickly resumes the periodic fashion. The similar features of the difference $\phi_1 - \phi_2$ are also displayed in Fig. 6(b). As i_{dc} is far from the critical value, more and more random large bursts take place more frequently. Although this behavior is similar to the characteristic of well-known intermittency, which were investigated in low-dimensional systems [Pomeau & Manneville, 1980], it is an essential type of spatiotemporal intermittency, which has not been found before in the rf-driven JJSA or other high dimensional globally chaotic systems. The above features do not depend on the specific cell and the number of cells. The spatial variable ($N \geq 2$), the dynamics of a single cell and the global coupling are of crucial importance for this interesting phenomenon.

In conclusion we analyzed the complex spatiotemporal dynamics of the rf-driven JJSA. Clustering bifurcation, clustering induced spatiotemporal chaos and spatiotemporal intermittency are shown to appear in these systems. The spatial variable, the dynamics of a single cell and the global coupling are of crucial importance for the existence of these interesting spatiotemporal phenomena.

References

Ben-Jacob, E., Goldhirsh, I., Imry, Y. & Fishman, S. [1982] "Intermittent chaos in Josephson junctions," *Phys. Rev. Lett.* **49**, 1599–1602.

Benz, S. P., Rzchowski, M. S., Tinkham, M. & Lobb, C. J. [1990] "Fractional giant Shapiro steps and spatially correlated phase motion in 2D Josephson arrays," *Phys. Rev. Lett.* **64**, 693–696.

Bhagavatula, R., Ebner, C. & Jayaprakash, C. [1992] "Dynamics of capacitive Josephson junction arrays subjected to electromagnetic radiation," *Phys. Rev.* **B45**, 4774–4787.

Bhattacharya, S., Stokes, J. P., Higgins, M. J. & Klemm, R. A. [1987] "Temporal coherence in the sliding charge-density wave condensate," *Phys. Rev. Lett.* **59**, 1849–1852.

Chernikov, A. A. & Schmidt, G. [1995] "Conditions for synchronization in Josephson-junction arrays," *Phys. Rev.* **E52**, 3415–3419.

Domínguez, D., Jose, J. V., Karma, A. & Wiecko, C. [1991] "Novel axisymmetric coherent vortex state in arrays of Josephson junction far from equilibrium," *Phys. Rev. Lett.* **67**, 2367–2370.

Domínguez, D. & Cerdeira, H. A. [1995] "Spatiotemporal chaos in rf-driven Josephson-junction series arrays," *Phys. Rev.* **B52**, 513–526.

Eikmans, H. & van Himbergen, J. E. [1991] "Stability analysis of Shapiro steps in Josephson-junction arrays," *Phys. Rev.* **B44**, 6937–6942.

Fisher, D. S. [1983] "Threshold behavior of charge-density waves pinned by impurities," *Phys. Rev. Lett.* **50**, 1486–1489.

Free, J. U., Benz, S. P., Rzchowski, M. S., Tinkham, M., Lobb, C. J. & Octavio, M. [1990] "Dynamical simulations of fractional giant Shapiro steps in two-dimensional Josephson arrays," *Phys. Rev.* **B41**, 7267–7269.

Grebogi, C., Ott, E. & Yorke, J. A. [1983] "Crises, sudden changes in chaotic attractors and transient chaos," *Physica* **D7**, 181–200.

Hadley, P. & Beasley, M. R. [1987] "Dynamical states and stability of linear arrays of Josephson junctions," *Appl. Phys. Lett.* **50**, 621–623.

Hadley, P., Beasley, M. R. & Wiesenfeld, K. [1988] "Phase locking of Josephson junction arrays," *Phys. Rev.* **B38**, 8712–8719.

Hebboul, S. E. & Garland, J. C. [1991] "Radiofrequency spectral response of two-dimensional Josephson-junction arrays," *Phys. Rev.* **B43**, 13703-13706.

Huberman, B. A., Crutchfield, J. P. & Packard, N. H. [1980] "Noise phenomena in Josephson junctions," *Appl. Phys. Lett.* **37**, 750–752.

Iansiti, M., Hu, Q., Westervelt, R. M. & Tinkham, M. [1985] "Noise and chaos in a fractal basin boundary regime of a Josephson junction," *Phys. Rev. Lett.* **55**, 746–749.

Jensen, M. H., Bak, P. & Bohr, T. [1984] "Transition to chaos by interaction of resonances in dissipative systems. II. Josephson junctions, charged density waves and standard maps," *Phys. Rev.* **A30**, 1970–1981.

Kaneko, K. [1989] "Chaotic but regular Posi-Nega switch among coded attractors by cluster-size variation," *Phys. Rev. Lett.* **63**, 219–223.

Kautz, R. L. & Monaco, R. [1985] "Survey of chaos in the rf-biased Josephson junction," *J. Appl. Phys.* **57**, 875–889.

Kvale, M. & Hebboul, S. E. [1991] "Theory of Shapiro steps in Josephson junction arrays and their topology," *Phys. Rev.* **B43**, 3720–3723.

Lee, H. C., Newrock, R. S., Mast, D. B., Hebboul, S. E., Garland, J. C. & Loff, C. J. [1991] "Subharmonics Shapiro steps in Josephson junction arrays," *Phys. Rev.* **B44**, 921–924.

McCumber, D. E. [1968] "Effect of ac-impedance on dc voltage-current characteristics of superconductor weak-link junctions," *J. Appl. Phys.* **39**, 3113–3118.

Middleton, A. A., Biham, O., Littlewood, P. B. & Sibam, P. [1992] "Complete mode locking in models of charge-density waves," *Phys. Rev. Lett.* **68**, 1586–1589.

Octavio, M. & Readi Nasser, C. [1984] "Chaos in a dc-bias Josephson junction in the presence of microwave radiation," *Phys. Rev.* **B30**, 1586–1588.

Pomeau, Y. & Manneville, P. [1980] "Intermittent transition to turbulence in dissipative dynamical systems," *Commun. Math. Phys.* **74**, 189–197.

Stewart, W. C. [1968] "Current-voltage characteristics of Josephson junctions," *Appl. Phys. Lett.* **12**, 277–279.

Strogatz, S. E. & Mirollo, R. E. [1993] "Splay states in globally coupled Josephson arrays: Analytical prediction of Floquet multipliers," *Phys. Rev.* **E47**, 220–227.

Tchistiakov, V. [1996] "Detecting symmetry breaking bifurcations in the system describing the dynamics of coupled arrays of Josephson junctions," *Physica* **D91**, 67–85.

Tsang, K. Y., Strogatz, S. H. & Wiesenfeld, K. H. [1991] "Reversibility and noise sensitivity of Josephson arrays," *Phys. Rev. Lett.* **66**, 1094–1097.

Tsang, K. Y. & Schwartz, I. B. [1992] "Interhyperhedral diffusion in Josephson-junction arrays," *Phys. Rev. Lett.* **68**, 2265–2268.

Watanabe, S. & Strogatz, S. E. [1993] "Integrability of a globally coupled oscillation array," *Phys. Rev. Lett.* **70**, 2391–2394.

Wiesenfeld, K., Colet, P. & Strogatz, S. H. [1996] "Attractor crowding in oscillator arrays," *Phys. Rev. Lett.* **76**, 404–407.

International Journal of Bifurcation and Chaos, Vol. 8, No. 8 (1998) 1719–1723

INHIBITION OF CHAOTIC ESCAPE BY AN ADDITIONAL DRIVEN TERM*

FRANCISCO BALIBREA
Departamento de Matemáticas, Universidad de Murcia, Murcia, Spain

RICARDO CHACÓN
Departamento de Electrónica e, Ingeniería Electromecánica, Escuela, de Ingenierías Industriales, Universidad de Extremadura, 06071, Badajoz, Spain

MIGUEL ANGEL LÓPEZ
Departamento de Matemáticas, Aplicada, Escuela Universitaria de, Arquitectura Técnica, Universidad de Castilla-La Mancha, 16002 Cuenca, Spain

Received July 31, 1997; Revised December 23, 1997

In this paper, we are devoted to the problem of escaping from a potential well which is present in a great number of physical situations. We use the Helmholtz oscillator as a model for those situations and consider the behavior of the oscillator under an additional driven perturbation. The Melnikov analysis reveals it as an adequate method. Some comparisons are made with the perturbations of the oscillator on the linear and quadratic terms.

1. Introduction

The problem of escaping from a potential well is present in a great number of different physical situations: The orbits described by a photon near a Schwarzschild black hole [Misner *et al.*, 1973], the capsizing of a boat under trains of regular waves [Thompson, 1989] and others (see [Chacón *et al.*, 1996]).

In this paper we continue developing the idea first introduced in [Chacón *et al.*, 1996] where the Helmholtz oscillator was considered as a model to treat most of the above problems.

In all those situations a common characteristic can be observed. Before the escape from a potential well, some chaotic transients of an unpredictable length can be produced and they can be observed in the orbits which start in the chaotic regions of the phase space, one of those being the region closed to separatrices [Chacón *et al.*, 1995].

In [Chacón *et al.*, 1996] we applied to the Helmholtz oscillator the technique of weak parametric modulations to the quadratic and linear terms in the equation of the oscillator. The technique attains good results in the task of the inhibition of the chaos which was present in the unperturbed oscillator.

The Helmholtz oscillator was chosen since it is a good example and a representative model of the behavior of the situations mentioned above.

In its integrable form its equation can be given by:

$$x''(t) - x(t) + \beta x(t)^2 = 0$$

where x denotes the displacement and $\beta > 0$.

When we introduce a weak perturbation in the integrable expression, the equation takes the form

$$x''(t) - x(t) + \beta x(t)^2 = -\delta x'(t) + \gamma \sin(\omega t)$$

*This work has been supported by Spanish D.G.I.C.Y.T. PB95-1004 grant and also by COM-20/96 MAT from Dirección General de Universidades, Comunidad Autónoma de Murcia.

with $\delta > 0$ and $\gamma \ll 1$. ω, δ and γ denote the normalized frequency, damping coefficient and driving term amplitude.

In this paper we are devoted to study the behavior of the oscillator under an additional driven perturbation given by:

$$x''(t) - x(t) + \beta x(t)^2 = -\delta x'(t) + \gamma \sin(\omega t) + \alpha\gamma \sin(\Omega t + \varphi) \quad (1)$$

where $0 < \alpha \ll 1$ and with Ω and φ we denote the normalized frequency and the initial phase of the perturbation.

We will compare the results with those obtained in [Chacón *et al.*, 1996] where perturbations of the quadratic and linear terms were considered. As a conclusion we will have that in some cases it is more advantageous to use the additional driven term (low frequencies) while in others the use of perturbations in the quadratic and linear terms (high frequencies) is better.

2. Melnikov Analysis

When detecting chaos in a dynamical system, one analytic procedure of great interest is the Melnikov's method [Wiggins, 1990]. It gives a useful criterion for detecting the presence of homoclinic or heteroclinic orbits. Nevertheless this procedure is limited in two senses: It is an approximative method of first order and is only valid for orbits which start in points sufficiently close to separatrices.

In the situation under consideration it gives good results. If we consider the phase space corresponding to Eq. (1), the separatrix of the system without perturbation has the following equations:

$$x_0(t) = 3/2\beta \sec h^2(t/2)$$

$$x_0'(t) = -3/2\beta \sec h^2(t/2)\, tgh(t/2)$$

The Melnikov's function associated to such an orbit is:

$$M(t_0) = -\delta \int_{-\infty}^{\infty} x_0'^2(t)dt + \gamma \int_{-\infty}^{\infty} x_0'(t) \sin[\omega(t+t_0)]dt + \alpha\gamma \int_{-\infty}^{\infty} x_0'(t) \sin[\Omega(t+t_0)+\varphi]dt$$

After some computations and using the integral tables [Gradshteyn *et al.*, 1994] we obtain:

$$M(t_0) = -C - A\cos(\omega t_0) - B\cos(\Omega t_0 + \varphi)$$

where

$$C = \frac{6\delta}{5\beta^2} \quad A = \frac{6\pi\gamma}{\beta}\omega^2 \cosh(\pi\omega)$$

$$B = \frac{6\pi\alpha\gamma}{\beta}\Omega^2 \cosh(\pi\omega)$$

Note that A, B and C are positive numbers in all the interval of the parameters.

It is well known that the Melnikov's function $M(t_0)$ gives a measure of the distance between the perturbed stable and unstable manifolds in the Poincaré section at a particular time t_0. When $M(t_0)$ has a simple zero, then we have a homoclinic bifurcation and therefore we have the possibility of the appearance of chaos. As a consequence $M(t_0) = 0$ is a necessary condition for such an appearance. But if $M(t_0)$ has never a zero then this is a sufficient condition for the opposite effect of the inhibition of even the transient chaos.

3. Inhibition of Chaos

When $\alpha = 0$ then $M(t_0) = -C - A\cos(\omega t_0)$ and we have a situation of chaotic escape if $A - C \equiv d \geq 0$ since in this case the Melnikov's function has simple zeros and it is equivalent to the previous condition $d \geq 0$.

If $\alpha \neq 0$ then $B > d$, that is $A - B - C < 0$. This last relationship is a necessary condition for $M(t_0)$ to have the same sign, in this case $M(t_0) < 0$ for every t_0 and can be written as

$$\alpha > \left(1 - \frac{C}{A}\right) R \quad \text{where} \quad R = \frac{\omega^2}{\Omega^2}\left[\frac{\sinh(\pi\Omega)}{\sinh(\pi\omega)}\right]$$

For general values of Ω and $0 \leq \varphi \leq 2\pi$ the above condition is not sufficient to assure that $M(t_0) < 0$ for every t_0. Now we can state the main result on inhibition of chaos for the Helmholtz oscillator.

Theorem 1. *Let $\Omega = p\omega$ with p a positive integer and such that $p = \frac{2m-(\varphi/\pi)}{2n+1}$ is satisfied for some positive integers m and n. Then $M(t_0)$ always has the same sign ($M(t_0) < 0$) for every t_0 if and only if*

$$\alpha_{\min} < \alpha \leq \alpha_{\max}$$

where $\alpha_{\min} = \left(1 - \frac{C}{A}\right) R \qquad \alpha_{\max} = \frac{R}{p^2}$

One observation on the theorem is that the length of the interval $[\alpha_{\min}, \alpha_{\max}]$ could be small, in fact this is the case if we observe the values of the parameters for which we have chaotic escape.

To prove the theorem we need some technical lemmas.

Lemma 2. *Let $p\omega = q\Omega$ for some positive integers p and q. Then there exists t_0^* satisfying $-\cos(\omega t_0^*) = \cos(\Omega t_0^* + \varphi) = 1$ if and only if $\frac{p}{q} = \frac{2m-(\varphi/\pi)}{2n+1}$ for some integers m and n.*

Proof. If $-\cos \omega t_0^* = 1$ then there is an integer n such that

$$\omega t_0^* = (2n+1)\pi \tag{2}$$

On the other hand if $\cos(\Omega t_0^* + \varphi) = 1$ then there is $m \in \mathbb{Z}$ such that $\Omega t_0^* + \varphi = 2m\pi$, that is, $\Omega t_0^* = 2m\pi - \varphi$. Using (2) we obtain

$$\frac{\Omega}{\omega} = \frac{2m\pi}{(2n+1)\pi} - \frac{\varphi}{(2n+1)\pi} = \frac{p}{q}$$

Therefore

$$\frac{p}{q} = \frac{2m\pi - \varphi}{(2n+1)\pi} = \frac{2m - \frac{\varphi}{\pi}}{2n+1} \quad \blacksquare$$

Lemma 3. *Let Ω and ω be incommensurable, that is, $\frac{\Omega}{\omega}$ is an irrational number. Then there exists $\bar{t}_0$ such that*

$$-B\cos(\Omega\bar{t}_0 + \varphi) - A\cos(\omega\bar{t}_0) > A - B$$

Proof. Using the change of variable $\varphi = \sigma + \frac{3\pi}{2}$ we have

$$-B\cos(\Omega\bar{t}_0 + \varphi) - A\cos(\omega\bar{t}_0)$$
$$= A\sin\left(\omega\bar{t}_0 + \frac{3\pi}{2}\right) - B\sin(\Omega\bar{t}_0 + \sigma)$$

We are looking for a $\bar{t}_0$ for which

$$A\sin\left(\omega\bar{t}_0 + \frac{3\pi}{2}\right) - B\sin(\Omega\bar{t}_0 + \sigma) > A - B$$

Let $\sigma = \frac{\pi}{2} - 3\pi\frac{\Omega}{\omega} = \frac{\pi}{2}(1 - \frac{6\Omega}{\omega})$ if $\omega > \Omega$. Then taking $\bar{t}_0 = \frac{\pi}{\omega}$ we obtain

$$A\sin\left(\omega\bar{t}_0 + \frac{3\pi}{2}\right) - B\sin(\Omega\bar{t}_0 + \sigma)$$
$$= A - B\cos\left(2\pi\frac{\Omega}{\omega}\right) > A - B$$

since Ω and ω are incommensurable and $\cos(2\pi\frac{\Omega}{\omega}) < 1$.

In an equivalent way we will take $\sigma = \frac{\pi}{2} - 3\pi\frac{\omega}{\Omega} = \frac{\pi}{2}(1 - \frac{6\omega}{\Omega})$ when $\omega < \Omega$. Let $\sigma \neq \frac{\pi}{2} - 3\pi\frac{\Omega}{\omega} = \frac{\pi}{2}(1 - \frac{6\Omega}{\omega})$. Then taking $\bar{t}_0 = \frac{3\pi}{\omega}$ we obtain

$$A\sin\left(\omega\bar{t}_0 + \frac{3\pi}{2}\right) - B\sin(\Omega\bar{t}_0 + \sigma)$$
$$= A - B\sin\left(3\pi\frac{\Omega}{\omega} + \sigma\right) > A - B$$

since in this case $\sigma \neq \frac{\pi}{2} - 3\pi\frac{\Omega}{\omega}$. $\blacksquare$

Lemma 4. *Let $g(\tau; p, q) = \frac{1-\cos(p\tau/q)}{1-\cos\tau}$ where $\tau \in \mathbb{R}$ and p and q are positive integers. Then g is finite if and only if $q = 1$. Moreover, we have that $0 \leq g(\tau; p, 1) \leq p^2$, where $\tau \in (-\infty, \infty)$.*

Proof. First we will compute $\lim_{\tau\to 2\pi l} g(\tau; p, q)$ where $l \in \mathbb{Z}$. A necessary condition to get g bounded is that its numerator has zeros in the same points that its denominator.

Consider first the case $q \neq 1$. The zeros of the numerator and denominator of g are $\tau = \frac{q}{p}2l\pi$ $\tau = 2\pi s$ where $l \in \mathbb{Z}$ and $s \in \mathbb{Z}$. It is evident that with arbitrary positive integers p, $q(q \neq 1)$ it is not always possible to find an integer l such that $s = l\frac{q}{p}$ where s is an arbitrary integer.

The above limit attains the value p^2 and since $g(\tau; p, 1) = \left[\frac{\sin(p\tau/2)}{\sin(\tau/2)}\right]^2$, using finite induction over p we immediately obtain $0 \leq g(\tau; p, 1) \leq p^2$.

Proof of Theorem 1. We ask under which conditions the condition $\alpha > (1 - \frac{C}{A})R$ is also a sufficient condition to obtain $M(t_0)$ for every t_0. It is immediate to observe that a sufficient condition is given by

$$A - B \geq -B\cos(\Omega t_0 + \varphi) - A\cos(\omega t_0) \tag{3}$$

Now we are looking for values of ω, Ω and φ in order that Eq. (3) be satisfied for every t_0. Lemma 3 says that if Ω and ω are incommensurable, this condition is not satisfied. Therefore a resonance condition $p\omega = q\Omega$ is necessary with p, q positive integers. In such case Lemma 2 supplies a sufficient condition for Eq. (3) to be held in a infinite number of values

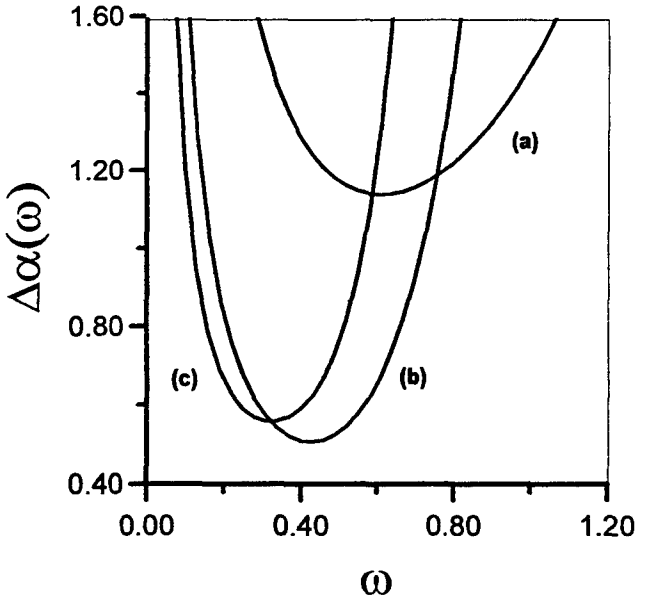

Fig. 1. Function $\Delta\alpha(\omega) = \alpha_{\max} - \alpha_{\min}$ versus ω for δ = const., β = const., γ = const. and $\Omega = p\omega$: (a) $p = 1$; (b) $p = 2$; (c) $p = 3$.

of t_0. In such a case (3) is written as

$$\frac{A}{B} \geq \frac{1 - \cos(\Omega t_0 + \varphi)}{1 + \cos(\omega t_0)}$$

$$= \frac{1 - \cos\left(\frac{p}{q}[\omega t_0 - (2n+1)\pi] + 2m\pi\right)}{1 + \cos(\omega t_0)}$$

Then

$$\frac{A}{B} \geq \frac{1 - \cos\left(\frac{p\tau}{q}\right)}{1 - \cos\tau} \quad \text{with} \quad \tau = \omega t_0 - (2n+1)\pi \tag{4}$$

But since $\frac{A}{B} = \frac{\omega^2}{\alpha\Omega^2}\left[\frac{\sinh(\pi\Omega)}{\sinh(\pi\omega)}\right] = \frac{R}{\alpha}$ we obtain

$$\frac{R}{\alpha} \geq \frac{1 - \cos\left(\frac{p\tau}{q}\right)}{1 - \cos\tau} \quad \text{with} \quad \tau = \omega t_0 - (2n+1)\pi$$

Finally if $q = 1$, Lemma 4 gives a condition for (4) to be satisfied for every τ (that is for every t_0). This condition is $\alpha \leq \frac{R}{p^2}$ where $R = \frac{\omega^2}{\Omega^2}\left[\frac{\sinh(\pi\Omega)}{\sinh(\pi\omega)}\right]$. ■

Remark 1. Suppose we have a set of parameters that satisfy the hypotheses of Theorem 1. As p increases, the interval of escape $(\alpha_{\min}, \alpha_{\max})$ shrinks rapidly. Figure 1 shows a plot of the width of the inhibition interval as a function of ω. For each p, $\Delta\alpha$ achieves a minimum value as a function of the frequency.

4. Comparisons with the Quadratic and Linear Parametric Perturbations Cases

In [Chacón *et al.*, 1996] the Helmholtz oscillator is perturbed by weak parametric modulations of the quadratic (5a) and linear (5b) terms in the following way:

$$x''(t) = x(t) - \beta[1 + \eta\,\sin(\Omega_1 t + \varphi_1)]x(t)^2 - \delta x'(t) + \gamma\,\sin(\omega t) \tag{5a}$$

$$x''(t) = x(t)[1 + \eta'\,\sin(\Omega' t + \varphi')] - \beta x(t)^2 - \delta x'(t) + \gamma\,\sin(\omega t) \tag{5b}$$

obtaining similar results as above. Nevertheless it is of great interest to compare those results from the point of view of inhibition of chaos with the situation considered in this paper. The results of this comparisons are shown in Figs. 2 and 3. In both pictures we represent the quotient $\frac{1}{\gamma\beta}\frac{\Delta\eta(\omega)}{\Delta\alpha(\omega)}$ versus ω for several values of p. In Fig. 2 we have

$$\frac{\Delta\eta(\omega)}{\Delta\alpha(\omega)} = \frac{10\gamma\beta}{(p^2\omega^2 + 1)(p^2\omega^2 + 4)}$$

and in Fig. 3

$$\frac{\Delta\eta'(\omega)}{\Delta\alpha(\omega)} = \frac{2\gamma\beta}{p^2\omega^2 + 1}$$

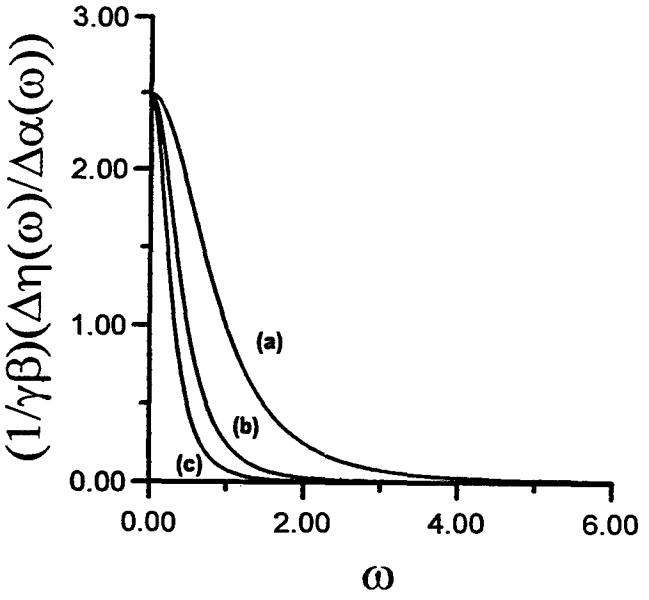

Fig. 2. The function $\frac{1}{\gamma\beta}\frac{\Delta\eta(\omega)}{\Delta\alpha(\omega)}$ versus ω for several values of p: (a) $p = 1$; (b) $p = 2$; (c) $p = 3$.

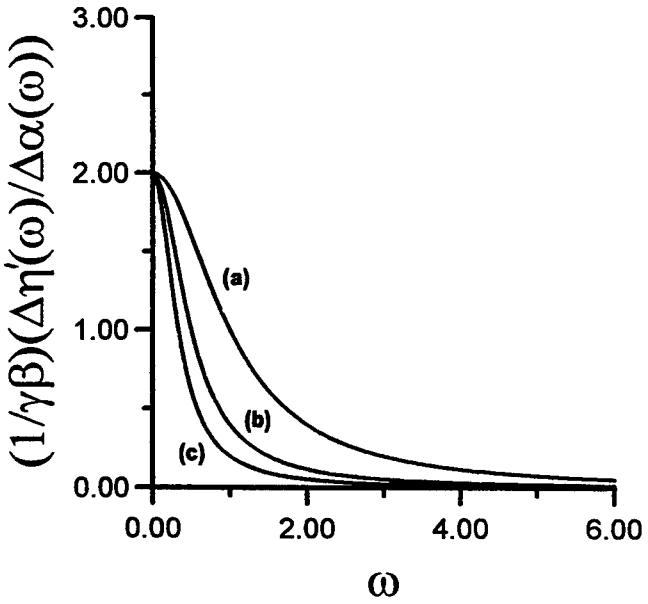

Fig. 3. The function $\frac{1}{\gamma\beta}\frac{\Delta\eta'(\omega)}{\Delta\alpha(\omega)}$ versus ω for several values of p: (a) $p = 1$; (b) $p = 2$; (c) $p = 3$.

From these two pictures we can see that for a fixed value of p, an additional damped perturbation of the oscillator is more efficient (in the frequency domain) than perturbations of the quadratic and linear terms for low frequencies ω for the inhibition of chaos. The opposite effect is obtained for large frequencies ω. It can be observed also that for $\omega = \frac{1}{p}$ we obtain $\Delta\eta = \Delta\alpha$ and $\Delta\eta' = \Delta\alpha$.

5. Conclusions

The application of an additional driven perturbation to the Helmholtz oscillator is an efficient method to suppress the chaotic escape from a potential well. We have estimated the range of parameters where the inhibition of chaos is possible through a systematic application of the Melnikov's method.

When we compare the results with those obtained by parametric perturbations of the quadratic and linear terms we obtain that for a fixed value of the resonance parameter p, at low frequencies ω the effectiveness of the suppression of chaos by an additional driven term is greater than in the other two methods. At large values of the frequency we obtain the opposite situation.

References

Chacón, R. & Cirac, J. I. [1995] "Chaotic and regular behavior of a trapped ion interacting with a laser field," *Phys. Rev.* **A51**, 4900–4906.

Chacón, R., Balibrea, F. & López Guerrero, M. A. [1996] "Inhibition of chaotic escape from a potential well using small parametric perturbations," *J. Math. Phys.* **37**(11), 5518–5523.

Gradshteyn, I. & Ryzhik, I. [1994] *Table of Integrals, Series and Products* (Academic Press, NY).

Misner, C. W., Thorne, K. S. & Wheeler, A. [1973] *Gravitation* (Freeman W.H., NY), pp. 679–680.

Thompson, J. M. T. [1989] "Chaotic phenomena triggering the escape from a potential well," *Proc. R. Soc. London* **A421**, 195–225.

Wiggins, S. [1990] *Introduction to Applied Nonlinear Dynamical Systems and Chaos* (Springer Verlag, Berlin), Chapter 4, pp. 483–519.

International Journal of Bifurcation and Chaos, Vol. 8, No. 8 (1998) 1725–1731

SIMULATION OF HEARTBEAT DYNAMICS: A NONLINEAR MODEL

MARIA G. SIGNORINI* and SERGIO CERUTTI
Department of Biomedical Engineering, Politechnic University of Milan, P.zza Leonardo da Vinci 32, 20133, Milan, Italy

DIEGO DI BERNARDO
Department of Electronic Engineering, University "Federico II" of Naples, Via Claudio 21, 80100, Naples, Italy

Received July 31, 1997; Revised November 28, 1997

The mathematical modeling of biological systems has proven to be a valuable tool by allowing experiments which would otherwise be unfeasible in a real situation. In this work we propose a system of nonlinear differential equations describing the macroscopic behavior of the cardiac conduction system. The model describes the interaction between the SinoAtrial and AtrioVentricular node. Its very simple structure consists of two nonlinear oscillators resistively coupled.

The numerical analysis detects different kinds of bifurcations whose pathophysiological meanings are discussed. Moreover, the model is able to classify different pathologies, such as several classes of arrhythmic events, as well as to suggest hypothesis on the mechanisms that induce them. These results also show that the mechanisms generating the heartbeat obey complex laws. The model provides a quite complete description of different pathological phenomena and its simplicity can be exploited for further studies on the control of cardiac dynamics.

1. The model

We propose to describe the interaction between the SinoAtrial node and the AtrioVentricular node by modeling them as two-coupled nonlinear oscillators. The model equations can be associated to an equivalent electronic circuit, depicted in Fig. 1.

The system of differential equations describing the model is then:

$$\begin{cases} \dot{x}_1 = \dfrac{1}{C_1}\, x_2 \\ \dot{x}_2 = -\dfrac{1}{L_1}\,[x_1 + g(x_2) + R(x_2 + x_4)] + A\,\cos(2\pi f t) \\ \dot{x}_3 = \dfrac{1}{C_2}\, x_4 \\ \dot{x}_4 = -\dfrac{1}{L_2}\,[x_3 + f(x_4) + R(x_2 + x_4)] \end{cases} \tag{1}$$

*Author to whom correspondence should be addressed
E-mail: signorini@biomed.polimi.it

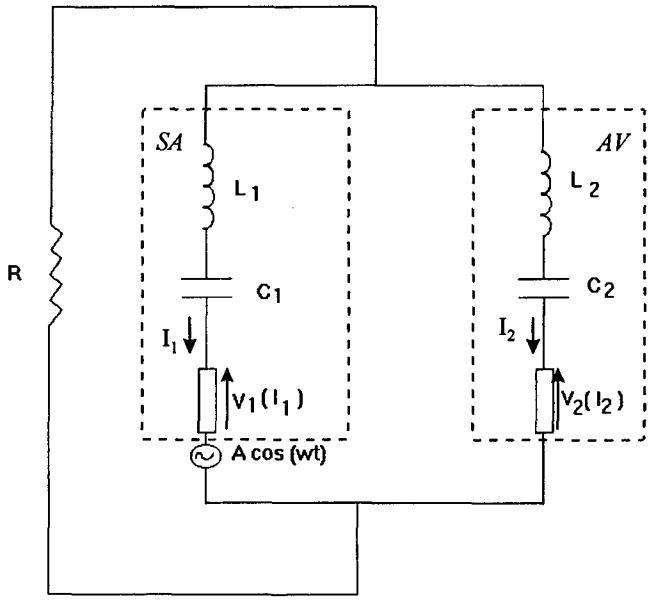

Fig. 1. Equivalent electrical circuit describing the model constituted by two oscillators: SA and AV. The parameters have the following values: $R = 0.9\ \Omega$, $C_1 = 0,\ 167$ F, $L_1 = 0,\ 033$ H, $C_2 = 0,\ 45$ F, $L_2 = 0,\ 018$ H.

where

$$f(x_4) = -x_4 + \frac{1}{3}x_4^3 \tag{2}$$

$$g(x_2) = -x_2 + \frac{1}{3}x_2^3 + h(x_2) \tag{3}$$

with

$$h(x_2) = \begin{cases} -x_2^2 - \dfrac{1}{4} & |x_2| < \dfrac{1}{2} \\ -x_2 & x_2 > \dfrac{1}{2} \\ x_2 & x_2 < \dfrac{1}{2} \end{cases} \tag{4}$$

We assume that x_2 and x_4, describe, respectively, the action potentials of the SA and AV nodes [di Bernardo *et al.*, 1998].

In the past ten years, even more if we consider the pioneering work of van der Pol [van der Pol & van der Mark, 1928], many attempts have been made to describe the macroscopic heart activity by means of mathematical modeling. All of these models can be classified in two categories: (1) discrete time models based on circle maps [Guevara & Glass, 1982; Bub & Glass, 1994; Honerkamp, 1983], and (2) continuous time models based on limit cycle oscillators [van der Pol & van der Mark, 1928; West *et al.*, 1985]. The time continuous model presented in this paper differs somewhat from others of its class in four main features:

(1) Each oscillator is described by a two-dimensional system, so that the system of ordinary differential equations [Eqs. (1)] describing the complete model is $4(2+2)$-dimensional, thus enabling complex behaviors such as aperiodic and chaotic solutions. In the model of West [West *et al.*, 1985], on the contrary, the oscillators are monodimensional, consequently, the complete model equations are $2(1+1)$-dimensional.
(2) Each oscillator is able to oscillate on its own, that is, without an external forcing, thus respecting the autoexcitatory nature of both SA and AV node cells (whereas, in the West model, a voltage generator is needed).
(3) The coupling between the two oscillators is bidirectional, therefore different from the van der Pol model [van der Pol & van der Mark, 1928], where it is monodirectional.
(4) Unlike other models of the same kind, the two oscillators are not identical as they should take into account the different physiological behavior of SA and AV nodes.

In short, our model put together the features of the van der Pol model with the West model one in a compact and simple set of equations.

1.1. *The choice of parameters values*

Parameters values were fixed respecting the following physiological constraints:

(1) The shape of the model outputs x_2 (SA node Action Potential) and x_4 (AV node action potential). They depend on the ratios $\varepsilon_1 = C_1/L_1$ and $\varepsilon_2 = C_2/L_2$. Figure 2 shows an example of this behavior. A change in the value of C_1 corresponds to different slopes of the rising wavefront of x_2. This is similar to the behavior experimentally observed in SA node cells as their depolarization frequency varies [DiFrancesco, 1995]. This change of the slope is the mechanism used by the Central Nervous System to control the heart rate and is achieved by changes in ionic currents and in cellular membranes permeability [DiFrancesco, 1995].
(2) We chose the physiological shooting value of the SA node. Indeed, the AV node is also a pacemaker site: in pathologies that prevent the SA node from depolarizing (e.g. Sinus Arrest

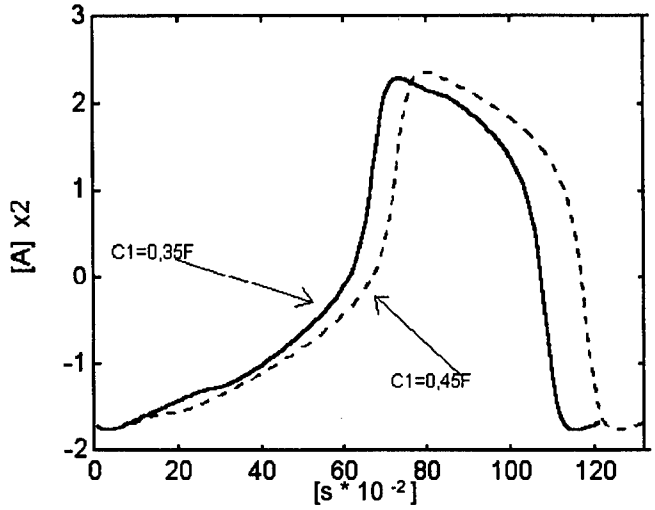

Fig. 2. Waveforms of x_2 for two different values of C_1. A larger value of C_1 corresponds to a smaller intrinsic frequency of the SA node oscillator.

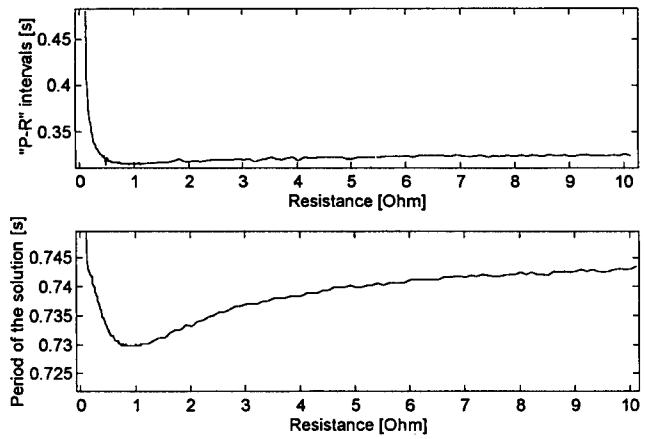

Fig. 3. Length of the simulated P–R intervals (top diagram) and the period of the first oscillator, that represent the SA node (bottom diagram), as a function of the coupling resistance. The parameters are chosen as in Eq. 2.

event), the AV node becomes the dominant pacemaker of the heart. However its shooting frequency is lower than the SA node one so that the heart rate also slows down. This phenomenon is known as *junction rhythm.* It has been found in experiments on canine hearts that the ratio between the physiological SA and AV nodes shooting frequencies can be considered equal to $T_{SA}/T_{AV} = 2/3$ [West *et al.*, 1985].

(3) In the normal ECG signal, the time delay between the P wave (onset of atrial contraction) and the R wave (onset of ventricular contraction) is in the range [0.12 s, 0.25 s]. In our model the P–R interval is the delay between the maximum value of x_2 (SA Action Potential) and the maximum value of x_4 (AV Action Potential). This time interval depends mainly on the coupling resistance R. Figure 3 shows both the obtained P–R and T_{SA} values as R varies. We observe an acceptable range of P–R intervals for $R \geq 0.8\ \Omega$. We set $R = 0.9\ \Omega$ so that the corresponding value of T_{SA} is physiological and approximately equal to 80 b/m.

The parameters values satisfying the above mentioned properties are:

$$C_1 = 0.167\text{ F} \quad L_1 = 0.033\text{ H} \quad C_2 = 0.45\text{ F}$$
$$L_2 = 0.018\text{ H} \quad R = 0.9\ \Omega \tag{5}$$

C_1, L_1	drive the frequency of the SA node
C_2, L_2	drive the frequency of the AV node
R	drives the coupling between the
	two oscillators, as well as, the
	P–R time delay

The absolute refractory period of the first oscillator (representing the SA node) with the parameters as in Eq. (5) is approximately 0.25 s, while for the second oscillator (representing the AV node) is approximately 0.15 s. This refractory periods where calculated by forcing the two oscillators, in uncoupled condition, with a square impulse with an amplitude of 5A and a duration of 10 ms.

Technical details together with the extensive model description can be found in [di Bernardo *et al.*, 1998].

2. Equilibrium Point Bifurcations

With the parameters as in Eq. (5) the system has got only one unstable equilibrium point at $(x_1, x_2, x_3, x_4) = (1/4, 0, 0, 0)$, where we set $x_1 = V_1$, $x_2 = I_1$, $x_3 = V_2$, $x_4 = I_2$.

We want to study the behavior of our model when the coupling resistance R and the capacitance C_1 vary.

The R parameter models the coupling "strength" between SA and the AV nodes. When R increases the coupling between the two oscillators increases, because a smaller current will flow through the resistance. Changing the value of

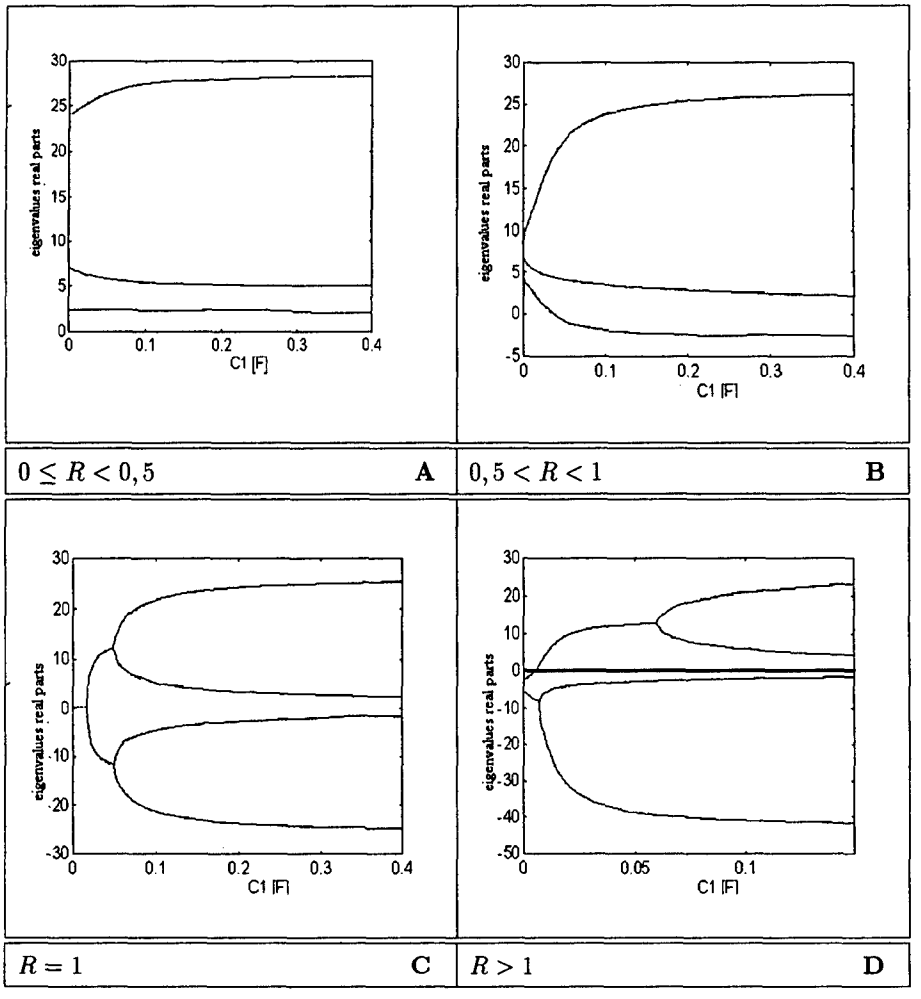

Fig. 4. Plot of the real parts of the Jacobian matrix eigenvalues, evaluated at the equilibrium point, when C_1 varies for different values of the coupling resistance R. When $[0 \leq R < 0, 5]$ all four eigenvalues have positive real parts (A). When $[0, 5 < R < 1]$ the real parts of two eigenvalues change their sign, and for small values of C_1, they are all 4 greater than 0 (B). When $[R = 1]$ no eigenvalues change sign (C). For small values of C_1 all four eigenvalues' real parts become equal to zero. When $[R > 1]$, the real parts of two eigenvalues change their sign, and for small values of C_1 become all 4 less than 0 (D).

C_1 means to increase or decrease the depolarization frequency of the SinoAtrial node. The SA frequency increases when C_1 decreases and vice-versa.

To study the possible bifurcations of the equilibrium point of our system as R and C_1 vary, we calculate the eigenvalues of the Jacobian matrix of our system at the equilibrium point. Figure 4 summarizes the results of our analysis. When $R < 1$, the equilibrium point remains always unstable, thus no interesting behavior is found. However when $R = 1$, there exist a value of C_1 for which all four eigenvalues become pure complex numbers. This suggests that a *double Hopf bifurcation* takes place. We will further show this bifurcation by using numerical simulations. When $R > 1$, two eigenvalues become pure complex numbers, for a specific value of C_1. Thus we can expect the occurrence of a *Hopf bifurcation* [Kuznetsov, 1995].

A numerical simulation confirms what we hypothesized above. Figure 5 shows the results for *double Hopf bifurcation.* By decreasing R from 1.1 Ω to 0.9 Ω with $C_1 = 0.0027$ F, the stable fixed points become unstable and a torus is generated.

Figure 6, instead, shows the *Hopf* bifurcation. We notice that this is a *subcritical Hopf bifurcation* for which the unstable limit cycle folds back and becomes stable.

This kind of scenario (Hopf bifurcation plus fold bifurcation) is typical for biological systems [Glass & Mackey, 1988; Seydel, 1994] and is known as *hard loss of stability* of the equilibrium point.

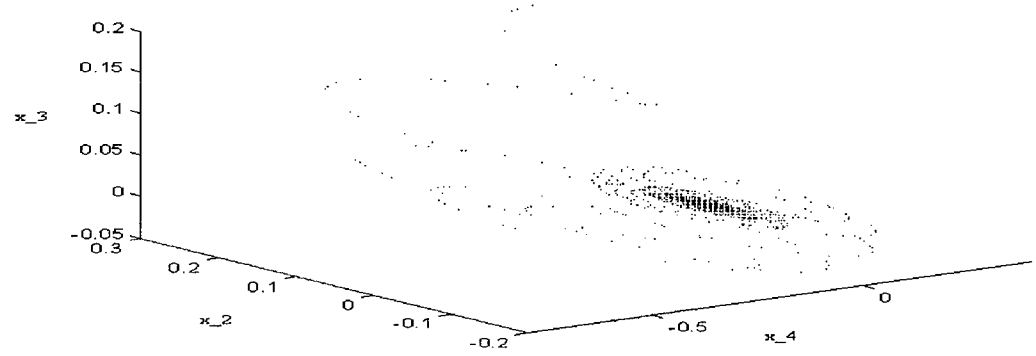

(a)

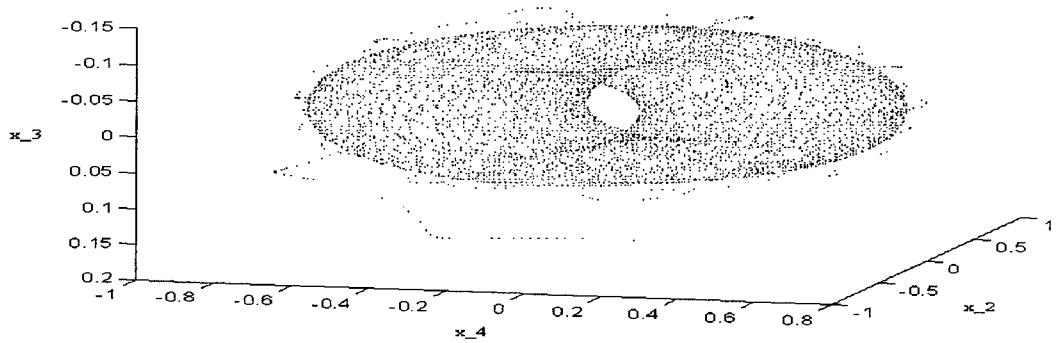

(b)

Fig. 5. (a) Projection of the four-dimensional trajectory falling in the equilibrium point on the (x_3, x_2, x_4) phase space. $R = 1.1\ \Omega$, $C_1 = 0.0027$ F, and the other parameters as in Eq. (2). (b) Projection of the torus in the (x_3, x_2, x_4) phase space. $R = 0.9\ \Omega$, $C_1 = 0.0027$ F, and the other parameters as in Eq. (2).

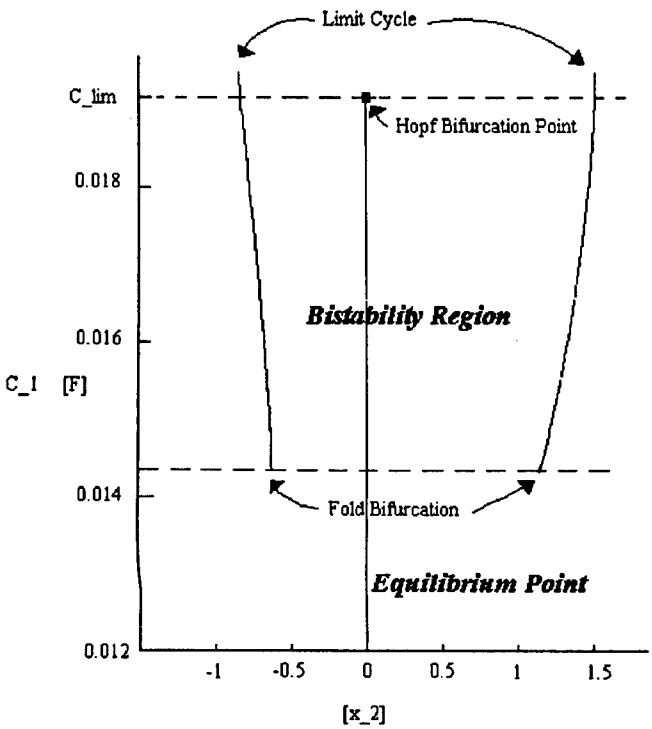

A physiologic interpretation of these bifurcations is possible: when the intrinsic frequency of the SA node increases (that is C_1 decreases) beyond a critical value, the AV node may not be able to shoot at the high frequency dictated by the SA node anymore (this corresponds, on the bifurcation diagram in Fig. 6, to the bistability region). The greater the increase of the SA node frequency, the higher the likelihood that the heart would stop: the bistability region ends and the only remaining stable attractor is the critical point.

3. Simulation of Cardiac Arrhythmias

In this section we will study the genesis of some cardiac arrhythmias that occur when some

Fig. 6. Subcritical Hopf bifurcation. The bistability region is shown as C_1 varies. The minima and maxima of x_2 are shown for different initial conditions, after a time interval long enough for the transient to be considered over. The unstable limit cycle is not shown. $R = 1.1\ \Omega$.

parameters of the system change. We will also force the system on the SA node oscillator using a sinusoidal voltage generator. The external generator action should model the influence of ectopic pacemakers in the atria that disturb the activity of the dominant pace-maker of the heart (the SA node).

3.1. *Unforced system*

The analysis for the unforced system begins by varying the coupling resistance R while the other parameters are constant with values as in Eq. (5).

We are interested in which kind of phase-locking between the two oscillators occurs. As a matter of fact, different phase-locking behaviors correspond to different kind of arrhythmias. In order to classify the solutions, a specific rotation number ρ is defined [di Bernardo *et al.*, 1998]. Intuitively ρ represents the average number of times the SA node depolarizes for a single depolarization of the AV node. For example $\rho = 1.5$ means that, on average, for every three depolarizations of the SA node, two depolarizations of the AV node occur. We calculated the rotation number ρ, for different values of the coupling resistance R. For $R > 0.11\ \Omega$ the two oscillators are 1:1 phase-locked. Every time SA depolarizes, there is one AV node depolarization. As R decreases a series of subharmonic bifurcations appear. Some of these solutions are aperiodic, but all of these resemble just one type of arrhythmia known as 2° *AV block of the Wenckebach type.*

A similar analysis is performed when R is fixed and C_1 varies. This corresponds to varying the frequency of the first oscillator (SA node). It happens that the rotation number assumes only integer values n, meaning that the phase-locking between the two oscillators is of the $n:1$ kind. These solutions resemble arrhythmic episodes known as n:1 *AV blocks.* Thus our model is able to simulate different kinds of arrhythmia depending on which parameter, R or C_1, is changed. However we are also interested in the study of solutions that could resemble atrial and ventricular fibrillation. Therefore we searched for chaotic solutions in the R–C_1 parameter space. We found a region of the parameter space ($0.967\ \Omega < R < 1$ and $0.012\ \text{F} < C_1 < 0.015\ \text{F}$) in which a series of period doubling bifurcations, leading to a chaotic attractor, takes place. From the pathophysiological point of view, this result is important because it shows that for high depolarization frequency of the SA node ($C_1 = 0.012$ F, period of SA oscillator $\triangleq 300$ beats per minute), a chaotic behavior, such as fibrillation can occur.

3.2. *Forced system*

We set the parameters as in Eq. (5), but $R = 0,\ 11\ \Omega$. This is done as more complex dynamics occur at the edge of the 1:1 phase-locking region, found for this value of R.

In order to identify different kind of arrhythmias, we classify the solutions by calculating Poincaré maps. The solution is sampled at intervals equal to the forcing function period. Using these maps it is possible to define a rotation number ρ_1 which has the same meaning given in the previous paragraph. Moreover, it is possible to calculate, when the solution is periodic, the number of periods n and m of the first and second oscillator, contained in one period of the forcing function.

The solutions obtained as the frequency and the amplitude of the forcing function vary, resemble both Wenckebach rhythms and AV blocks and also atrial bigeminy like and chaotic solutions. The rotation number of Wenckebach-like solutions assumes rational values; AV blocks like solutions, instead, have integer rotation numbers. The solutions that seem to be chaotic are generated at high frequency and low amplitude values of the forcing function. This result suggests that an ectopic pacemaker (modeled by the forcing function) can initiate a chaotic event in the heart muscle.

Atrial bigeminy episodes were obtained for small values of the frequency of the forcing function, smaller than half of the free shooting frequency of the SA oscillator.

By increasing the coupling "strength" (R from $0.11\ \Omega$ to $0.13\ \Omega$), the kind of arrhythmia simulated by the solution (atrial bigeminy) remains the same. Only the R–R interval series change.[1] For $R = 0.13\ \Omega$ the R–R series, shown in Fig. 7, seems to be modulated by an aperiodic function, whereas for $R = 0.11\ \Omega$, R–R interval series remains periodic and alternates between two fixed values.

This behavior is significant as it has been experimentally found [Babloyantz & Destexhe, 1988] that the normal heart is not a perfect periodic

[1]The time interval between two consecutive QRS complexes is known as R–R interval. We calculated them in our model as the time intervals between two consecutive maxima in x_4.

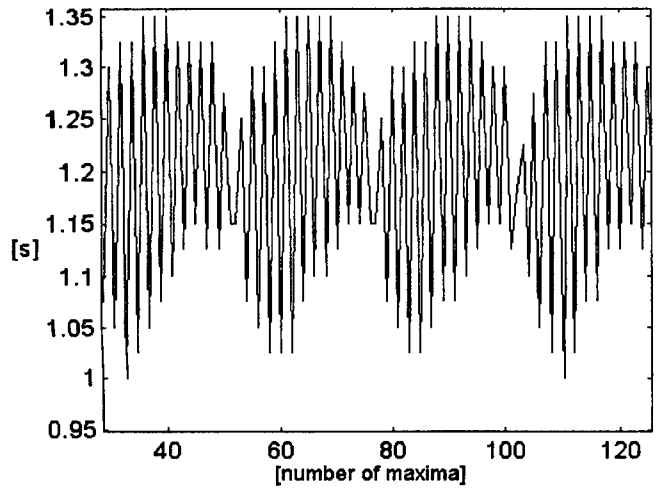

Fig. 7. Intervals between two successive x_4 maxima during atrial bigeminy event. Forcing function amplitude $A = 1.1$ V, frequency $f = 0.4$ Hz and coupling resistance $R = 0.13\ \Omega$. The other parameters as in Eq. (5).

oscillator. Its dynamics, indeed, are very rich and complex. In particular R–R interval series have been extensively investigated suggesting the presence of nonlinear mechanisms of chaotic nature contributing to their generation and control [Guzzetti *et al.*, 1996].

4. Conclusions

The simple nonlinear model (someone can say raw!) proposed in this paper allows the characterization of several pathophysiological conditions that could occur or affect the real heart.

It is able to reproduce many episodes like arrhythmias or other alterations in the normal heart rhythm. This is for example the case of cardiac arrest event. It can be explained through a transition marked by a Hopf plus a Fold bifurcation when the frequency of the driving oscillator reaches values that are too high.

Moreover in many regions of the parameters space, bifurcation diagram allows the interpretation of heart dynamics in terms of generating mechanisms. In this way, the analysis of the model by means of the powerful tool introduced by the bifurcation theory applied to biological systems not only produces a new description of the heartbeat generation but also helps in the identification of possible causes for these events.

The results of the analysis could lead to applications in heart rate prediction and control by exploiting one of the features of the model such as the reduced number of parameters and their strong correspondence to the physiological cardiovascular system behavior.

References

Babloyantz, A. & Destexhe, A. [1988] "Is the normal heart a periodic oscillator?" *Biol. Cybern.* **58**, 203–211.

Bub, G. & Glass, L. [1994] "Bifurcations in a continous circle map: A theory for chaotic cardiac arrhythmia," *Int. J. Bifurcation and Chaos* **5**(2), 359–371.

Chialvo, D. R., Gilmour, R. F. & Jalife, J. [1990] "Low dimensional chaos in cardiac tissue," *Nature* **343**(6259), 653–657.

Chua, L. O., Desoer, C. A. & Kuh, E. S. [1989] *Linear and Nonlinear Circuits*, Italian edition (Gruppo Editoriale Jackson, Milan), Chapter 7, pp. 420–467.

di Bernardo D., Signorini, M. G. & Cerutti, S. [1998] "A model of two nonlinear coupled oscillators for the study of heartbeat dynamics," *Int. J. Bifurcation and Chaos* **8**(10), to appear.

DiFrancesco, D. [1995] "The onset and autonomic regulation of cardiac pacemaker activity: Relevance of the f current," *Cardiovasc. Res.* **29**, 449–456.

Glass, L. & Mackey, M. C. [1988] *From Clocks to Chaos. The Rhythms of Life* (Princeton University Press, Princeton), Chapter 5, pp. 93–95.

Guevara, M. R. & Glass, L. [1982] "Phase locking, period doubling bifurcations and chaos in a mathematical model of a periodically driven oscillator: A theory for the entrainment of biological oscillators and the generation of cardiac dysrhythmias," *J. Math. Biol.* **14**, 1–23.

Guzzetti, S., Signorini, M. G., Cogliati, C., Mezzetti, S., Porta, A., Cerutti, S. & Malliani, A. [1996] "Deterministic chaos indices in heart rate variability of normal subjects and heart transplanted patients," *Cardiovasc. Res.* **31**, 441–446.

Honerkamp, J. [1983] "The heart as a system of coupled nonlinear oscillators," *J. Math. Biol.* **18**, 69–88.

Kuznetsov, Y. [1995] *Elements of Applied Bifurcation Theory* (Springer-Verlag, Berlin).

Seydel, R. [1994] *Practical Bifurcation and Stability Analysis. From Equilibrium to Chaos* (Springer-Verlag, NY), Chapter 4, pp. 144–146.

van der Pol, B. & van der Mark, J. [1928] "The heartbeat considered as a relaxation oscillation and an electrical model of the heart," *Phil. Mag.* **6**, 763–775.

West, B. J., Goldberger, A. L., Rovner, G. & Bhargava, V. [1985] "Nonlinear dynamics of the heartbeat. The AV junction: Passive conduit or active oscillator?" *Physica* **D17**, 198–206.

International Journal of Bifurcation and Chaos, Vol. 8, No. 8 (1998) 1733–1738

DESYNCHRONIZATION TRANSITIONS IN RINGS OF COUPLED CHAOTIC OSCILLATORS

I. P. MARIÑO* and V. PÉREZ-MUÑUZURI
Group of Nonlinear Physics, Faculty of Physics, University of Santiago de Compostela, 15706 Santiago de Compostela, Spain

M. A. MATÍAS†
Físca Teórica, Facultad de Ciencias, Universidad de Salamanca, 37008 Salamanca, Spain

Received July 31, 1997; Revised November 25, 1997

Rings of chaotic oscillators coupled unidirectionally through driving are studied. While synchronization is observed for small sizes of the ring, beyond a certain critical size a desynchronizing transition occurs. In the two examples studied here the system exhibits a transition to periodic rotating waves for rings of Lorenz systems, while one finds a sort of chaotic rotating waves when Chua's circuit is used.

1. Introduction

Synchronization phenomena are pervasive in nature [Winfree, 1980; Strogatz & Stewart, 1993] and, thus, many studies have been carried out, focusing particularly on limit-cycle oscillators. Less intuitive is probably the finding that chaotic systems may be made to get in synchrony [Fujisaka & Yamada, 1983; Pecora & Carroll, 1990], as chaos has been described as a situation in which a system gets out of synchronization with itself [Tang *et al.*, 1982]. In the present work we shall use the synchronization method introduced in [Güémez & Matías, 1995], that amounts to a generalization of the method introduced by Pecora and Carroll (PC). The idea is to avoid partitioning the response system in subsystems, introducing, instead, the driving signal at a particular place of the response system, i.e. without reducing the size of the latter. This property is particularly useful in the case that we are interested here: the design of arrays of coupled chaotic oscillators, as all the units in the array will be of the same type (will have the same dimension), without reducing the richness in possible dynamical behaviors of the system. This method has been used before and synchronization waves in linear arrays of chaotic oscillators have been obtained [Sánchez *et al.*, 1997].

In the present work, we shall consider rings of coupled chaotic oscillators. These geometries may be relevant in a biological context, like in morphogenesis [Turing, 1952] or in the context of neural systems. Thus, for example, Central Pattern Generators (CPGs), i.e. assemblies of small number of neurons, capable of providing the necessary rhythm of muscular activity even in the absence of external stimuli. These CPGs are believed to play an important role in animal locomotion. In these CPGs the relevant points to be considered are the dynamics of the isolated neurons, e.g. periodic or chaotic, the interaction between the oscillators, and the way in which information is processed. An important aspect is that the resulting spatiotemporal patterns can be analyzed through symmetry arguments [Collins & Stewart, 1994], and this

*E-mail: ines@fmmeteo.usc.es
†E-mail: mam@sonia.usal.es

allows one to study the different possible behaviors, stemming from symmetry-breaking bifurcations, and, thus, the transition between different animal gaits has been explained in this way by considering a model composed out of a ring of coupled oscillators [Collins & Stewart, 1994]. Regarding the possibility that single neurons are chaotic, some evidences point in this direction [Hayashi & Ishizuka, 1992].

In the present work we shall explore further the richness of dynamical behaviors that are possible in rings of unidirectionally coupled chaotic oscillators, considering as case examples the Lorenz and Chua systems. We shall perform our study by considering a reference state in which the behavior of the coupled systems is chaotic and uniform (synchronized), studying then the onset of instability, characterized in a Fourier representation by the instability in the $k = 1$ mode. This will yield rotating waves that in one case are periodic while in the other chaotic.

2. Rings of Lorenz Oscillators

In this case we shall consider rings coupled in such a way that the dynamical behavior is defined by,

$$\left.\begin{aligned} \dot{x}_j &= \sigma(y_j - x_j) \\ \dot{y}_j &= R\,\overline{x}_j - y_j - x_j\,z_j \\ \dot{z}_j &= x_j\,y_j - b\,z_j \end{aligned}\right\} \quad j = 1, \ldots, N\,, \qquad (1)$$

where the coupling enters through $\overline{x}_j$, that is defined as $\overline{x_j} = x_{j-1}$, with $\overline{x}_1 = x_N$.

In this situation it was observed [Matías *et al.*, 1997a] that the synchronized chaotic state is stable if the size of the ring is small enough, e.g. $N = 2$ (see Fig. 1), while for a certain critical number, $N_c = 3$ in the case of Lorenz model, an instability that destroys the uniform chaotic state occurs, leading to a rotating chaotic wave (see Fig. 2). We have performed studies in which the parameters of the system have been varied, with the result that the critical size, $N_c = 3$ in all cases. Anyway, so far we have explored only the region in which all the oscillators are identical.

A noteworthy aspect of this desynchronization transition is that the time scale of the emerging rotating wave is, roughly, one order of magnitude faster than that of the uncoupled oscillators. This instability can be characterized by performing a linear stability of the small deviations around the synchronized state (see e.g. [Turing, 1952; Heagy

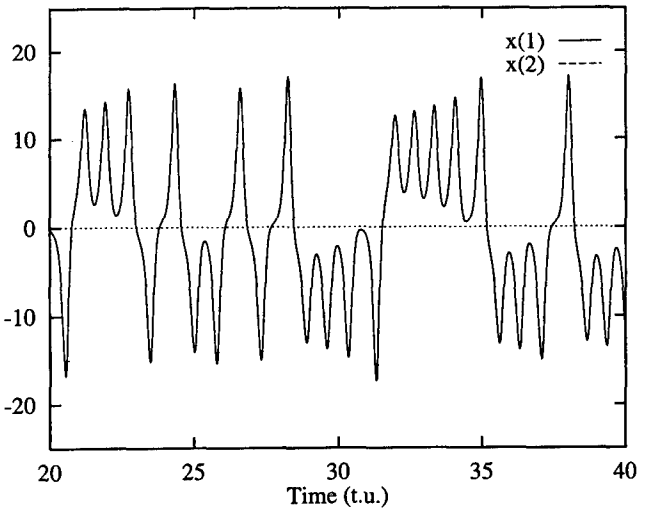

Fig. 1. Temporal evolution of the variable x of the two oscillators in a ring of $N = 2$ Lorenz oscillators. The values of the parameters are $(\sigma, R, b) = (10, 28, 8/3)$.

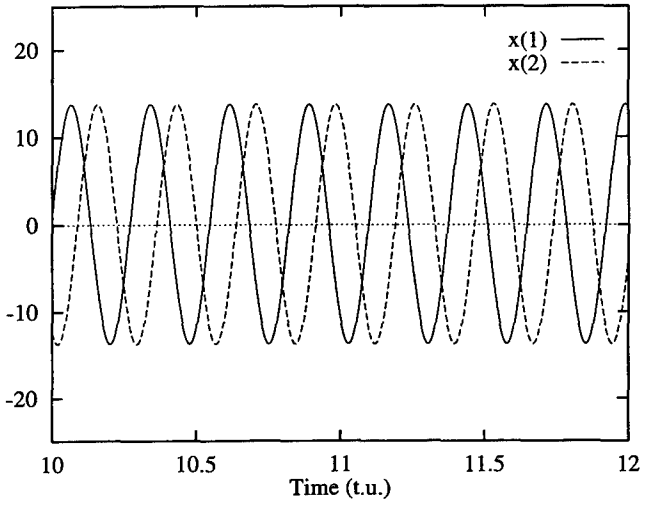

Fig. 2. Temporal evolution of the variable x of two contiguous oscillators in a ring of $N = 3$ Lorenz oscillators. Notice the time scale of this figure compared to that of Fig. 1. The values of the parameters are the same as in Fig. 1.

et al., 1994]). The time evolution of small differences around the synchronized state is governed by the equation,

$$\dot{\delta\mathbf{x}} = \mathbf{H}\,\delta\mathbf{x} \qquad (2)$$

where the $\mathbf{H}$ matrix is organized in a series of blocks corresponding to the uncoupled oscillators plus a number of off-diagonal terms arising from coupling.

However, the structure of this matrix is circulant, and for this reason one can put these equations in a more convenient form through the use of Discrete Fourier Transform (DFT) [Turing, 1952;

Heagy *et al.*, 1994]. As a result, the following equations are obtained,

$$\dot{\eta}^{(k)} = \mathbf{C}^{(k)}\,\eta^{(k)} \tag{3}$$

where in the case of the Lorenz model the structure of each block can be cast in the form,

$$\mathbf{C}^{(k)} = \begin{pmatrix} -\sigma & \sigma & 0 \\ (R\,e_k - z) & -1 & -x \\ y & x & -b \end{pmatrix}, \tag{4}$$

with $e_k = \exp(i\,2\pi\,k/N)$ and being $k = 0, \ldots, (N-1)$ the Fourier modes of the system.

The $\mathbf{C}^{(k)}$ matrices have time-dependent (chaotically varying) coefficients, and, thus, we have chosen to characterize its stability by determining the corresponding Lyapunov spectrum considering the infinite-time limit of the real part of the eigenvalues of this matrix. This has been done by generalizing Wolf's algorithm [Wolf *et al.*, 1985] to the case of complex vector spaces, while the different possible values of k and N have been joined through the definition of the reduced wavenumber $q = k/N$, and this yields the function $\lambda(q)$, that represents the highest Lyapunov exponent as a function of this variable. According to linear stability theory [Heagy *et al.*, 1994] the stability of the synchronized state will occur whenever the transverse Lyapunov exponent is negative. However, if one assumes that the dependence of λ on q is smooth, the fact that the uniform dynamics is chaotic, i.e. that $\lambda(0) > 0$, implies that the uniform chaotic state must be unstable for perturbations of some characteristic wavelength (see also [Bohr *et al.*, 1987] for an analogous argument).

In a more quantitative fashion, it can be shown that for the parameters used in this work, and reported in Fig. 3, this crossing occurs for $q_c \sim 0.37$, what implies that it occurs already for $N = 3$. This can be confirmed through numerical simulation of Eq. (1), as can be seen in Fig. 2. An easily acknowledged point from these results is that when the instability occurs the behavior of each oscillator becomes periodic, and neighboring oscillators exhibit a phase difference of $2\pi/N$. The first aspect, i.e. the transition from chaotic to periodic cannot be explained in the framework of a linear stability theory, and the observed behavior implies, probably, a global bifurcation.

However, the other aspect can be understood by noticing that the instability occurs through a

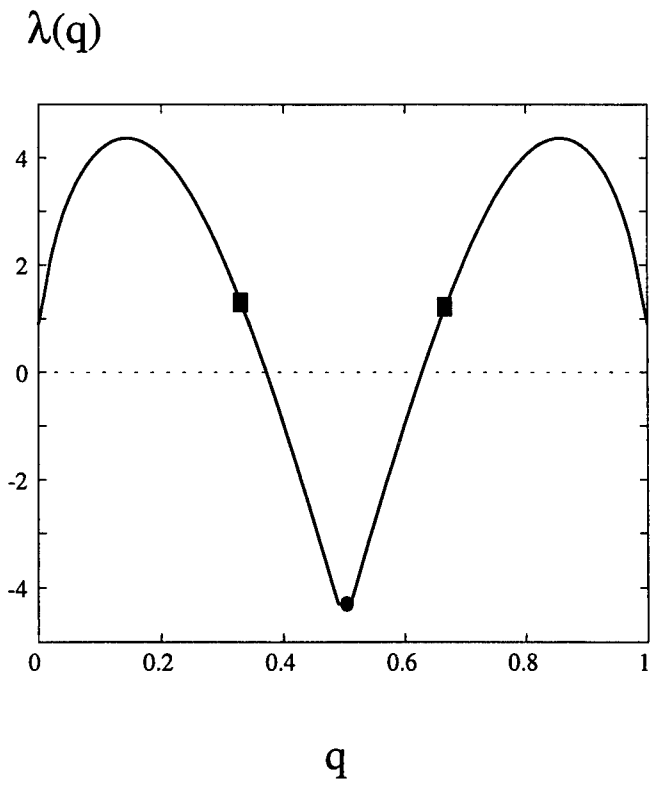

Fig. 3. Representation of the highest Lyapunov exponent $\lambda(q)$ as a function of $q = k/N$, i.e. $\lambda(q)$ versus q. The circles indicate the highest transverse Lyapunov exponent for a ring of $N = 2$ Lorenz oscillators, whereas the squares indicate the same for $N = 3$. The values of the parameters are the same as in Fig. 1.

symmetric Hopf bifurcation [Collins & Stewart, 1994]. This bifurcation is allowed because the presence of the e_k terms in Eq. (4) implies that half of the Fourier modes are complex conjugate to other half. In particular this implies that when a given mode crosses the instability threshold there will be another mode that also exhibits the same type of crossing. Whether these two complex conjugate unstable modes are real or complex will depend on the structure of the matrix, although in the present case, and by resorting to an approximate procedure [Güémez *et al.*, 1997], we have shown that the modes are indeed complex. The result is immediate: A Hopf bifurcation occurs, implying the appearance of a discrete rotating wave, in which neighboring oscillators exhibit the reported phase difference.

Symmetry is here a very helpful tool as it determines the properties of the different bifurcation branches. In the case of unidirectional coupling that we are considering here, and that it is the most relevant one in the case of CPGs, symmetry indicates that a single branch of rotating waves is obtained

[Collins & Stewart, 1994], where a single rotation direction is allowed.

3. Rings of Chua's Oscillators

An analogous study to that of the previous section has been carried out with rings of Chua's oscillators, a well-known paradigm of chaos in electronic circuits. In this case the oscillators have been coupled according to the following scheme, where the evolution equations for each coupled oscillator are reported,

$$\left.\begin{aligned} \dot{x}_j &= \alpha[y_j - x_j - f(\overline{x}_j)] \\ \dot{y} &= x_j - y_j + z_j \\ \dot{z}_j &= -\beta y_j - \gamma z_j \end{aligned}\right\} \quad j = 1, \ldots, N. \quad (5)$$

A theoretical study of this situation has been carried out in [Matías *et al.*, 1997b], while the predictions have been confirmed experimentally in [Sánchez *et al.*, 1997]. The nonlinear resistor $f(x)$ in (5) is given by,

$$f(x) = \left\{ bx + \frac{1}{2}(a-b)[|x+1| - |x-1|] \right\} . \quad (6)$$

Driving is introduced through the nonlinear term $f(x)$ in (5), such that $\overline{x}_k = x_{k-1}$ for $k \neq 1$, whereas for $k = 1$, $\overline{x}_1 = x_N$.

The same type of linear stability analysis discussed in the previous section can be applied here. In this case the matrix $\mathbf{C}^{(k)}$ takes the following form,

$$\mathbf{C}^{(k)} = \begin{pmatrix} -\alpha[1 + f'(x)e_k] & \alpha & 0 \\ 1 & -1 & 1 \\ 0 & -\beta & -\gamma \end{pmatrix} , \quad (7)$$

which leads to the representation of the highest transverse Lyapunov exponent as a function of the reduced wave number, plotted in Fig. 4. In the present case it is found that the onset of instability occurs at $q_c = 0.21$, which implies that the ring becomes unstable when $N \geq 5$. This can be seen from Fig. 5 that presents results for $N = 4$, while the behavior past the instability is presented in Fig. 6, that shows results for $N = 5$. The interesting feature is now that the behavior of the oscillators is not periodic, but chaotic, while neighboring oscillators present a phase difference that is approximately equal to $2\pi/N$. Thus, the ring can be better characterized as exhibiting a rotating chaotic wave.

Regarding the stability of chaotic synchronization as a function of the parameters of the model, by increasing α and γ one sees that the critical size N_c increases, as shown in Table 1. Thus,

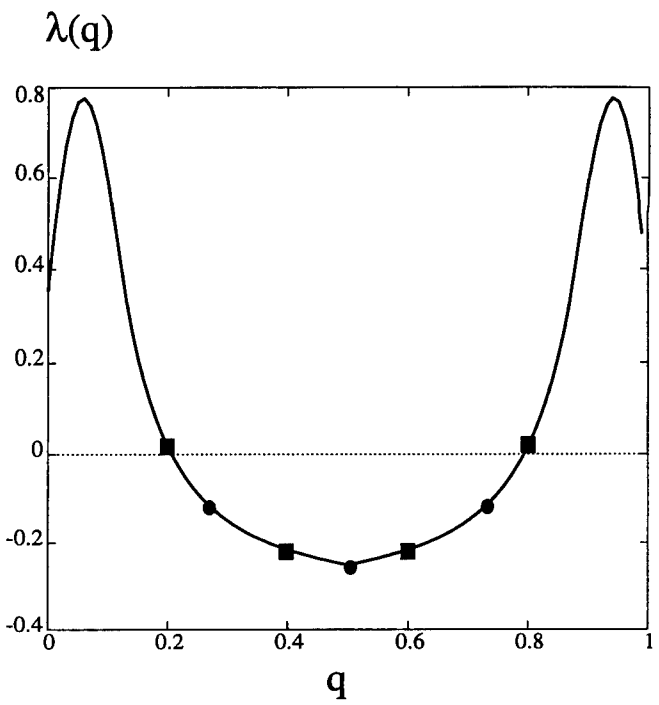

Fig. 4. Representation of the highest Lyapunov exponent $\lambda(q)$ as a function of $q = k/N$, i.e. $\lambda(q)$ versus q. The circles indicate the highest transverse Lyapunov exponent for a ring of $N = 4$ Chua oscillators, whereas the squares indicate the same for $N = 5$. The values of the parameters are $(\alpha, \beta, \gamma, a, b) = (10, 14.87, 0.06, -1.27, -0.68)$.

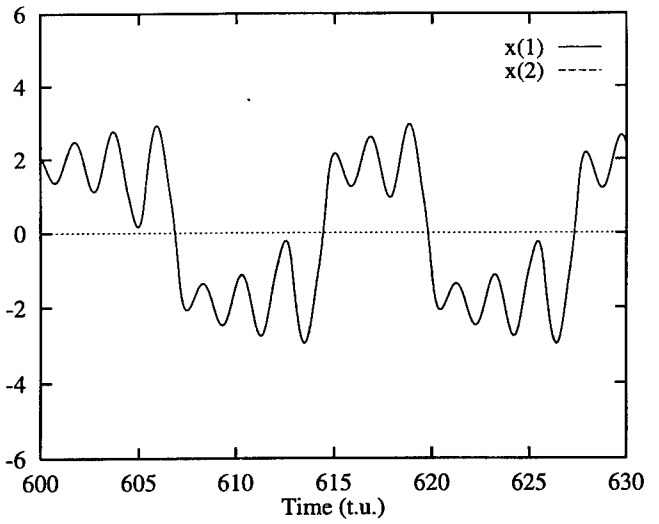

Fig. 5. Temporal evolution of the variable x of two contiguous oscillators in a ring of $N = 4$ Chua oscillators. The values of the parameters are the same as in Fig. 4.

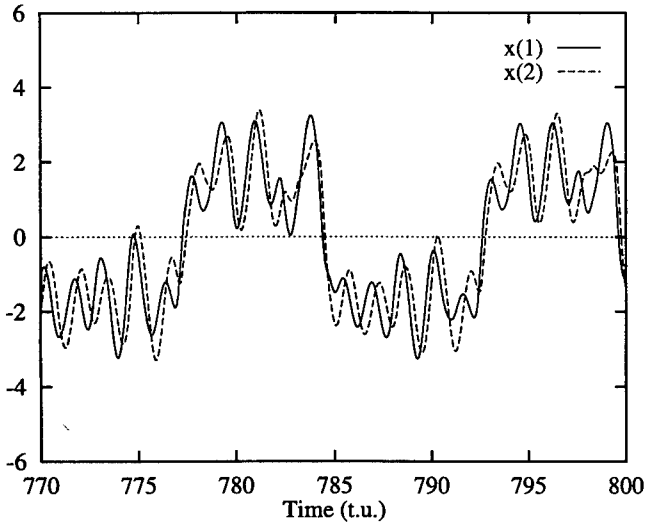

Fig. 6. Temporal evolution of the variable x of two contiguous oscillators in a ring of $N = 5$ Chua oscillators. The values of the parameters are the same as in Fig. 4.

Table 1. Critical number of chaotic Chua's circuits in a ring, N_c, that supports chaotic (uniform) synchronization.

N_c	$(\alpha;\gamma)$
4	$\alpha = 10; \gamma \leq 0.15$
5	$\alpha = 10; 0.15 < \gamma < 0.2$
6	$\alpha = 12; \gamma = 0.2$

for the value $\gamma = 10$ used in all our calculations for $\gamma \leq 0.15$ one gets $N_c = 4$, while when $0.15 < \gamma < 0.20$ this critical value becomes $N_c = 5$. Considering higher values of γ is meaningless, as the system becomes periodic. However, one can stabilize the $N = 6$ ring in the chaotic synchronized state by increasing simultaneously α (e.g. for $\alpha = 12$ and $\gamma = 0.2$).

4. Conclusions

In the present work we have considered the behavior of rings of unidirectionally coupled identical chaotic oscillators. In particular, we have considered the cases of Lorenz and Chua systems. In both cases it is found that the uniform chaotic state of the ring is unstable to perturbations of some finite wavelength, or, equivalently, a finite size N. This leads to an instability in the uniform state, that is conveniently characterized by performing a Discrete Fourier Transform on the linear stability matrix of the problem. However, the behavior exhibited by these two types of rings is different in that in one case (Lorenz system) one obtains discrete periodic rotating waves, while in the second case (Chua system) these waves are chaotic.

These discrete spatiotemporal structures are interesting in the context of dynamical systems theory, as they reveal the richness of dynamical behaviors that one may obtain in coupled arrays of chaotic oscillators, beyond synchronization. In addition, they can be potentially useful in connection to CPGs, i.e. rings of coupled neuron models. It has been found that these structures can be useful in locomotion, where the different symmetry-breaking solutions would be responsible for the different gaits that the animal exhibits [Collins & Stewart, 1994]. In particular, in this context it is useful to notice that in the case of rings of Lorenz systems the pattern that emerges is periodic, although the dynamics of the uncoupled oscillators was chaotic. It is also interesting to notice the time scale of the emerging rotating wave: It is, at least, one order of magnitude faster than the uncoupled oscillators, and this could be relevant in a neuronal context. As well, one should bear in mind that the brain is able to perform various tasks in a short time, although the neurons in which these tasks base are relatively slow.

Acknowledgments

We would like to thank N. Lorenzo for helpful discussions. This work was supported in part by DGICYT (Spain) Research Grants No. PB95-0570 and No. PB96-0937.

References

Bohr, T., Grinstein, G., He, Y. & Jayaprakash, C. [1987] "Coherence, chaos, and broken symmetry in classical, many-body systems," *Phys. Rev. Lett.* **58**, 2155–2158.

Collins, J. J. & Stewart, I. [1994] "A group-theoretic approach to rings of coupled biological oscillators," *Biol. Cybern.* **71**, 95–103.

Fujisaka, H. & Yamada, T. [1983] "Stability theory of synchronized motion in coupled-oscillator systems," *Prog. Theor. Phys.* **69**, 32–47.

Güémez, J. & Matías, M. A. [1995] "Modified method for synchronizing and cascading chaotic systems," *Phys. Rev.* **E52**, R2145–R2148.

Güémez, J., Martín, C. & Matías, M. A. [1997] "Approach to the chaotic synchronized state of some driving methods," *Phys. Rev.* **E55**, 124–134.

Hayashi, H. & Ishizuka, S. [1992] "Chaotic nature of bursting discharges in the Onchidium pacemaker neuron," *J. Theor. Biol.* **156**, 269–291.

Heagy, J. F., Carroll, T. L. & Pecora, L. M. [1994] "Synchronous chaos in coupled oscillator systems," *Phys. Rev.* **E50**, 1874–1885.

Matías, M. A., Pérez-Muñuzuri, V., Lorenzo, M. N., Mariño, I. P. & Pérez-Villar, V. [1997a] "Observation of a fast rotating wave in rings of coupled chaotic oscillators," *Phys. Rev. Lett.* **78**, 219–222.

Matías, M. A., Güémez, J., Pérez-Muñuzuri, V., Mariño, I. P., Lorenzo, M. N. & Pérez-Villar, V. [1997b] "Size instabilities in rings of chaotic synchronized systems," *Europhys. Lett.* **37**, 379–384.

Pecora, L. M. & Carroll, T. L. [1990] "Synchronization in chaotic systems," *Phys. Rev. Lett.* **64**, 821–824.

Sánchez, E., Matías, M. A. & Pérez-Muñuzuri, V. [1998] "Chaotic synchronization in linear arrays and rings of chaotic systems," *IEEE Trans. Circuits Syst. I*, in press.

Strogatz, S. H. & Stewart, I. [1993] "Coupled oscillators and biological synchronization," *Sci. Am.* **269**(6), 102–109.

Tang, Y. S., Mees, A. I. & Chua, L. O. [1983] "Synchronization and chaos," *IEEE Trans. Circuits Syst.* **I30**, 620–626.

Turing, A. M. [1952] "The chemical basis of morphogenesis," *Phil. Trans. R. Soc. London* **B237**, 37–72.

Winfree, A. T. [1980] *The Geometry of Biological Time* (Springer, NY).

Wolf, A., Swift, J. B., Swinney, H. L. & Vastano, J. A. [1985] "Determining Lyapunov exponents from a time series," *Physica* **D16**, 285–317.

International Journal of Bifurcation and Chaos, Vol. 8, No. 8 (1998) 1739–1742

SUPPRESSION AND EXCITATION OF CHAOS: THE EXAMPLE OF THE GLOW DISCHARGE

THOMAS BRAUN
Instituto de Física – UFRGS, Caixa Postal 15051, 91501-970 Porto Alegre-RS, Brazil

Received July 31, 1997; Revised December 23, 1997

I report on the experimental observation of excitation and suppression of chaos through time dependent perturbations in the dynamical variable of a glow discharge. The interaction of the external signal with the dynamical system is explained in terms of the 1D map associated to the glow discharge. Numerical simulations are also performed with the logistic map. The proposed mechanism of exciting and/or suppressing chaos is in accordance with the OGY method of controlling chaos.

1. Introduction

Very often a dynamical system may be modeled by a discrete time evolution equation that can be cast in the form $x_{i+1} = f(x_i, \mu)$. This is a generic example of a unidimensional (1D) map, where x_i represents the dynamical variable and μ is a control parameter. It is well known that by varying μ the system may present bifurcations (i.e. qualitative changes in its dynamical behavior) leading to a very complex evolution that we assume to be chaotic. The properties of this road to chaos have been extensively studied in the literature for several 1D mappings, as for instance the logistic map: $x_{i+1} = \mu x_i(1 - x_i)$.

In this work, besides the logistic map, an experimental system is analyzed: the glow discharge. Experimental systems are dissipative, thus their phase-space volumes contract in all directions. One direction has the slowest convergence and defines a line along which the universality theory applies [Collet & Eckmann, 1980] and therefore their chaotic dynamics can be modeled by 1D maps.

In the example of the glow discharge the dynamical variable is the electric current flowing through the discharge and the control parameter is the DC voltage feeding the discharge. Under suitable conditions the current of the discharge presents a self-generated periodic oscillation that, by changing the applied voltage, may turn into a chaotic oscillation. The associated bifurcation sequences eventually reaching chaos are characterized elsewhere [Braun *et al.*, 1987, 1992, 1994, 1995]. In this paper suppression and excitation of chaos in the glow discharge are analyzed by using time-dependent perturbations on the current of the discharge. The mechanism of control is explained in terms of the 1D map associated to the discharge and complemented with the example of the logistic map.

This paper is organized as follows: in Sec. 2, I describe the experimental apparatus. The measurements and their analysis are presented in Sec. 3. Conclusions are presented in Sec. 4.

2. Experimental

The experimental arrangement is shown schematically in Fig. 1. The main setup consists of a discharge cell connected to an adjustable DC power supply (Ortec, model 456) and a ballast resistor of 1 MΩ in a series circuit. The discharge cell is assembled with a glass tube 24 mm in diameter and has brass electrodes which are ~ 1 cm apart. The cathode has a diameter of 12 mm while the anode has a diameter of 19.2 mm. Inside the cell there is an argon pressure of ~ 2 mbar. The cathode is

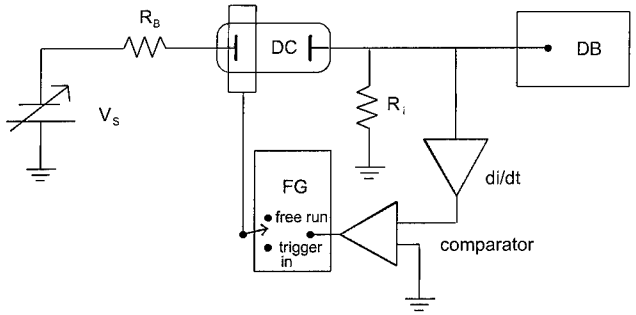

Fig. 1. Experimental setup. V_S, power supply; $R_B = 1$ MΩ; $R_i = 2$ kΩ; DC, discharge cell; DB, digitizing board; FG, function generator.

connected to the voltage source and the anode is grounded through a 2 kΩ resistor which is used to measure the current. The current was monitored by a digitizing board (Sonix STR825) in a personal microcomputer. The magnitude of this current is of the order of some μA when the power supply furnishes a voltage that ranges between 300 and 500 V.

Depending on the value of this voltage, the current through the discharge shows periodic or chaotic oscillations. In order to excite or suppress chaos in the glow discharge the current is perturbed by an external signal. The perturbation arrangement is shown in Fig. 1 by the drawing in gray. The perturbation signal was applied to the discharge by a capacitive coupling. The output from a variable frequency function generator (Tektronix FG 504) was connected to a copper tube of 20 mm in length which just fitted the outside of the glass discharge cell. In this way the electric field distribution inside the discharge cell is perturbed by the signal generator. I adopted the following criterion to define a small perturbation. With the discharge out of operation I measured the voltage induced by the external signal between electrodes. This voltage must be less than 5% of the voltage furnished by the power supply when the discharge is in operation. As will be explained later, the perturbation signal may be periodic or not.

3. Results and Analysis

An example of the chaotic evolution of the current in the discharge is displayed at the left of Fig. 2, whereas at the right the corresponding next amplitude map is shown. This map is obtained by sampling only the amplitudes (A_i) of the current oscillations and arranging them in a plot $A_i \times A_{i+1}$. The result is a noticeable 1D map.

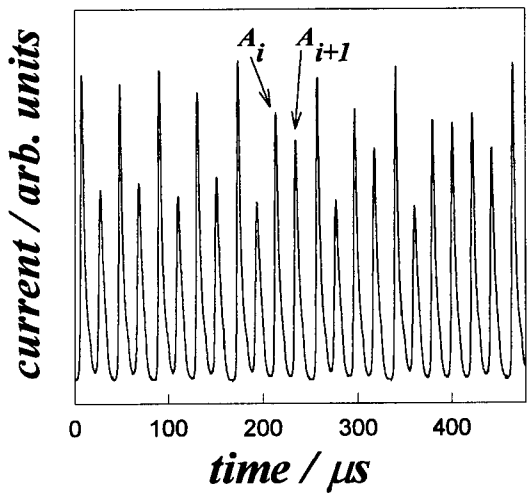

(a)

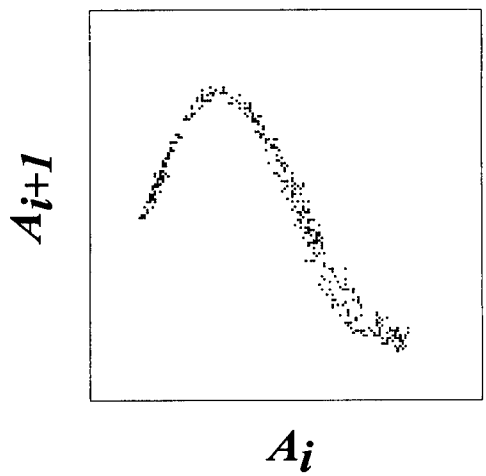

(b)

Fig. 2. (a) Chaotic current in the glow discharge. Two successive amplitudes (A_i and A_{i+1}) are identified. (b) Next amplitude map corresponding to (a).

By perturbing the electrical discharge with an external periodic signal, the dynamics changes drastically. This can be seen in Figs. 3 and 4. Both diagrams are obtained digitizing only the amplitudes of the oscillations. The continuous lines in this diagram characterize a periodic evolution whereas a blurred collection of points indicates a chaotic evolution. Also, both diagrams show a drastic change in dynamics when the perturbation is switched on and off. While the perturbation is active, its amplitude is slowly increased linearly.

In Fig. 3 the initially periodic oscillations (period one) on the current make an abrupt transition to chaos with a very small external perturbation demonstrating the excitation of chaos. As the

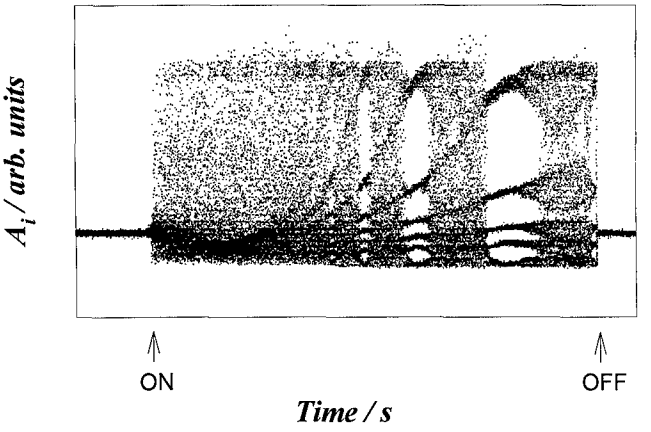

Fig. 3. Excitation of chaos in the glow discharge. The two arrows indicate where the perturbation is turned, respectively, on and off.

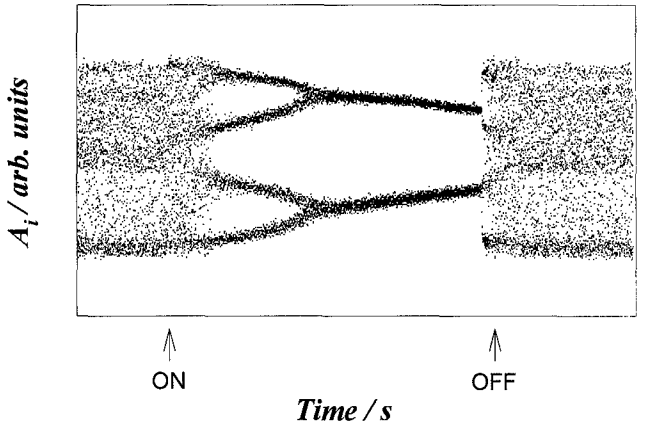

Fig. 4. Suppression of chaos in the glow discharge.

amplitude of the perturbation is increased, a sequence of oscillations with period ...-8-7-6-5-... is clearly observed between chaotic regions. When the external signal is switched off, the current returns to its initial state.

The suppression of chaos is shown in Fig. 4. The initially chaotic behavior of the current changes to an oscillation of period four as the amplitude of the external signal is increased. The oscillation undergoes a reverse period doubling, resulting in a period-two oscillation at a higher amplitude of the perturbation. The current returns to its initial noisy appearance when the external oscillator is switched off.

Similar results are obtained for different external periodic signals: a sine wave, a triangular wave, and a square wave. All of them have a frequency very close to the one of the auto-oscillations of the current. Also, a nonperiodic signal is effective in exciting and/or suppressing chaos. For example, instead of using the function generator in the free run mode, it may be triggered such that the output of the generator is always synchronized with the amplitudes of the oscillation. For this purpose, the trigger input was generated by injecting the discharge current oscillations in a peak detector (differentiator plus comparator in Fig. 1). In this way, the perturbation has always the same periodicity of the oscillations in the discharge current. For instance, if the current is chaotic then the perturbation signal is also chaotic, but as the the perturbation increases and achieves suppression of chaos then the signal becomes periodic.

I used an external perturbation in the form of "delta" pulses synchronized with the amplitudes of the current oscillation to excite and/or suppress chaos. In this way the perturbation systematically changes the variable of the next amplitude map. The latter observation suggests that the interaction of the external signal with the dynamical system (discharge) can best be understood in terms of the 1D map associated to the system as the next amplitude map. I empirically propose that this interaction takes then the form: $x_{i+1} = f(x_i, \mu)|_{\mu=\text{constant}} - \varepsilon_i$. ε_i represents the external perturbation; its amplitude increases linearly with the successive iterations. This linear growth better fits the experimental results presented previously.

To check this proposition, I have made some numerical simulations using the logistic map: $x_{i+1} = \mu x_i(1 - x_i) + \sigma\xi - \varepsilon i$ (see Fig. 5). Concerning the glow discharge, this map may be considered as "equivalent" to the 1D map ruling the dynamics such as the next amplitude map or a Poincaré return map that can be obtained from the phase

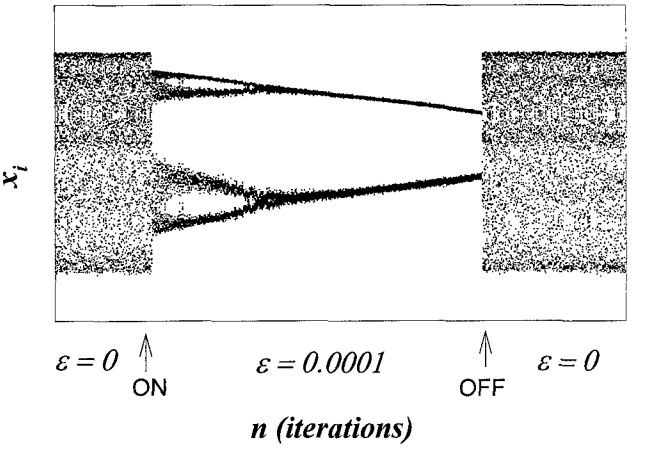

Fig. 5. Simulation for the logistic map with $\mu = 3.75$.

space flow through a Poincaré section. I considered $\varepsilon_i = \varepsilon i$, ε being constant and i corresponding to the iteration. A Gaussian noise $\sigma\xi$ (σ = amplitude = 0.002, $\langle\xi\rangle = 0$; $\langle\xi^2\rangle = 1$) was introduced in another term to represent external noise, always present in experimental conditions. The noise does not disturb the proposed control mechanism. It may be concluded that the dynamical state of the system with μ = constant varies according to the amplitude of the perturbation ε_i. In fact, ε_i works as a "new" control parameter and, changing linearly its amplitude, it results a similar bifurcation sequence as that observed in the nonperturbed system.

Related procedures of perturbing the variables in 1D discrete time systems (maps) have been studied by Güémez and Matías [1993] and Parthasarathy and Sinha [1995]. The present work, besides demonstrating new features of such ideas in 1D maps, extends them to continuous time systems (flows) like the glow discharge. The mechanism of exciting and suppressing chaos outlined in this paper has also been applied to a numerical Rössler system. It turned out that this control procedure is also effective in a numerical continuous time system [Braun, 1997].

As a final remark, I want to stress that the proposed mechanism of exciting and/or suppressing chaos is in accordance with the OGY method of controlling chaos [Ott *et al.*, 1990; Shinbrot *et al.*, 1993], which consists of stabilizing an unstable periodic orbit present in the system under control. The mechanism proposed in this work does not change the control parameter, it only displaces up- or downwards the entire function $f(x_i, \mu)$ of the 1D map by an amount ε_i. The direction of the displacement depends on the sign of ε. Possible period-n orbits of the map ($n = 1, 2, 3, \ldots$) are given by the intersection of $f^{(n)}$ with the diagonal $y = x$. They are stable or unstable whether $f^{(n)'}(x_i)$ is respectively greater or less than one. By displacing $f^{(n)}$, the stability of these periodic points is changed and thus chaos can be controlled by stabilizing an unstable periodic orbit, what is the essential idea of the OGY method. In the same way a stable periodic orbit can be turned into an unstable one.

4. Conclusions

I demonstrated that it is possible to suppress and/or excite chaos through time dependent perturbations in the variable of a dynamical system. I investigated experimentally the glow discharge and numerically the logistic map. The proposed control mechanism is easily understood in terms of the 1D map associated to the dynamical system. Essentially it consists in changing the stability of the periodic points of the map.

Acknowledgments

I thank the Brazilian agencies CNPq, FINEP, and FAPERGS for support.

References

Braun, T., Lisbôa, J. A., Francke, R. E. & Gallas, J. A. C. [1987] "Observation of deterministic chaos in electrical discharges in gases," *Phys. Rev. Lett.* **59**, 613–616.

Braun, T., Lisbôa, J. A. & Gallas, J. A. C. [1992] "Evidence of homoclinic chaos in the plasma of a glow discharge," *Phys. Rev. Lett.* **68**, 2770–2773.

Braun, T. & Lisboa, J. A. [1994] "Characterization of homoclinic chaos in a glow discharge through return maps," *Int. J. Bifurcation and Chaos* **4**, 1483–1493.

Braun, T., Correia, R. R. B. & Altmann, N. [1995] "Topological model of homoclinic chaos in a glow discharge," *Phys. Rev.* **E51**, 4165–4168.

Braun, T. [1997] to be published.

Collet, P. & Eckmann, J.-P. [1980] *Iterated Maps on the Interval as Dynamical Systems* (Birkhäuser, Boston).

Güémez, J. & Matías, M. A. [1993] "Control of chaos in unidimensional maps," *Phys. Lett.* **A181**, 29–32.

Ott, E., Grebogi, C. & Yorke, J. A. [1990] "Controlling chaos," *Phys. Rev. Lett.* **64**, 1196–1199.

Parthasarathy, S. & Sinha, S. [1995] "Controlling chaos in unidimensional maps using constant feedback," *Phys. Rev.* **E51**, 6239–6242.

Shinbrot, T., Grebogi, C., Ott, E. & Yorke, J. A. [1993] "Using small perturbations to control chaos," *Nature* **363**, 411–417.

International Journal of Bifurcation and Chaos, Vol. 8, No. 8 (1998) 1743–1747

FUZZY CONTROL OF CHAOS

OSCAR CALVO*
CICpBA, L.E.I.C.I., Departamento de Electrotecnia, Facultad de Ingeniería, Universidad Nacional de La Plata, 1900 La Plata, Argentina

JULYAN H. E. CARTWRIGHT†
Departament de Física & Centre de Càlcul i Informatització, Universitat de les Illes Balears, 07071 Palma de Mallorca, Spain

Received July 31, 1997; Revised January 15, 1998

We introduce the idea of the fuzzy control of chaos: we show how fuzzy logic can be applied to the control of chaos, and provide an example of fuzzy control used to control chaos in Chua's circuit.

1. Introduction

Chaos control exploits the sensitivity to initial conditions and to perturbations that is inherent in chaos as a means to stabilize unstable periodic orbits within a chaotic attractor. The control can operate by altering system variables or system parameters, and either by discrete corrections or by continuous feedback. Many methods of chaos control have been derived and tested [Chen & Dong, 1993; Lindner & Ditto, 1995; Ogorzałek, 1993]. Why then consider fuzzy control of chaos?

A fuzzy controller works by controlling a conventional control method. We propose that fuzzy control can become useful together with one of these other methods — as an extra layer of control — in order to improve the effectiveness of the control in terms of the size of the region over which control is possible, the robustness to noise, and the ability to control long period orbits.

In this paper, we put forward the idea of fuzzy control of chaos, and we provide an example showing how a fuzzy controller applying occasional proportional feedback to one of the system parameters can control chaos in Chua's circuit.

2. Fuzzy Control

Fuzzy control [Driankov *et al.*, 1993; Terano *et al.*, 1994] is based on the theory of fuzzy sets and fuzzy logic [Yager & Zadeh, 1991; Bezdek, 1993]. The principle behind the technique is that imprecise data can be classified into sets having fuzzy rather than sharp boundaries, which can be manipulated to provide a framework for approximate reasoning in the face of imprecise and uncertain information. Given a datum, x, a fuzzy set A is said to contain x with a degree of membership $\mu_A(x)$, where $\mu_A(x)$ can take any value in the domain $[0, 1]$. Fuzzy sets are often given descriptive names (called linguistic variables) such as FAST; the membership function $\mu_{\mathrm{FAST}}(x)$ is then used to reflect the similarity between values of x and a contextual meaning of FAST. For example, if x represents the speed of a car in kilometres per hour, and FAST is to be used to classify cars travelling fast, then FAST might have a membership function equal to zero for speeds below 90 km/h and equal to one for speeds above 130 km/h, with a curve joining these two extremes for speeds between these values. The degree of truth of the statement

*E-mail: calvo@athos.fisica.unlp.edu.ar
†E-mail: julyan@hp1.uib.es, URL: http://formentor.uib.es/~julyan

the car is travelling fast is then evaluated by reading off the value of the membership function corresponding to the car's speed.

Logical operations on fuzzy sets require an extension of the rules of classical logic. The three fundamental Boolean logic operations, intersection, union, and complement, have fuzzy counterparts defined by extension of the rules of Boolean logic. A fuzzy expert system uses a set of membership functions and fuzzy logic rules to reason about data. The rules are of the form "if x is FAST and y is SLOW then z is MEDIUM", where x and y are input variables, z is an output variable, and SLOW, MEDIUM, and FAST are linguistic variables. The set of rules in a fuzzy expert system is known as the rule base, and together with the data base of input and output membership functions it comprises the knowledge base of the system.

A fuzzy expert system functions in four steps. The first is *fuzzification*, during which the membership functions defined on the input variables are applied to their actual values, to determine the degree of truth for each rule premise. Next under *inference*, the truth value for the premise of each rule is computed, and applied to the conclusion part of each rule. This results in one fuzzy set to be assigned to each output variable for each rule. In *composition*, all of the fuzzy sets assigned to each output variable are combined together to form a single fuzzy set for each output variable. Finally comes *defuzzification*, which converts the fuzzy output set to a crisp (nonfuzzy) number.

A fuzzy controller may then be designed using a fuzzy expert system to perform fuzzy logic operations on fuzzy sets representing linguistic variables in a qualitative set of control rules (see Fig. 1).

As a simple metaphor of fuzzy control in practice, consider the experience of balancing a stick

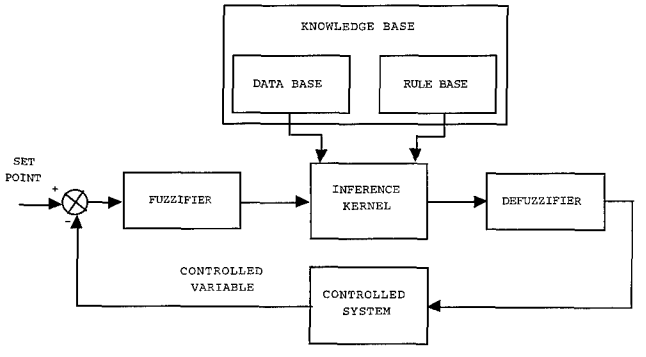

Fig. 1. Fuzzy logic controller block diagram.

vertically on the palm of one's hand. The equations of motion for the stick (a pendulum at its unstable fixed point) are well-known, but we do not integrate these equations in order to balance the stick. Rather, we stare at the top of the stick and carry out a type of fuzzy control to keep the stick in the air: We move our hand slowly when the stick leans by a small angle, and fast when it leans by a larger angle. Our ability to balance the stick despite the imprecision of our knowledge of the system is at the heart of fuzzy control.

3. Techniques for Fuzzy Chaos Control

To control a system necessitates perturbing it. Whether to perturb the system via variables or parameters depends on which are more readily accessible to be changed, which in turn depends on what type of system is to be controlled — electronic, mechanical, optical, chemical, biological, etc. Whether to perturb continuously or discretely is a question of intrusiveness — it is less intrusive to the system, and less expensive to the controller, to perturb discretely. Only when discrete control is not effective might continuous control be considered.

Ott, Grebogi and Yorke [Ott *et al.*, 1990] invented a method of applying small feedback perturbations to an accessible system parameter in order to control chaos. The OGY method uses the dynamics of the linearized map around the orbit one wishes to control. Using the OGY method, one can pick any unstable periodic orbit that exists within the attractor and stabilize it. The control is imposed when the orbit crosses a Poincaré section constructed close to the desired unstable periodic orbit. Since the perturbation applied is small, it is supposed that the unstable periodic orbit is unaffected by the control.

Occasional proportional feedback [Hunt, 1991; Lindner & Ditto, 1995] is a variant of the original OGY chaos control method. Instead of using the unstable manifold of the attractor to compute corrections, it uses one of the dynamical variables, in a type of one-dimensional OGY method. This feedback could be applied continuously or discretely in time; in occasional proportional feedback it is applied discretely. Occasional proportional feedback exploits the strongly dissipative nature of the flows often encountered, enabling one to control them with a one-dimensional map. The method is easy

to implement, and in many cases one can stabilize high period unstable orbits by using multiple corrections per period. It is a suitable method on which to base a fuzzy logic technique for the control of chaos, since it requires no knowledge of a system model, but merely an accessible system parameter.

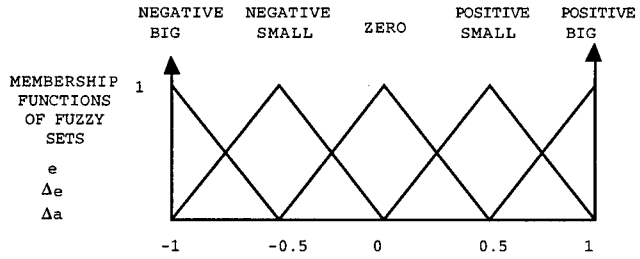

Fig. 2. Membership functions of the input and output variables e, Δe, and Δa.

4. An Example: Fuzzy Control of Chaos in Chua's Circuit

Chua's circuit [Matsumoto, 1984; Kennedy, 1993] exhibits chaotic behavior that has been extensively studied, and whose dynamics is well known [Madan, 1993]. Recently, occasional proportional feedback has been used to control the circuit [Johnson *et al.*, 1993]. The control used an electronic circuit to sample the peaks of the voltage across the negative resistance and if it fell within a window, centred about a by a set-point value, modified the slope of the negative resistance by an amount proportional to the difference between the set point and the peak value. The nonlinear nature of this system and the heuristic approach used to find the best set of parameters to take the system to a given periodic orbit suggest that a fuzzy controller that can include knowledge rules to achieve periodic orbits may provide significant gains over occasional proportional feedback alone.

We have implemented a fuzzy controller to control the nonlinearity of the nonlinear element (a three segment nonlinear resistance) within Chua's circuit. The block diagram of the controller is

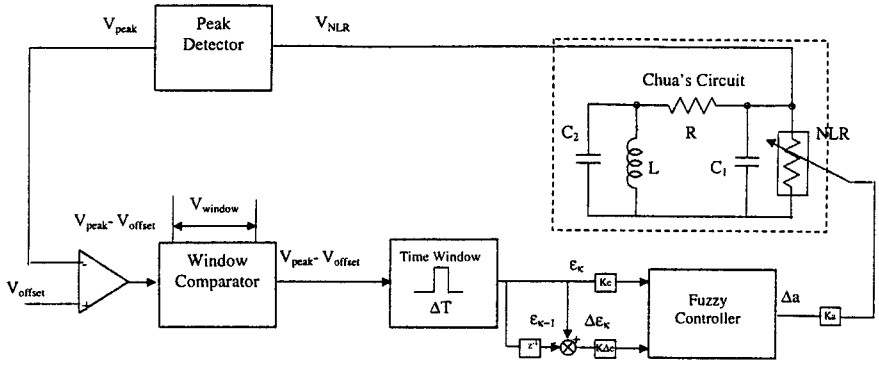

Fig. 3. The whole controller and control system in the form of a block diagram, including the fuzzy controller, the peak detector, the window comparator, and the Chua's circuit system being controlled.

Table 1. Quantification levels and membership functions.

Error, e	−1	−0.75	−0.5	−0.25	0	0.25	0.5	0.75	1
Change in error, Δe	−1	−0.75	−0.5	−0.25	0	0.25	0.5	0.75	1
Control, Δa	−1	−0.75	−0.5	−0.25	0	0.25	0.5	0.75	1
Quantification level	−4	−3	−2	−1	0	1	2	3	4
Linguistic Variables	Membership Functions								
Positive Big, PB	0	0	0	0	0	0	0	0.5	1
Positive Small, PS	0	0	0	0	0	0.5	1	0.5	0
Approximately Zero, AZ	0	0	0	0.5	1	0.5	0	0	0
Negative Small, NS	0	0.5	1	0.5	0	0	0	0	0
Negative Big, NB	1	0.5	0	0	0	0	0	0	0

Table 2. Rule table for the linguistic variables in Table 1.

Δe \ e	NB	NS	AZ	PS	PB
NB	NB	NS	NS	AZ	AZ
NS	NS	AZ	AZ	PS	
AZ	NS	AZ	PS	PS	
PS	AZ	AZ	PS	PB	
PB	AZ	PS	PS	PB	

shown in Fig. 1. It consists of four blocks: knowledge base, fuzzification, inference and defuzzification. The knowledge base is composed of a data base and a rule base. The data base consists of the input and output membership functions (Fig. 2). It provides the basis for the fuzzification, defuzzification and inference mechanisms. The rule base is made up of a set of linguistic rules mapping inputs to control actions. Fuzzification converts the input signals e and Δe into fuzzified signals with membership values assigned to linguistic sets. The inference mechanisms operate on each rule, applying fuzzy operations on the antecedents and by compositional inference methods derives the consequents. Finally, defuzzification converts the fuzzy outputs to control signals, which in our case control the slope of the negative resistance Δa in Chua's circuit (Fig. 3). The fuzzification maps the error e, and the change in the error Δe, to labels of fuzzy sets. Scaling and quantification operations are applied to the inputs. Table 1 shows the quantified levels and the linguistic labels used for inputs and output. The knowledge rules (Table 2) are represented as control statements such as "if e is NEGATIVE BIG and Δe is NEGATIVE SMALL then Δa is NEGATIVE BIG".

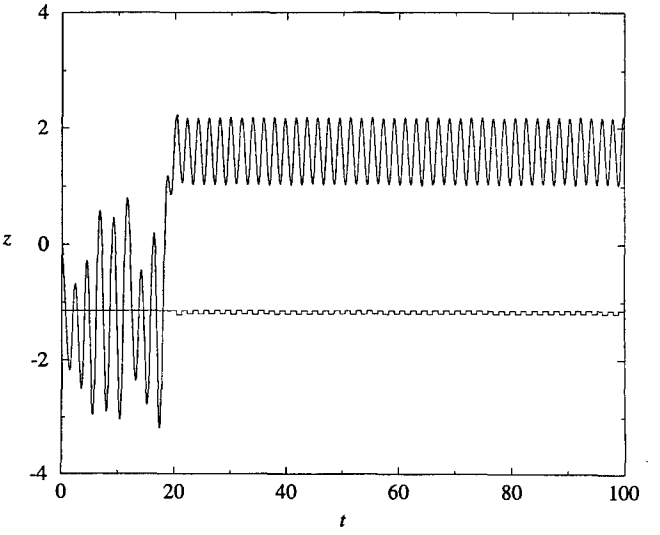

Fig. 4. The fuzzy controller stabilizes a previously unstable period-1 orbit. The control is switched on at time 20. The lower trace shows the correction pulses applied by the controller.

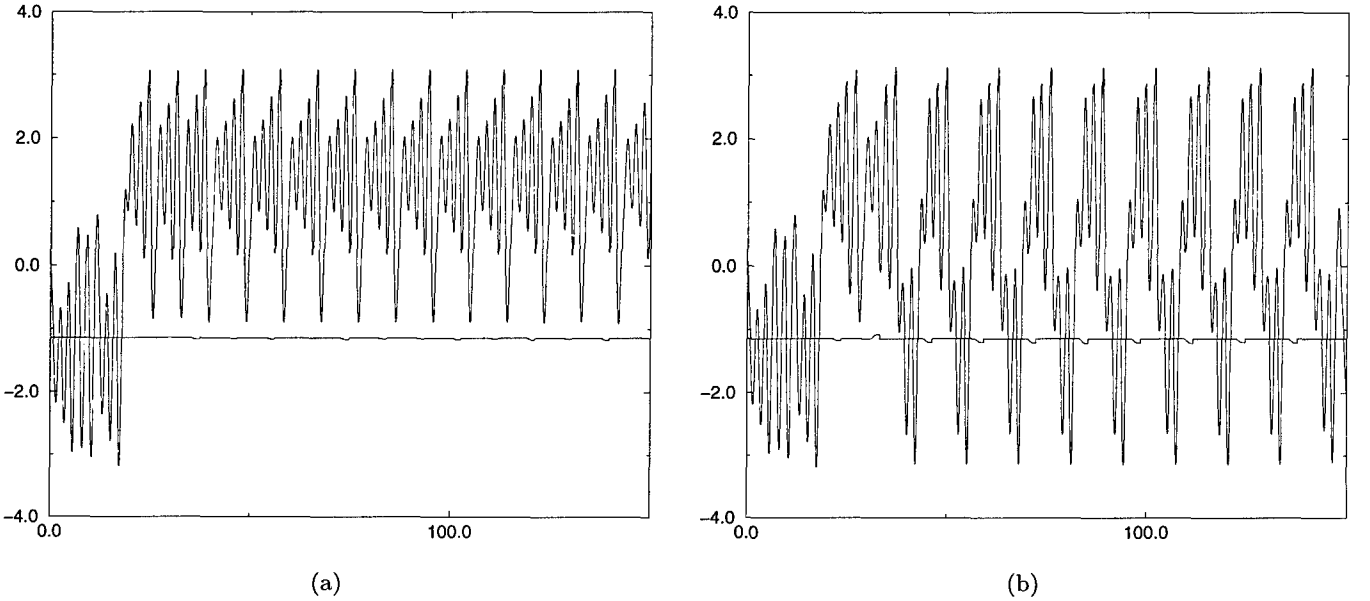

Fig. 5. Trajectory traces show higher period orbits stabilized by the controller. As before, the lower trace shows the correction pulses applied by the fuzzy control.

The normalized equations representing the circuit are

$$\begin{aligned} \dot{x} &= \alpha(y - x - f(x)) , \\ \dot{y} &= x - y + z , \\ \dot{z} &= -\beta y , \end{aligned} \tag{1}$$

where $f(x) = bx + \frac{1}{2}(a-b)(|x+1| - |x-1|)$ represents the nonlinear element of the circuit. Changes in the negative resistance were made by changing a by an amount

$$\Delta a = \text{Fuzzy Controller Output} \times \text{Gain} \times a . \tag{2}$$

We have performed numerical simulations, both in C and in Simulink, of Chua's circuit controlled by the fuzzy logic controller. Figure 3 shows the whole control system in the form of a block diagram, including Chua's circuit, the fuzzy controller, the peak detector, and the window comparator. Figure 4 gives a sample output of the fuzzy controller stabilizing an unstable period-1 orbit by applying a single correction pulse per cycle of oscillation. By changing the control parameters we can stabilize orbits of different periods. In Fig. 5 we illustrate more complex higher period orbits stabilized by the controller. One can tune the fuzzy control over the circuit to achieve the type of response required in a given situation by modifying some or all of the rules in the knowledge base of the system.

Of course, in the case of Chua's circuit the system equations are available and fuzzy logic is thus not necessary for control, but this simple example permits us to see the possibilities that fuzzy control provides, by allowing a nonlinear gain implemented in the form of knowledge based rules.

5. Conclusions

We have introduced the idea of using fuzzy logic for the control of chaos. Fuzzy logic controllers are commonly used to control systems whose dynamics is complex and unknown, but for expositional clarity here we have given an example of its use with a well-studied chaotic system. We have shown that it is possible to control chaos in Chua's circuit using fuzzy control. Further work is necessary to quantify the effectiveness of fuzzy control of chaos compared with alternative methods, to identify ways in which to systematically build the knowledge base for fuzzy control of a particular chaotic system, and to apply the fuzzy controller to future chaotic systems.

References

Bezdek, J. C. [1993] "Fuzzy models — What are they, and why?" *IEEE Trans. Fuzzy Syst.* **1**, 1–6.

Chen, G. & Dong, X. [1993] "From chaos to order — Perspectives and methodologies in controlling chaotic nonlinear dynamical systems," *Int. J. Bifurcation and Chaos* **3**, 1363–1409.

Driankov, D., Hellendoorn, H. & Reinfrank, M. [1993] *An Introduction to Fuzzy Control* (Springer).

Hunt, E. R. [1991] "Stabilizing high period orbits in a chaotic system," *Phys. Rev. Lett.* **67**, 1953–1955.

Johnson, G. A., Tigner, T. E. & Hunt, E. R. [1993] "Controlling chaos in Chua's circuit," *J. Circuits Syst. Comput.* **3**, 109–117.

Kennedy, M. P. [1993] "Three steps to chaos — Part II: A Chua's circuit primer," *IEEE Trans. Circuits Syst.* **40**, 657–674.

Lindner, J. F. & Ditto, W. L. [1995] "Removal, suppression, and control of chaos by nonlinear design," *Appl. Mech. Rev.* **48**, 795–808.

Madan, R. N. (ed.) [1993] *Chua's Circuit: A Paradigm for Chaos* (World Scientific, Singapore).

Matsumoto, T. [1984] "A chaotic attractor from Chua's circuit," *IEEE Trans. Circuits Syst.* **31**, 1055–1058.

Ogorzałek, M. J. [1993] "Taming chaos: Part II — control," *IEEE Trans. Circuits Syst.* **40**, 700–706.

Ott, E., Grebogi, C. & Yorke, J. A. [1990] "Controlling chaos," *Phys. Rev. Lett.* **64**, 1196–1199.

Terano, T., Asai, K. & Sugeno, M. (eds.) [1994] *Applied Fuzzy Systems* (Academic Press).

Yager, R. R. & Zadeh, L. A. [1991] *An Introduction to Fuzzy Logic Applications in Intelligent Systems* (Kluwer).

SUBSCRIPTION INFORMATION

Home Page: **http://www.wspc.com.sg**

USA **World Scientific Publishing Co., Inc.**
1060 Main Street, River Edge, NJ 07661, USA
Toll-Free-Tel: 1-800-227-7562 Toll-Free-Fax: 1-888-977-2665 E-mail: sales@wspc.com

UK **World Scientific Publishing (UK) Ltd.**
57 Shelton Street, Covent Garden, London WC2H 9HE, UK
Fax: 44-171-836-2020 Tel: 44-171-836-0888 E-mail: sales@wspc2.demon.co.uk

SINGAPORE **World Scientific Publishing Co. Pte. Ltd.**
Farrer Road, P O Box 128, SINGAPORE 912805 Cable Address: "COSPUB" Telex: RS 28561 WSPC
Fax: 65-382-5919 Tel: 65-382-5663 E-mail: sales@wspc.com.sg

HONG KONG **World Scientific Publishing (HK) Co. Ltd.**
P O Box 72482, Kowloon Central Post Office, HONG KONG
Fax: 852-2-771-8155 Tel: 852-2-771-8791 E-mail: wsped@hk.super.net

INDIA **World Scientific Publishing Co. Pte. Ltd.**
4911, 9th Floor, High Point IV, 45 Palace Road, Bangalore 560 001, INDIA
Telex: 0845-2900- PCO IN **Fax: 91-80-334-4593** Tel: 91-80-220-5972

TAIWAN **World Scientific Publishing Co. Pte. Ltd.**
5F-6, No. 88, Sec 3, Hsin-Sheng S Road, Taipei, Taiwan, ROC
Fax:886-2-2366-0460 Tel: 886-2-2369-1366 E-mail: wsptw@ms13.hinet.net

❑ Please enter my subscription:

IJBC (ISSN: 0218-1274)	Vol. 8/1998 (12 issues)		
Institutions/libraries	❑ US$1399	❑ DM2331	❑ S$1888
SPECIAL RATES			
Institutions/libraries from developing countries	❑ US$803	❑ DM1398	❑ S$1133
Individuals	❑ US$536	❑ DM932	❑ S$755
For airmail, please add	❑ US$96	❑ DM167	❑ S$135
For surface mail, please add	❑ US$55	❑ DM96	❑ S$78

- *Customers from Europe, please pay in DM.*
- *Customers from Asia-Pacific and Australasia, please pay in Singapore dollars (S$)*
- *Customers from America and the rest of the world, please pay in US$.*

❑ **Please send me a complimentary copy of *International Journal of Bifurcation and Chaos in Applied Sciences and Engineering***

Name:_____ Organization/institution:_____

Address:_____ E-mail:_____

City:_____ State:_____ Zip:_____ Country:_____

METHODS OF PAYMENT

- For cheque payment in USA, please make cheque payable to "World Scientific Publishing Co. Inc."
- For cheque payment from the rest of the world, please make cheque payable to "World Scientific Publishing Co. Pte. Ltd."
- **Please enclose your personal cheque or details of your credit card for INDIVIDUAL subscription.**

❑ Cheque/bank draft enclosed for the amount of _____

❑ Charge my ❑ Visa ❑ MasterCard ❑ Amex ❑ Diners Club

Card No:_____ Expiry date:_____

Signature:_____ Tel:_____

❑ Bill my company/institution:_____ (Please attach purchase order.)

Please add my name to your mailing list. My field of interest is_____

RUSH ORDERS
In USA and Canada,
☎call toll-free:
1-800-227-7562
In Europe, fax:
44-171-836-2020
In other countries, fax:
65-382-5919

SINGAPORE • NEW JERSEY • LONDON • HONG KONG • BANGALORE • TAIPEI

Preparation of Manuscript

(a) The whole manuscript should be written in proper English and typed single-sided on letter-size paper with double spacing and wide margins around the text. All pages should be numbered consecutively. Type references, tables and figure captions on separate pages.

(b) The first page of the manuscript should contain the title of the paper, the name(s), affiliation(s) and address(es) of the author(s) and the abstract. The abstract should be less than 500 words. A shortened version of the title of the paper (less than 50 characters) should be provided. This will be used as the running title.

(c) There is no artificial limit to the length of a paper, but letters to the Editor should preferably be restricted to four printed pages in order to speed up the refereeing process.

(d) The words "section"/"sections," "figure"/"figures" and "equation"/"equations" should be abbreviated to Sec./Secs., Fig./Figs. and Eq./Eqs., respectively, whenever they occur within a sentence, e.g., Eq. (24), Eqs. (7)–(10), Fig. 11, Figs. 12–13, Sec. 5. They should, however, be written in full when they occur at the beginning of a sentence.

(e) Number sections, figures and tables using arabic numerals. Subsections should be numbered using the decimal system (e.g., "3.2" means subsection 2 under section 3). To avoid cumbersome numbering, sub-subsections may be labeled as, for example, "3.2(A)," "3.2(B)," etc.

(f) For section headings, capitalize the first letter of each word except for articles, conjunctions and prepositions (e.g., Bifurcation and Chaos in the Synaptic Circuit Model). For subsection headings, only the first letter of the first word is capitalized.

(g) Equations are labeled with arabic numbers which are enclosed within parentheses and set on the right-hand margin, e.g.,

$$x_{n+1} = -(ax_n + b) \bmod 1 \quad . \tag{7}$$

When an equation is cited in the text, the equation number should be in parentheses, e.g., Eq. (7), not Eq. 7.

(h) All mathematical symbols should be easily recognizable. Identify symbols in the margin if confusion might arise, e.g., between certain capital and lower-case letters, the letter O and zero, etc. Italics should either be typed as such or underlined.

(i) References cited in the text should be placed within square brackets and stated as [surname of author(s), year of publication], e.g., [Smith, 1964], [Smith & Thomas, 1964] and, with three or more authors, [Smith *et al.*, 1964]. If the reference reads as part of the sentence, the square brackets enclose only the year of publication, e.g., "According to Smith [1964], ... "

A complete list of references cited, arranged in alphabetical order according to the surname of the first author, should be provided. References by the same author will follow a chronological sequence, i.e., Smith [1969] precedes Smith [1971]. Article titles should be stated in full but standard abbreviations should be used for journal names.

Examples

Journal reference:
Sharkovsky, A. N. & Romanenko, E. Y. [1992] "Ideal turbulence: attractors of deterministic systems may lie in the space of random fields," *Int. J. Bifurcation and Chaos* **2**(1), 31–36.

Book reference:
Hao, B.-L. [1989] *Elementary Symbolic Dynamics and Chaos in Dissipative Systems* (World Scientific, Singapore) Chap. 2, pp. 25–100.

Kaplan, J. L. & Yorke, J. A. [1979] "Chaotic behavior of multi-dimensional differential equations," in *Functional Differential Equations and Approximations of Fixed Points*, eds. Peitgen, H. O. & Walther, H. O. (Springer-Verlag, Berlin) pp. 228–237.

Proceedings reference:
Barnsley, M. & Demko, S. [1985] "Iterated function systems and the global construction of fractals," *Proc. Roy. London* **A399**, 243–275.

(j) Indicate all footnotes in the text with superscript arabic numerals. Type each footnote at the bottom of the page where it is called for, and separate it from the text by a short bar, e.g.,

---

[2]This equation will be solved in Sec. 5.

(k) Figures, including all labeling, should be professionally done and provided in the form of glossy prints or Indian ink drawings. Low-resolution computer-generated charts or graphics should be avoided. All essential details (e.g., labeling) must be legible after a reduction of at least 50%. Each figure should occupy a separate page with the author's name and figure number clearly stated.

(l) High-quality color pictures will be reproduced by the four-color process. For best results, authors should send transparencies (35 mm slides or preferably larger ones) for reproduction, but color prints should also be provided for color matching and quality control purposes. All color pictures in each paper will be printed on one page or on selected pages.

(m) All acknowledgments (for individuals, organizations or funding agencies) should appear as a separate section before the list of references.

(n) Appendices, if any, should be placed at the end of the paper, after the list of references. Subsections within the appendix should be numbered as A.1, A.2, etc.

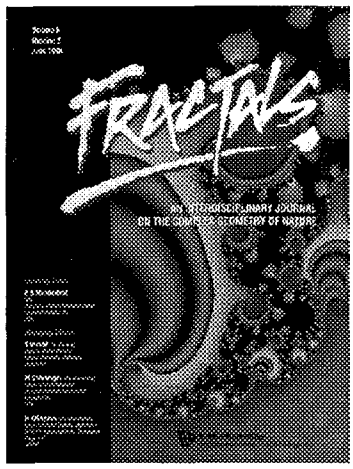

FRACTALS

An Interdisciplinary Journal on the Complex Geometry of Nature

A leading journal devoted exclusively to fractals, FRACTALS publishes an attractive mix of theory and experiments, simulations and proofs. The scope of the journal is broad: it publishes papers on fractal geometry as well as contributions on all kinds of complex scaling behavior in any interesting systems. This journal is essential reading for all scientists and students involved in fractal research.

Aims and Scope

The investigation of phenomena involving fractals has gone through spectacular developments in the past decade. During this relatively short time, fractals have been shown to represent the common aspects of many complex processes ocurring in an unusually diverse range of fields, including physics, mathematics, biology, chemistry, economics and technology. As a rule, the complex nature of a phenomenon is manifested in the intricate underlying geometry, which in most cases can be described in terms of objects with non-integer (fractal) dimension.

By using fractal geometry as a language in related theoretical, numerical and experimental investigations, it has been possible to get a deeper insight into previously intractable problems. Among many others, a better understanding of growth phenomena, turbulence, iterative functions, colloidal aggregation, biological pattern formation and inhomogeneous materials has emerged through the application of such concepts as scale invariance, self-affinity and multifractality.

The aim of this journal is to bring together the most recent developments in fractals research, so that a fruitful interaction of the various approaches and scientific views on the complex spatial and temporal behaviors can take place.

"...next to the innumerable existing journals and without any desire to supersede them, a need has now arisen for a journal on fractals.

...I welcome the initiative of my friends Tamás Vicsek, Michael Shlesinger and Mitsugu Matsushita, and of the World Scientific Publishing Company of Singapore. I wish them all the best, and feel honored by being asked to play a small role in their new journal. Furthermore, I would be pleased to see it publish several papers of mine."

Extracts from Foreword to the first issue of FRACTALS
by Benoit B Mandelbrot

World Scientific
An International Publisher

Home Page:
http://www.worldscientific.com/

For price information, please contact your nearest World Scientific office:

USA office: 1060 Main Street, River Edge, NJ 07661, USA
Toll-free Fax:1-888-977-2665 Toll-free: 1-800-227-7562 E-mail:sales@wspc.com

UK office: 57 Shelton Street, Covent Garden, London WC2H 9HE, UK **Fax: 44-171-836-2020**
Tel: 44-171-836-0888 E-mail:sales@wspc2.demon.co.uk

Singapore office: Farrer Road, P O Box 128, Singapore 912805 Cable: "COSPUB"
Fax: 65-466-5775 Tel: 65-467-7667 E-mail:sales@wspc.com.sg

INSTRUCTIONS FOR CONTRIBUTORS

Organization of Manuscript

To promote the cross-fertilization of ideas among different disciplines, all manuscripts should preferably be organized so that the main results, as well as their significance and potential applications, appear in the earlier sections. Terminologies not generally known outside a main discipline should be defined at the outset. An introductory textbook and/or tutorial paper reference for readers outside the main discipline should also be provided. The technical details, mathematical proofs, and experimental procedure should preferably be given in the latter sections so that a nonspecialist interested only in learning the main results and potential applications need not plow through the complete manuscript in order to filter out this information. Long mathematical proofs should preferably be decomposed into several propositions and/or lemmas so that the main idea of the proof can be understood without having to sift through the fine details.

Submission of Manuscript

Manuscripts should be submitted in **four** copies to:

Professor Leon O. Chua
Editor, *International Journal of Bifurcation and Chaos*
University of California, Berkeley
Dept. of Electrical Engineering & Computer Sciences
Berkeley, CA 94720, USA

To expedite publication, manuscripts of letters to the Editor must include all original line drawings, figures, and photographs.

The cover letter for each contribution should include the author's full postal address, telephone number, computer mail address (if available) and fax number (if available). In the case of a multi-author paper, the cover letter should designate a single author responsible for all future communications.

If available, computer text files ($\TeX$, $\LaTeX$, ASCII or Microsoft Word) should be submitted in a diskette together with the final, revised manuscript.

All manuscripts will be refereed, but they will not be returned to the authors.

Detailed instructions for the preparation of manuscripts are given on the final two printed pages of this issue.

INTERNATIONAL JOURNAL OF
BIFURCATION AND CHAOS
IN APPLIED SCIENCES AND ENGINEERING

MITA (P) No. 310/05/98